

REVISED RESPONSE TO REQUEST FOR ADDITIONAL INFORMATION**APR1400 Design Certification****Korea Electric Power Corporation / Korea Hydro & Nuclear Power Co., LTD****Docket No. 52-046**

RAI No.: 287-8272
SRP Section: 09.01.02 – New and Spent Fuel Storage
Application Section: 9.1.2
Date of RAI Issue: 11/02/2015

Question No. 09.01.02-20

1. The 10 CFR Part 50, Appendix A, General Design Criteria (GDC) 1, 2, 4, 5, 63, and 10CFR 52.80 (a) provide the regulatory requirements for the design of the new and spent fuel storage facilities. Standard Review Plan (SRP) Sections 9.1.2 and 3.8.4, Appendix D describes specific SRP acceptance criteria for the review of the fuel racks that are acceptable to meet the relevant requirements of the Commission's regulations identified above. The SRP 3.8.4 Appendix D section I.5, 'Design and analysis Procedure' requires that "Details of the mathematical model, including a description of how the important parameters are obtained, should be provided". The seismic response of the freestanding fuel storage rack modules is highly nonlinear and involves a complex combination of motions (sliding, rocking, and twisting). The staff did not find sufficient information of the mathematical model and its parameters considered for the seismic evaluation of the new and the spent fuel racks. In accordance with SRP 3.8.4 Appendix D section I.5, the applicant is requested to provide the following information so that the staff can perform its safety evaluation of the seismic analysis.

a. In Subsection 3.3 (3), it is stated that "Each concentrated mass has a degree of freedom in horizontal direction". The applicant is requested to clarify if the same mass is considered effective in both the horizontal directions. Also, the applicant is requested to provide the technical basis for not including the rack and the fuel lumped masses associated with the rocking and twisting degrees of freedom to simulate sliding, rocking and twisting of the free standing racks.

b. In Figures 3-1 and 3-3 (APR1400-H-N-NR-14012, Rev.0), dynamic analysis model of new fuel and spent fuel storage racks respectively, rack equivalent element and fuel assembly equivalent element are shown. Please describe the methodology for determining the rack and fuel assembly equivalent element properties including the acceptance criteria for dynamic equivalency. Provide a comparison of natural frequencies and significant modes of vibrations of the equivalent rack-fuel assembly with the actual rack-fuel assembly.

c. In Figure 3-4 (APR1400-H-N-NR-14012-P, Rev.0), schematic of spring elements used for SF SR are shown. The applicant is requested to provide the spring values and explain how the different spring stiffness values are determined. Since the impact forces are affected by the impact spring stiffness, the applicant is also requested to explain how the sensitivity of the impact forces and rack responses to variation in these spring constants is considered in the nonlinear seismic analyses. Provide the results of any sensitivity analysis performed.

d. Provide the integration time step used in performing the nonlinear time history analyses for SSE. Please explain the sensitivity of the numerical results to the integration time step used in the nonlinear seismic analyses. Provide the results of any sensitivity analysis performed.

e. The applicant is also requested to explain the methods used to incorporate gaps between the racks, fuel bundles and the guide tubes and how the sensitivity of variation in gaps is considered in the nonlinear seismic analyses. Provide the results of any sensitivity analysis performed.

f. The applicant is requested to discuss how the effect of the installation tolerances for the nominal gap are considered in the seismic analysis and design of the NFSR and SF SR and provide the results of any sensitivity analysis performed.

The applicant is requested to identify any proposed changes to and provide a mark-up of Subsections in the DCD Tier 2 and the report APR1400-H-N-NR-14012, Rev.0, as appropriate.

Response – (Rev. 0)

a. Each concentrated mass of fuel assembly model has two degree of freedom in horizontal direction (X and Y direction) and time history seismic loading for two horizontal directions (X and Y direction) are applied simultaneously in nonlinear seismic analyses. All fuel assemblies move simultaneously in one direction. The assumption included in this model brings about larger impact on the rack module than the actual case, and results in the conservative loads to the storage rack. The response of a free-standing rack module to seismic inputs is highly nonlinear and involves a complex combination of motions such as sliding, rocking, twisting, and turning by impacts and friction effects. Therefore, as stated in the response for question number 09.01.02-16, Dynamic Simulations, the analysis is conducted with five separate time histories. Each of the five time histories is then evaluated three different coefficients of friction for the pedestal to the bottom of pool.

b. Dynamic analysis model of the new fuel and spent fuel storage racks are generated using a simplified beam element. A simplified beam model is developed in ways to have similar dynamic characteristics (natural frequency and mode shapes) with actual model. A simplified beam model is generated by repetitive change in moment of inertia (I_{yy} , I_{zz}) for rack element so that the natural frequency of a simplified beam model is tuned to that of a actual models. The following table shows the modal analysis results of a actual and a simplified beam model.

1) New Fuel Storage Rack

Module Type	Direction	FEM Model	Mode	Natural Frequency (Hz)		
7 x 8	Horizontal	Actual Model (A)	1	22.88		
			2	23.01		
		Simplified Beam Model (B)	1	22.87		
			2	23.01		
		Difference of natural frequency*			Less than 5%	

2) Spent Fuel Storage Rack

Region I :

Module Type	Direction	FEM Model	Mode	Natural Frequency (Hz)		
8 x 8	Horizontal	Actual Model (A)	1	41.61		
			2	47.70		
		Simplified Beam Model (B)	1	41.34		
			2	47.40		
		Difference of natural frequency			Less than 5%	
		6 x 8	Horizontal	Actual Model (A)	1	34.34
2	50.43					
Simplified Beam Model (B)	1			34.45		
	2			50.66		
Difference of natural frequency*				Less than 5%		

Region II :

Module Type	Direction	FEM Model	Mode	Natural Frequency (Hz)		
8 x 8	Horizontal	Actual Model (A)	1	38.26		
			2	44.17		
		Simplified Beam Model (B)	1	38.38		
			2	44.95		
		Difference of natural frequency*			Less than 5%	
		8 x 7	Horizontal	Actual Model (A)	1	36.07
2	43.88					
Simplified Beam Model (B)	1			36.35		
	2			43.45		
Difference of natural frequency*				Less than 5%		

(*)Difference of natural frequency = $(1 - B/A) \times 100$

Dynamic analysis model of a fuel assembly is generated using lumped mass and a simplified beam elements. Methodology for determining the fuel assembly equivalent element is shown in the response for question number 09.01.02-30.a.

c Spring stiffness value of fuel assembly-to-rack cell is calculated by multiplying the grid stiffness of a fuel assembly and the total number of fuel assembly grid (11 EA). Stiffness value of the fuel assembly grid is determined by evaluation of the simplified analysis model for the impact test result of the fuel assembly.

And the spring stiffness value of pedestal-to-spent fuel pool floor is calculated using the following formula:

$$K_{ped} = \frac{1}{\frac{1}{K_{bp}} + \frac{1}{K_{fp}} + \frac{1}{K_{mp}}}$$

Where,

- K_{ped} : pedestal stiffness
- K_{bp} : baseplate vertical stiffness
- K_{fp} : female support stiffness
- K_{mp} : male support stiffness

And the method of calculating the spring stiffness value for rack baseplate-to-rack baseplate is shown in the response for question number 09.01.02-31. A sensitivity analysis is performed in which the spring stiffness value is uniformly decreased or increased by 20%, respectively. A sensitivity analysis results are shown in the response for question number 09.01.02-16.

The following table shows spring stiffness values of the rack baseplate-to-rack baseplate, fuel assembly-to-rack cell, and pedestal-to-spent fuel pool floor.

Spring Element	Stiffness Value (lbs/in)
Rack baseplate-to-Rack baseplate	2.717E+7
Fuel Assembly-to-Rack Cell	2.0E+4 x 11
Pedestal-to-Spent Fuel Pool Floor	2.011E+7

d. Integration time step for nonlinear time history analyses is determined automatically from ANSYS during the total record length. The accuracy of the transient dynamic solution depends on the integration time step. Use of small time step size can get accurate results at transient analysis, but transient analysis can be very inefficient. At other parts larger time step size can get accurate results. Automatic time stepping of ANSYS optimize the time step size for this inefficiency. Therefore, sensitivity analysis of integration time step is not performed.

e. Gaps between the racks are used in hydrodynamic mass calculation. The hydrodynamic mass is dependent upon the size of the gap. As the fluid gap size decreases, the hydrodynamic mass increases. As the gap size is increased, the hydrodynamic mass decreases. The hydrodynamic mass is calculated based upon the initial gap sizes. For the rack-to-rack, the initial gap sizes are expected to be reasonably maintained during a seismic response. The rack-to-pool wall gaps change during seismic response based upon the sliding displacements. The hydrodynamic mass increases as the rack moves to close the gap on one side, but the increase is not large until the gap becomes very small. The

hydrodynamic mass is not updated during a seismic response because the maximum displacement of the outmost rack is small in comparison with the gap size of the outmost rack and the pool wall. This is conservative because as the racks approach the wall, the increase in hydrodynamic mass would reduce the sliding response of the racks. Therefore, it is a conservative methodology for maximizing the amount of rack sliding and the potential for rack-to-wall and rack-to-rack impacts. This is also consistent with the discussion of fluid effects in NUREG/CR-5912. In NUREG/CR-5912, it is stated, "...the change was not significant and that the practice of using a constant hydrodynamic mass based on initial gaps is reasonable."

Therefore, the sensitivity analysis of variation in gaps is not performed.

- f. Installation gap as shown in Figures 2-1 and 2-4 of the report APR1400-H-N-NR-14012, Rev.0 is minimum value. Evaluation results for the maximum relative displacement of the adjacent rack show that the structural integrity of rack is maintained. Also, the gap size is increased, the hydrodynamic mass decreases. Therefore, the sensitivity analysis of installation tolerances for the gap is not performed.

Response – (Rev. 1)

Technical report, APR1400-H-N-NR-14012-NP was submitted as Rev. 0 in December, 2014. KHNP responses to RAI 287-8272 were based in part on the Technical Report. Subsequent to issuance of the Technical Report and RAI responses, the NRC provided feedback on both the Technical Report and RAI 287-8272 responses. In response to this NRC feedback, Technical report, APR1400-H-N-NR-14012-NP will be revised (as Rev. 3) to incorporate additional information pertaining to the fuel racks. This RAI revision contains the specific Technical Report revisions relevant to this response and associated DCD changes, where necessary. A summary of the additional information is in the below paragraphs.

Details for Rack and Fuel Assembly Model

The NFSR and fuel assembly model are of a single rack and includes 3-D elastic beam elements (ANSYS BEAM4) and lumped mass elements (ANSYS MASS21) with properties derived from the dynamic characteristics of the detailed 3-D shell model of the NFSR. Effective structural properties for the dynamic model are determined from the natural frequencies and mode shapes of the detailed model. Vertical portions of the NFSR cells and fuel assemblies are each represented by five nodes. Nodes are located at the rack baseplate, $\frac{1}{4} H$, $\frac{1}{2} H$, $\frac{3}{4} H$, and H (where H is the rack height measured above the baseplate). Each rack node has six degrees of freedom (three translations and three rotations) and a lumped mass associated with it. The nodes for the rack and the fuel assembly are connected by contact elements (ANSYS CONTAC52) in the horizontal direction. There is a single contact element in the vertical direction between the fuel assembly bottom node and the baseplate node.

The SFSR model is similar to the NFSR model and is composed of elastic beam elements and lumped mass elements with properties derived from the dynamic characteristics of the detailed 3-D shell model of the SFSR. All the fuel assemblies in each storage rack module are

modeled as one beam of which the mass equals the sum of the masses of all the fuel assemblies in a rack module. Because the fuel assemblies in a rack module are modeled together, all fuel assemblies move simultaneously in one direction. This assumption results in larger impact forces on the rack module than the actual case and results in conservative loads on the storage rack. Because the fuel assembly is modeled with five nodes, the calculated impact loads on the nodes will be larger than the actual value because the fuel assembly actually has eleven spacer grids. The maximum fuel assembly grid horizontal impact load is determined by dividing the maximum impact load at each node by the number of grids associated with that node (2.75 for Nodes 10, 11, and 12, and 1.375 for Nodes 9 and 13). Lumped masses of the rack and fuel assemblies are distributed among the five nodes for spent fuel storage rack cells and fuel assemblies as shown in the table below.

Node No.		Location	Total Mass Distribution
Rack	Fuel Assembly		
13	18	Top of Rack	12.5 %
12	17	3/4 Height	25 %
11	16	1/2 Height	25 %
10	15	1/4 Height	25 %
9	14	Bottom (Baseplate) of Rack	12.5 %

Movement of Fuel Assembly

The following assumption is used in the WPMR dynamic analysis:

“When the SSE occurs, the rack is affected by irregular movement of every single fuel assembly. For conservative evaluation, all the fuel assemblies within the rack rattle in unison (model as a single beam) throughout the seismic event, which exaggerates the impact against the cell wall.”

Stiffness of Model

Two types of stiffness are used in the SFSR model: 3-D elastic beam elements, as discussed above, and contact elements. The contact elements are used to calculate horizontal loads due to friction (between the rack pedestal and embedment plate) and impacts (fuel-to-cell wall, rack-to-rack, and pedestal-to-embedment plate). The contact element used is ANSYS CONTAC52.

CONTAC52 represents two surfaces that may maintain or break physical contact and may slide relative to each other. This element is capable of supporting only compression in the direction normal to the surfaces and shear (coulomb friction) in the tangential direction. The element has three degrees of freedom at each node (x, y, and z). A specified stiffness acts in the normal and tangential directions when the gap is closed. The stiffness values (i.e., spring constants) for the rack baseplates and pedestal are calculated in Appendix E of Reference 1. For these contact elements, the location of the element determines which values are used:



(1) Fuel Assembly-to-Cell Wall

Each node of the fuel assembly beam and the corresponding node of the rack beam is connected using a contact element in order to represent impact between the fuel assembly and the rack cell wall. The normal direction stiffness of this element is calculated assuming a series spring connection of the stiffness of the fuel assembly spacer grid and the local stiffness of the cell in the horizontal direction. To be conservative, the cell wall local stiffness is neglected. The fuel assembly/rack cell contact element has a local stiffness (K_i) to account for impact phenomena of the fuel assembly-to-cell wall. The grid stiffness for a fuel assembly beam is multiplied by the number of fuel assemblies assumed to be in the rack. The stiffness of fuel assembly grid is applied by dividing the total grid stiffness at each node by number of grid associated with node ($K_i/4$ for Nodes 15, 16, and 17, and $K_i/8$ for Nodes 14 and 18).

(2) Pedestal-to-Embedment Plate

Four nodes corresponding to the rack pedestals are connected to the pool floor using contact elements. The stiffness of these elements is a series spring connection of the vertical stiffness of the rack baseplate and pedestal. The baseplate vertical stiffness is calculated from FEM analysis. The stiffness values for the rack baseplates and pedestal are calculated in Appendix E of Reference 1. Therefore, pedestal-to-embedment plate stiffness value is calculated using the following formula:



(3) Rack-to-Rack and Rack-to-Pool Wall

The stiffness for the rack-to-rack contact element is based on connections of the horizontal rack stiffness at the base plate. Analysis results show that the rack-to-rack and rack-to-pool wall displacements are less than the available rack-to-rack and rack-to-pool wall clearances. Consequently, contact elements are not included on the racks except for baseplate-to-baseplate and pedestal rack-to-floor interaction.

Because rack-to-rack impact other than at the baseplates does not occur, no sensitivity is performed. Therefore, the sensitivity of the impact force to the impact spring constant is evaluated for rack baseplate-to-rack baseplate only. A sensitivity analysis is performed in which the spring constant value is uniformly decreased or increased by 20%, respectively.

Sensitivity Analysis for Spring Constants

Three sensitivities were performed on spring constants (i.e., stiffness) in the model, as shown in:

- The rack-to-floor stiffness was evaluated at $\pm 20\%$ of the nominal value.
- The rack-to-rack stiffness was evaluated at $\pm 20\%$ of the nominal value.
- The fuel-to-rack stiffness was evaluated at $\pm 20\%$ of the nominal value.

The effect of the sensitivities was a change in predicted loads within the variation found for different time histories and less than the variation for different COFs.

Sensitivity Analysis for Integration Time Step

Comparison of a run at one half the fixed time step used for all other runs showed small changes in calculated results comparable to the run to run variation with different time histories. Small differences, vice identical results, are expected because the time step used affects where in each time history the acceleration is taken and how long it is applied. The 5% convergence value for dynamic simulation is applied to calculate the force and displacement quantities of interest. Displacement plots of one of the racks to compare results between time steps for the time step sensitivity are as shown in Figure 1.

Fluid Coupling

For seismic conditions, the submerged SFSR is influenced by fluid coupling as well as by mechanical contact. When the racks displace toward each other and the gaps between them are reduced, the fluid coupling effect increases. Because the racks are densely arranged in the spent fuel pool, the fluid coupling effect can be significant. Fluid coupling is included in the SFSR models by use of hydrodynamic mass based on the potential flow theory of Fritz (References 2 and 3).

Hydrodynamic masses are defined at fuel assembly-to-cell wall gaps, rack-to-rack gaps, rack-to-pool wall gaps, and rack baseplate-to-pool floor gaps based on the size of the gaps at those locations.

As gap size is increased, the hydrodynamic mass decreases. The hydrodynamic mass is calculated based upon the initial gap sizes. The initial SFSR rack-to-rack baseplate gaps are the minimum physically possible. Although the hydrodynamic mass increases as the rack moves to close the gap, the increase is not meaningful until the gap becomes very small. Therefore, hydrodynamic mass is not updated during a seismic response run because the maximum displacement of the outermost rack is small in comparison with the gap size of the outermost rack and the pool wall. If applied, the increase in hydrodynamic mass would reduce the sliding response of the racks. Therefore, it is conservative for maximizing the amount of rack sliding and the potential for rack-to-pool wall and rack-to-rack impacts to not increase the hydrodynamic mass. This is also consistent with the discussion of fluid effects in NUREG/CR-5912, Section 6.4.3, Fluid Effects, which states "...the change was not significant and that the practice of using a constant hydrodynamic mass based on initial gaps is reasonable."

Therefore, a sensitivity analysis of variation in gaps (i.e., installation tolerances for the gap) was not performed.

Hydrodynamic mass is calculated based on Fritz's classical two-body fluid coupling model (Reference 3) extended to multiple bodies. In its simplest form, the fluid coupling effect can be explained by considering the proximate motion of two bodies (such as a rack and a wall) under water.

The effect of hydrodynamic mass is implemented through the use of the ANSYS MATRIX27 element.

The NFSRs have no hydrodynamic effect because they are installed in air.

Impacts of Rack-to-Rack and Rack-to-Pool Wall

SFSRs are installed as closely as possible with the protruding baseplate intended to be in contact with the adjacent baseplates. If the racks were initially installed with slight separation, conclusions would not change since it would be no different than a few time steps into a transient when the rack bases have moved slightly apart. The upper part of the racks do not come into contact. Therefore, the only rack-to-rack contact is between the baseplate of racks. Also, the racks do not contact the SFP wall. Therefore, no rack to pool wall impact loads are calculated. This is consistent with SRP Section 3.8.4, Appendix D, Structural Acceptance Criteria, which states:

“In the consideration of the effects of seismic loads, factors of safety against gross sliding and overturning of racks and rack modulus [sic] under all probable service conditions should be in accordance with SRP Section 3.8.5, Subsection II.5. This position on factors of safety against sliding and tilting need not be met provided that the applicant meets any one of the following conditions:

“a. Detailed nonlinear dynamic analyses show that the amplitudes of sliding motion are minimal and impact between adjacent rack modules or between a rack module and the pool walls is prevented provided that the factors of safety against tilting are within the allowable values provided in SRP Section 3.8.5, Subsection II.5....”

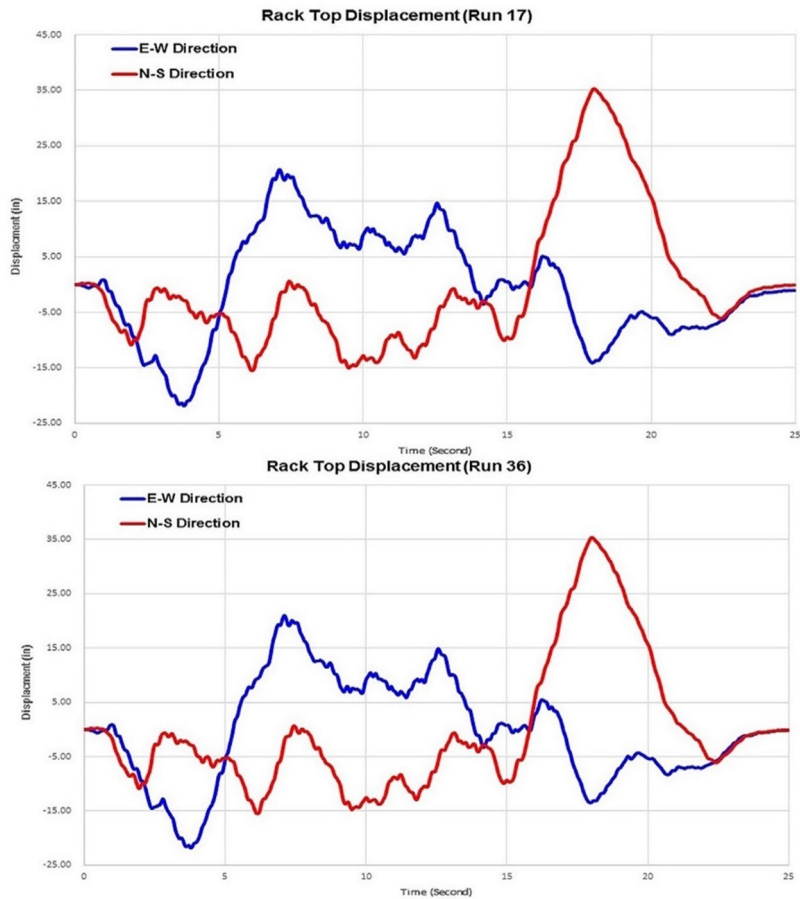


Figure 1 Comparison of Rack Top Displacements at the Time Step Sensitivity Runs

References:

1. Doosan, "Structural and Seismic Analysis Report for New and Spent Fuel Storage Racks," N14014-224CN-0001, Rev.3, Aug. 2017.
2. S. Singh, et. Al., "Structural Evaluation of Onsite Spent Fuel Storage: Recent Developments," Proceedings of the Third Symposium, Orlando, Florida, December 1990, North Carolina State University, Raleigh, NC 27695, pp V/4-1 through V/4-18.
3. Fritz, R.J., "The Effects of Liquids on the Dynamic Motions of Immersed Solids," Journal of Engineering for Industry, Trans. of ASME, February 1972, pp 167-172.

Impact on DCD

There is no impact on the DCD.

Impact on PRA

There is no impact on the PRA.

Impact on Technical Specifications

There is no impact on the Technical Specifications.

Impact on Technical/Topical/Environmental Reports

APR1400-H-N-NR-14012-NP (Rev. 3), will be revised as shown in Attachment 1 to this response (see below).

- a) Section 3.1.2.2 and 3.3
- b) Section 3.1.2.2
- c) Section 3.1.2.4 and 3.7.4
- d) Section 3.7.4.6 and Table 3-6
- e) Section 3.1.2.1(5)
- f) Section 3.1.2.1(5) and 3.7.1.3(2)

3.1.2.2 Details for Rack and Fuel Assembly Model

The sections below provide details on the rack and fuel assembly modeling.

(1) New Fuel Storage Rack Model

The dynamic analysis model for the NFSR and fuel assemblies are shown in Figure 3-1. The NFSR and fuel assembly model are of a single rack and includes 3-D elastic beam elements (ANSYS BEAM4) and lumped mass elements (ANSYS MASS21) with properties derived from the dynamic characteristics of the detailed 3-D shell model of the NFSR. Effective structural properties for the dynamic model are determined from the natural frequencies and mode shapes of the detailed model (see Section 3.1.2.7). Details of effective structural properties for fuel racks are shown in Appendix H of Reference 17. Structural properties (i.e. Young's modulus and flexural rigidity) for fuel assemblies are shown in Table 3-3.

Vertical portions of the NFSR cells and fuel assemblies are each represented by five nodes. Nodes are located at the rack baseplate, $\frac{1}{4} H$, $\frac{1}{2} H$, $\frac{3}{4} H$, and H (where H is the rack height measured above the baseplate). Each rack node has six degrees of freedom (three translations and three rotations) and a lumped mass associated with it. The nodes for the rack and the fuel assembly are connected by contact elements (ANSYS CONTAC52) in the horizontal direction. There is a single contact element in the vertical direction between the fuel assembly bottom node and the baseplate node.

Lumped masses of the NFSR and fuel assemblies are distributed among the five nodes for rack cells and fuel assemblies as shown in the table below:

Node No. (Figure 3-1)		Location	Total Mass Distribution
Rack	Fuel Assembly		
13	18	Top of Rack	12.5 %
12	17	3/4 Height	25 %
11	16	1/2 Height	25 %
10	15	1/4 Height	25 %
9	14	Bottom (Baseplate) of Rack	12.5 %

(2) Spent Fuel Storage Rack Model

To model the interaction among the multiple SFSTRs, the WPMR shown in Figure 3-3 is comprised of a dynamic analysis model for individual SFSTRs, as shown in Figure 3-2. This model is similar to the NFSR model and is composed of elastic beam elements and lumped mass elements with properties derived from the dynamic characteristics of the detailed 3-D shell model of the SFSTR. An underlying assumption in the modeling of the rack as a single beam using the overall bending stiffness of the entire rack is that the cell-to-cell welds remain intact and can carry the internal forces. This assumption is confirmed by structural evaluation of the welds (see Section 3.7.3.3).

Effective structural properties for the dynamic model are determined from the natural frequencies and mode shapes of the detailed model (see Section 3.1.2.7).

Figure 3-2 shows a schematic depicting five nodes representing masses of fuel and rack cells and their associated elements, which are used to represent the interactions and vertical and horizontal motions of support pedestals, respectively. Contact (i.e., gap) elements are used in the representation of rack sliding and impact. A directional stiffness is assigned to the contact element. The pool floor is assumed to be a rigid body initially in contact with the rack pedestals. The contact elements are used to represent potential impact of a rack pedestal on the pool floor. The coefficient of friction between the rack pedestals and pool floor is incorporated into a contact (gap) element.

RAI 287-8272 - Question 09.01.02-20_Rev.1

The hydrodynamic masses for the fuel assembly-to-cell wall, rack-to-rack and rack-to-pool wall are modeled as ANSYS mass MATRIX27 elements. The hydrodynamic masses for rack baseplate-to-pool floor are considered as added masses to each rack baseplate.

Lumped masses of the rack and fuel assemblies are distributed among the five nodes for spent fuel storage rack cells and fuel assemblies as shown in the table below.

Node No. (Figure 3-2)		Location	Total Mass Distribution
Rack	Fuel Assembly		
13	18	Top of Rack	12.5 %
12	17	3/4 Height	25 %
11	16	1/2 Height	25 %
10	15	1/4 Height	25 %
9	14	Bottom (Baseplate) of Rack	12.5 %

All the fuel assemblies in each storage rack module are modeled as one beam of which the mass equals the sum of the masses of all the fuel assemblies in a rack module. Structural properties (i.e. Young's modulus and flexural rigidity) for fuel assemblies are shown in Table 3-3. Because the fuel assemblies in a rack module are modeled together, all fuel assemblies move simultaneously in one direction. This assumption results in larger impact forces on the rack module than the actual case and results in conservative loads on the storage rack. Because the fuel assembly is modeled with five nodes, the calculated impact loads on the nodes will be larger than the actual value because the fuel assembly actually has eleven spacer grids. The maximum fuel assembly grid horizontal impact load is determined by dividing the maximum impact load at each node by the number of grids associated with that node (2.75 for Nodes 10, 11, and 12, and 1.375 for Nodes 9 and 13).

Fluid damping and form drag are conservatively omitted.

Figure 3-3 shows the WPMR analysis model, which combines the single rack models described above to represent the entire spent fuel pool.

3.1.2.3 Hydrodynamic Mass

In addition to the structural mass of racks and fuel assemblies, hydrodynamic masses are included in the SFSR model to account for fluid coupling. Hydrodynamic mass is included in the SFSR model with the ANSYS MATRIX27 element and added mass, which represents an arbitrary element whose geometry is undefined but whose kinematic response can be specified by mass coefficients. Details of hydrodynamic masses are shown in Appendix H of Reference 17.

(1) Fuel Assembly-to-Cell Wall

A fuel assembly consists of fuel rods, guide tubes, top and bottom nozzles, and spacer grids. The hydrodynamic mass coefficients between the rack cell wall and the fuel assembly are calculated assuming the rack cell and fuel assembly are long coaxial cylinders. Hydrodynamic masses acting at the centers of two rigid cylinders with a fluid-filled annulus are represented using the following formula in Reference 15:

$$\begin{pmatrix} F_1 \\ F_2 \end{pmatrix} = \begin{bmatrix} -M_H & M_1 + M_H \\ M_1 + M_H & -(M_1 + M_2 + M_H) \end{bmatrix} \begin{pmatrix} X_1'' \\ X_2'' \end{pmatrix}$$

$$M_H = \left[\frac{R_2^2 + R_1^2}{R_2^2 - R_1^2} \right] \pi \rho R_1^2 h$$

$$M_2 = \rho h (2 C + g_2) \left[2B + \left(\frac{g_1 + g_3}{2} \right) \right]$$

Where,

M_H = Hydrodynamic mass that depends on the fluid flow when the two bodies move relative to each other,

M_1 = Mass of fluid displaced by inner body,

M_2 = Mass of fluid inside the outer body in the absence of the inner body,

h = height of the storage rack,

ρ = density of the fluid, and

g_1, g_2, g_3 = initial gaps between the two bodies.

If g_2 is not the same on both sides, an average value of g_2 is used. If two or more racks overlap each other, the hydrodynamic mass is calculated using a weighted average gap.

(3) Rack Baseplate-to-Pool Floor

The hydrodynamic mass under the baseplate of each rack is calculated using the following formula in accordance with Table 1 of Reference 16.

$$M_{\text{baseplate}} = K \cdot (\pi \cdot \rho \cdot a^2 \cdot b / 4)$$

Where,

K = hydrodynamic mass coefficient ($K = 0.478$ is used for the SFSR),

a, b = length a and width b dimensions of the rack, and

ρ = density of the fluid.

3.1.2.4 Stiffness of Model

Two types of stiffness are used in the SFSR model: 3-D elastic beam elements, as discussed above, and contact elements. The contact elements are used to calculate horizontal loads due to friction (between the rack pedestal and embedment plate) and impacts (fuel-to-cell wall, rack-to-rack, and pedestal-to-embedment plate). The contact element used is ANSYS CONTAC52.

CONTAC52 represents two surfaces that may maintain or break physical contact and may slide relative to each other. This element is capable of supporting only compression in the direction normal to the surfaces and shear (Coulomb friction) in the tangential direction. The element has three degrees of freedom at each node ($x, y,$ and z). A specified stiffness acts in the normal and tangential directions when the gap is closed. The stiffness values (i.e., spring constants) for the rack baseplates and pedestal are calculated in Appendix E of Reference 17. For these contact elements, the location of the element determines which values are used:



(1) Fuel Assembly-to-Cell Wall

Each node of the fuel assembly beam and the corresponding node of the rack beam is connected using a contact element in order to represent impact between the fuel assembly and the rack cell wall. The normal direction stiffness of this element is calculated assuming a series spring connection of the stiffness of the fuel assembly spacer grid and the local stiffness of the cell in the horizontal direction. To be conservative, the cell wall local stiffness is neglected. The fuel assembly/rack cell contact element has a local stiffness (K_i) to account for impact phenomena of the

RAI 287-8272 - Question 09.01.02-20 Rev.1

fuel assembly-to-cell wall. The grid stiffness for a fuel assembly beam is multiplied by the number of fuel assemblies assumed to be in the rack. The stiffness of fuel assembly grid is applied by dividing the total grid stiffness at each node by number of grid associated with node ($K_i/4$ for Nodes 15, 16, and 17, and $K_i/8$ for Nodes 14 and 18).

(2) Pedestal-to-Embedment Plate

Four nodes corresponding to the rack pedestals are connected to the pool floor using contact elements. The stiffness of these elements is a series spring connection of the vertical stiffness of the rack baseplate and pedestal. The baseplate vertical stiffness is calculated from FEM analysis. The stiffness values for the rack baseplates and pedestal are calculated in Appendix E of Reference 17. Therefore, pedestal-to-embedment plate stiffness value is calculated using the following formula:

$$\left[\begin{array}{c} \\ \\ \\ \\ \end{array} \right]^{TS}$$

(3) Rack-to-Rack and Rack-to-Pool Wall

The stiffness for the rack-to-rack contact element is based on connections of the horizontal rack stiffness at the base plate. Analysis results show that the rack-to-rack and rack-to-pool wall displacements are less than the available rack-to-rack and rack-to-pool wall clearances. Consequently, contact elements are not included on the racks except for baseplate-to-baseplate and pedestal rack-to-floor interaction.

Because rack-to-rack impact other than at the baseplates does not occur, no sensitivity is performed. Therefore, the sensitivity of the impact force to the impact spring constant is evaluated for rack baseplate-to-rack baseplate only. A sensitivity analysis is performed in which the spring constant value is uniformly decreased or increased by 20%, respectively.

3.1.2.5 Friction Coefficient

Because SFSRs are not fixed to the storage pool, sliding could occur between the rack pedestals and the embedment plates or pool floor. The contact element is used to model this effect. Based on experimental data (Reference 14), the COF is bounded within the range from 0.2 to 0.8 with a mean value of 0.5. A low friction coefficient may increase sliding distance, while a high friction coefficient may increase rack load.

3.1.2.6 Buoyant Force

The SFSRs are submerged in water; therefore, buoyant forces are calculated and applied to the applicable nodes as concentrated loads in the vertical direction as follows:

$$\text{Buoyant force acting on rack} = W_{\text{rack}} - [(\rho_{\text{rack}} - \rho_{\text{water}}) / \rho_{\text{rack}}] \times W_{\text{rack}}$$

$$\text{Buoyant force acting on fuel assembly} = V_{\text{FA}} \times \rho_{\text{water}} \times \text{gravity}$$

Where,

ρ_{rack} = Density of storage rack, 8,000 kg/m³ (0.289 lbm/in³),

ρ_{water} = Density of fluid, 1,000 kg/m³ (0.036 lbm/in³),

W_{rack} = Weight of rack in air, and

- (4) For welds, the Level D allowable weld stress is not specified in Appendix F of the ASME Code. Therefore, a limit for weld throat stress is used conservatively as follows:

$$F_w = (0.3 S_u) \times \text{Factor}$$

Where,

$$\text{Factor} = (\text{Level D shear stress limit}) / (\text{Level A shear stress limit}) = 0.72 \times S_y / 0.4 \times S_y = 1.8$$

3.2.2.4 Stress Limit for NFSR Stud Bolt

The allowable tensile and shear stresses in the stud bolt are in accordance with ASME Code Section III, Subsection NF and Appendix F for Service Level A and D, respectively. The appropriate stress limit factors K_{bo} are given in Table NF-3225.2-1 in accordance with the load condition. The NFSR stud bolt subjected to combined shear and tension shall be proportioned so that the combined effects of shear and tensile stress satisfy the ellipse equation as shown below.

Load Condition	Tensile (F_{tb})	Shear (F_{vb})	Combined ⁽¹⁾
Level A	$S_u/3.33$	$0.62S_u/5$	$\frac{f_t^2}{F_{tb}^2} + \frac{f_v^2}{F_{vb}^2} \leq 1$
Level D ⁽²⁾	$\text{Min}(0.7S_u, S_y)$	$\text{Min}(0.42S_u, 0.6S_y)$	

(1) f_t and f_v are calculated tensile and shear stresses, respectively.

(2) Specified in Appendix F-1335 of ASME Code, Section III, Division 1.

3.2.3 Dimensionless Stress Factors

Dimensionless stress factors are calculated by the ratio of the calculated stress to the allowable stress for the combined and the individual loads according to ASME Code Section III, Division 1, Subsection NF. When the calculated stress factor does not exceed 1.0, it is considered to meet stress limit requirements for each service condition. In this report, a stress factor as described below is calculated using the load combination for each service condition.

FACT1 = Stress factor of member subject to combined bending and compression (as defined in subsection 3.2.2.1(5)).

FACT2 = Stress factor of member subject to combined flexure and tension (or compression) (as defined in subsection 3.2.2.1(6)).

FACT3 = Stress factor of gross shear on a net section.

3.3 Assumptions

The following assumptions are used in the WPMR dynamic analysis:

- (1) Fluid damping is conservatively neglected.
- (2) Sloshing of the SFP water during a seismic event does not influence the dynamic response of the racks in either horizontal direction because the height of the racks is approximately equal to 3/8 times the depth of water in the spent fuel pool (see Reference 21).
- (3) The fuel assembly is considered as 3-D elastic beam with concentrated masses at the upper and lower ends and at three equally spaced intermediate points of the rack (total of 5 nodes).
- (4) When the SSE occurs, the rack is affected by irregular movement of every single fuel assembly. For conservative evaluation, all the fuel assemblies within the rack rattle in unison (model as a single beam) throughout the seismic event, which exaggerates the impact against the cell wall.

$\frac{S_y}{\sqrt{3}}$ (shear stress limit according to the distortion energy theory of yielding),

S_y (yield strength of baseplate) = 147.5 MPa (21,400 psi),
 L (side length of the pedestal block) = 285 mm (11.2 in), and
 t (thickness of the baseplate) = 25 mm (0.984 in).

The punching shear capacity of the baseplate calculated using the above equation exceeds the maximum pedestal load per Table 3-7 as shown in Table 3-15. Therefore, a punching shear failure of the rack baseplate will not occur.

b. Punching due to Fuel Impact Load

A punching shear analysis due to the maximum impact load of fuel assembly-to-baseplate is performed for the rack baseplate under seismic loading conditions and compared with the allowable stress limit ($0.72 \times S_y = 106.2$ MPa (15,408 psi)) for the Level D condition as follows:

$$\sigma_{\text{shear}} = F_{\text{impact}} / (4 \times L \times t/2)$$

Where,

F_{impact} (Maximum fuel assembly-to-baseplate impact load in vertical direction)
 = 55.7 kN (12,516 lbf) per Table 3-8,
 L (Side length of the square cross-section of fuel assembly) = 206.5 mm (8.128 in), and
 t (Thickness of the baseplate) = 25 mm (0.984 in).

The resultant stress (σ_{shear}) does not exceed the allowable stress limit as shown in Table 3-15. Therefore, a punching shear failure of the rack baseplate will not occur.

3.7.4 Sensitivity Studies

Since the NFSRs are secured in place and do not slide, the following sensitivities (except for the first, rack EI) are not considered applicable. Therefore, discussion of these sensitivities is for the SFSRs only.

3.7.4.1 Rack EI

For both the NFSR and SFSR, sensitivities of $\pm 20\%$ of the product of rack elastic modulus and moment of inertia are evaluated in runs 21 through 24. For the NFSR, fuel assembly grid to cell impact loads were similar. For the SFSR, all loads were similar to those for the base case.

3.7.4.2 Coefficient of Friction

Each of the five time histories was applied to both Region I and Region II racks at COF values of 0.2, 0.5, and 0.8, as shown in Table 3-5 and Figure 3-20. The following trends were noted:

- For loads on a single pedestal, horizontal loads increase with increasing COF
- Baseplate-to-baseplate impact loads increase with increasing COF
- COF does not affect the other loads.

3.7.4.3 Spring constant

Three sensitivities were performed on spring constants (i.e., stiffness) in the model, as shown

- in:
- The rack-to-floor stiffness was evaluated at $\pm 20\%$ of the nominal value.
 - The rack-to-rack stiffness was evaluated at $\pm 20\%$ of the nominal value.
 - The fuel-to-rack stiffness was evaluated at $\pm 20\%$ of the nominal value.

The effect of the sensitivities was a change in predicted loads within the variation found for different time histories and less than the variation for different COFs. Figure 3-24 show the effect on pedestal and baseplate impact loads, respectively.

3.7.4.4 Fuel Assembly EI

One case (Run 33) evaluates the effect of end of life fuel assembly properties. Fuel-to-cell wall and fuel assembly grid impact loads were consistent with those of the BOL case.

3.7.4.5 Rack Loading

The free standing SFSRs do slide and different fuel loading arrangements were considered, as shown in Table 3-5 and described in most runs used fully loaded racks, but one sensitivity involved all racks being empty (Run 34) and another (Run 35) had one quarter full rack and also two half full racks loaded uniformly (see Figure 3-4). The results showed that the displacements of empty fuel racks were less than those of fully loaded racks.

3.7.4.6 Calculational Time Step

Comparison of a run at one half the fixed time step used for all other runs showed small changes in calculated results comparable to the run to run variation with different time histories. Small differences, vice identical results, are expected because the time step used affects where in each time history the acceleration is taken and how long it is applied. Used convergence values for dynamic simulation were 5% for both force and displacement quantities of interest.

3.7.5 Conservatism in Seismic Analysis

The APR1400 fuel rack seismic analytical approach includes significant conservatism:

- All of the fuel mass at each elevation in the rack is assumed to move as a unit, resulting in a conservative impact force and rack response.
- The damping applied in the time history analyses is a conservative value. The ANSYS analyses are based on full integration of the equations of motion and necessarily use frequency dependent damping. For frequency dependent damping, the damping curve is anchored at the lower and upper bounds of the frequency range of interest. For all frequencies between the lower and upper bound, a conservative, lower damping value will then be applied.
- When evaluating stresses, the calculated loads are combined conservatively. For all horizontal loads except fuel assembly grid impact, the combination uses the maximum E-W and the maximum N-S load at any time during the transient, even if they do not occur during the same time step. The grid loads use the values during the same time step to find the maximum. The times of maximum load in the two directions are in general not the same.
- Fluid drag in the spent fuel pool is conservatively neglected. If considered, fluid drag would result in lower impact loads.

Consequently, the reported results include considerable conservatism that are not quantified.

3.7.6 Review of Results

Following completion of the analyses described above, results were reviewed for unexpected or inconsistent behavior. The following high level conclusions were noted.

The analyses performed for loads results from a SSE show satisfactory performance to regulatory acceptance criteria.

Mechanical Analysis for New and Spent Fuel Storage Racks

APR1400-H-N-NR-14012-NP, Rev.3

RAI 287-8272 - Question 09.01.02-20_Rev.1

Table 3-6 Displacement of Racks for All Simulations

Rack	Run Number	Top of Rack (in)		Reduction in Gap between Adjacent Racks (in)*				Displacement of Pedestal Relative to Pool Floor (in)		Coefficient of Friction
				Region I		Region II				
		E-W	N-S	E-W	N-S	E-W	N-S	E-W	N-S	
NFSR	1	0.478	0.617	-	-	-	-	-	-	N/A
	2	0.585	0.557	-	-	-	-	-	-	
	3	0.556	0.602	-	-	-	-	-	-	
	4	0.471	0.652	-	-	-	-	-	-	
	5	0.446	0.664	-	-	-	-	-	-	
SFSR	6	0.149	0.203	0.119	0.185	0.174	0.279	3.171	2.696	0.2
	7	0.159	0.231	0.119	0.208	0.193	0.182	1.565	2.775	
	8	0.138	0.188	0.127	0.224	0.152	0.210	1.906	2.054	
	9	0.125	0.181	0.106	0.166	0.147	0.158	1.944	1.804	
	10	0.140	0.201	0.112	0.232	0.210	0.157	4.108	2.261	
	11	0.206	0.269	0.202	0.278	0.181	0.179	2.032	1.591	0.5
	12	0.219	0.240	0.180	0.232	0.179	0.206	1.463	1.209	
	13	0.226	0.267	0.139	0.292	0.159	0.205	1.248	1.161	
	14	0.218	0.270	0.197	0.285	0.144	0.186	1.652	1.026	
	15	0.225	0.251	0.129	0.258	0.171	0.159	2.334	1.487	
	16	0.278	0.334	0.233	0.365	0.182	0.254	1.957	1.171	0.8
	17	0.285	0.314	0.199	0.307	0.196	0.208	1.157	1.213	
	18	0.268	0.367	0.162	0.361	0.197	0.227	0.837	0.860	
	19	0.276	0.331	0.162	0.309	0.195	0.224	1.380	1.187	
	20	0.329	0.318	0.176	0.369	0.196	0.182	1.130	1.207	
Sensitivity Runs										
NFSR	21	0.410	0.471	-	-	-	-	-	-	N/A
	22	0.595	0.670	-	-	-	-	-	-	
SFSR	23	0.239	0.250	0.156	0.257	0.161	0.139	1.056	0.941	0.8
	24	0.358	0.392	0.188	0.335	0.210	0.270	1.159	1.266	
	25	0.277	0.293	0.189	0.274	0.215	0.243	1.206	1.247	0.8
	26	0.279	0.336	0.190	0.289	0.175	0.183	1.150	1.252	
	27	0.220	0.233	0.131	0.243	0.134	0.191	1.305	1.073	0.5
	28	0.217	0.256	0.183	0.283	0.186	0.172	1.373	1.246	
	29	0.249	0.336	0.203	0.327	0.149	0.243	1.080	0.889	0.8
	30	0.280	0.338	0.167	0.328	0.186	0.220	0.835	0.845	
	31	0.269	0.331	0.169	0.344	0.196	0.271	1.323	0.965	0.8
	32	0.260	0.323	0.194	0.391	0.178	0.270	1.324	1.004	
	33	0.292	0.308	0.165	0.330	0.176	0.198	1.236	0.816	0.8
	34	0.106	0.090	0.078	0.092	0.094	0.068	0.569	0.514	
	35	0.165	0.170	0.155	0.185	0.166	0.123	1.085	1.162	0.5
	36	0.294	0.306	0.189	0.357	0.166	0.183	1.125	1.241	

* Maximum displacements of less than 2.36 in (60 mm) (Region I) and 1.18 in (30 mm) (Region II) indicate no contact occurs.

(3) Contact Elements

Gaps between fuel assemblies and rack cell walls/baseplate, adjacent rack baseplates, and pedestals and embedment plates are modeled with contact elements in the WPMR analysis, as described in Section 3.1.2.4.

(4) Coefficient of Friction

Because the SFSTRs are free-standing, they may slide during an earthquake. The pedestal-to-embedment plate interface is assigned a coefficient of friction (COF) that represents contact between stainless steel surfaces in a wet environment. Based on experimental data (Reference 14), the COF is bounded within the range from 0.2 to 0.8 with a mean value of 0.5.

Since the NFSRs are attached to the floor, COF is not applicable as long as the stud bolts remain intact.

For both the NFSRs and SFSTRs, a COF of 0.5 between the fuel assembly and the rack was used.

(5) Fluid Coupling

For seismic conditions, the submerged SFSTR is influenced by fluid coupling as well as by mechanical contact. When the racks displace toward each other and the gaps between them are reduced, the fluid coupling effect increases. Because the racks are densely arranged in the spent fuel pool, the fluid coupling effect can be significant. Fluid coupling is included in the SFSTR models by use of hydrodynamic mass based on the potential flow theory of Fritz (References 15 and 16).

Hydrodynamic masses are defined at fuel assembly-to-cell wall gaps, rack-to-rack gaps, rack-to-pool wall gaps, and rack baseplate-to-pool floor gaps based on the size of the gaps at those locations. Figure 2-5 and Figure 2-6 show the installation gaps for the SFSTRs.

As gap size is increased, the hydrodynamic mass decreases. The hydrodynamic mass is calculated based upon the initial gap sizes. The initial SFSTR rack-to-rack baseplate gaps are the minimum physically possible. Although the hydrodynamic mass increases as the rack moves to close the gap, the increase is not meaningful until the gap becomes very small. Therefore, hydrodynamic mass is not updated during a seismic response run because the maximum displacement of the outermost rack is small in comparison with the gap size of the outermost rack and the pool wall. If applied, the increase in hydrodynamic mass would reduce the sliding response of the racks. Therefore, it is conservative for maximizing the amount of rack sliding and the potential for rack-to-pool wall and rack-to-rack impacts to not increase the hydrodynamic mass. This is also consistent with the discussion of fluid effects in NUREG/CR-5912, Section 6.4.3, Fluid Effects, which states "...the change was not significant and that the practice of using a constant hydrodynamic mass based on initial gaps is reasonable."

Therefore, a sensitivity analysis of variation in gaps (i.e., installation tolerances for the gap) was not performed.

Hydrodynamic mass is calculated based on Fritz's classical two-body fluid coupling model (Reference 16) extended to multiple bodies. In its simplest form, the fluid coupling effect can be explained by considering the proximate motion of two bodies (such as a rack and a wall) under water.

The effect of hydrodynamic mass is implemented through the use of the ANSYS MATRIX27 element as discussed in Section 3.1.2.3.

The NFSRs have no hydrodynamic effect because they are installed in air.

The maximum relative displacement of the rack pedestal from its starting point is 104.3 mm (4.1 in) as shown in Table 3-6. The minimum size of the embedment plate is about 610 mm (24 in) x 610 mm (24 in) (Reference 27). Therefore, rack pedestals do not slide off the embedment plates onto the spent fuel pool liner because the maximum displacement of rack pedestal is not large enough to move off of the embedment plate.

The maximum rotations of the rack are obtained from a post-processing of the rack time history response output. The SF SR should not exhibit rotations sufficient to cause the rack to overturn (i.e., the rack does not exhibit a rotation sufficient to bring the center of mass over the corner pedestal). Based on the width and height of a 8x7 rack, the rotation required to produce incipient tipping for this rack is approximately equal to:

$$\tan^{-1}[(1/2 * \text{Distance to bring center of gravity over pedestal}) / (1/2 * \text{Height of rack})]$$

$$\tan^{-1}[(1,610/2) / (4,775/2)] = 18.5^\circ$$

As shown in Table 3-10, the safety factor for allowable angle is greater than the acceptance criteria of 1.5 from SRP 3.8.5. Therefore, overturning of a rack module does not occur.

3.7.1.2 Support Pedestal Loads of Rack

The maximum horizontal and vertical loads generated on support pedestal with the application of SSE loads are shown in Table 3-7 and Figure 3-22 and are used to perform structural integrity evaluation of support pedestal and rack. The dynamic simulations of the racks give results for the vertical and two horizontal forces (i.e., E-W and N-S directions) throughout the transient. From those values, the maximum axial force in the vertical direction and the maximum shear forces of the two horizontal directions per pedestal are determined. The resultant shear force for each run is conservatively calculated by combining the maximum horizontal loads on any single pedestal as shown in Table 3-7 using the square root of the sum of the squares (SRSS) method. The maximum bending moment at the bottom baseplate-to-pedestal interface is computed by multiplying the maximum shear force and the distance from the bottom baseplate to the contact point surface underneath of the NFSRs and SF SRs, which is 185 mm (7.28 inches) and 160 mm (6.3 inches) as shown in Tables 2-1 and 2-2, respectively. Additional detail is provided in Appendix F of Reference 17.

3.7.1.3 Impact Loads

The impact loads for fuel-to-cell wall, rack-to-rack and rack-to-pool wall of the NFP and SFP are calculated as follows:

(1) Fuel-to-Cell Wall

For purposes of assessing the effect on rack structural integrity, the maximum impact loads of fuel assembly-to-cell wall for the NFSRs and the SF SRs are as shown in Table 3-8. These loads are determined by dividing the maximum total fuel assembly beam to cell wall load by the number of fuel assemblies in the rack under evaluation (e.g., divide by 64 for a full rack, 32 for a half full rack).

For purposes of determining the effect on the fuel assembly grids, the impact load on each of the fuel support grids at each time step is determined by dividing the maximum calculated impact load per cell at each of the five nodes by number of spacer grids at each of the nodes. For each run, the impact loads in the East-West and North-South directions are combined using the SRSS method at the same time. The combined maximum impact loads on fuel support grid of the NFSRs and the SF SRs are shown in Table 3-8.

(2) Impacts of Rack-to-Rack and Rack-to-Pool Wall

RAI 287-8272 - Question 09.01.02-20_Rev.1

SFSRs are installed as closely as possible with the protruding baseplate intended to be in contact with the adjacent baseplates. If the racks were initially installed with slight separation, conclusions would not change since it would be no different than a few time steps into a transient when the rack bases have moved slightly apart. As reported in Section 3.7.1.1, the upper part of the racks do not come into contact. Therefore, the only rack-to-rack contact is between the baseplate of racks. The maximum impact load at the SFSR baseplates is shown in Table 3-8.

Also as reported in Section 3.7.1.1, the racks do not contact the SFP wall. Therefore, no rack to pool wall impact loads are calculated. This is consistent with SRP Section 3.8.4, Appendix D, Structural Acceptance Criteria, which states:

“In the consideration of the effects of seismic loads, factors of safety against gross sliding and overturning of racks and rack modulus [sic] under all probable service conditions should be in accordance with SRP Section 3.8.5, Subsection II.5. This position on factors of safety against sliding and tilting need not be met provided that the applicant meets any one of the following conditions:

“a. Detailed nonlinear dynamic analyses show that the amplitudes of sliding motion are minimal and impact between adjacent rack modules or between a rack module and the pool walls is prevented provided that the factors of safety against tilting are within the allowable values provided in SRP Section 3.8.5, Subsection II.5....”

3.7.2 Fuel Structural Evaluation

Lateral impact load on the spent fuel assembly is evaluated for two acceptance criteria: fuel spacer grid buckling and fuel cladding yield stress.

The maximum impact load per cell applied to fuel assembly is evaluated for the peak load shown in Table 3-8. Therefore, the maximum acceleration load that the rack imparts on the fuel assembly can be conservatively calculated as follows:

$$a = \frac{F}{w}$$

Where,

- a = Maximum lateral acceleration in g's (= 22.8 g) per section 7.2 of Reference 17,
- F = Maximum fuel-to-cell wall impact load per cell, and
- w = Weight of one fuel assembly (6.27 kN (1408.6 lbf)).

The structural integrity of fuel assembly cladding is evaluated for the maximum lateral acceleration load, obtained by combining (i.e., SRSS) the simultaneous impact load in the E-W and N-S directions to find the maximum value at any time step. The fuel assembly spacer grid is evaluated for the maximum grid impact load, obtained by combining (i.e., SRSS) the simultaneous impact load in the E-W and N-S directions at the same time.

3.7.2.1 Structural Integrity Evaluation of Fuel Spacer Grid

The lateral impact loads on a single fuel spacer grid is compared against its buckling load capacity, which is shown in the Table 3-3. The critical buckling load of the fuel spacer grid for the APR1400 design is 31.3 kN (7,045 lbf) and compared with the combined fuel grid impact load as shown in Table 3-8. The resulting safety factor on fuel assembly spacer grid is as summarized in Table 3-11.

3.7.2.2 Stress Evaluation of Fuel Cladding

The maximum lateral acceleration acting on the fuel mass is used to calculate a load uniformly distributed

REVISED RESPONSE TO REQUEST FOR ADDITIONAL INFORMATION**APR1400 Design Certification****Korea Electric Power Corporation / Korea Hydro & Nuclear Power Co., LTD****Docket No. 52-046**

RAI No.: 287-8272
SRP Section: 09.01.02 – New and Spent Fuel Storage
Application Section: 9.1.2
Date of RAI Issue: 11/02/2015

Question No. 09.01.02-21

1. The 10 CFR Part 50, Appendix A, General Design Criteria (GDC) 1, 2, 4, 5, 63, and 10CFR 52.80 (a) provide the regulatory requirements for the design of the new and spent fuel storage facilities. Standard Review Plan (SRP) Sections 9.1.2 and 3.8.4, Appendix D describes specific SRP acceptance criteria for the review of the fuel racks that are acceptable to meet the relevant requirements of the Commission's regulations identified above. In DCD Tier 2, Section 9.1.2.2.3, "New and Spent Fuel Storage Rack Design", the applicant stated that "The dynamic and stress analyses are performed as described in report APR1400-H-N-NR-14012-P & NP". In the report APR1400-H-N-NR-14012-P, Rev.0, Section 3.1.2.3 "Hydrodynamic Mass", the staff notes that the Applicant did not describe the hydrodynamic mass under the baseplate of each rack. The SRP 3.8.4 Appendix D section I.5, "Design and analysis Procedure" requires that the effect of effective mass from submergence in water should be quantified. In accordance with SRP 3.8.4 Appendix D section I.5, the Applicant is requested to (1) clarify whether the hydrodynamic mass under the rack baseplate of each rack has been considered in all nonlinear seismic analyses and (2) provide the methodology for calculating this hydrodynamic mass. If the hydrodynamic mass under the base plate of each rack is not considered in the nonlinear dynamic analyses, the applicant is requested to provide the technical basis and justification to show that ignoring the hydrodynamic mass under the baseplate of each rack is conservative. The second part of Subsection 3.1.2.3 states "(2) Hydrodynamic masses between Rack-to-Rack and Rack-to-Pool Wall are calculated based on height of rack, density of fluid and gap of adjacent racks, assuming that the fluid is filled between two objects." The applicant is requested to provide a technical reference to any recognized method for this calculation. Also, describe how changes in the gap during seismic response affect the gap-dependent hydrodynamic mass and the subsequent seismic response due to the revised hydrodynamic mass. This could potentially be significant for low coefficient of friction cases where more sliding is expected.

Response – (Rev. 0)

- (1) The hydrodynamic mass under the rack baseplate of each rack is not considered in the dynamic analysis. The analysis will be redone taking into consideration the hydrodynamic mass under the rack baseplate of each rack and a revised report APR1400-H-N-NR-4012-P will be provided by April 30, 2016.
- (2) The hydrodynamic mass under the rack baseplate of each rack is calculated using the following formula in accordance with Table 1 of the effect of liquids on the dynamic motions of immersed solids of Reference 5 in APR1400-H-N-NR-14012-P.

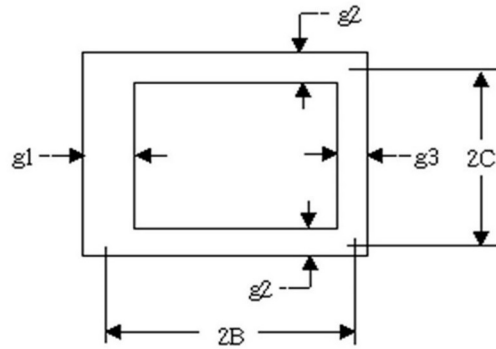
$$M_{\text{baseplate}} = K (\pi \rho a^2 b / 4)$$

Where, $K = 0.478$, a and b are the dimensions of the rack baseplate, and ρ is density of fluid.

The following table shows the calculated hydrodynamic mass under the baseplate of each rack.

TS

The hydrodynamic mass between rack-to-rack and rack-to-storage pool wall is calculated based on the height of the rack, density of the fluid, and the gap of adjacent racks assuming the fluid is filled between two objects consisting of a rigid body, and the center is eccentric. If there is a storage rack with one or more separate gaps at the surface in contact with an adjacent rack, the hydrodynamic mass is calculated based on the average gap with weight. Hydrodynamic masses between rack-to-rack and rack-to-pool wall was calculated using the following formula in accordance with Reference 4 in the report APR1400-H-N-NR-14012-P.



$$M_{H(\text{horiz})} = 2 \rho h C^2 \left[\frac{C}{3 g_1} + \frac{C}{3 g_3} + \frac{2B}{g_2} \right]$$

$$M_1 = \rho h (2C - g_2) \left[2b - \left(\frac{g_1 + g_3}{2} \right) \right]$$

$$M_2 = \rho h (2C + g_2) \left[2b + \left(\frac{g_1 + g_3}{2} \right) \right]$$

Where, h means height of storage rack, ρ means density of fluid, g_1, g_2, g_3 means gap. If gaps are different from each other, the hydrodynamic mass is calculated using the average gap. If two or more racks overlap each other, the hydrodynamic mass is calculated using the average gap with weighted value.

The hydrodynamic mass is dependent upon the size of the gap. As the fluid gap size decreases, the hydrodynamic mass increases. As the gap size is increased, the hydrodynamic mass decreases. The hydrodynamic mass is calculated based upon the initial gap sizes. For the rack-to-rack, the initial gap sizes are expected to be reasonably maintained during a seismic response. The rack-to-pool wall gaps change during seismic response based upon the sliding displacements. The hydrodynamic mass increases as the rack moves to close the gap on one side, but the increase is not large until the gap becomes very small. The hydrodynamic mass is not updated during a seismic response because the maximum displacement of the outmost rack is small in comparison with the gap size of the outmost rack and the pool wall. This is conservative because as the racks approach the wall, the increase in hydrodynamic mass would reduce the sliding response of the racks. Therefore, it is a conservative methodology for maximizing the amount of rack sliding and the potential for rack-to-wall and rack-to-rack impacts. This is also consistent with the discussion of fluid effects in NUREG/CR-5912. In NUREG/CR-5912, it is stated, "...the change was not significant and that the practice of using a constant hydrodynamic mass based on initial gaps is reasonable."

Response – (Rev. 1)

Technical report, APR1400-H-N-NR-14012-NP was submitted as Rev. 0 in December, 2014. KHNP responses to RAI 287-8272 were based in part on the Technical Report. Subsequent to issuance of the Technical Report and RAI responses, the NRC provided feedback on both the Technical Report and RAI 287-8272 responses. In response to this NRC feedback, Technical report, APR1400-H-N-NR-14012-NP will be revised (as Rev. 3) to incorporate additional information pertaining to the fuel racks. This RAI revision contains the specific Technical Report revisions relevant to this response and associated DCD changes, where necessary. A summary of the additional information is in the below paragraphs.

Hydrodynamic Mass for Rack Baseplate-to-Pool Floor

In addition to the structural mass of racks and fuel assemblies, hydrodynamic masses are included in the SFSR model to account for fluid coupling. Hydrodynamic mass is included in the SFSR model with the ANSYS MATRIX27 element and added mass, which represents an arbitrary element whose geometry is undefined but whose kinematic response can be specified by mass coefficients. Details of hydrodynamic masses are shown in Appendix H of Reference 1.

The hydrodynamic mass under the baseplate of each rack is calculated using the following formula in accordance with Table 1 of Reference 2.

$$M_{\text{baseplate}} = K \cdot (\pi \cdot \rho \cdot a^2 \cdot b / 4)$$

Where,

K = hydrodynamic mass coefficient (K = 0.478 is used for the SFSR),

a, b = length a and width b dimensions of the rack, and

ρ = density of the fluid.

References:

1. Doosan, "Structural and Seismic Analysis Report for New and Spent Fuel Storage Racks," N14014-224CN-0001, Rev.3, Aug. 2017 (Doosan Proprietary).
2. Fritz, R.J., "The Effects of Liquids on the Dynamic Motions of Immersed Solids," Journal of Engineering for Industry, Trans. of ASME, February 1972, pp 167-172.

Impact on DCD

There is no impact on the DCD.

Impact on PRA

There is no impact on the PRA.

Impact on Technical Specifications

There is no impact on the Technical Specifications.

Impact on Technical/Topical/Environmental Reports

[APR1400-H-N-NR-14012-NP \(Rev. 3\), Section 3.1.2.3\(3\)](#) will be revised as shown in Attachment 1 to this response.

$$M_2 = \rho h (2 C + g_2) \left[2B + \left(\frac{g_1 + g_3}{2} \right) \right]$$

Where,

M_H = Hydrodynamic mass that depends on the fluid flow when the two bodies move relative to each other,

M_1 = Mass of fluid displaced by inner body,

M_2 = Mass of fluid inside the outer body in the absence of the inner body,

h = height of the storage rack,

ρ = density of the fluid, and

g_1, g_2, g_3 = initial gaps between the two bodies.

If g_2 is not the same on both sides, an average value of g_2 is used. If two or more racks overlap each other, the hydrodynamic mass is calculated using a weighted average gap.

(3) Rack Baseplate-to-Pool Floor

The hydrodynamic mass under the baseplate of each rack is calculated using the following formula in accordance with Table 1 of Reference 16.

$$M_{\text{baseplate}} = K \cdot (\pi \cdot \rho \cdot a^2 \cdot b / 4)$$

Where,

K = hydrodynamic mass coefficient ($K = 0.478$ is used for the SFSR),

a, b = length a and width b dimensions of the rack, and

ρ = density of the fluid.

3.1.2.4 Stiffness of Model

Two types of stiffness are used in the SFSR model: 3-D elastic beam elements, as discussed above, and contact elements. The contact elements are used to calculate horizontal loads due to friction (between the rack pedestal and embedment plate) and impacts (fuel-to-cell wall, rack-to-rack, and pedestal-to-embedment plate). The contact element used is ANSYS CONTAC52.

CONTAC52 represents two surfaces that may maintain or break physical contact and may slide relative to each other. This element is capable of supporting only compression in the direction normal to the surfaces and shear (coulomb friction) in the tangential direction. The element has three degrees of freedom at each node ($x, y,$ and z). A specified stiffness acts in the normal and tangential directions when the gap is closed. The stiffness values (i.e., spring constants) for the rack baseplates and pedestal are calculated in Appendix E of Reference 17. For these contact elements, the location of the element determines which values are used:



(1) Fuel Assembly-to-Cell Wall

Each node of the fuel assembly beam and the corresponding node of the rack beam is connected using a contact element in order to represent impact between the fuel assembly and the rack cell wall. The normal direction stiffness of this element is calculated assuming a series spring connection of the stiffness of the fuel assembly spacer grid and the local stiffness of the cell in the horizontal direction. To be conservative, the cell wall local stiffness is neglected. The fuel assembly/rack cell contact element has a local stiffness (K_i) to account for impact phenomena of the

REVISED RESPONSE TO REQUEST FOR ADDITIONAL INFORMATION**APR1400 Design Certification****Korea Electric Power Corporation / Korea Hydro & Nuclear Power Co., LTD****Docket No. 52-046**

RAI No.: 287-8272
SRP Section: 09.01.02 – New and Spent Fuel Storage
Application Section: 9.1.2
Date of RAI Issue: 11/02/2015

Question No. 09.01.02-22

The 10 CFR Part 50, Appendix A, General Design Criteria (GDC) 1, 2, 4, 5, 63, and 10CFR 52.80 (a) provide the regulatory requirements for the design of the new and spent fuel storage facilities. Standard Review Plan (SRP) Sections 9.1.2 and 3.8.4, Appendix D describes specific SRP acceptance criteria for the review of the fuel racks that are acceptable to meet the relevant requirements of the Commission's regulations identified above. In DCD Tier 2, Section 9.1.2.2.3, "New and Spent Fuel Storage Rack Design", the applicant stated that "The dynamic and stress analyses are performed as described in report APR1400-H-N-NR-14012-P & NP". In the report APR1400-H-N-NR-14012-P, Rev.0, Subsection 3.7.3.4 (3) "Secondary Stress by Temperature Effects", it is stated that "a conservative estimate of the weld stresses along the length of an isolated hot cell is obtained by considering a beam strip uniformly heated by 65° F and restrained from growth along one long edge. The Applicant further stated that temperature rise envelops the difference between the maximum local spent fuel pool water temperature (155°F) inside a storage cell and the bulk pool temperature (121°F) based on the thermal-hydraulic analysis of the spent fuel pool". The Applicant is requested to provide appropriate references and the methodology to calculate the maximum local spent fuel pool water temperature inside a storage cell and the bulk pool temperature.

Response – (Rev. 0)

Bulk pool temperature and the maximum local spent fuel pool water temperature contained in APR1400-H-N-NR-14012-P & NP are based on thermal-hydraulic analysis of abnormal operating conditions, which is one refueling core (100FA) plus one full core (241FA) discharging to the spent fuel pool (SFP) with two cooling trains. The methodology and the references for the calculation of each temperature are as follows;

1. Methodology

1) Bulk pool temperature

In the thermal-hydraulic analysis, the bulk pool temperature for the spent fuel pool is determined based on time, and this temperature can be calculated by using the law of conservation of energy according to the interaction between heat load and heat loss. The mathematical model can be expressed as follows:

$$\frac{d}{dt}(C_W M_W T_W) = Q_{Load} - Q_{Loss}$$

where,

C_W = Specific heat of coolant (J/kg-K)

M_W = Mass of coolant in SFP (kg)

T_W = Bulk SFP temperature (K)

The heat load can be distinguished as decay heat that is generated from the stored spent fuel assemblies in the spent fuel pool. Basically, it is assumed that the spent fuel pool is almost at capacity and has just enough storage space for the newly discharged fuel assemblies. The heat load can be calculated using ORIGEN ARP computer code from Scale6.1, developed at Oak Ridge National Laboratory (ORNL) in 2011.

The heat loss can be distinguished as cooling of the pool mainly through the spent fuel pool cooling system (SFPCS). The pump and heat exchanger in SFPCS, circulate water in the spent fuel pool to remove the heat from the spent fuel assemblies. The other sources of heat loss are evaporation and natural convection of heat transfer process.

For calculating the bulk pool temperature conservatively, the following assumptions are used in the analysis.

- For all discharge scenarios, all the freshly discharged fuel into the SFP from reactor are assumed to be discharged all at one time, after a specified hold time in the shutdown reactor. This is a more conservative assumption than the fact that SFAs are transferred one by one from reactor to SFP.
- All previously discharged fuel and freshly discharged fuel are assumed to have the maximum irradiation exposure, with up to 1,643 effective full power days (3 cycles) in the reactor. This conservatively maximizes the decay heat load associated with all fuel stored in SFP.
- The thermal capacity of the SFP is based on the net water volume above the top of the spent fuel racks SFRs. Since this conservative assumption disregards total thermal capacity, it results in faster computed heat-up rates.
- The decay heat load of the previously discharged fuel assemblies is assumed constant in all discharge scenarios.

2) Maximum local spent fuel pool water temperature

In the thermal-hydraulic analysis, the maximum local spent fuel pool water temperatures are calculated using the CFD program, Fluent. The inputs required for the calculation are: (1) the spent fuel pool and spent fuel rack dimensional data for three-dimensional CFD model; (2) the spent fuel rack and fuel assembly dimensional data for calculating the hydraulic resistance of the spent fuel assembly stored in the spent fuel rack; (3) the heat load of the discharged spent fuel assembly according to the time after reactor shutdown; (4) the temperature and velocity of coolant from spent fuel pool cooling system.

The configuration of the spent fuel racks and fuel assemblies is modeled as a porous media which is mainly used for flow field analysis and geometric structure. According to the Fluent code user's guide, calculating the hydraulic resistance (i.e., permeability and inertial resistance) is performed assuming a porous media for spent fuel racks and fuel assemblies. For calculating the maximum local spent fuel pool water temperature conservatively, the following assumptions are used in the analysis.

- 50 % SFR cells are assumed to be blocked at the top of the cell. This assumption provides conservative results by increasing the flow resistance of the coolant.
- The hottest among the SFRs are grouped together.
- All SFAs are assumed to be located entirely in pedestal cells. These cells have more restrictive flow resistance characteristics compared to non-pedestal cells.
- The decay heat load contribution of the discharged fuel assemblies is assumed constant in all discharge scenarios. Since it disregards the time-varying exponential decay of the heat generation of spent fuel assembly, this assumption is conservative.

2. References

For characterizing the thermal-hydraulic response of the bulk and local spent fuel pool and demonstrating an adequate margin of safety, the applicant had performed the thermal-hydraulic analysis. And for the NRC staff audit of the spent fuel rack (SFR) and the spent fuel pool (SFP) cooling conducted in July, the applicant had submitted the thermal-hydraulic analysis report for SFR & SFP for review.

As a result of the audit, the applicant received follow-up questions from the NRC staff. After addressing the questions, the applicant will submit the thermal-hydraulic analysis report in the form of a technical report.

3. Modification

According to the results of the thermal-hydraulic analysis, the maximum local spent fuel pool water temperature in abnormal operating conditions is 164°F. However, even considering the temperature differential (44°F) applying the revised maximum local temperature, the temperature differential (65°F) described in APR1400-H-N-NR-14012-P & NP is more conservative.

APR1400-H-N-NR-14012-P, Section 3.7.3.4.(3) second paragraph will be revised to include the revised maximum local SFP water temperature of 164°F.

Response – (Rev. 1)

Results of each temperature for spent fuel pool (SFP) contained in APR1400-H-N-NR-14012-P & NP are based on abnormal offloading (Case III) in the thermal-hydraulic analysis for spent fuel racks (Reference 1), which is one refueling core (100FA) plus one full core (241FA) discharging to the spent fuel pool with two cooling trains. The methodology and the references for the calculation of each temperature are as follows;

1. Methodology

1) Bulk pool temperature

In the thermal-hydraulic analysis, the bulk pool temperature for the spent fuel pool is determined based on time, and this temperature can be calculated by using the law of conservation of energy according to the interaction between heat load and heat loss. The mathematical model can be expressed as follows:

$$\frac{d}{dt}(C_W M_W T_W) = Q_{Load} - Q_{Loss}$$

where,

- C_W = Specific heat of coolant (Btu/lb-°F)
- M_W = Mass of coolant in SFP (lb)
- T_W = Bulk SFP temperature (°F)

The heat load can be distinguished as decay heat that is generated from the stored spent fuel assemblies in the spent fuel pool. Basically, it is assumed that the spent fuel pool is almost at capacity and has just enough storage space for the recently offloaded spent fuel assemblies. The heat load can be calculated using ORIGEN ARP computer code from Scale6.1, developed at Oak Ridge National Laboratory (ORNL) in 2011.

The heat loss can be distinguished as cooling of the pool mainly through the spent fuel pool cooling system (SFPCS). The pump and heat exchanger in SFPCS, circulate water in the spent fuel pool to remove the heat from the spent fuel assemblies. The other sources of heat loss are evaporation and natural convection of heat transfer process. (assumed to be neglected for conservatism)

For calculating the bulk pool temperature conservatively, the following assumptions are used in the analysis.

- For all discharge scenarios, all the recently offloaded spent fuel assemblies into the SFP from reactor are assumed to be offloaded all at one time, after a specified hold time in the shutdown reactor. This is a more conservative assumption than the fact that spent fuel assemblies are transferred one by one from reactor to SFP.
- All previously offloaded spent fuel assemblies and recently offloaded spent fuel assemblies are assumed to have the maximum irradiation exposure, with up to 1,643 effective full power days (3 cycles) in the reactor. This conservatively maximizes the decay heat load associated with all spent fuel assemblies stored in SFP.
- The thermal capacity of the SFP is based on the net water volume above the top of the spent fuel racks. Since this conservative assumption disregards total thermal capacity, it results in faster computed heat-up rates.
- The decay heat load of the previously offloaded spent fuel assemblies are assumed constant in all operating scenarios.

2) Maximum local spent fuel pool water temperature

In the thermal-hydraulic analysis, the maximum local spent fuel pool water temperatures are calculated using the CFD program, Fluent. The inputs required for the calculation are: (1) the spent fuel pool and spent fuel rack dimensional data for three-dimensional CFD model; (2) the spent fuel rack and fuel assembly dimensional data for calculating the hydraulic resistance of the spent fuel assembly stored in the spent fuel rack; (3) the heat load of the

offloaded spent fuel assembly according to the time after reactor shutdown; (4) the temperature and velocity of coolant from spent fuel pool cooling system.

TS

For calculating the maximum local spent fuel pool water temperature conservatively, the following assumptions are used in the analysis.

- 50 % SFR cells are assumed to be blocked at the top of the cell. This assumption provides conservative results by increasing the flow resistance of the coolant.
- The hottest among the spent fuel assemblies are grouped together.
- All spent fuel assemblies are assumed to be located entirely in pedestal cells. These cells have more restrictive flow resistance characteristics compared to non-pedestal cells.
- The decay heat load contribution of the offloaded fuel assemblies is assumed constant in all operating scenarios. Since it disregards the time-varying exponential decay of the heat generation of spent fuel assembly, this assumption is conservative.

2. Modification

Technical report, APR1400-H-N-NR-14012-NP was submitted as Rev. 0 in December, 2014. KHNP responses to RAI 287-8272 were based in part on the Technical Report. Subsequent to issuance of the Technical Report and RAI responses, the NRC provided feedback on both the Technical Report and RAI 287-8272 responses. In response to this NRC feedback, Technical report, APR1400-H-N-NR-14012-NP will be revised (as Rev. 3) to incorporate additional information pertaining to the fuel racks. This RAI revision contains the specific Technical Report revisions relevant to this response and associated DCD changes, where necessary. A summary of the additional information is in the below paragraphs.

Secondary Stress by Temperature Effects

The temperature gradients across the rack structure caused by differential heating effects between one or more filled cells and one or more adjacent empty cells are considered. The worst thermal stress in a fuel rack is obtained when a storage cell has a fuel assembly generating heat at the maximum postulated rate and the surrounding storage cells contain no fuel. The thermal stress stresses that occur in this scenario are secondary stresses as defined by the ASME Code Section III, Division 1. Therefore, it is independently evaluated without combining with primary stress of other load conditions.

A conservative estimate of the weld stresses along the length of an isolated hot cell is obtained by considering a beam strip uniformly heated by $\Delta T = 36 \text{ }^\circ\text{C}$ (65 $^\circ\text{F}$), and restrained from growth along one long edge. The temperature rise envelops the difference between the maximum local spent fuel pool water temperature (76.2 $^\circ\text{C}$ (169 $^\circ\text{F}$) bounding) inside a storage cell and the bulk pool temperature (48.9 $^\circ\text{C}$ (120 $^\circ\text{F}$)) based on the thermal-hydraulic analysis of the spent fuel pool (Reference 1). This analysis assumes an almost full SFP to which freshly discharged fuel with worst case decay heat is added in adjacent cells and SFP thermal capacity of only the water above the top of the SFRs. The maximum shear stress due to temperature change for isolated hot cell weld is calculated as follows:

$$\tau_{max} = E \times \alpha \times \Delta T$$

Where,

$E = 1.896E+05 \text{ N/mm}^2 (27.5E+06 \text{ psi})$,

$\alpha = 9.5E-06 \text{ in/in-}^\circ\text{F}$, and

$\Delta T = 36 \text{ }^\circ\text{C} (65 \text{ }^\circ\text{F})$.

The maximum shear stress due to the temperature gradient for an isolated hot cell is calculated given that this thermal stress is classified as secondary stress, the allowable shear stress criteria for Level D condition ($0.42 S_u = 191.4 \text{ MPa} (27,762 \text{ psi})$) is used as the limit of allowable. Therefore, the maximum shear stress due to the temperature gradient is acceptable.

Another possible source of temperature induced stress is expansion of adjacent SFSRs with increased temperature resulting in a contact load between pedestals and baseplates of adjacent racks or relatively different expansion for a fuel assembly and the cell surrounding it. For the former, it is likely that a fuel assembly would cool over time so that it would not generate an increase stress. However, in the event of a loss of SFP cooling, the fuel and the surrounding cell could heat up at different rates. The fuel assembly grid typical dimension is 206.45 mm (8.128 in) square, and a SFSR cell inner dimension is $220.0 \pm 3 \text{ mm}$ square, for a gap of 10.55 mm (0.415 in). Assuming that thermal expansion of the fuel assembly and the rack material is identical, the elongation of SA-240 Type 304L material due to thermal expansion is:

$$\epsilon = \alpha (T_2 - T_1) = 0.001 \text{ in/in}$$

Where,

ϵ : Differential thermal expansion elongation (in/in),

α : Thermal expansion coefficient of SA-240 Type 304L = $8.9E-6 \text{ (in/in-}^\circ\text{F)}$,

T_2 : Temperature = 223.7°F [Maximum fuel clad cladding temperature of spent fuel assembly at abnormal condition per thermal-hydraulic analysis], and

T_1 : Temperature = $115.5 \text{ }^\circ\text{F}$ [Bulk temperature on normal condition of spent fuel pool].

Given the fuel assembly dimensions, the total differential expansion is 0.21 mm (0.008 in), which is a small fraction of the available gap.

As for the load due to expansion of each SFSR causing a contact stress, assuming the racks are installed touching at $21^\circ\text{C} (70^\circ\text{F})$ and heat up to $48.9^\circ\text{C} (120^\circ\text{F})$, the expansion of each rack is about 0.43 mm (0.017 in). In order to develop a load due to constraint of free end displacement, more than two adjacent racks must be in hard contact this is extremely unlikely. Therefore, the development of any significant thermal load due to restraint of free end displacement is not considered credible. Any incidental forces that might develop if some baseplates are in contact are self-limiting as a very small displacement, or shifting of the racks, relieves the stress. Self-limiting stresses developed by constraint of the structure and relieved by minor deformation are, by definition (NF-3121.3), secondary stresses.

According SRP Section 3.8.4, Appendix D, Section I.2, "Design, fabrication, and installation of fuel racks of stainless steel material may be performed based on ASME Code, Section III, Division 1, Subsection NF requirements for Class 3 component supports." For the design of

Class 3 component supports, Table NF-3251.2-1, does not require the evaluation of secondary stresses. Based on this, it is concluded that the development of significant thermal loads due to constraint of the baseplates is not credible and any postulated incidental loads need not be considered since they result in secondary stresses. Therefore, loads from the restraint of adjacent racks do not need to be explicitly considered in the design analysis.

Reference:

1. Doosan, "Thermal-Hydraulic Analysis for Spent Fuel Racks," APR1400-H-N-NR-14013-P/NP, Rev. 0, December 2016.

Impact on DCD

There is no impact on the DCD.

Impact on PRA

There is no impact on the PRA.

Impact on Technical Specifications

There is no impact on the Technical Specifications.

Impact on Technical/Topical/Environmental Reports

APR1400-H-N-NR-14012-NP (Rev. 3), Section 3.7.3.5(3) will be revised as shown in Attachment 1 to this response.

3.7.3.5 Local Stress Evaluation

(1) Cell Wall Impact

The maximum fuel-to-cell wall impact loads for the NFSRs and the SFSRs are as shown in Table 3-8. The evaluation for cell wall for impact is performed to guarantee that local impact does not affect criticality of stored fuel. Integrity of local cell wall is evaluated conservatively using the peak impact load. The limiting impact load to induce overall permanent deformation is calculated by plastic analysis. The cell walls of the new and the spent fuel storage racks can withstand a side load of a maximum of 273.2 kN (61,410 lbf) and 47.4 kN (10,660 lbf), respectively (Reference 17). Therefore, the cell wall of racks satisfies the requirement with the maximum impact loads less than the allowable loads.

(2) Cell Wall Buckling

The cell wall buckling analysis is performed to evaluate the buckling capacity of the spent fuel storage rack cells at the base of the racks using ANSYS program. The cell wall acts alone in compression for a length of about 130 mm (5.12 in) up to the point where the neutron absorbing material sheathing is attached. The sheathing provides additional strength against cell wall buckling. Therefore, the buckling analysis is considered on the lower 130 mm (5.12 in) of the cell wall.

The analysis is evaluated for Region II cells because the maximum stress factor on Region I racks is less than the maximum stress factor (i.e. FACT 2) for the region II racks as shown in Table 3-9 of the TeR. A compressive force for cell wall buckling evaluation is calculated as follows:

$$\sigma_{\text{comp}} = 1.2 \times 21400 \times \text{FACT2} = 71.0 \text{ MPa (10,298 psi)}$$

Where,

FACT2 = 0.401, the stress factor is taken from Table 3-9.

Above calculation is based on the maximum stress factor for the net vertical force on the gross cell cross-section. The vertical forces on the rack support pedestal reflects the weight of the rack plus the stored fuel assemblies during the seismic event. Since the stored fuel assemblies are supported by the rack baseplate, the actual compressive load on the rack cell structure is significantly less than the value determined by the results of dynamic simulations. It is appropriate to use a FACT2 value for cell wall buckling evaluation.

The critical elastic buckling load of cell wall is calculated by ANSYS eigenvalue analysis. Two by two cells of spent fuel storage rack are considered in the buckling analysis. The FE model reflects a reinforcement plate that is welded to outer side of cells. The boundary condition and applied unit load (1 MPa) of FE mode is shown in Figure 3-28. Fixed boundary condition is applied on bottom surface of FE model. Figure 3-29 shows the results of buckling analysis. The minimum value of load multiplier represents the critical elastic buckling pressure of fuel rack cell wall, which is 136.68 MPa (19,823 psi). Therefore, two-thirds of the critical buckling stress as the limit under Service Level D condition is calculated as 91.12 MPa (13,215 psi).

The ANSYS analysis demonstrates that the spent fuel storage rack cells remain in a stable configuration under the maximum seismic load without any gross yielding of the storage cell wall, which satisfies the ASME Code requirements for Level D conditions. Therefore, a buckling of the rack cell wall does not occur.

(3) Secondary Stress by Temperature Effects

The temperature gradients across the rack structure caused by differential heating effects between one or more filled cells and one or more adjacent empty cells are considered. The worst thermal stress in a fuel rack is obtained when a storage cell has a fuel assembly generating heat at the maximum postulated rate and the surrounding storage cells contain no fuel. The thermal stress stresses that occur in this scenario

RAI 287-8272 - Question 09.01.02-22_Rev.1

are secondary stresses as defined by the ASME Code Section III, Division 1. Therefore, it is independently evaluated without combining with primary stress of other load conditions.

A conservative estimate of the weld stresses along the length of an isolated hot cell is obtained by considering a beam strip uniformly heated by $\Delta T = 36\text{ }^{\circ}\text{C}$ ($65\text{ }^{\circ}\text{F}$), and restrained from growth along one long edge. The temperature rise envelops the difference between the maximum local spent fuel pool water temperature ($76.2\text{ }^{\circ}\text{C}$ ($169\text{ }^{\circ}\text{F}$) bounding) inside a storage cell and the bulk pool temperature ($48.9\text{ }^{\circ}\text{C}$ ($120\text{ }^{\circ}\text{F}$)) based on the thermal-hydraulic analysis of the spent fuel pool (Reference 29). This analysis assumes an almost full SFP to which freshly discharged fuel with worst case decay heat is added in adjacent cells and SFP thermal capacity of only the water above the top of the SFRs. The maximum shear stress due to temperature change for isolated hot cell weld is calculated as follows:

$$\tau_{max} = E \times \alpha \times \Delta T$$

Where,

$E = 1.896\text{E}+05\text{ N/mm}^2$ ($27.5\text{E}+06\text{ psi}$),

$\alpha = 9.5\text{E}-06\text{ in/in-}^{\circ}\text{F}$, and

$\Delta T = 36\text{ }^{\circ}\text{C}$ ($65\text{ }^{\circ}\text{F}$).

The maximum shear stress due to the temperature gradient for an isolated hot cell is calculated given that this thermal stress is classified as secondary stress, the allowable shear stress criteria for Level D condition ($0.42 S_u = 191.4\text{ MPa}$ ($27,762\text{ psi}$)) is used as the limit of allowable. Therefore, the maximum shear stress due to the temperature gradient is acceptable.

Another possible source of temperature induced stress is expansion of adjacent SFSRs with increased temperature resulting in a contact load between pedestals and baseplates of adjacent racks or relatively different expansion for a fuel assembly and the cell surrounding it. For the former, it is likely that a fuel assembly would cool over time so that it would not generate an increase stress. However, in the event of a loss of SFP cooling, the fuel and the surrounding cell could heat up at different rates. The fuel assembly grid typical dimension is 206.45 mm (8.128 in) square, and a SFSR cell inner dimension is $220.0 \pm 3\text{ mm}$ square, for a gap of 10.55 mm (0.415 in). Assuming that thermal expansion of the fuel assembly and the rack material is identical, the elongation of SA-240 Type 304L material due to thermal expansion is:

$$\epsilon = \alpha (T_2 - T_1) = 0.001\text{ in/in}$$

Where,

ϵ : Differential thermal expansion elongation (in/in),

α : Thermal expansion coefficient of SA-240 Type 304L = $8.9\text{E}-6\text{ (in/in-}^{\circ}\text{F)}$,

T_2 : Temperature = $223.7\text{ }^{\circ}\text{F}$ [Maximum fuel clad cladding temperature of spent fuel assembly at abnormal condition per thermal-hydraulic analysis], and

T_1 : Temperature = $115.5\text{ }^{\circ}\text{F}$ [Bulk temperature on normal condition of spent fuel pool].

Given the fuel assembly dimensions, the total differential expansion is 0.21 mm (0.008 in), which is a small fraction of the available gap.

As for the load due to expansion of each SFSR causing a contact stress, assuming the racks are installed touching at $21\text{ }^{\circ}\text{C}$ ($70\text{ }^{\circ}\text{F}$) and heat up to $48.9\text{ }^{\circ}\text{C}$ ($120\text{ }^{\circ}\text{F}$), the expansion of each rack is about 0.43 mm (0.017 in). In order to develop a load due to constraint of free end displacement, more than two adjacent racks must be in hard contact this is extremely unlikely. Therefore, the development of any significant thermal load due to restraint of free end displacement is not considered credible. Any incidental forces that might develop if some baseplates are in contact are self-limiting as a very small displacement, or shifting of the racks, relieves the stress. Self-limiting stresses developed by constraint of the structure and relieved by minor deformation are, by definition (NF-3121.3), secondary stresses.

According to SRP Section 3.8.4, Appendix D, Section I.2, "Design, fabrication, and installation of fuel racks of stainless steel material may be performed based on ASME Code, Section III, Division 1, Subsection NF requirements for Class 3 component supports." For the design of Class 3 component supports, Table NF-3251.2-1, does not require the evaluation of secondary stresses. Based on this, it is concluded that the development of significant thermal loads due to constraint of the baseplates is not credible and any postulated incidental loads need not be considered since they result in secondary stresses. Therefore, loads from the restraint of adjacent racks do not need to be explicitly considered in the design analysis.

(4) Punching Shear Analysis of Rack Baseplate

a. Punching due to Vertical Pedestal Load

A punching shear analysis has been performed for the rack baseplate under seismic loading conditions. The analysis demonstrates that the maximum vertical load on a single support pedestal is less than the force necessary for the 285 mm (11.2 in) square pedestal block to punch through the 25 mm (0.984 in) thickness of the baseplate. The punching shear capacity of the baseplate (F_v) can be calculated by following equation.

$$F_v = \frac{S_y}{\sqrt{3}} \times 4 \times L \times t$$

Where,

$\frac{S_y}{\sqrt{3}}$ (shear stress limit according to the distortion energy theory of yielding),

S_y (yield strength of baseplate) = 147.5 MPa (21,400 psi),

L (side length of the pedestal block) = 285 mm (11.2 in), and

t (thickness of the baseplate) = 25 mm (0.984 in).

The punching shear capacity of the baseplate calculated using the above equation exceeds the maximum pedestal load per Table 3-7 as shown in Table 3-15. Therefore, a punching shear failure of the rack baseplate will not occur.

b. Punching due to Fuel Impact Load

A punching shear analysis due to the maximum impact load of fuel assembly-to-baseplate is performed for the rack baseplate under seismic loading conditions and compared with the allowable stress limit ($0.72 \times S_y = 106.2$ MPa (15,408 psi)) for the Level D condition as follows:

$$\sigma_{\text{shear}} = F_{\text{impact}} / (4 \times L \times t/2)$$

Where,

F_{impact} (Maximum fuel assembly-to-baseplate impact load in vertical direction)
= 55.7 kN (12,516 lbf) per Table 3-8,

L (Side length of the square cross-section of fuel assembly) = 206.5 mm (8.128 in), and

t (Thickness of the baseplate) = 25 mm (0.984 in).

The resultant stress (σ_{shear}) does not exceed the allowable stress limit as shown in Table 3-15. Therefore, a punching shear failure of the rack baseplate will not occur.

3.7.4 Sensitivity Studies

Since the NFSRs are secured in place and do not slide, the following sensitivities (except for the first, rack EI) are not considered applicable. Therefore, discussion of these sensitivities is for the SFSTRs only.

REVISED RESPONSE TO REQUEST FOR ADDITIONAL INFORMATION**APR1400 Design Certification****Korea Electric Power Corporation / Korea Hydro & Nuclear Power Co., LTD****Docket No. 52-046**

RAI No.: 287-8272

SRP Section: 09.01.02 – New and Spent Fuel Storage

Application Section: 9.1.2

Date of RAI Issue: 11/02/2015

Question No. 09.01.02-23

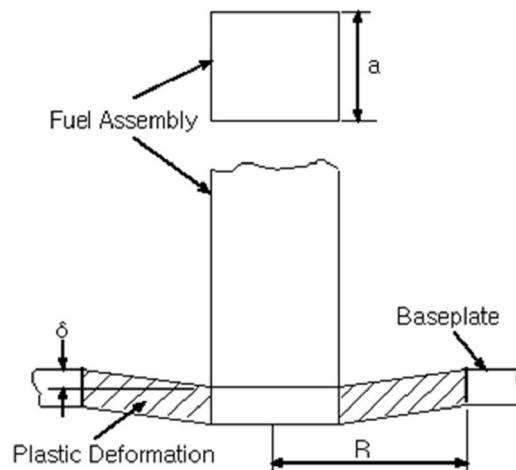
1. The 10 CFR Part 50, Appendix A, General Design Criteria (GDC) 1, 2, 4, 5, 63, and 10CFR 52.80 (a) provide the regulatory requirements for the design of the new and spent fuel storage facilities. Standard Review Plan (SRP) Sections 9.1.2 and 3.8.4, Appendix D describes specific SRP acceptance criteria for the review of the fuel racks that are acceptable to meet the relevant requirements of the Commission's regulations identified above. In DCD Tier 2, Section 9.1.2.2.3, "New and Spent Fuel Storage Rack Design", the applicant stated that "The dynamic and stress analyses are performed as described in report APR1400-H-N-NR-14012-P & NP". In the report APR1400-H-N-NR-14012-P, Rev.0, Section 4.1 "Description of Mechanical Accident", the applicant considered a drop of fuel assembly in an interior cell away from the support pedestal for one of the 'Straight Deep Drops' scenario. The applicant is requested to provide specific location(s) of the drop on the rack base plate that were considered to maximize the deformation of the rack base plate and whether it also considered a deep drop into a cell along the perimeter and half way between the supports. It is not clear from the description whether the rack baseplate evaluation due to fuel impact assumed that other fuel assemblies are in place when a fuel assembly drops through an empty cell. A full load of fuel assemblies may introduce progressive deformation of the baseplate after a fuel assembly impacts the rack baseplate. The maximum downward deformation of the baseplate may be significant enough to initiate a progressive deformation. Therefore, the applicant is also requested to provide (1) the technical basis and justification for not considering all other fuel assemblies in place when a fuel assembly drops through an empty cell and (2) the design basis for the rack baseplate including the basis for determining the most critical locations of the fuel assembly drop.

The applicant is requested to identify any proposed changes to and provide a mark-up of Subsections in the DCD Tier 2 and the report APR1400-H-N-NR-14012-P, Rev.0, as appropriate.

Response – (Rev. 0)

- (1) The calculated deflection of the baseplate due to the deep drop conservatively ignores the reinforcing effect of the cell-to-baseplate welds. The strength provided by the cell-to-baseplate weld reinforcement would offset the added static load of the fuel assemblies. Therefore, all other fuel assemblies in place is not considered when a fuel assembly drops through an empty cell.
- (2) When a fuel assembly drops to the baseplate of a rack, the baseplate must not experience gross failure (i.e., puncture), and the deformed baseplate must not impact the pool liner. In the deep drop analysis (away from the pedestal), a specific location on the rack baseplate was not considered because the maximum deformation of the rack baseplate is calculated without a support under the rack baseplate.

The figure below shows the final deformed shape of the baseplate considered in deep drop analysis.



Deformed Shape of the Rack Baseplate

Response – (Rev. 1)

Technical report, APR1400-H-N-NR-14012-NP was submitted as Rev. 0 in December, 2014. KHNP responses to RAI 287-8272 were based in part on the Technical Report. Subsequent to issuance of the Technical Report and RAI responses, the NRC provided feedback on both the Technical Report and RAI 287-8272 responses. In response to this NRC feedback, Technical report, APR1400-H-N-NR-14012-NP will be revised (as Rev. 3) to incorporate additional information pertaining to the fuel racks. This RAI revision contains the specific Technical Report revisions relevant to this response and associated DCD changes, where necessary. A summary of the additional information is in the below paragraphs.

Straight Deep Drop Away from a Pedestal

For assessing the impact of a drop on baseplate deformation, drops as far away from the support provided by a pedestal are considered at two locations (a central cell and a peripheral cell at the midpoint of a side) that maximize the distance to the points of support. A fuel assembly along with the handling tool (total mass = 1,100 kg (2,425 lbm)) is dropped from a fuel bottom height of 0.61 m (2 ft) above the racks. The falling assembly is assumed to enter an unoccupied storage cell away from a pedestal and impact the rack baseplate. This scenario is also evaluated for the NFSR, and analysis for this scenario is the same as done for the SFSR, except speed at impact is higher because the drop does not have the viscous drag associated with falling through water.

Assumption for Straight Deep Drop Scenario

The fuel assemblies on rack are fully loaded.

Finite Element Model

All drops were analyzed by developing a finite element model in ANSYS LS-DYNA. The impactor (e.g., the fuel assembly and its handling tool, dropped transport container handling tool) is conservatively modeled as a rigid solid with no energy absorption capacity except for drop scenario 3. The detailed configurations of the impact target (i.e., the rack) are modeled in all analyzed events. The deep drop analysis model considers the effects of all of the stored fuel assemblies in the rack by modifying the density of the baseplate to simulate the loading effects of the other fuel assemblies. In most cases, the model of the rack did not include any the structure underneath the rack, but for the deep drop over a pedestal, the effect of the impact on concrete underneath the pedestal baseplate was evaluated. Figure 1 through Figure 7 show the finite element models and results for straight deep drop scenario 2. ANSYS LS-DYNA Elements, SHELL163 (explicit thin structural shell) and SOLID164 (explicit 3-D structural solid), are used to mesh the cell walls, baseplate and rack feet. SHELL163 is a 4-node element with both bending and membrane capabilities. Both in-plane and normal loads are permitted. The element has 12 degrees of freedom at each node: translations, accelerations, and velocities in the nodal x, y, and z directions and rotations about the nodal x, y, and z-axes. SOLID164 is used for the 3-D modeling of solid structures. The element is defined by eight nodes having the degrees of freedom at each node: translations, velocities, and accelerations in the nodal x, y, and z directions. The bottom of the modeled rack feet is fixed in the finite element model because the NFSRs are bolted and horizontal motion is not relevant to a SFSR or NFSR straight vertical drop.



TS

Figure 1 NFSR Model – Deep Drop Away from Pedestal (Scenario 2)



TS

Figure 2 NFSR Impact Location-1 (left) and Location-2 (right) on Baseplate



TS

Figure 3 SFSR Model – Deep Drop Away from Pedestal (Scenario 2)



TS

Figure 4 SFSR Impact Location on Baseplate



Figure 5 Plastic Strain of Baseplate - NFSR Drop Location 1



Figure 6 NFSR Peripheral Deep Drop – Baseplate Plastic Strain



Figure 7 Plastic Strain of Baseplate – SFSR Deep Drop Away from Pedestal

Impact on DCD

There is no impact on the DCD.

Impact on PRA

There is no impact on the PRA.

Impact on Technical Specifications

There is no impact on the Technical Specifications.

Impact on Technical/Topical/Environmental Reports

APR1400-H-N-NR-14012-NP (Rev. 3), Sections 4.1(2), 4.3.1, and 4.3.3 will be revised as shown in Attachment 1 to this response.

4 MECHANICAL ACCIDENTS ANALYSIS

This chapter presents the structural integrity evaluation for new and spent fuel storage racks for dropped and stuck fuel assembly scenarios. Only the effect of the accident scenarios on the racks is considered. The postulated fuel handling accident including a drop of fuel assemblies is addressed in the APR1400 Design Control Document, Section 15.7.4.

The accident analyses demonstrate that the APR1400 fuel racks meet the acceptance criteria specified in Appendix D of SRP 3.8.4 (Reference 1).

4.1 Description of Mechanical Accidents

The NRC SRP 3.8.4, Appendix D (Reference 1) identifies load combinations for SFSR that are to be evaluated in accordance with ASME Code, Section III, Division 1, Subsection NF. Specifically, a stuck fuel assembly analysis should meet Class 3 Level B service limits, while a dropped fuel assembly analysis should demonstrate that the functional capability of the fuel rack is maintained. A subset of accident scenarios is applied to the NFSR due to their different design and environment (e.g., not underwater, no neutron absorber plates). The pedestal of NFSR is supported by the overlapped intermediate plate and embedment plate on concrete slab as shown in Figure 2-3. The following scenarios have been evaluated:

(1) Straight Shallow Drop (Scenario 1)

In the so-called "straight shallow drop" accident, the fuel assembly and handling tool (total mass = 1,100 kg (2,425 lbm)) are dropped from a height of 0.61 m (2 ft) [or the transport container handling tool (= 214.55 kg (473 lbm)) drops from a height of 5.0 m (196.8 in)] above the top of the SFSR and impacts on a top edge of the rack. The dropping mass is assumed to impact the top edge of the rack. Potential for damage to a neutron absorber plate is evaluated. A schematic of the straight shallow drop is shown as Figure 4-1. The shallow drop accident for the NFSR is not relevant since there is no neutron absorber to damage.

(2) Straight Deep Drop Away from a Pedestal (Scenario 2)

For assessing the impact of a drop on baseplate deformation, drops as far away from the support provided by a pedestal are considered at two locations (a central cell and a peripheral cell at the midpoint of a side) that maximize the distance to the points of support. A fuel assembly along with the handling tool (total mass = 1,100 kg (2,425 lbm)) is dropped from a fuel bottom height of 0.61 m (2 ft) above the racks. The falling assembly is assumed to enter an unoccupied storage cell away from a pedestal (as shown in Figure 4-2) and impact the rack baseplate. This scenario is also evaluated for the NFSR, and analysis for this scenario is the same as done for the SFSR, except speed at impact is higher because the drop does not have the viscous drag associated with falling through water.

(3) Straight Deep Drop Over a Pedestal (Scenario 3)

In this case, the fuel assembly enters a corner storage cell which is above a pedestal (as shown in Figure 4-3). This is most limiting for evaluating the concentrated loading on the concrete underlying the baseplate on which the pedestal rests.

(4) Stuck Fuel Assembly (Scenario 4)

In this scenario, it is assumed that a fuel assembly becomes stuck while being lifted out of an SFSR cell resulting in the lifting force of the crane being applied against the SFSR structure. The fuel hoists are provided with load-measuring devices and interlocks to interrupt hoisting if the load increases above the overload setpoint, as identified in DCD Section 9.1.4.5. A tensile force of 22.2 kN (5,000 lbf) on the

SFSR (limited by the motor stall torque or load-limiting device of the crane used to load fuel into the racks) represents the maximum uplift force of a stuck fuel assembly.

4.2 Acceptance Criteria

For mechanical accidents above, the acceptance criteria to ensure damage of the racks is limited as described below:

(1) Straight Shallow Drop (Scenario 1)

For the postulated shallow drop event, the crushed rack walls must not extend down into the "poison zone" that shadows the entire length of the active fuel. This will ensure that the configuration analyzed in the criticality evaluation remains valid. The distance measured from the top of the rack to the upper boundary of the "poison zone" is 610 mm (24.0 in). The depth of damage to the impacted cell walls must be demonstrated to remain limited to the portion of the cell above the top of the "poison zone", which is the elevation of the top of the neutron absorber. This will ensure that the configuration analyzed in the criticality evaluation remains valid. The distance measured from the top of the rack to the upper boundary of the "poison zone" is 0.61 m (2 ft).

(2) Straight Deep Drop (Scenario 2; Away from the pedestal)

The dropping mass impacts the rack baseplate. The acceptance criteria are that the baseplate is not pierced and that the deformed baseplate of the rack must not impact the concrete floor (NFSRs) or pool liner (SFSRs). The normal separation between the underside of the NFSR baseplate and the pit floor is 185 mm (7.28 in) and between the underside of the SFSR baseplate and pool liner is 160 mm (6.30 in).

(3) Straight Deep Drop (Scenario 3; Over a pedestal)

For the postulated deep drop event (over a pedestal), the compressive stress on the concrete floor underneath the embedment plates shall not exceed the maximum allowable stress of 16.4 MPa (2,375 psi) as specified on the paragraph 5.3.4.4 of design specification (Reference 22).

(4) Stuck Fuel Assembly (Scenario 4)

The stuck fuel assembly is evaluated to Level B service limits to ensure the integrity of the rack is unaffected.

4.3 Analysis Method

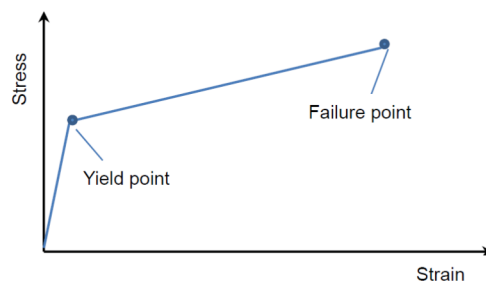
The finite element method is used for the impact analysis of the postulated drop accidents. ANSYS LS-DYNA, a commercial computer code that has been independently validated by Doosan (Reference 30), is used to numerically simulate the impact events. For uplift force, a classical strength of materials calculation is used to determine the amount of area needed to support the forces.

4.3.1 Assumptions

- Scenario masses and heights are constrained as follows:
 - Fuel assembly plus handling tool (1,100 kg (2,425 lbm)) drops from a maximum initial height of 0.61 m (2 ft) above the top of the rack in accordance with paragraph 5.3.4.4.2 of the rack design specification (Reference 22) for all drop scenarios.
 - Transport container handling tool (214.55 kg (473 lbm)) drops from a maximum initial height of 5.0 m (196.8 in) above the top of the rack for shallow drop scenario rack in accordance with paragraph 5.3.4.4.2 of the rack design specification (Reference 22).

RAI 287-8272 - Question 09.01.02-23_Rev.1

- A tensile force of 22.2 kN (5,000 lbf) on the SFSR (limited by the motor stall torque or load-limiting device of the crane used to load fuel into the racks) represents the maximum uplift force of a stuck fuel assembly.
 - In addition, interlocks are installed so that movement of the refueling machine is not possible when the hoist is withdrawing or inserting a fuel assembly. The movement of bridge and trolley is allowed when the fuel assembly has reached the up-limit.
 - The fuel hoists are provided with load-measuring devices and interlocks to interrupt hoisting if the load increases above the overload setpoint and to interrupt lowering if the load decreases below the underload setpoint.
 - Heavy loads, as described in DCD Subsection 9.1.4.2.1, are prevented from traveling over the NFSRs by the use of mechanical and electrical interlocks on the cask handling hoist.
- The spent fuel rack is in a stationary status before the impact. The only postulated means by which the racks could move is a seismic event. Mechanical accidents, however, are not postulated to occur concurrently with a seismic event.
 - The fuel assemblies on rack are fully loaded.
 - The trajectory of the dropped objects is vertical which minimizes the fluid drag. This assumption increases the impact velocity and results in higher energy impacts.
 - In the initial impact velocity calculations, the dropped fuel assembly is treated as a solid rectangular bar. In reality, the fuel assembly is not a solid bar; the lower nozzle block of the fuel assembly may have numerous small flow holes, which allow water to pass between the fuel rods. Although these flow holes reduce the form drag of the lower nozzle, they introduce significant energy loss at the entrance of each flow hole and significant internal flow resistance at the grid spacers and on the fuel rod surfaces. Thus, a solid rectangular bar is considered to reasonably represent the real behavior of the fuel assembly.
 - The ultimate load that can be sustained by a cell wall is based on the load carrying capacity of thin plate sections.
 - The stainless steels used to fabricate the new and spent fuel rack are considered to be bilinear elastoplastic materials with a stress-strain curve to that shown in the following sketch.



- The fuel assembly is assumed to hit a periphery cell wall in the shallow drop event. This is a conservative assumption, since the periphery cell wall has less support from adjacent cells than an interior cell and, therefore, is more vulnerable in a shallow drop accident.
- The concrete steel reinforcement, which is designed to take the tension load, is conservatively neglected in the SFP slab concrete model.
- The energy absorbed through failure of connecting welds is ignored in the analysis.
- Impact damping is conservatively neglected in the finite element analysis.

RAI 287-8272 - Question 09.01.02-23_Rev.1

For a given drop height, impact velocities for shallow drops are identical for both SFSR regions. However, some of the Region II periphery cells, which are formed by welding a panel plate to three adjacent box cells, are structurally weaker. Therefore, a shallow drop over a Region II rack periphery panel plate governs.

For deep drops over a pedestal, impact velocities are the same for both regions. For deep drops away from a pedestal, the impact velocities for Region I and Region II SFSRs are calculated based on the inner dimension of damaged fuel canister cells and that of other cells, respectively. It cause different drag conditions of Region I and Region II SFSRs. Therefore, the impact velocity for Region I SFSRs is greater than that of Region II.

Since a drop into a NFSR is through air, rather than water, it has a higher impact velocity.

4.3.3 Finite Element Model

All drops were analyzed by developing a finite element model in ANSYS LS-DYNA. The impactor (e.g., the fuel assembly and its handling tool, dropped transport container handling tool) is conservatively modeled as a rigid solid with no energy absorption capacity except for drop scenario 3. The detailed configurations of the impact target (i.e., the rack) are modeled in all analyzed events. The deep drop analysis model considers the effects of all of the stored fuel assemblies in the rack by modifying the density of the baseplate to simulate the loading effects of the other fuel assemblies. In most cases, the model of the rack did not include any the structure underneath the rack, but for the deep drop over a pedestal, the effect of the impact on concrete underneath the pedestal baseplate was evaluated. Figure 4-4 through Figure 4-16 show the finite element models and results for individual scenarios, which are discussed in the following sections. ANSYS LS-DYNA Elements, SHELL163 (explicit thin structural shell) and SOLID164 (explicit 3-D structural solid), are used to mesh the cell walls, baseplate and rack feet. SHELL163 is a 4-node element with both bending and membrane capabilities. Both in-plane and normal loads are permitted. The element has 12 degrees of freedom at each node: translations, accelerations, and velocities in the nodal x, y, and z directions and rotations about the nodal x, y, and z-axes. SOLID164 is used for the 3-D modeling of solid structures. The element is defined by eight nodes having the degrees of freedom at each node: translations, velocities, and accelerations in the nodal x, y, and z directions. The bottom of the modeled rack feet is fixed in the finite element model because the NFSRs are bolted and horizontal motion is not relevant to a SFSR or NFSR straight vertical drop.

4.3.4 Methodology for Straight Shallow Drop Accident onto a SFSR

The straight shallow drop accident analysis determines the extent of the damage to the rack structure due to the impact of the dropping object. The impact velocity of the dropping mass is calculated first to determine the bounding kinetic energy that will be used to evaluate the postulated shallow drop accident. In analyzing the shallow drop, the rack model consists of 25 cells as shown in Figure 4-4. Modeling only 25 of 56 or 64 SFSR cells has negligible effect since damage is locally limited to the top of cell walls at the point of impact.

4.3.5 Methodology for Straight Deep Drop Accident (Away from Pedestal)

When a dropping object impacts the baseplate of a rack, the deformation of the baseplate and the potential for impact on the pool liner is evaluated. In analyzing the deep drop scenario 1 (away from the pedestal), the NFSR model consists of 56 cells as shown in Figure 4-5. Figure 4-7 shows the 16 cell model used for the SFSR. The deep drop analysis model considers the effects of all of the stored fuel assemblies in the rack by modifying the density of the baseplate to simulate the dynamic effects of the other fuel assemblies.

REVISED RESPONSE TO REQUEST FOR ADDITIONAL INFORMATION**APR1400 Design Certification****Korea Electric Power Corporation / Korea Hydro & Nuclear Power Co., LTD****Docket No. 52-046**

RAI No.: 287-8272

SRP Section: 09.01.02 – New and Spent Fuel Storage

Application Section: 9.1.2

Date of RAI Issue: 11/02/2015

Question No. 09.01.02-24

1. The 10 CFR Part 50, Appendix A, General Design Criteria (GDC) 1, 2, 4, 5, 63, and 10CFR 52.80 (a) provide the regulatory requirements for the design of the new and spent fuel storage facilities. Standard Review Plan (SRP) Sections 9.1.2 and 3.8.4, Appendix D describes specific SRP acceptance criteria for the review of the fuel racks that are acceptable to meet the relevant requirements of the Commission's regulations identified above. In DCD Tier 2, Section 9.1.2.2.3, "New and Spent Fuel Storage Rack Design", the applicant stated that "The dynamic and stress analyses are performed as described in report APR1400-H-N-NR-14012-P & NP". In the report APR1400-H-N-NR-14012-P, Rev.0, Section 4.3 "Analysis Method", the applicant presented empirical methodologies to analyze the straight shallow and deep drop accidents. The applicant is requested to provide a validation and verification of the proposed empirical methodologies for nonlinear impact phenomena in order for the staff to evaluate whether the proposed methodologies are conservative in predicting the nonlinear deformations of the rack and the rack baseplate, and the impact force on the rack pedestal that is transmitted to the liner and the concrete structure of the spent fuel pool. A nonlinear dynamic analysis for the impact effects of drop accidents, considering a finite element model of the spent fuel rack, rack base plate, a fuel assembly and the pedestal support using appropriate shell, beam, and solid body elements is one approach acceptable to the staff.

Response – (Rev. 0)

The finite element method is used to evaluate whether the proposed methodologies (i.e. energy balance method) are conservative in predicting the nonlinear deformations of the rack and the rack baseplate, and the impact force on the rack pedestal that is transmitted to the embedment plate and the concrete structure of the spent fuel pool. ANSYS LS-DYNA, a commercial computer code that has been validated by DOOSAN's quality control procedure, is used to numerically simulate the impact events.

The results predicted using the energy balance method is conservative compared to the computer program LS-DYNA results as follows:

Summary of comparison results

Rack	Cases	Category	Calculated Value		Acceptance Criteria
			LS-DYNA	Energy Balance Method	
SFSR	Shallow drop	Deformation	6.56 inch	6.64 inch(*)	24.0 inch
	Deep drop SC1 (Away from the pedestal)	Deformation	1.45 inch	4.61 inch	6.3 inch
	Deep drop SC2 (over a pedestal)	Compressive Stress	647 psi (Maximum)	581 psi (Average)	2,375 psi (Average)

Notes:

Once the ultimate load carrying capacity of a cell wall is calculated, the maximum crush depth, δ , of the cell walls due to the dropped fuel assembly impact is obtained using the following formula:

$$\delta = \frac{U_{fa}}{[N_{walls} \cdot P_{ult} - W_{fa} \cdot (1 - \epsilon_{fa})]}$$

where,

U_{fa} : Kinetic energy of the dropping object (i.e. fuel assembly and its handling tool),

N_{walls} : Number of cell walls crushed,

P_{ult} : Ultimate load carrying capacity in the cell wall,

W_{fa} : Weight of dropped object (dry), and

ϵ_{fa} : Ratio of buoyant mass divided by dry mass of dropping object.

(*) We assumed that a number of cell walls crushed are three (3) on calculation of the report APR1400-H-N-NR-14012-P, Rev.0. This value will be reflected on the next revision of the report APR1400-H-N-NR-14012-P based on one (1) cell wall crushed.

Detailed description of Analyses

An elastic-plastic finite element model for each drop event is prepared with the computer code LS-DYNA.

The model simulates the transient collision event with the consideration of plastic and deformation of the fuel rack, rack base plate, and the pedestal support using appropriate shell, beam, and solid body elements. The impactor (i.e., the fuel assembly and its handling tool) is conservatively modeled as a rigid solid with no energy absorption capacity. And the detailed configurations of the impact target (i.e., the rack or SFP floor) are modeled in all analyzed events. The structurally weakest impact region is considered in performing the “shallow” and the “deep” drop analyses.

In analyzing the shallow drop and the deep drop scenario 1 (away from the pedestal), the rack model consists of 64 cells as shown on the Figures 1 and 3. ANSYS Elements, SHELL163 and SOLID164, are used to mesh the cell walls, base plate and rack feet, respectively. The bottom of the modeled rack feet is fixed in the finite element model.

The model for deep drop scenario 2 (over a pedestal) is developed mainly for capturing the structural responses of the rack pedestal, the SFP embedment plate and the underlying concrete slab as shown on the Figure 5. ANSYS Elements, SOLID164 are used to mesh the base plate, rack feet, embedment plate and spent fuel pool (SFP) slab, respectively. Since the SFP slab is supported on grade, the slab model is fixed at the bottom surface with the periphery boundary surface nodes restrained laterally.

And the elastic and elastic-plastic material properties are used to model the rack material behavior as follows:

Material Properties	Material Data	
	SA-240 Type 304L	SA-564 Grade 630 (Hardened at 1100°F)
Yield Strength (ksi)	21.4	106.3
Ultimate Strength (ksi)	66.1	140.0
Young's Modulus (10^6 x psi)	27.5	27.8
Failure Strain/Elongation (in/in)(*)	0.4	0.14

(*) Per ASME Code Section II, Part A

The spent fuel pool floor is assumed as constructed using 4,500 psi concrete and the thickness of the spent fuel pool floor embedment plate is considered to be 2 inch thickness.

The results from the analyses are shown in Figures 2, 4 and 6.

Figures for Finite Element Model and Analysis Results

TS



Figure 1 Finite Element Model – Shallow Drop (Drop Location)

TS



Figure 2 Plastic Strain of the Cell Wall – Shallow Drop

TS



Figure 3 Finite Element Model – Deep Drop Scenario 1 (Drop Location)

TS



Figure 4 Maximum Baseplate Deformation – Deep Drop Scenario 1



Figure 5 Finite Element Model – Deep Drop Scenario 2



Figure 6 Compressive stresses on SFP slab – Deep Drop Scenario 2

Response – (Rev. 1)

Technical report, APR1400-H-N-NR-14012-NP was submitted as Rev. 0 in December, 2014. KHNP responses to RAI 287-8272 were based in part on the Technical Report. Subsequent to issuance of the Technical Report and RAI responses, the NRC provided feedback on both the Technical Report and RAI 287-8272 responses. In response to this NRC feedback, Technical report, APR1400-H-N-NR-14012-NP will be revised (as Rev. 3) to incorporate additional information pertaining to the fuel racks. This RAI revision contains the specific Technical Report revisions relevant to this response and associated DCD changes, where necessary. A summary of the additional information is in the below paragraphs.

Finite Element Model

All drops were analyzed by developing a finite element model in ANSYS LS-DYNA. The impactor (e.g., the fuel assembly and its handling tool, dropped transport container handling tool) is conservatively modeled as a rigid solid with no energy absorption capacity except for drop scenario 3. The detailed configurations of the impact target (i.e., the rack) are modeled in all analyzed events. The deep drop analysis model considers the effects of all of the stored fuel assemblies in the rack by modifying the density of the baseplate to simulate the loading effects of the other fuel assemblies. In most cases, the model of the rack did not include any the structure underneath the rack, but for the deep drop over a pedestal, the effect of the impact on concrete underneath the pedestal baseplate was evaluated. ANSYS LS-DYNA Elements, SHELL163 (explicit thin structural shell) and SOLID164 (explicit 3-D structural solid), are used to mesh the cell walls, baseplate and rack feet. SHELL163 is a 4-node element with both bending and membrane capabilities. Both in-plane and normal loads are permitted. The element has 12 degrees of freedom at each node: translations, accelerations, and velocities in the nodal x, y, and z directions and rotations about the nodal x, y, and z-axes. SOLID164 is used for the 3-D modeling of solid structures. The element is defined by eight nodes having the degrees of freedom at each node: translations, velocities, and accelerations in the nodal x, y, and z directions. The bottom of the modeled rack feet is fixed in the finite element model because the NFSRs are bolted and horizontal motion is not relevant to a SFSR or NFSR straight vertical drop.

Methodology for Straight Shallow Drop Accident onto a SFSR

The straight shallow drop accident analysis determines the extent of the damage to the rack structure due to the impact of the dropping object. The impact velocity of the dropping mass is calculated first to determine the bounding kinetic energy that will be used to evaluate the postulated shallow drop accident. In analyzing the shallow drop, the rack model consists of 25 cells as shown in Figure 1. Modeling only 25 of 56 or 64 SFSR cells has negligible effect since damage is locally limited to the top of cell walls at the point of impact.

Methodology for Straight Deep Drop Accident (Away from Pedestal)

When a dropping object impacts the baseplate of a rack, the deformation of the baseplate and the potential for impact on the pool liner is evaluated. In analyzing the deep drop scenario

1 (away from the pedestal), the NFSR model consists of 56 cells as shown in Figure 2. Figure 3 shows the 16 cell model used for the SFSR. The deep drop analysis model considers the effects of all of the stored fuel assemblies in the rack by modifying the density of the baseplate to simulate the dynamic effects of the other fuel assemblies.

Methodology for Straight Deep Drop Accident (Over a Pedestal of SFSR)

The model was developed mainly for capturing the structural responses of the rack pedestal, the SFP embedment plate and the underlying concrete slab as shown in the Figure 4. The impactor (i.e., the fuel assembly and its handling tool, drop of transport container handling tool) model consists of two parts: a bottom end nozzle with instrument tube and an elastic beam representing the fuel rods. The mass and cross-sectional area properties of the elastic beam are based on the entire array of fuel rods (cladding material only). The other mass properties including handling tool are distributed on a model of the bottom end nozzle with instrument tube. Therefore, the impactor model has the same mass as an actual fuel assembly and handling tool. Using the impact velocity described in Section 4.3.2 of the Technical report, APR1400-H-N-NR-14012-NP, ensures that the impact energy will be representative of an actual drop accident. Bi-linear material properties have been assigned to the bottom end nozzle with instrument tube. The fuel cladding is modeled using beam elements with elastic material properties for conservatism. ANSYS LS-DYNA Elements, BEAM161 (explicit 3-D beam) and SOLID164 (explicit 3-D structural solid), are used to mesh the fuel assembly. ANSYS LS-DYNA Element SOLID164 is used to mesh the base plate, rack feet, embedment plate and SFP slab. The slab model is fixed at the bottom surface with the peripheral boundary surface nodes restrained laterally. The deep drop analysis model considers the effects of all of the stored fuel assemblies in the rack by modifying the density of the baseplate to simulate the dynamic effects of the other fuel assemblies.

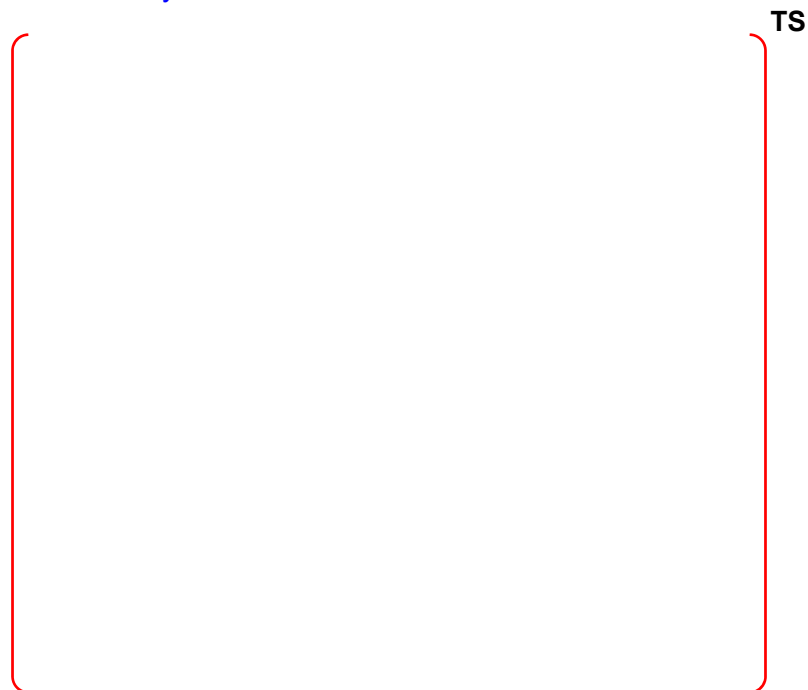


Figure 1 Finite Element Model – Shallow Drop

TS



Figure 2 NFSR Model – Deep Drop Away from Pedestal (Scenario 2)

TS



Figure 3 SFSR Model – Deep Drop Away from Pedestal (Scenario 2)

TS



Figure 4 SFSR Model – Deep Drop Over a Pedestal (Scenario 3)

Impact on DCD

There is no impact on the DCD.

Impact on PRA

There is no impact on the PRA.

Impact on Technical Specifications

There is no impact on the Technical Specifications.

Impact on Technical/Topical/Environmental Reports

APR1400-H-N-NR-14012-NP (Rev. 3), Sections 4.3.3, 4.3.4, 4.3.5, 4.3.6, and Figure 4-4 through Figure 4-9 will be revised as shown in Attachment 1 to this response.

For a given drop height, impact velocities for shallow drops are identical for both SFSR regions. However, some of the Region II periphery cells, which are formed by welding a panel plate to three adjacent box cells, are structurally weaker. Therefore, a shallow drop over a Region II rack periphery panel plate governs.

For deep drops over a pedestal, impact velocities are the same for both regions. For deep drops away from a pedestal, the impact velocities for Region I and Region II SFSRs are calculated based on the inner dimension of damaged fuel canister cells and that of other cells, respectively. It cause different drag conditions of Region I and Region II SFSRs. Therefore, the impact velocity for Region I SFSRs is greater than that of Region II.

Since a drop into a NFSR is through air, rather than water, it has a higher impact velocity.

4.3.3 Finite Element Model

All drops were analyzed by developing a finite element model in ANSYS LS-DYNA. The impactor (e.g., the fuel assembly and its handling tool, dropped transport container handling tool) is conservatively modeled as a rigid solid with no energy absorption capacity except for drop scenario 3. The detailed configurations of the impact target (i.e., the rack) are modeled in all analyzed events. The deep drop analysis model considers the effects of all of the stored fuel assemblies in the rack by modifying the density of the baseplate to simulate the loading effects of the other fuel assemblies. In most cases, the model of the rack did not include any the structure underneath the rack, but for the deep drop over a pedestal, the effect of the impact on concrete underneath the pedestal baseplate was evaluated. Figure 4-4 through Figure 4-16 show the finite element models and results for individual scenarios, which are discussed in the following sections. ANSYS LS-DYNA Elements, SHELL163 (explicit thin structural shell) and SOLID164 (explicit 3-D structural solid), are used to mesh the cell walls, baseplate and rack feet. SHELL163 is a 4-node element with both bending and membrane capabilities. Both in-plane and normal loads are permitted. The element has 12 degrees of freedom at each node: translations, accelerations, and velocities in the nodal x, y, and z directions and rotations about the nodal x, y, and z-axes. SOLID164 is used for the 3-D modeling of solid structures. The element is defined by eight nodes having the degrees of freedom at each node: translations, velocities, and accelerations in the nodal x, y, and z directions. The bottom of the modeled rack feet is fixed in the finite element model because the NFSRs are bolted and horizontal motion is not relevant to a SFSR or NFSR straight vertical drop.

4.3.4 Methodology for Straight Shallow Drop Accident onto a SFSR

The straight shallow drop accident analysis determines the extent of the damage to the rack structure due to the impact of the dropping object. The impact velocity of the dropping mass is calculated first to determine the bounding kinetic energy that will be used to evaluate the postulated shallow drop accident. In analyzing the shallow drop, the rack model consists of 25 cells as shown in Figure 4-4. Modeling only 25 of 56 or 64 SFSR cells has negligible effect since damage is locally limited to the top of cell walls at the point of impact.

4.3.5 Methodology for Straight Deep Drop Accident (Away from Pedestal)

When a dropping object impacts the baseplate of a rack, the deformation of the baseplate and the potential for impact on the pool liner is evaluated. In analyzing the deep drop scenario 1 (away from the pedestal), the NFSR model consists of 56 cells as shown in Figure 4-5. Figure 4-7 shows the 16 cell model used for the SFSR. The deep drop analysis model considers the effects of all of the stored fuel assemblies in the rack by modifying the density of the baseplate to simulate the dynamic effects of the other fuel assemblies.

4.3.6 Methodology for Straight Deep Drop Accident (Over a Pedestal of SFSR)

The model was developed mainly for capturing the structural responses of the rack pedestal, the SFP embedment plate and the underlying concrete slab as shown in the Figure 4-9. The impactor (i.e., the fuel assembly and its handling tool, drop of transport container handling tool) model consists of two parts: a bottom end nozzle with instrument tube and an elastic beam representing the fuel rods. The mass and cross-sectional area properties of the elastic beam are based on the entire array of fuel rods (cladding material only). The other mass properties including handling tool are distributed on a model of the bottom end nozzle with instrument tube. Therefore, the impactor model has the same mass as an actual fuel assembly and handling tool. Using the impact velocity described in Section 4.3.2 above ensures that the impact energy will be representative of an actual drop accident. Bi-linear material properties have been assigned to the bottom end nozzle with instrument tube. The fuel cladding is modeled using beam elements with elastic material properties for conservatism. ANSYS LS-DYNA Elements, BEAM161 (explicit 3-D beam) and SOLID164 (explicit 3-D structural solid), are used to mesh the fuel assembly. ANSYS LS-DYNA Element SOLID164 is used to mesh the base plate, rack feet, embedment plate and SFP slab. The slab model is fixed at the bottom surface with the peripheral boundary surface nodes restrained laterally. The deep drop analysis model considers the effects of all of the stored fuel assemblies in the rack by modifying the density of the baseplate to simulate the dynamic effects of the other fuel assemblies.

4.3.7 Methodology for Stuck Fuel Accident

This analysis evaluates the ability of the rack walls to withstand the uplift force due to a stuck fuel assembly. There are a number of ways that a fuel assembly can become stuck in a cell, and most involve contact with more than one cell wall (i.e., wedging). Assuming that the uplift force is imposed on a single cell wall is conservative. A classical strength of materials equation is used to determine the amount of area needed to support the uplift force on a stuck fuel assembly.

(1) Vertical uplift force at top of cell

The critical location for load application is to have this load applied near the top of the rack along or against a single cell wall. If the vertical uplift load is resisted only by shear stress and the allowable in shear is the Level B limit. The depth (h_{sf}) of the cell that can support the applied load is obtained from the classical strength of materials equation to determine the amount of area needed to support the forces. If the damage depth of the cell is above the active fuel area, the vertical uplift force is not a safety concern.

$$h_{sf} = \frac{F_{Uplift}}{2 \cdot \tau_y \cdot t_{cell}}$$

Where,

F_{Uplift} : Uplift force applied to the rack,

τ_y : Allowable in shear of cell wall for Level B limit (=1.33 x 0.4 x S_y), and

t_{cell} : Cell wall thickness.

(2) Vertical uplift along length of cell

The cell wall stress (σ) due to vertical uplift force along length of cell is determined as follows:

$$\sigma = \frac{F_{Uplift}}{D_{cell} \cdot t_{cell}}$$

Where,

D_{cell} : Cell Inside dimension

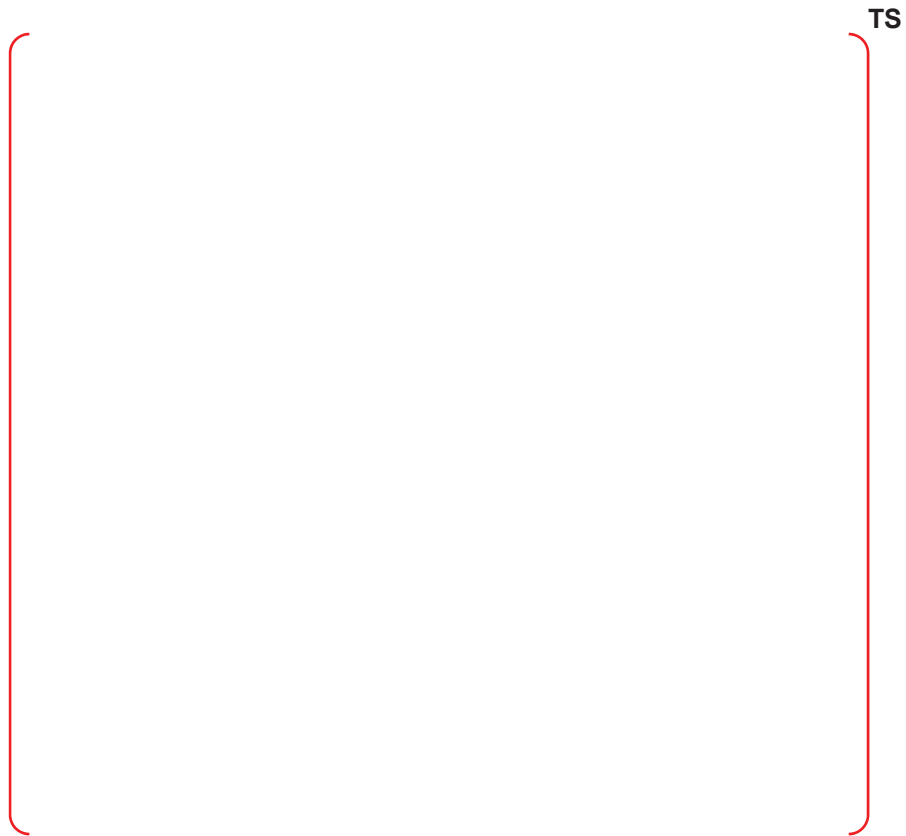


Figure 4-4 Finite Element Model – Shallow Drop

RAI 287-8272 - Question 09.01.02-24_Rev.1

TS

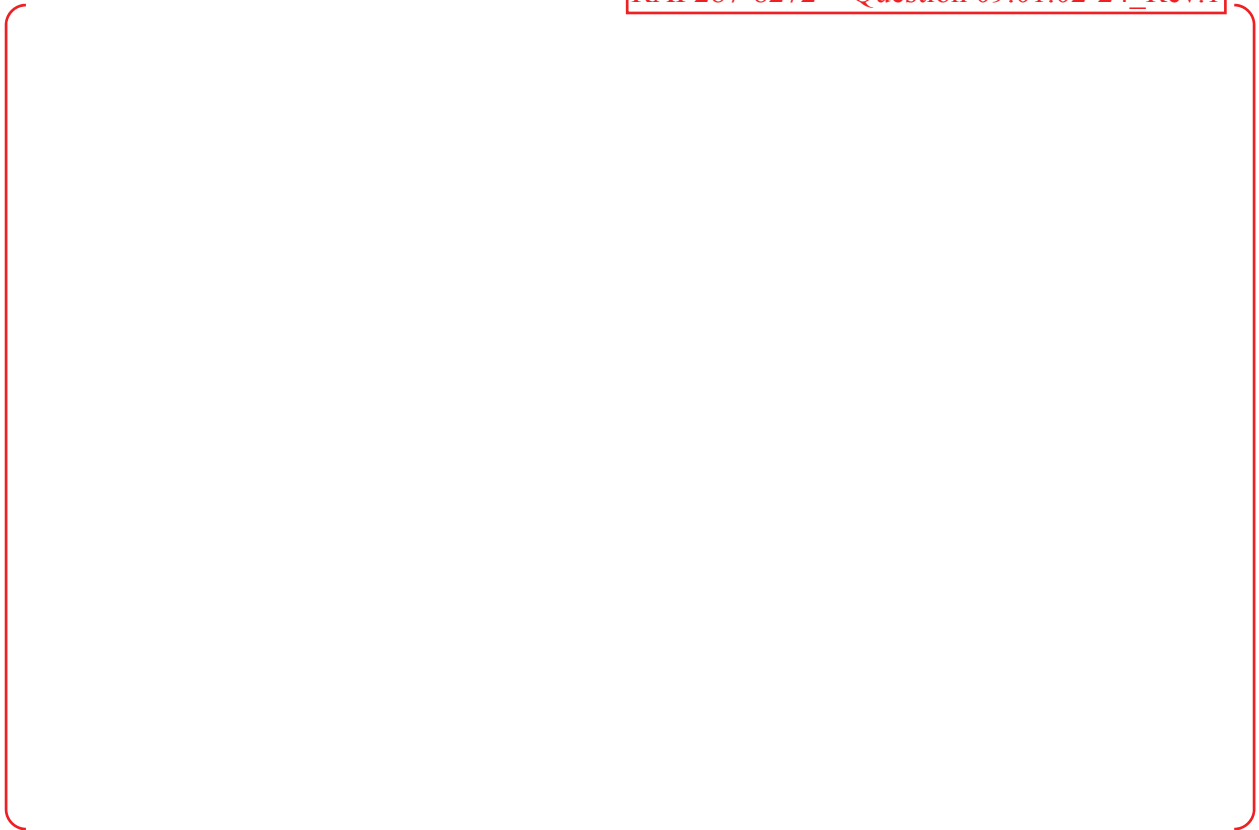


Figure 4-5 NFSR Model – Deep Drop Away from Pedestal (Scenario 2)

TS



Figure 4-6 NFSR Impact Location-1 (left) and Location-2 (right) on Baseplate

RAI 287-8272 - Question 09.01.02-24_Rev.1

TS

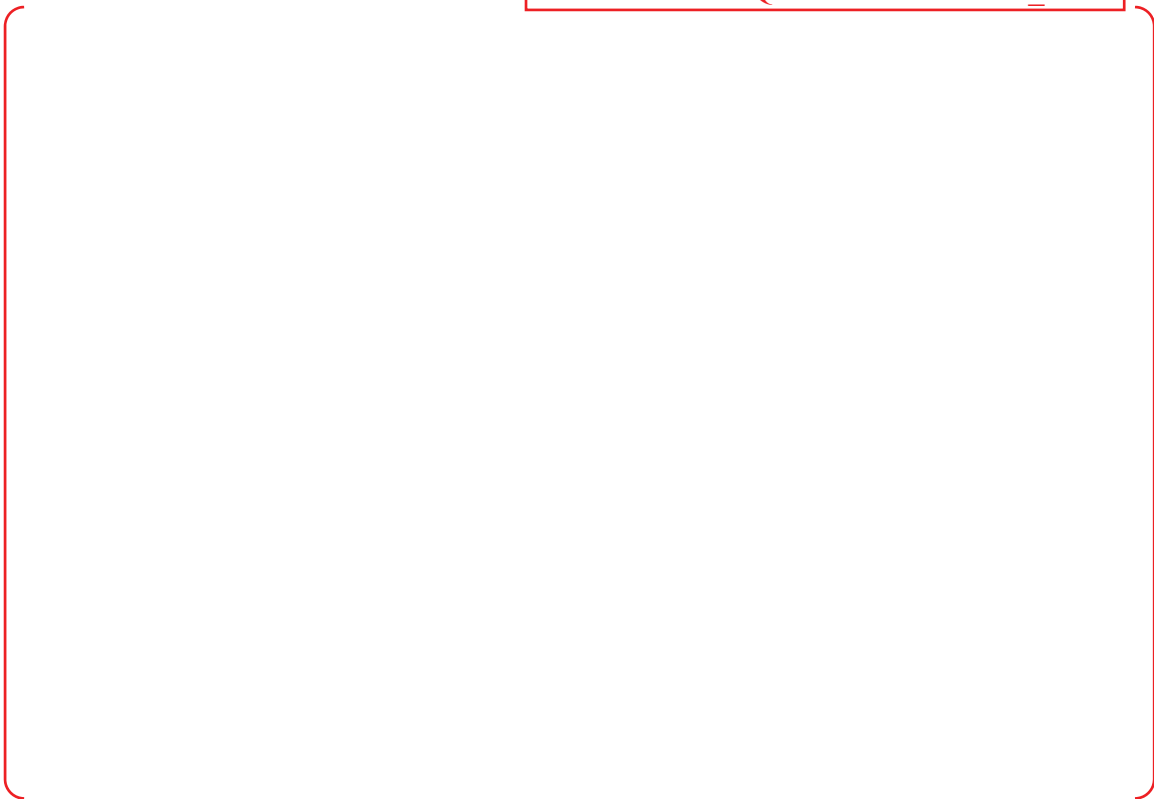


Figure 4-7 SFSR Model – Deep Drop Away from Pedestal (Scenario 2)



TS

Figure 4-8 SFSR Impact Location on Baseplate

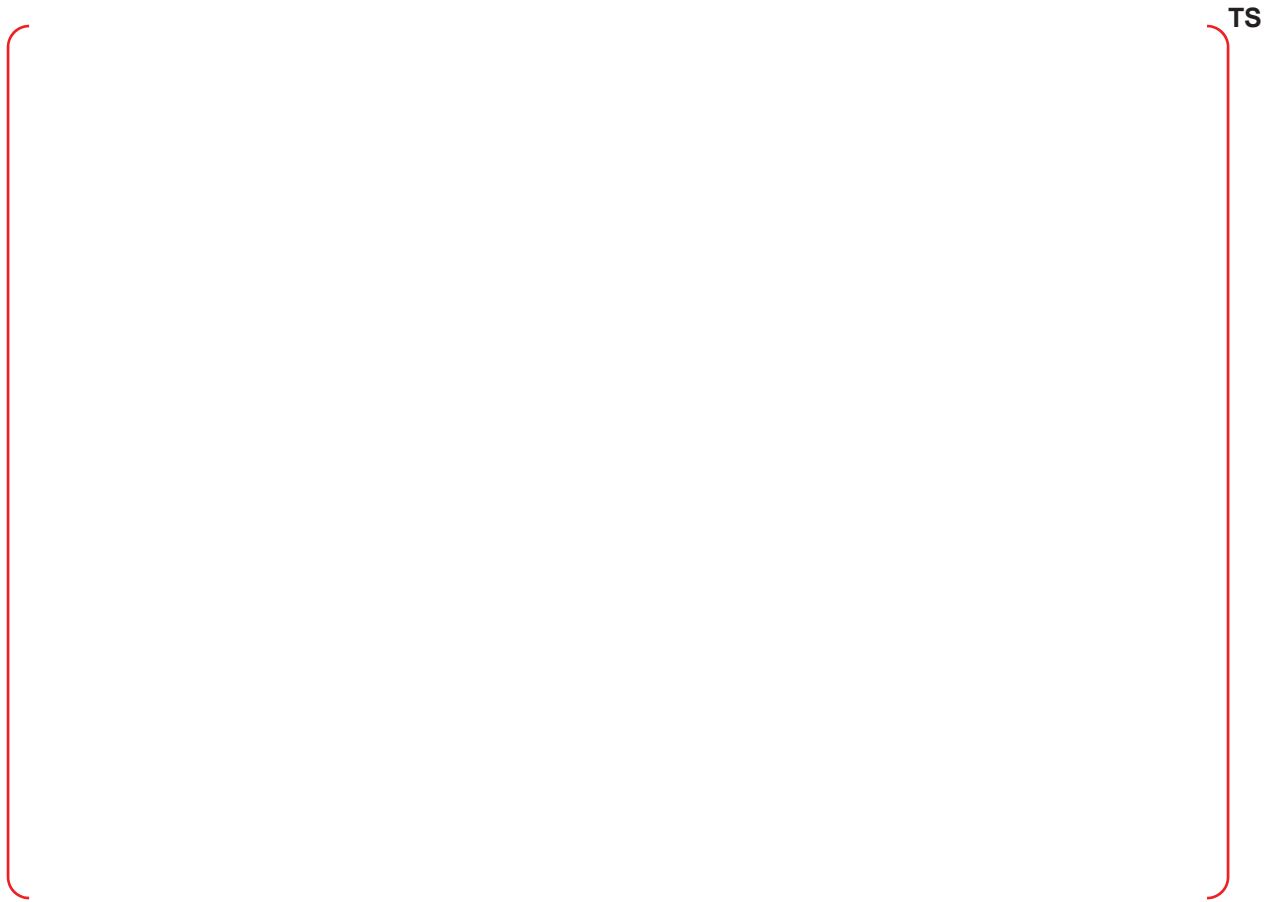


Figure 4-9 SFSR Model – Deep Drop Over a Pedestal (Scenario 3)

REVISED RESPONSE TO REQUEST FOR ADDITIONAL INFORMATION**APR1400 Design Certification****Korea Electric Power Corporation / Korea Hydro & Nuclear Power Co., LTD****Docket No. 52-046**

RAI No.: 287-8272
SRP Section: 09.01.02 – New and Spent Fuel Storage
Application Section: 9.1.2
Date of RAI Issue: 11/02/2015

Question No. 09.01.02-25

1. The 10 CFR Part 50, Appendix A, General Design Criteria (GDC) 1, 2, 4, 5, 63, and 10CFR 52.80 (a) provide the regulatory requirements for the design of the new and spent fuel storage facilities. Standard Review Plan (SRP) Sections 9.1.2 and 3.8.4, Appendix D describes specific SRP acceptance criteria for the review of the fuel racks that are acceptable to meet the relevant requirements of the Commission's regulations identified above. In DCD Tier 2, Section 9.1.2.2.3, "New and Spent Fuel Storage Rack Design", the applicant stated that "The dynamic and stress analyses are performed as described in report APR1400-H-N-NR-14012-P & NP". In the report APR1400-H-N-NR-14012-P, Rev.0, Section 4.5 "Results of Analyses", the applicant provided the results of fuel assembly drop analyses but did not provide the structural assessment of the dropped fuel assemblies due to impact with the rack and the rack baseplate. The staff notes that the applicant in Subsection 3.7.2 of the report provided structural evaluation of the fuel for the lateral impact loads on the fuel assembly due to fuel-to-cell wall impact. The applicant is requested to provide the results of its structural evaluation of the fuel assembly from the mechanical drop accident scenarios described in Section 4.1 of the report.

The applicant is requested to identify any proposed changes to and provide a mark-up of Subsections in the DCD Tier 2 and the report APR1400-H-N-NR-14012-P, Rev.0, as appropriate.

Response – (Rev. 0)

The structural integrity evaluation of new and spent fuel storage rack under the mechanical drop accident scenarios is described in the Section 4.5 of the report APR1400-H-N-NR-14012-P, Mechanical Accident Analysis, includes descriptions of the straight shallow drop and two straight deep drop scenarios. In the "straight shallow" and "straight deep" drop events,

the fuel assembly is treated as a rigid mass with conservative frontal area and total weight (total weight is the sum of fuel assembly and handling tool).

The radiological fuel damage caused by a fuel handling accident is evaluated in accordance with NRC RG 1.183, Appendix B. The radiological consequence for fuel assembly in postulated fuel handling accident is addressed in DCD Tier 2, Section 15.7.4.

Response – (Rev. 1)

Technical report, APR1400-H-N-NR-14012-NP was submitted as Rev. 0 in December, 2014. KHNP responses to RAI 287-8272 were based in part on the Technical Report. Subsequent to issuance of the Technical Report and RAI responses, the NRC provided feedback on both the Technical Report and RAI 287-8272 responses. In response to this NRC feedback, Technical report, APR1400-H-N-NR-14012-NP will be revised (as Rev. 3) to incorporate additional information pertaining to the fuel racks. This RAI revision contains the specific Technical Report revisions relevant to this response and associated DCD changes, where necessary. A summary of the additional information is in the below paragraphs.

Structural Evaluation of the Fuel Assembly from the Mechanical Drop Accident

The postulated fuel handling accident including a drop of fuel assemblies is addressed in the APR1400 Design Control Document, Section 15.7.4.

Impact on DCD

There is no impact on the DCD.

Impact on PRA

There is no impact on the PRA.

Impact on Technical Specifications

There is no impact on the Technical Specifications.

Impact on Technical/Topical/Environmental Reports

APR1400-H-N-NR-14012-P (Rev. 3), Section 4 will be revised as shown in Attachment 1 to this response.

4 MECHANICAL ACCIDENTS ANALYSIS

This chapter presents the structural integrity evaluation for new and spent fuel storage racks for dropped and stuck fuel assembly scenarios. Only the effect of the accident scenarios on the racks is considered. The postulated fuel handling accident including a drop of fuel assemblies is addressed in the APR1400 Design Control Document, Section 15.7.4.

The accident analyses demonstrate that the APR1400 fuel racks meet the acceptance criteria specified in Appendix D of SRP 3.8.4 (Reference 1).

4.1 Description of Mechanical Accidents

The NRC SRP 3.8.4, Appendix D (Reference 1) identifies load combinations for SFSR that are to be evaluated in accordance with ASME Code, Section III, Division 1, Subsection NF. Specifically, a stuck fuel assembly analysis should meet Class 3 Level B service limits, while a dropped fuel assembly analysis should demonstrate that the functional capability of the fuel rack is maintained. A subset of accident scenarios is applied to the NFSR due to their different design and environment (e.g., not underwater, no neutron absorber plates). The pedestal of NFSR is supported by the overlapped intermediate plate and embedment plate on concrete slab as shown in Figure 2-3. The following scenarios have been evaluated:

(1) Straight Shallow Drop (Scenario 1)

In the so-called "straight shallow drop" accident, the fuel assembly and handling tool (total mass = 1,100 kg (2,425 lbm)) are dropped from a height of 0.61 m (2 ft) [or the transport container handling tool (= 214.55 kg (473 lbm)) drops from a height of 5.0 m (196.8 in)] above the top of the SFSR and impacts on a top edge of the rack. The dropping mass is assumed to impact the top edge of the rack. Potential for damage to a neutron absorber plate is evaluated. A schematic of the straight shallow drop is shown as Figure 4-1. The shallow drop accident for the NFSR is not relevant since there is no neutron absorber to damage.

(2) Straight Deep Drop Away from a Pedestal (Scenario 2)

For assessing the impact of a drop on baseplate deformation, drops as far away from the support provided by a pedestal are considered at two locations (a central cell and a peripheral cell at the midpoint of a side) that maximize the distance to the points of support. A fuel assembly along with the handling tool (total mass = 1,100 kg (2,425 lbm)) is dropped from a fuel bottom height of 0.61 m (2 ft) above the racks. The falling assembly is assumed to enter an unoccupied storage cell away from a pedestal (as shown in Figure 4-2) and impact the rack baseplate. This scenario is also evaluated for the NFSR, and analysis for this scenario is the same as done for the SFSR, except speed at impact is higher because the drop does not have the viscous drag associated with falling through water.

(3) Straight Deep Drop Over a Pedestal (Scenario 3)

In this case, the fuel assembly enters a corner storage cell which is above a pedestal (as shown in Figure 4-3). This is most limiting for evaluating the concentrated loading on the concrete underlying the baseplate on which the pedestal rests.

(4) Stuck Fuel Assembly (Scenario 4)

In this scenario, it is assumed that a fuel assembly becomes stuck while being lifted out of an SFSR cell resulting in the lifting force of the crane being applied against the SFSR structure. The fuel hoists are provided with load-measuring devices and interlocks to interrupt hoisting if the load increases above the overload setpoint, as identified in DCD Section 9.1.4.5. A tensile force of 22.2 kN (5,000 lbf) on the

REVISED RESPONSE TO REQUEST FOR ADDITIONAL INFORMATION**APR1400 Design Certification****Korea Electric Power Corporation / Korea Hydro & Nuclear Power Co., LTD****Docket No. 52-046**

RAI No.: 287-8272
SRP Section: 09.01.02 – New and Spent Fuel Storage
Application Section: 9.1.2
Date of RAI Issue: 11/02/2015

Question No. 09.01.02-28

1. The 10 CFR Part 50, Appendix A, General Design Criteria (GDC) 1, 2, 4, 5, 63, and 10CFR 52.80 (a) provide the regulatory requirements for the design of the new and spent fuel storage facilities. Standard Review Plan (SRP) Sections 9.1.2 and 3.8.4, Appendix D describes specific SRP acceptance criteria for the review of the fuel racks that are acceptable to meet the relevant requirements of the Commission's regulations identified above. In DCD Tier 2, Section 9.1.2.2.3, "New and Spent Fuel Storage Rack Design", the applicant stated that "The dynamic and stress analyses are performed as described in report APR1400-H-N-NR-14012-P & NP". In the technical report APR1400-H-N-NR-14012-P, Rev 0, Subsection 3.7.3.3, "Stresses on Welds", the applicant evaluated stresses in cell-to-baseplate and baseplate-to-pedestal welds but did not calculate the base metal shear stress. The safety factor (ratio of allowable to actual shear stress) for the base metal may be lower than that for the weld. This reduction is noted in safety factors in Table 3-13 "Stress Evaluation for Fuel Racks. The staff notes that the safety factor for the cell-to cell weld stress is 5.42 that is reduced to 3.68 for the base metal shear. The applicant is requested to provide the base metal shear stress and corresponding safety factor for the cell-to-baseplate and baseplate-to-pedestal weld connections so the staff can make safety conclusions related to the rack welded connections.

Response – (Rev. 0)

The evaluation results of the base metal shear stress for the cell-to-baseplate and baseplate-to-pedestal weld are as follows:

Region	Type	Calculated Stress, MPa (psi)	Allowable Stress, MPa (psi) ^(*)	Safety Factor (-)
Rack Cell-to-Baseplate	Base Metal Shear	84 (12,183)	118.0 (17,120)	1.41
Baseplate-to-Pedestal		87.7 (12,721)	118.0 (17,120)	1.35

(*) The allowable stress is calculated using 304 material yield strength.

Table 3-13 will be revised to include the base metal shear values.

Response – (Rev. 1)

Technical report, APR1400-H-N-NR-14012-NP was submitted as Rev. 0 in December, 2014. KHNP responses to RAI 287-8272 were based in part on the Technical Report. Subsequent to issuance of the Technical Report and RAI responses, the NRC provided feedback on both the Technical Report and RAI 287-8272 responses. In response to this NRC feedback, Technical report, APR1400-H-N-NR-14012-NP will be revised (as Rev. 3) to incorporate additional information pertaining to the fuel racks. This RAI revision contains the specific Technical Report revisions relevant to this response and associated DCD changes, where necessary. A summary of the additional information is in the below paragraphs.

Cell-to-Baseplate Weld

As given in ASME Code Section III, Subsection NF, for Level A or B conditions, an allowable shear stress of a weld is $0.3 S_u = 136.7 \text{ MPa (19,830 psi)}$ conservatively based on the base metal material. The allowable weld stress may be increased for Level D by a factor of 1.8, giving an allowable of $0.54 S_u = 246.1 \text{ MPa (35,694 psi)}$. Stresses in the cell-to-baseplate welds are determined through the use of a simple conversion factor (ratio) applied to the corresponding stress factor in the adjacent rack material. The conversion factor (ratio) values are developed from consideration of the differences in material thickness and length versus weld throat dimension and length, as follows:

$$\text{Ratio} = [(220 + 2.5) \times 2.5] / (180 \times 2.5 \times 0.707) = 1.75 \text{ (for the SFSRs)}$$

Where,

- Inner cell dimension (220 mm (8.66 in)),
- Cell wall thickness (2.5 mm (0.098 in)),
- Weld length (180 mm (7.09 in)), and
- Weld throat thickness (= $2.5 \times 0.707 = 1.767 \text{ mm (0.069 in)}$) are used.

For the NFSRs, the cell wall thickness and weld thickness are 6.0 mm (0.236 in) and 4.24 mm (0.167 in), respectively. The conversion factor (ratio) for the NFSRs is calculated as 1.54. The highest predicted cell-to-baseplate weld stress is conservatively calculated based on the highest FACT2 for the rack cell region tension stress factor and FACT3 for the rack cell region shear stress factor. The maximum stress factors used do not all occur at the same time instant

and the shear stress factors are the maximum for all load conditions. The total cell-to-baseplate weld stress is calculated by combining the shear stress on the weld with the axial shear stress on the weld by tension stress using the SRSS method. The stress on the weld of cell-to- baseplate is calculated as follows:

1) Shear stress calculation of cell-to-baseplate weld:

$$S_{\text{shear}} = (\text{FACT3}) \times \text{Min.}(0.72 \times S_y \text{ or } 0.42 \times S_u) \times \text{Ratio}$$

Where,

FACT3 : Shear stress factor of cell wall in Table 3-9 of Technical Report, and
 0.72 x S_y or 0.42 x S_u : Allowable stress of cell wall under Level D condition.

2) Axial shear stress calculation of cell-to-baseplate weld:

$$S_{\text{axialshear}} = (\text{FACT2}) \times \text{Min.}(1.2 \times S_y \text{ or } 0.7 \times S_u) \times \text{Ratio}$$

Where,

FACT2 : Tension stress factor of cell wall in Table 3-9 of Technical Report, and
 1.2 x S_y or 0.7 x S_u : Allowable stress of cell wall under Level D condition.

3) The total cell-to-baseplate weld stress:

$$S_{\text{combined}} = \sqrt{S_{\text{shear}}^2 + S_{\text{axialshear}}^2}$$

The calculated stress value is less than the allowable weld stress value of 246.1 MPa (35,694 psi). Therefore, all weld stresses between the cell wall and the baseplate are acceptable.

Baseplate-to-Pedestal Weld

The stress in the baseplate-to-pedestal weld is evaluated using the maximum horizontal pedestal load and the maximum compressive vertical load. The weld stress is derived from simultaneous application of the maximum tensile force obtained from ANSYS and the maximum pedestal friction forces in the horizontal directions. The calculated maximum stress identified in Table 1 is well below the Level D allowable of 246.1 MPa (35,694 psi). Therefore, all weld stresses between baseplate and support pedestal are acceptable.

Table 1 Stress Evaluation for Fuel Racks

Region	Rack	Type	Calculated Stress, MPa (psi)	Allowable Stress, MPa (psi)	Safety Factor (-)
Rack Cell-to-Baseplate	SFSR	Weld	125.4 (18,188)	246.1 (35,694)	1.96
		Base Metal Shear	88.7 (12,865)	106.2 ⁽¹⁾ (15,408)	1.19

Baseplate-to-Pedestal ⁽¹⁾	NFSR	Weld	123.3 (17,885)	246.1 (35,694)	1.99
		Base Metal Shear	87.0 (12,645)	106.2 ⁽¹⁾ (15,408)	1.22
	SFSR	Weld	99.6 (14,443)	246.1 (35,694)	2.47
		Base Metal Shear	70.4 (10,211)	106.2 ⁽¹⁾ (15,408)	1.51

Note:

(1) The allowable stress is calculated using 304 material yield strength.

Impact on DCD

There is no impact on the DCD.

Impact on PRA

There is no impact on the PRA.

Impact on Technical Specifications

There is no impact on the Technical Specifications.

Impact on Technical/Topical/Environmental Reports

APR1400-H-N-NR-14012-NP (Rev. 3), Section 3.7.3.3 and Table 3-12 will be revised as shown in Attachment 1 to this response.

time. In particular, maximum values for the stress factors which are defined in Section 3.2.2 can be determined for each pedestal in each rack. Using this information, the structural integrity of the pedestals can be assessed.

The net section maximum bending moments and shear forces can also be determined at the bottom of the rack structure. From these loads, the stress factors for the NFSRs and the SFSR cell walls just above the baseplate can be also determined in the rack. Because they are at the end of fuel rack beam, these locations are the most heavily loaded net sections in the structure so that satisfaction of the stress factor criteria at these locations ensures that the overall structural criteria set forth in Section 3.2 are met.

As shown in Table 3-9:

- Maximum pedestal stress factors for the NFSRs and SFSRs are less than the allowable of 1.0.
- Maximum cell wall stress factors for the NFSRs and SFSRs are less than the allowable of 1.0.

Therefore, the rack cells and the support pedestals are able to maintain their structural integrity under the worst loading conditions.

3.7.3.2 Pedestal Thread Stress Evaluation

The integrity for the support pedestal thread is evaluated using the maximum load on the support pedestal in vertical direction as shown in Table 3-7. Using this load, the maximum shear stress of thread in the engagement region is calculated. The allowable shear stress of SA-240 Type 304L material for Level D condition is the lesser of $0.72 S_y = 106.2 \text{ MPa}$ (15,408 psi) or $0.42 S_u = 191.4 \text{ MPa}$ (27,762 psi) as stated on Section 3.2.2. Therefore, the former criteria controls, and the calculated shear stress of pedestal thread is acceptable, as shown on Table 3-13.

3.7.3.3 Stresses on Welds

Weld locations of the NFSRs subjected to SSE loading are at the bottom of the rack at the cell-to-baseplate connection, and at the top of the pedestal support at the baseplate connection.

SFSR welds are at the bottom of the rack at the cell-to-baseplate connection, at the top of the pedestal support at the baseplate connection, and at cell-to-cell connections. The maximum values of resultant loads are used to evaluate the structural integrity of these welds. The calculated stresses on fuel rack welds are summarized in Table 3-12.

(1) Cell-to-Baseplate Weld

As given in ASME Code Section III, Subsection NF, for Level A or B conditions, an allowable shear stress of a weld is $0.3 S_u = 136.7 \text{ MPa}$ (19,830 psi) conservatively based on the base metal material. As stated in Section 3.2.2.3, the allowable weld stress may be increased for Level D by a factor of 1.8, giving an allowable of $0.54 S_u = 246.1 \text{ MPa}$ (35,694 psi).

Stresses in the cell-to-baseplate welds are determined through the use of a simple conversion factor (ratio) applied to the corresponding stress factor in the adjacent rack material. This stress factor is discussed in Section 3.2.3, and given in Table 3-9. The conversion factor (ratio) values are developed from consideration of the differences in material thickness and length versus weld throat dimension and length, as follows:

$$\text{Ratio} = [(220 + 2.5) \times 2.5] / (180 \times 2.5 \times 0.707) = 1.75 \text{ (for the SFSRs)}$$

Where,

Inner cell dimension (220 mm (8.66 in)),

Cell wall thickness (2.5 mm (0.098 in)),
Weld length (180 mm (7.09 in)), and
Weld throat thickness ($= 2.5 \times 0.707 = 1.767$ mm (0.069 in)) are
used.

For the NFSRs, the cell wall thickness and weld thickness are 6.0 mm (0.236 in) and 4.24 mm (0.167 in), respectively. The conversion factor (ratio) for the NFSRs is calculated as 1.54.

The highest predicted cell-to-baseplate weld stress is conservatively calculated based on the highest FACT2 for the rack cell region tension stress factor and FACT3 for the rack cell region shear stress factor. The maximum stress factors used do not all occur at the same time instant and the shear stress factors are the maximum for all load conditions. The total cell-to-baseplate weld stress is calculated by combining the shear stress on the weld with the axial shear stress on the weld by tension stress using the SRSS method. The stress on the weld of cell-to- baseplate is calculated as follows:

1) Shear stress calculation of cell-to-baseplate weld:

$$S_{\text{shear}} = (\text{FACT3}) \times \text{Min.}(0.72 \times S_y \text{ or } 0.42 \times S_u) \times \text{Ratio}$$

Where, FACT3 : Shear stress factor of cell wall in Table 3-9, and

0.72 $\times S_y$ or 0.42 $\times S_u$: Allowable stress of cell wall under Level D condition.

2) Axial shear stress calculation of cell-to-baseplate weld:

$$S_{\text{axialshear}} = (\text{FACT2}) \times \text{Min.}(1.2 \times S_y \text{ or } 0.7 \times S_u) \times \text{Ratio}$$

Where, FACT2 : Tension stress factor of cell wall in Table 3-9, and

1.2 $\times S_y$ or 0.7 $\times S_u$: Allowable stress of cell wall under Level D condition.

3) The total cell-to-baseplate weld stress:

$$S_{\text{combined}} = \sqrt{S_{\text{shear}}^2 + S_{\text{axialshear}}^2}$$

The calculated stress value is less than the allowable weld stress value of 246.1 MPa (35,694 psi). Therefore, all weld stresses between the cell wall and the baseplate are acceptable.

(2) Baseplate-to-Pedestal Weld

The stress in the baseplate-to-pedestal weld is evaluated using the maximum horizontal pedestal load and the maximum compressive vertical load. The weld stress is derived from simultaneous application of the maximum tensile force obtained from ANSYS and the maximum pedestal friction forces in the horizontal directions in Table 3-7. The calculated maximum stress identified in Table 3-12 is well below the Level D allowable of 246.1 MPa (35,694 psi). Therefore, all weld stresses between baseplate and support pedestal are acceptable.

(3) Cell-to-Cell Weld

Cell-to-cell connections are a series of connecting welds along the cell height. Stresses in the SFSR cell-to-cell welds develop due to fuel assembly impacts with the cell wall. Weld stress is calculated based on the maximum fuel-to-cell wall impact load and shear stress, which is obtained by using the cell wall shear stress coefficient under Level D conditions from the dynamic analysis results. These weld stresses are conservatively considered by assuming that fuel assemblies in adjacent cells are moving out of phase with one another so that impact loads in two adjacent cells are in opposite directions and are applied simultaneously. This load application tends to separate the two cells from each other at the weld.

Table 3-11 Stress Evaluation for Fuel Assembly

Location	Category	Calculated Value	Allowable Limit	Safety Factor (-)
Fuel spacer grid	Buckling Load	19.9 kN (4,481 lbf)	31.3 kN (7,045 lbf)	1.57
Fuel rod cladding	Bending Stress	65.2 MPa (9,449 psi)	540.3 MPa (78,365 psi)	8.3
	Yield Strain	0.0007 in/in	0.0058 in/in	8.3

Table 3-12 Stress Evaluation for Fuel Racks

Region	Rack	Type	Calculated Stress, MPa (psi)	Allowable Stress, MPa (psi)	Safety Factor (-)
Rack Cell-to-Baseplate	SFSR	Weld	125.4 (18,188)	246.1 (35,694)	1.96
		Base Metal Shear	88.7 (12,865)	106.2 ⁽¹⁾ (15,408)	1.19
Baseplate-to-Pedestal ⁽¹⁾	NFSR	Weld	123.3 (17,885)	246.1 (35,694)	1.99
		Base Metal Shear	87.0 (12,645)	106.2 ⁽¹⁾ (15,408)	1.22
	SFSR	Weld	99.6 (14,443)	246.1 (35,694)	2.47
		Base Metal Shear	70.4 (10,211)	106.2 ⁽¹⁾ (15,408)	1.51
Cell-to-Cell	SFSR	Weld	66.2 (9,603)	246.1 (35,694)	3.72
		Base Metal Shear	46.8 (6,789)	106.2 ⁽¹⁾ (15,408)	2.27

Note:

(1) The allowable stress is calculated using 304 material yield strength.

REVISED RESPONSE TO REQUEST FOR ADDITIONAL INFORMATION**APR1400 Design Certification****Korea Electric Power Corporation / Korea Hydro & Nuclear Power Co., LTD****Docket No. 52-046**

RAI No.: 287-8272
SRP Section: 09.01.02 – New and Spent Fuel Storage
Application Section: 9.1.2
Date of RAI Issue: 11/02/2015

Question No. 09.01.02-29

1. The 10 CFR Part 50, Appendix A, General Design Criteria (GDC) 1, 2, 4, 5, 63, and 10CFR 52.80 (a) provide the regulatory requirements for the design of the new and spent fuel storage facilities. Standard Review Plan (SRP) Sections 9.1.2 and 3.8.4, Appendix D describes specific SRP acceptance criteria for the review of the fuel racks that are acceptable to meet the relevant requirements of the Commission's regulations identified above. In DCD Tier 2, Section 9.1.2.2.3, "New and Spent Fuel Storage Rack Design", the applicant stated that "The dynamic and stress analyses are performed as described in report APR1400-H-N-NR-14012-P & NP". In the technical report APR1400-H-N-NR-14012-P, Rev 0, Subsection 3.7.3.3, "Stresses on Welds", the applicant evaluated stresses in cell-to-cell welds. An underlying assumption in the modeling of the rack as a single beam using the overall bending stiffness of the entire rack is that the cell-to-cell welds are intact and can carry the internal forces necessary to validate this assumption. This is not addressed in the report. The applicant is requested to provide a quantitative evaluation demonstrating that this loading in conjunction with the other loadings discussed in the report does not create an overstress condition in the cell-to-cell welds.

Response – Rev. 0

The cell-to-cell weld stress is calculated based on the maximum fuel-to-cell impact load and the cell wall shear stress. Overstress in the cell-to-cell weld can be caused by using this load in conjunction with other loads, which include cell wall tensile and bending loads. The tensile and bending stress on the cell wall is calculated by multiplying the tensile or bending allowable stress under Level D conditions and the cell wall stress coefficient, $FACT2 = 0.314$, per Table 3-12 of the report APR1400-H-N-NR-14012-P. The cell-to-cell weld evaluation results including the cell wall tensile and bending stress are as shown below:

Region	Type	Calculated Stress, MPa (psi)	Allowable Stress, MPa (psi)	Safety Factor (-)
Cell-to-Cell	Weld	71.8 (10,408)	246.1 (35,694)	3.43
	Base Metal Shear	50.7 (7,358)	118.0 (17,120)	3.49

Therefore, the cell-to-cell weld does not create an overstress condition.

Response – Rev. 1

Technical report, APR1400-H-N-NR-14012-NP was submitted as Rev. 0 in December, 2014. KHNP responses to RAI 287-8272 were based in part on the Technical Report. Subsequent to issuance of the Technical Report and RAI responses, the NRC provided feedback on both the Technical Report and RAI 287-8272 responses. In response to this NRC feedback, Technical report, APR1400-H-N-NR-14012-NP will be revised (as Rev. 3) to incorporate additional information pertaining to the fuel racks. This RAI revision contains the specific Technical Report revisions relevant to this response and associated DCD changes, where necessary. A summary of the additional information is in the below paragraphs.

Cell-to-Cell Weld

Cell-to-cell connections are a series of connecting welds along the cell height. Stresses in the SFSR cell-to-cell welds develop due to fuel assembly impacts with the cell wall. Weld stress is calculated based on the maximum fuel-to-cell wall impact load and shear stress, which is obtained by using the cell wall shear stress coefficient under Level D conditions from the dynamic analysis results. These weld stresses are conservatively considered by assuming that fuel assemblies in adjacent cells are moving out of phase with one another so that impact loads in two adjacent cells are in opposite directions and are applied simultaneously. This load application tends to separate the two cells from each other at the weld.

Stress in the cell-to-cell weld is combined by the square root of the sum of the squares (SRSS) method for the shear stress due to horizontal load acting on rack and the shear stress due to impact load of rack fuel-to-cell wall, and the stress due to cell wall axial shear load.

The shear stress on the cell wall is calculated by multiplying shear allowable stress under Level D conditions and the cell wall stress coefficient, FACT3 from Table 3-9 of Technical report, APR1400-H-N-NR-14012-P. The total shear stress acting on the weld is calculated by combining the shear stress acting on cell wall with the fuel-to-cell impact stress using the SRSS method. The calculated stresses of the cell-to-cell weld and the base metal shear are well below the allowable.

In summary, the stress on the cell-to-cell weld is calculated using the following formulas.

- 1) Stress calculation of base metal adjacent to weld due to impact load:

$$S_{impact} = \frac{F_{impact}}{A_{weld}}$$

Where,

F_{impact} : Maximum fuel assembly to cell impact load in Table 3-8 of Technical report, and
 A_{weld} : Total area of weld.

2) Shear stress calculation of the cell wall:

$$S_{shear} = FACT3 * V_{sse}$$

Where,

FACT3 : Shear stress factor of cell wall in Table 3-9 of Technical report, and
 V_{sse} : Allowable stress of cell wall under Level D condition.

3) Axial shear stress calculation of the cell wall:

$$S_{a_shear} = \frac{F_{a_shear}}{A_{weld}}$$

Where,

F_{a_shear} : Axial shear force of cell wall,
 $= FACT2 * V_{sse_axial} * A_{cell}$

FACT2 : Tensile or bending stress factor of cell wall in Table 3-9 of Technical report, and,
 V_{sse_axial} : Allowable stress of cell wall under Level D condition, and
 A_{cell} : Area of cell.

4) Total shear stress calculation acting at cell-to-cell weld:

$$S_{combined} = \sqrt{S_{impact}^2 + S_{shear}^2 + S_{a_shear}^2}$$

The cell-to-cell weld evaluation results are as shown below:

Region	Type	Calculated Stress, MPa (psi)	Allowable Stress, MPa (psi)	Safety Factor (-)
Cell-to-Cell	Weld	66.2 (9,603)	246.1 (35,694)	3.72
	Base Metal Shear	46.8 (6,789)	106.2 (15,408)	2.27

Impact on DCD

There is no impact on the DCD.

Impact on PRA

There is no impact on the PRA.

Impact on Technical Specifications

There is no impact on the Technical Specifications.

Impact on Technical/Topical/Environmental Reports

[APR1400-H-N-NR-14012-NP \(Rev. 3\)](#), Section 3.7.3.3 will be revised as shown in Attachment 1 to this response.

Cell wall thickness (2.5 mm (0.098 in)),
Weld length (180 mm (7.09 in)), and
Weld throat thickness (= 2.5 x 0.707 = 1.767 mm (0.069 in)) are used.

For the NFSRs, the cell wall thickness and weld thickness are 6.0 mm (0.236 in) and 4.24 mm (0.167 in), respectively. The conversion factor (ratio) for the NFSRs is calculated as 1.54.

The highest predicted cell-to-baseplate weld stress is conservatively calculated based on the highest FACT2 for the rack cell region tension stress factor and FACT3 for the rack cell region shear stress factor. The maximum stress factors used do not all occur at the same time instant and the shear stress factors are the maximum for all load conditions. The total cell-to-baseplate weld stress is calculated by combining the shear stress on the weld with the axial shear stress on the weld by tension stress using the SRSS method. The stress on the weld of cell-to- baseplate is calculated as follows:

1) Shear stress calculation of cell-to-baseplate weld:

$$S_{\text{shear}} = (\text{FACT3}) \times \text{Min.}(0.72 \times S_y \text{ or } 0.42 \times S_u) \times \text{Ratio}$$

Where, FACT3 : Shear stress factor of cell wall in Table 3-9, and

0.72 x S_y or 0.42 x S_u : Allowable stress of cell wall under Level D condition.

2) Axial shear stress calculation of cell-to-baseplate weld:

$$S_{\text{axialshear}} = (\text{FACT2}) \times \text{Min.}(1.2 \times S_y \text{ or } 0.7 \times S_u) \times \text{Ratio}$$

Where, FACT2 : Tension stress factor of cell wall in Table 3-9, and

1.2 x S_y or 0.7 x S_u : Allowable stress of cell wall under Level D condition.

3) The total cell-to-baseplate weld stress:

$$S_{\text{combined}} = \sqrt{S_{\text{shear}}^2 + S_{\text{axialshear}}^2}$$

The calculated stress value is less than the allowable weld stress value of 246.1 MPa (35,694 psi). Therefore, all weld stresses between the cell wall and the baseplate are acceptable.

(2) Baseplate-to-Pedestal Weld

The stress in the baseplate-to-pedestal weld is evaluated using the maximum horizontal pedestal load and the maximum compressive vertical load. The weld stress is derived from simultaneous application of the maximum tensile force obtained from ANSYS and the maximum pedestal friction forces in the horizontal directions in Table 3-7. The calculated maximum stress identified in Table 3-12 is well below the Level D allowable of 246.1 MPa (35,694 psi). Therefore, all weld stresses between baseplate and support pedestal are acceptable.

(3) Cell-to-Cell Weld

Cell-to-cell connections are a series of connecting welds along the cell height. Stresses in the SF SR cell-to-cell welds develop due to fuel assembly impacts with the cell wall. Weld stress is calculated based on the maximum fuel-to-cell wall impact load and shear stress, which is obtained by using the cell wall shear stress coefficient under Level D conditions from the dynamic analysis results. These weld stresses are conservatively considered by assuming that fuel assemblies in adjacent cells are moving out of phase with one another so that impact loads in two adjacent cells are in opposite directions and are applied simultaneously. This load application tends to separate the two cells from each other at the weld.

RAI 287-8272 - Question 09.01.02-29_Rev.1

Stress in the cell-to-cell weld is combined by the square root of the sum of the squares (SRSS) method for the shear stress due to horizontal load acting on rack and the shear stress due to impact load of rack fuel-to-cell wall, and the stress due to cell wall axial shear load.

The maximum fuel-to-cell wall impact load is taken from Table 3-8. The shear stress on the cell wall is calculated by multiplying shear allowable stress under Level D conditions and the cell wall stress coefficient, FACT3 from Table 3-9. The total shear stress acting on the weld is calculated by combining the shear stress acting on cell wall with the fuel-to-cell impact stress using the SRSS method. The calculated stresses of the cell-to-cell weld and the base metal shear are well below the allowable, and the results are summarized in Table 3-12.

Figure 3-19 shows a free-body diagram explaining how the loads were transferred and used to evaluate the cell-to-cell welds.

In summary, the stress on the cell-to-cell weld is calculated using the following formulas as described in Reference 17.

1) Stress calculation of base metal adjacent to weld due to impact load:

$$S_{impact} = \frac{F_{impact}}{A_{weld}}$$

Where,

F_{impact} : Maximum fuel assembly to cell impact load in Table 3-8,
and A_{weld} : Total area of weld.

2) Shear stress calculation of the cell wall:

$$S_{shear} = FACT3 * V_{sse}$$

Where, FACT3 : Shear stress factor of cell wall in Table 3-9, and V_{sse} :
Allowable stress of cell wall under Level D condition.

3) Axial shear stress calculation of the cell wall:

$$S_{a_shear} = \frac{F_{a_shear}}{A_{weld}}$$

Where,

F_{a_shear} : Axial shear force of cell wall,
= $FACT2 * V_{sse_axial} * A_{cell}$

FACT2 : Tensile or bending stress factor of cell wall in Table 3-9,
 V_{sse_axial} : Allowable stress of cell wall under Level D condition,
and A_{cell} : Area of cell.

4) Total shear stress calculation acting at cell-to-cell weld:

$$S_{combined} = \sqrt{S_{impact}^2 + S_{shear}^2 + S_{a_shear}^2}$$

3.7.3.4 Stress Evaluation of Stud Bolt for NFSR

The integrity for the stud bolt is evaluated for the maximum loads on NFSR module. Detailed calculation is provided in Appendix F (Reference 17). Stud bolt stress is evaluated against the criteria for Level D. The calculated stresses of stud bolt are well below the allowable, and the results are summarized in Table 3-14.

REVISED RESPONSE TO REQUEST FOR ADDITIONAL INFORMATION**APR1400 Design Certification****Korea Electric Power Corporation / Korea Hydro & Nuclear Power Co., LTD****Docket No. 52-046**

RAI No.: 287-8272

SRP Section: 09.01.02 – New and Spent Fuel Storage

Application Section: 9.1.2

Date of RAI Issue: 11/02/2015

Question No. 09.01.02-30

1. The 10 CFR Part 50, Appendix A, General Design Criteria (GDC) 1, 2, 4, 5, 63, and 10CFR 52.80 (a) provide the regulatory requirements for the design of the new and spent fuel storage facilities. Standard Review Plan (SRP) Sections 9.1.2 and 3.8.4, Appendix D describes specific SRP acceptance criteria for the review of the fuel racks that are acceptable to meet the relevant requirements of the Commission's regulations identified above. SRP 3.8.4 Appendix D I (5) states that "Details of the mathematical model, including a description of how the important parameters are obtained, should be provided". In DCD Tier 2, Section 9.1.2.2.3, "New and Spent Fuel Storage Rack Design", the applicant stated that "The dynamic and stress analyses are performed as described in report APR1400-H-NNR-14012-P & NP". In the technical report APR1400-H-N-NR-14012-P, Rev 0, Subsection 3.1.2.2, "Details of Rack and Fuel Assembly" the staff finds that the information of the rack and fuel assembly mathematical model and the computer program used for the nonlinear seismic analysis is insufficient. The applicant is requested to provide the following additional information so that the staff can perform its safety evaluation of the seismic analysis of the rack and fuel assembly.

a. The applicant stated that "There are three nodes for rack cells and fuel assemblies". The applicant did not provide any technical basis to show that the three node model of the fuel assembly adequately represents the dynamic characteristics of the fuel assembly. The applicant is requested to provide the fuel frequencies of the three lumped mass fuel model along with a comparison with frequency of the fuel assuming the fuel assembly as a simply supported beam, and with any physical test measurements of a PWR fuel assembly.

b. The applicant stated that "All the fuel assemblies in each storage rack module are modeled as one beam of which the mass equals the sum of the masses of all the fuel assemblies in a rack". The applicant is requested to discuss and provide the details of how the stiffness properties of the beam that represents all the fuel assemblies in a rack are calculated to capture the dynamic characteristics of the free standing racks under seismic loading. The

applicant is also requested to provide the assumptions and computational details of the contact stiffness between the fuel and the rack's cell wall that is used to predict the maximum fuel-to-cell impact loads.

c. The applicant used ANSYS, Version 10 finite element program for the nonlinear dynamic analysis. The applicant is requested to provide reference to operating or new nuclear power plants free standing fuel racks that have been licensed using ANSYS Version 10. The applicant is also requested to provide the details of benchmarking, validation and verification of ANSYS computer program for the specific application to the nonlinear seismic analysis of the free standing submerged fuel rack structures that includes nonlinear springs.

The applicant is requested to identify any proposed changes to and provide a mark-up of Subsections in the DCD Tier 2 and the report APR1400-H-N-NR-14012-P, Rev.0, as appropriate.

Response – (Rev. 0)

- a. The mass (M) and the flexural rigidity (EI) values of a PWR fuel assembly are applied to the fuel assembly model for the fuel rack dynamic and stress analyses to reflect the dynamic characteristics of the PWR fuel assembly. These values are provided by the supplier of the PWR fuel assembly. Therefore, the dynamic analysis of rack do not use the frequencies of the three lumped mass fuel model. All the fuel assemblies in each storage rack are modeled as an individual distributed mass and beam elements. All fuel assemblies move simultaneously in one direction. The assumption included in this model brings about larger impact on the rack module than the actual case and results in the conservative loads to the storage rack.
- b. The report APR1400-H-N-NR-14012-P, Section 3.2.1.4 (1), explains the contact stiffness between the fuel assembly and rack cell. A fuel assembly within the rack is modeled as three lumped masses equally spaced over the height of the rack. The node of the fuel assembly beam model and the node of rack beam model is connected using CONTAC52 element. The stiffness of the fuel assembly only is applied in consideration of conservatism.
- c. The benchmarking of the ANSYS computer program for the specific application to the nonlinear seismic analysis will be performed by comparing the ANSYS calculated results to the results of a previously approved fuel rack analysis. The rack seismic analysis of Shin-Kori Units 1 and 2 (2005) was performed by Doosan using Holtec's program, DYNARACK. The results of benchmarking of the ANSYS computer program will be submitted by April 30, 2016.

Response – (Rev. 1)

- a. The mass (M) and the flexural rigidity (EI) values of a PWR fuel assembly are applied to the fuel assembly model for the fuel rack dynamic and stress analyses to reflect the dynamic characteristics of the PWR fuel assembly. These values are provided by the supplier of the PWR fuel assembly. Therefore, the dynamic analysis of rack do not use the frequencies of the three lumped mass fuel model. All the fuel assemblies in each storage

rack are modeled as an individual distributed mass and beam elements. All fuel assemblies move simultaneously in one direction. The assumption included in this model brings about larger impact on the rack module than the actual case and results in the conservative loads to the storage rack.

- b. The report APR1400-H-N-NR-14012-P, Section 3.2.1.4 (1), explains the contact stiffness between the fuel assembly and rack cell. A fuel assembly within the rack is modeled as three lumped masses equally spaced over the height of the rack. The node of the fuel assembly beam model and the node of rack beam model is connected using CONTACT52 element. The stiffness of the fuel assembly only is applied in consideration of conservatism.
- c. The benchmarking of the ANSYS computer program for the specific application to the nonlinear seismic analysis is performed by comparing the ANSYS calculated results with the DYNARACK analysis tests. The rack seismic analysis of Shin-Kori Nuclear Power Plant Units 1 and 2 (SKN 1&2) was performed using the DYNARACK program. Benchmark test results for nonlinear seismic analysis using the ANSYS and the DYNARACK program are shown in attachment.

Response – (Rev. 2)

Technical report, APR1400-H-N-NR-14012-NP was submitted as Rev. 0 in December, 2014. KHNP responses to RAI 287-8272 were based in part on the Technical Report. Subsequent to issuance of the Technical Report and RAI responses, the NRC provided feedback on both the Technical Report and RAI 287-8272 responses. In response to this NRC feedback, Technical report, APR1400-H-N-NR-14012-NP will be revised (as Rev. 3) to incorporate additional information pertaining to the fuel racks. This RAI revision contains the specific Technical Report revisions relevant to this response and associated DCD changes, where necessary. A summary of the additional information is in the below paragraphs.

Details for Rack and Fuel Assembly Model

The NFSR and fuel assembly model are of a single rack and includes 3-D elastic beam elements (ANSYS BEAM4) and lumped mass elements (ANSYS MASS21) with properties derived from the dynamic characteristics of the detailed 3-D shell model of the NFSR. Effective structural properties for the dynamic model are determined from the natural frequencies and mode shapes of the detailed model. Vertical portions of the NFSR cells and fuel assemblies are each represented by five nodes. Nodes are located at the rack baseplate, $\frac{1}{4} H$, $\frac{1}{2} H$, $\frac{3}{4} H$, and H (where H is the rack height measured above the baseplate). Each rack node has six degrees of freedom (three translations and three rotations) and a lumped mass associated with it. The nodes for the rack and the fuel assembly are connected by contact elements (ANSYS CONTACT52) in the horizontal direction. There is a single contact element in the vertical direction between the fuel assembly bottom node and the baseplate node.

The SFSR model is similar to the NFSR model and is composed of elastic beam elements and lumped mass elements with properties derived from the dynamic characteristics of the

detailed 3-D shell model of the SFSR. All the fuel assemblies in each storage rack module are modeled as one beam of which the mass equals the sum of the masses of all the fuel assemblies in a rack module. Because the fuel assemblies in a rack module are modeled together, all fuel assemblies move simultaneously in one direction. This assumption results in larger impact forces on the rack module than the actual case and results in conservative loads on the storage rack. Because the fuel assembly is modeled with five nodes, the calculated impact loads on the nodes will be larger than the actual value because the fuel assembly actually has eleven spacer grids. The maximum fuel assembly grid horizontal impact load is determined by dividing the maximum impact load at each node by the number of grids associated with that node (2.75 for Nodes 10, 11, and 12, and 1.375 for Nodes 9 and 13). Lumped masses of the rack and fuel assemblies are distributed among the five nodes for spent fuel storage rack cells and fuel assemblies as shown in the table below.

Node No.		Location	Total Mass Distribution
Rack	Fuel Assembly		
13	18	Top of Rack	12.5 %
12	17	3/4 Height	25 %
11	16	1/2 Height	25 %
10	15	1/4 Height	25 %
9	14	Bottom (Baseplate) of Rack	12.5 %

Stiffness of Model for Fuel Assembly-to-Cell Wall

Each node of the fuel assembly beam and the corresponding node of the rack beam is connected using a contact element in order to represent impact between the fuel assembly and the rack cell wall. The normal direction stiffness of this element is calculated assuming a series spring connection of the stiffness of the fuel assembly spacer grid and the local stiffness of the cell in the horizontal direction. To be conservative, the cell wall local stiffness is neglected. The fuel assembly/rack cell contact element has a local stiffness (K_i) to account for impact phenomena of the fuel assembly-to-cell wall. The grid stiffness for a fuel assembly beam is multiplied by the number of fuel assemblies assumed to be in the rack. The stiffness of fuel assembly grid is applied by dividing the total grid stiffness at each node by number of grid associated with node ($K_i/4$ for Nodes 15, 16, and 17, and $K_i/8$ for Nodes 14 and 18).

Natural Frequencies

The dynamic analysis models for the NFSR and SFSRs are generated using simplified beam elements. Each simplified beam model is developed to have dynamic characteristics (1st and 2nd mode of natural frequency and mode shapes) similar to the detailed finite element model. Appendix H of Reference 1 documents the comparison of the simplified and detailed three-dimensional models.

The fundamental frequencies of the NFSR are above 20 Hz and of the SFSR are above 30 Hz.

The range of frequencies considered is from 1 to 100 Hz according to the floor response spectra of design specification (Reference 2).

ANSYS

A benchmarking study (Reference 3) was performed to demonstrate that ANSYS Version 15.0 is an acceptable computer code for the seismic analysis of the SFSR and NFSR. While the SRP Section 3.8.1 Subsection II.4.F states that meeting any one of the following methods is sufficient to validate computer programs used for design analysis, the benchmarking study addressed all three:

- 1) The computer program is recognized in the public domain and has had sufficient history of use to justify its applicability and validity without further demonstration.
- 2) The computer program's solutions to a series of test problems have been demonstrated to be substantially identical to those obtained from classical solutions or from accepted experimental tests or to analytical results published in technical literature. The test problems should be demonstrated to be similar to or within the range of applicability of the classical problems analyzed to justify acceptance of the program.
- 3) The computer program's solutions to a series of test problems have been demonstrated to be substantially identical to those obtained by a similar and independently written and recognized program in the public domain. The test problems should be demonstrated to be similar to or within the range of applicability of the problems analyzed by the public domain computer program.

ANSYS has been used in the nuclear energy industry for nearly 40 years. The ANSYS software is developed within an ISO 9001 quality program that meets both ASME NQA-1 and 10 CFR 50 Appendix B. ANSYS software has previously been accepted by the NRC for SFSR seismic structural analysis.

Five test cases were run with ANSYS Version 15.0 to provide a comparison of ANSYS results to analytical results published in technical literature. These test cases exercised the ANSYS elements (MASS21, COMBIN14, CONTAC52, BEAM4, and MATRIX27) and features (direct integration time history, mass, spring, friction, impact and hydrodynamic coupling) used for the ARP1400 fuel rack seismic analysis. The five test cases involved coulomb friction, a two degree of freedom system with inertial coupling, mass impact on a beam, mass impact on a flexible surface, and the Fritz methodology for modeling hydrodynamic mass. The results of these five test problems compared very well to the published analytical results.

To further validate the use of ANSYS for APR1400 fuel rack seismic analysis, a single SFSR was analyzed with both ANSYS and LS-DYNA for five different sets of acceleration time histories. ANSYS is an implicit finite element code used for structural analysis with the capability to perform both static and dynamic simulations, while LS-DYNA is an explicit finite element code used for transient analysis. The results showed reasonable agreement, considering the highly non-linear nature of the response of the free-standing racks to a seismic base excitation. Maximum forces for design purposes were comparable between the two analyses.

References:

1. Doosan, "Structural and Seismic Analysis Report for New and Spent Fuel Storage Racks," N14014-224CN-0001, Rev.3, Aug. 2017(Doosan Proprietary).

-
2. KEPCO Engineering & Construction Co. Inc., KEPCO E&C Job No. 11E47, 1-423-N462-003, Rev. 2, "Design Specification for Fuel Storage Rack," October 2016.
 3. MPR, "APR1400 Fuel Rack Dynamic Analysis Benchmarking," 0938-0006-RPT-001, Rev. 0, October 2016 (Doosan Proprietary).
-

Impact on DCD

There is no impact on the DCD.

Impact on PRA

There is no impact on the PRA.

Impact on Technical Specifications

There is no impact on the Technical Specifications.

Impact on Technical/Topical/Environmental Reports

APR1400-H-N-NR-14012-NP (Rev. 3), Sections 3.1.2.2, 3.1.2.4, 3.1.2.7, 3.5.1, and 3.5 will be revised as shown in Attachment 1 to this response.

3.1.2.2 Details for Rack and Fuel Assembly Model

The sections below provide details on the rack and fuel assembly modeling.

(1) New Fuel Storage Rack Model

The dynamic analysis model for the NFSR and fuel assemblies are shown in Figure 3-1. The NFSR and fuel assembly model are of a single rack and includes 3-D elastic beam elements (ANSYS BEAM4) and lumped mass elements (ANSYS MASS21) with properties derived from the dynamic characteristics of the detailed 3-D shell model of the NFSR. Effective structural properties for the dynamic model are determined from the natural frequencies and mode shapes of the detailed model (see Section 3.1.2.7). Details of effective structural properties for fuel racks are shown in Appendix H of Reference 17. Structural properties (i.e. Young's modulus and flexural rigidity) for fuel assemblies are shown in Table 3-3.

Vertical portions of the NFSR cells and fuel assemblies are each represented by five nodes. Nodes are located at the rack baseplate, $\frac{1}{4} H$, $\frac{1}{2} H$, $\frac{3}{4} H$, and H (where H is the rack height measured above the baseplate). Each rack node has six degrees of freedom (three translations and three rotations) and a lumped mass associated with it. The nodes for the rack and the fuel assembly are connected by contact elements (ANSYS CONTAC52) in the horizontal direction. There is a single contact element in the vertical direction between the fuel assembly bottom node and the baseplate node.

Lumped masses of the NFSR and fuel assemblies are distributed among the five nodes for rack cells and fuel assemblies as shown in the table below:

Node No. (Figure 3-1)		Location	Total Mass Distribution
Rack	Fuel Assembly		
13	18	Top of Rack	12.5 %
12	17	3/4 Height	25 %
11	16	1/2 Height	25 %
10	15	1/4 Height	25 %
9	14	Bottom (Baseplate) of Rack	12.5 %

(2) Spent Fuel Storage Rack Model

To model the interaction among the multiple SFSRs, the WPMR shown in Figure 3-3 is comprised of a dynamic analysis model for individual SFSRs, as shown in Figure 3-2. This model is similar to the NFSR model and is composed of elastic beam elements and lumped mass elements with properties derived from the dynamic characteristics of the detailed 3-D shell model of the SFSR. An underlying assumption in the modeling of the rack as a single beam using the overall bending stiffness of the entire rack is that the cell-to-cell welds remain intact and can carry the internal forces. This assumption is confirmed by structural evaluation of the welds (see Section 3.7.3.3).

Effective structural properties for the dynamic model are determined from the natural frequencies and mode shapes of the detailed model (see Section 3.1.2.7).

Figure 3-2 shows a schematic depicting five nodes representing masses of fuel and rack cells and their associated elements, which are used to represent the interactions and vertical and horizontal motions of support pedestals, respectively. Contact (i.e., gap) elements are used in the representation of rack sliding and impact. A directional stiffness is assigned to the contact element. The pool floor is assumed to be a rigid body initially in contact with the rack pedestals. The contact elements are used to represent potential impact of a rack pedestal on the pool floor. The coefficient of friction between the rack pedestals and pool floor is incorporated into a contact (gap) element.

RAI 287-8272 - Question 09.01.02-30_Rev.2

The hydrodynamic masses for the fuel assembly-to-cell wall, rack-to-rack and rack-to-pool wall are modeled as ANSYS mass MATRIX27 elements. The hydrodynamic masses for rack baseplate-to-pool floor are considered as added masses to each rack baseplate.

Lumped masses of the rack and fuel assemblies are distributed among the five nodes for spent fuel storage rack cells and fuel assemblies as shown in the table below.

Node No. (Figure 3-2)		Location	Total Mass Distribution
Rack	Fuel Assembly		
13	18	Top of Rack	12.5 %
12	17	3/4 Height	25 %
11	16	1/2 Height	25 %
10	15	1/4 Height	25 %
9	14	Bottom (Baseplate) of Rack	12.5 %

All the fuel assemblies in each storage rack module are modeled as one beam of which the mass equals the sum of the masses of all the fuel assemblies in a rack module. Structural properties (i.e. Young's modulus and flexural rigidity) for fuel assemblies are shown in Table 3-3. Because the fuel assemblies in a rack module are modeled together, all fuel assemblies move simultaneously in one direction. This assumption results in larger impact forces on the rack module than the actual case and results in conservative loads on the storage rack. Because the fuel assembly is modeled with five nodes, the calculated impact loads on the nodes will be larger than the actual value because the fuel assembly actually has eleven spacer grids. The maximum fuel assembly grid horizontal impact load is determined by dividing the maximum impact load at each node by the number of grids associated with that node (2.75 for Nodes 10, 11, and 12, and 1.375 for Nodes 9 and 13).

Fluid damping and form drag are conservatively omitted.

Figure 3-3 shows the WPMR analysis model, which combines the single rack models described above to represent the entire spent fuel pool.

3.1.2.3 Hydrodynamic Mass

In addition to the structural mass of racks and fuel assemblies, hydrodynamic masses are included in the SFSR model to account for fluid coupling. Hydrodynamic mass is included in the SFSR model with the ANSYS MATRIX27 element and added mass, which represents an arbitrary element whose geometry is undefined but whose kinematic response can be specified by mass coefficients. Details of hydrodynamic masses are shown in Appendix H of Reference 17.

(1) Fuel Assembly-to-Cell Wall

A fuel assembly consists of fuel rods, guide tubes, top and bottom nozzles, and spacer grids. The hydrodynamic mass coefficients between the rack cell wall and the fuel assembly are calculated assuming the rack cell and fuel assembly are long coaxial cylinders. Hydrodynamic masses acting at the centers of two rigid cylinders with a fluid-filled annulus are represented using the following formula in Reference 15:

$$\begin{pmatrix} F_1 \\ F_2 \end{pmatrix} = \begin{bmatrix} -M_H & M_1 + M_H \\ M_1 + M_H & -(M_1 + M_2 + M_H) \end{bmatrix} \begin{pmatrix} X_1'' \\ X_2'' \end{pmatrix}$$

$$M_H = \left[\frac{R_2^2 + R_1^2}{R_2^2 - R_1^2} \right] \pi \rho R_1^2 h$$

$$M_2 = \rho h (2 C + g_2) \left[2 B + \left(\frac{g_1 + g_3}{2} \right) \right]$$

Where,

M_H = Hydrodynamic mass that depends on the fluid flow when the two bodies move relative to each other,

M_1 = Mass of fluid displaced by inner body,

M_2 = Mass of fluid inside the outer body in the absence of the inner body,

h = height of the storage rack,

ρ = density of the fluid, and

g_1, g_2, g_3 = initial gaps between the two bodies.

If g_2 is not the same on both sides, an average value of g_2 is used. If two or more racks overlap each other, the hydrodynamic mass is calculated using a weighted average gap.

(3) Rack Baseplate-to-Pool Floor

The hydrodynamic mass under the baseplate of each rack is calculated using the following formula in accordance with Table 1 of Reference 16.

$$M_{\text{baseplate}} = K \cdot (\pi \cdot \rho \cdot a^2 \cdot b / 4)$$

Where,

K = hydrodynamic mass coefficient ($K = 0.478$ is used for the SFSR),

a, b = length a and width b dimensions of the rack, and

ρ = density of the fluid.

3.1.2.4 Stiffness of Model

Two types of stiffness are used in the SFSR model: 3-D elastic beam elements, as discussed above, and contact elements. The contact elements are used to calculate horizontal loads due to friction (between the rack pedestal and embedment plate) and impacts (fuel-to-cell wall, rack-to-rack, and pedestal-to-embedment plate). The contact element used is ANSYS CONTAC52.

CONTAC52 represents two surfaces that may maintain or break physical contact and may slide relative to each other. This element is capable of supporting only compression in the direction normal to the surfaces and shear (coulomb friction) in the tangential direction. The element has three degrees of freedom at each node ($x, y,$ and z). A specified stiffness acts in the normal and tangential directions when the gap is closed. The stiffness values (i.e., spring constants) for the rack baseplates and pedestal are calculated in Appendix E of Reference 17. For these contact elements, the location of the element determines which values are used:



(1) Fuel Assembly-to-Cell Wall

Each node of the fuel assembly beam and the corresponding node of the rack beam is connected using a contact element in order to represent impact between the fuel assembly and the rack cell wall. The normal direction stiffness of this element is calculated assuming a series spring connection of the stiffness of the fuel assembly spacer grid and the local stiffness of the cell in the horizontal direction. To be conservative, the cell wall local stiffness is neglected. The fuel assembly/rack cell contact element has a local stiffness (K_i) to account for impact phenomena of the

RAI 287-8272 - Question 09.01.02-30_Rev.2

fuel assembly-to-cell wall. The grid stiffness for a fuel assembly beam is multiplied by the number of fuel assemblies assumed to be in the rack. The stiffness of fuel assembly grid is applied by dividing the total grid stiffness at each node by number of grid associated with node ($K_i/4$ for Nodes 15, 16, and 17, and $K_i/8$ for Nodes 14 and 18).

(2) Pedestal-to-Embedment Plate

Four nodes corresponding to the rack pedestals are connected to the pool floor using contact elements. The stiffness of these elements is a series spring connection of the vertical stiffness of the rack baseplate and pedestal. The baseplate vertical stiffness is calculated from FEM analysis. The stiffness values for the rack baseplates and pedestal are calculated in Appendix E of Reference 17. Therefore, pedestal-to-embedment plate stiffness value is calculated using the following formula:

$$\left[\begin{array}{c} \\ \\ \\ \\ \end{array} \right] TS$$

(3) Rack-to-Rack and Rack-to-Pool Wall

The stiffness for the rack-to-rack contact element is based on connections of the horizontal rack stiffness at the base plate. Analysis results show that the rack-to-rack and rack-to-pool wall displacements are less than the available rack-to-rack and rack-to-pool wall clearances. Consequently, contact elements are not included on the racks except for baseplate-to-baseplate and pedestal rack-to-floor interaction.

Because rack-to-rack impact other than at the baseplates does not occur, no sensitivity is performed. Therefore, the sensitivity of the impact force to the impact spring constant is evaluated for rack baseplate-to-rack baseplate only. A sensitivity analysis is performed in which the spring constant value is uniformly decreased or increased by 20%, respectively.

3.1.2.5 Friction Coefficient

Because SFSRs are not fixed to the storage pool, sliding could occur between the rack pedestals and the embedment plates or pool floor. The contact element is used to model this effect. Based on experimental data (Reference 14), the COF is bounded within the range from 0.2 to 0.8 with a mean value of 0.5. A low friction coefficient may increase sliding distance, while a high friction coefficient may increase rack load.

3.1.2.6 Buoyant Force

The SFSRs are submerged in water; therefore, buoyant forces are calculated and applied to the applicable nodes as concentrated loads in the vertical direction as follows:

$$\text{Buoyant force acting on rack} = W_{\text{rack}} - [(\rho_{\text{rack}} - \rho_{\text{water}}) / \rho_{\text{rack}}] \times W_{\text{rack}}$$

$$\text{Buoyant force acting on fuel assembly} = V_{\text{FA}} \times \gamma_{\text{water}}$$

Where,

ρ_{rack} = Density of storage rack, 8,000 kg/m³ (0.289 lbm/in³),

ρ_{water} = Density of fluid, 1,000 kg/m³ (0.036 lbm/in³),

W_{rack} = Weight of rack in air, and

V_{FA} = Volume of water displaced by fuel assembly, 0.743 m³ (2.625 ft³).

γ_{water} = Specific weight of fluid, 1000 kgf/m³ (0.036 lbf/in³)

The calculated buoyant forces were applied as follows:

Buoyant Force Acting on Rack and Fuel Assembly		
	Node(s) (See Figure 3-2)	Buoyant Force Applied to Each Node
Rack	1,2,3,4	Buoyant Force acting on rack /8
	9	Buoyant Force acting on rack /2
Fuel Assembly	18	Buoyant Force acting on fuel assembly

3.1.2.7 Natural Frequencies

The dynamic analysis models for the NFSR and SFSRs are generated using simplified beam elements. Each simplified beam model is developed to have dynamic characteristics (1st and 2nd mode of natural frequency and mode shapes) similar to the detailed finite element model. Appendix H of Reference 17 documents the comparison of the simplified and detailed three-dimensional models.

The fundamental frequencies of the NFSR are above 20 Hz and of the SFSR are above 30 Hz.

The range of frequencies considered is from 1 to 100 Hz according to the floor response spectra of design specification (Reference 22).

3.1.3 Simulation and Solution Methodology

The SFSR WPMR analysis is performed to calculate the displacements and loads for each rack and determine the presence or absence of specific rack-to-rack or rack-to-pool wall impacts during the seismic event. The analysis of the SFSR is performed as follows:

- (1) Use the ANSYS program (Reference 18) to prepare a 3-D WPMR model that includes hydrodynamic effects and nonlinear elements to produce realistic simulations of rack and fuel assembly motion during a seismic event.
- (2) Perform transient dynamic analyses for various combinations of friction coefficient values and rack loading conditions (full, partially full, and empty) with multiple input motion time histories to determine the response of the rack and fuel assemblies.

The basic equation of motion solved by a transient dynamic analysis is

$$(M)\{\ddot{u}\} + (C)\{\dot{u}\} + (K)\{u\} = \{F(t)\}$$

Where,

(M) = mass matrix,

(C) = damping matrix,

(K) = stiffness matrix,

$\{\ddot{u}\}$ = nodal acceleration vector,

$\{\dot{u}\}$ = nodal velocity vector,

$\{u\}$ = nodal displacement vector, and

$\{F(t)\}$ = load vector.

RAI 287-8272 - Question 09.01.02-30_Rev.2

- (4) When the SSE occurs, the rack is affected by irregular movement of every single fuel assembly. For conservative evaluation, all the fuel assemblies within the rack rattle in unison (model as a single beam) throughout the seismic event, which exaggerates the impact against the cell wall.

3.4 Input Data

3.4.1 Rack Data

Dimensions and mass of the new and the spent fuel storage racks used in the analysis are in accordance with the design drawings (References 5 and 6) and are summarized in the Tables 2-1, 2-2 and 3-2.

3.4.2 Fuel Assembly Data

Dimensions and mass of the fuel assembly used in the analysis are based on the pressurized water reactor (PWR) PLUS7 fuel assembly data (References 22 and 23) and are summarized in the Table 3-3.

3.4.3 Structural Damping

Rayleigh damping is used to specify mass (M) and stiffness (K) proportional damping (C):

$$C = \alpha \times M + \beta \times K$$

The constants α and β are calculated in the range of the lowest and highest frequencies of interest in the dynamic analysis (Reference 17). M corresponds to real mass of the rack-fuel system and does not include any hydrodynamic mass. Only material damping for the fuel and rack is used in calculating the damping matrix C. The design basis damping value for the NFSRs and the SF SRs is 4% for a SSE event in accordance with the regulatory guide (RG) 1.61 (Reference 24) for welded steel. The frequency range from 2 Hz to 85 Hz is applied to NFSR, while 2 Hz to 65 Hz is applied to SF SR considering installation in the water. The frequencies selected bound the natural frequencies of interest (e.g., for the NFSRs and SF SRs, frequencies of the fuel assemblies and rack structure). The damping model underpredicts damping (i.e., is conservative) at intermediate frequencies where the highest input accelerations occur.

3.4.4 Material Data

Material properties of a fuel assembly are taken from the PWR PLUS7 fuel assembly data (References 22 and 23) as shown in the Table 3-3. In addition, those of the racks are obtained from ASME Code Section II, Part D (Reference 19). The values listed correspond to a design temperature of 93.3 °C (200 °F); higher temperatures reduce material strength compared to normal conditions.

3.5 Computer Codes

3.5.1 ANSYS

A benchmarking study (Reference 25) was performed to demonstrate that ANSYS Version 15.0 (Reference 18) is an acceptable computer code for the seismic analysis of the SF SR and NFSR. While the SRP Section 3.8.1 Subsection II.4.F (Reference 26) states that meeting any one of the following methods is sufficient to validate computer programs used for design analysis, the benchmarking study addressed all three:

- 1) The computer program is recognized in the public domain and has had sufficient history of use to justify its applicability and validity without further demonstration.
- 2) The computer program's solutions to a series of test problems have been demonstrated to be substantially identical to those obtained from classical solutions or from accepted experimental tests

or to analytical results published in technical literature. The test problems should be demonstrated to be similar to or within the range of applicability of the classical problems analyzed to justify acceptance of the program.

- 3) The computer program's solutions to a series of test problems have been demonstrated to be substantially identical to those obtained by a similar and independently written and recognized program in the public domain. The test problems should be demonstrated to be similar to or within the range of applicability of the problems analyzed by the public domain computer program.

ANSYS has been used in the nuclear energy industry for nearly 40 years. The ANSYS software is developed within an ISO 9001 quality program that meets both ASME NQA-1 and 10 CFR 50 Appendix B. ANSYS software has previously been accepted by the NRC for SFSR seismic structural analysis.

Five test cases were run with ANSYS Version 15.0 to provide a comparison of ANSYS results to analytical results published in technical literature. These test cases exercised the ANSYS elements (MASS21, COMBIN14, CONTAC52, BEAM4, and MATRIX27) and features (direct integration time history, mass, spring, friction, impact and hydrodynamic coupling) used for the ARP1400 fuel rack seismic analysis. The five test cases involved coulomb friction, a two degree of freedom system with inertial coupling, mass impact on a beam, mass impact on a flexible surface, and the Fritz methodology for modeling hydrodynamic mass. The results of these five test problems compared very well to the published analytical results.

To further validate the use of ANSYS for APR1400 fuel rack seismic analysis, a single SFSR was analyzed with both ANSYS and LS-DYNA for five different sets of acceleration time histories. ANSYS is an implicit finite element code used for structural analysis with the capability to perform both static and dynamic simulations, while LS-DYNA is an explicit finite element code used for transient analysis. The results showed reasonable agreement, considering the highly non-linear nature of the response of the free-standing racks to a seismic base excitation. Maximum forces for design purposes were comparable between the two analyses.

3.6 Dynamic Simulations

The simulations listed in Table 3-5 are performed for the new and the spent fuel racks to investigate the structural integrity of each rack. The loading conditions for the racks are based on the SSE event.

The SFSR configurations at the full, empty, and mixed loadings are considered in the dynamic simulations. To consider the effect of the friction coefficient between pedestal and embedment plate as discussed in Section 3.1.2.5, simulations are performed by using the friction coefficient with upper and lower bound values and a mean value.

The nonlinear dynamic analyses for dynamic simulations of the NFSRs and the SFSRs are performed using the ANSYS (Reference 18) finite element program. The results of the simulations are compared to the stress and kinematic criteria in Section 3.2.

Run numbers 1 through 5 are dynamic simulations of the NFSR. For the SFSR, run numbers 6 through 10 use the coefficient of friction (COF) value 0.2, run numbers 11 through 15 are with the COF value 0.5, and run numbers 16 through 20 are with the COF value 0.8.

Run numbers 21 through 36 are sensitivity runs. The inputs (e.g., which time history, which COF for the SFSRs) for the sensitivity analysis were chosen from those used for base runs 1 to 5 for the NFSRs and 6 to 20 for the SFSRs, using the following rationale:

- Maximum vertical load on a single pedestal and fuel-to-cell wall impact load among the base runs.
- Maximum rack-to-rack baseplate impact load from among the base runs.

REVISED RESPONSE TO REQUEST FOR ADDITIONAL INFORMATION**APR1400 Design Certification****Korea Electric Power Corporation / Korea Hydro & Nuclear Power Co., LTD****Docket No. 52-046**

RAI No.: 287-8272

SRP Section: 09.01.02 – New and Spent Fuel Storage

Application Section: 9.1.2

Date of RAI Issue: 11/02/2015

Question No. 09.01.02-31

1. The 10 CFR Part 50, Appendix A, General Design Criteria (GDC) 1, 2, 4, 5, 63, and 10CFR 52.80 (a) provide the regulatory requirements for the design of the new and spent fuel storage facilities. Standard Review Plan (SRP) Sections 9.1.2 and 3.8.4, Appendix D describes specific SRP acceptance criteria for the review of the fuel racks that are acceptable to meet the relevant requirements of the Commission's regulations identified above. In DCD Tier 2, Section 9.1.2.2.3, "New and Spent Fuel Storage Rack Design", the applicant stated that "The dynamic and stress analyses are performed as described in report APR1400-H-N-NR-14012-P & NP". In the technical report APR1400-H-N-NR-14012-P, Rev 0, Subsection 3.7.1.3, "Impact Loads", for the case of rack-to-rack impacts, states that "The prominent baseplate of the fuel storage rack for the APR1400 design is installed almost in contact with the adjacent baseplate. According to the analysis result, the impact occurs not between the pool wall and the upper part of the rack, but between the baseplate of racks. SRP 3.8.4 Appendix D I(5) states that "Details of the mathematical model, including a description of how the important parameters are obtained, should be provided". In order for the staff to conclude that the applicant has adequately evaluated the rack-to-rack impact effects using a reasonable estimate of the impact spring rate, the applicant is requested to provide in accordance with the SRP 3.8.4 Appendix D I(5) the technical basis for calculating the impact spring constant for the rack-to-rack and rack baseplate-to-rack baseplate impact analysis in order to maximize the impact force. The applicant is also requested to address how the sensitivity of the impact force to the impact spring constant was considered in the analysis and design.

The applicant is requested to identify any proposed changes to and provide a mark-up of Subsections in the DCD Tier 2 and the report APR1400-H-N-NR-14012-P, Rev.0, as appropriate.

Response – (Rev. 0)

The spring constant value is assigned to the impact spring. Stiffness of the prismatic bar is calculated using the following formula:

$$K = \frac{E \cdot A}{L}$$

Where,
K is stiffness,
E is young's modulus,
A is cross section area, and
L is length.

Therefore, the spring constant of the rack baseplate is calculated using the following formula:

$$K = E \cdot \frac{L \cdot t}{W}$$

Where, K is spring constant of rack baseplate, E is young's modulus of rack baseplate, L is length of rack baseplate, t is thickness of rack baseplate, and W is width of rack baseplate.

The rack-to-rack impact does not occur as specified in the report APR1400-H-N-NR-14012-P, Section 3.7.7.1. Therefore, the sensitivity of the impact force to the impact spring constant is evaluated for rack baseplate-to-rack baseplate only. A sensitivity analysis is performed in which the spring constant value is uniformly decreased or increased by 20%, respectively. A sensitivity analysis results are shown in the response for question number 09.01.02-16.

Response – (Rev. 1)

Technical report, APR1400-H-N-NR-14012-NP was submitted as Rev. 0 in December, 2014. KHNP responses to RAI 287-8272 were based in part on the Technical Report. Subsequent to issuance of the Technical Report and RAI responses, the NRC provided feedback on both the Technical Report and RAI 287-8272 responses. In response to this NRC feedback, Technical report, APR1400-H-N-NR-14012-NP will be revised (as Rev. 3) to incorporate additional information pertaining to the fuel racks. This RAI revision contains the specific Technical Report revisions relevant to this response and associated DCD changes, where necessary. A summary of the additional information is in the below paragraphs.

Impact spring constant for the rack baseplate-to-rack baseplate

The spring constant value is assigned to the impact spring. Stiffness of the prismatic bar is calculated using the following formula:

$$K = \frac{E \cdot A}{L}$$

Where,

K is stiffness,
E is young's modulus,
A is cross section area, and
L is length.

Therefore, the spring constant of the rack baseplate is calculated using the following formula:

$$K = E \cdot \frac{L \cdot t}{W}$$

Where, K is spring constant of rack baseplate, E is young's modulus of rack baseplate, L is length of rack baseplate, t is thickness of rack baseplate, and W is width of rack baseplate.

Impacts of Rack-to-Rack and Rack-to-Pool Wall

SFSRs are installed as closely as possible with the protruding baseplate intended to be in contact with the adjacent baseplates. If the racks were initially installed with slight separation, conclusions would not change since it would be no different than a few time steps into a transient when the rack bases have moved slightly apart. The upper part of the racks do not come into contact. Therefore, the only rack-to-rack contact is between the baseplate of racks.

Also, the racks do not contact the SFP wall. Therefore, no rack to pool wall impact loads are calculated. This is consistent with SRP Section 3.8.4, Appendix D, Structural Acceptance Criteria, which states:

“In the consideration of the effects of seismic loads, factors of safety against gross sliding and overturning of racks and rack modulus [sic] under all probable service conditions should be in accordance with SRP Section 3.8.5, Subsection II.5. This position on factors of safety against sliding and tilting need not be met provided that the applicant meets any one of the following conditions:

“a. Detailed nonlinear dynamic analyses show that the amplitudes of sliding motion are minimal and impact between adjacent rack modules or between a rack module and the pool walls is prevented provided that the factors of safety against tilting are within the allowable values provided in SRP Section 3.8.5, Subsection II.5....”

Sensitivity Analysis for Spring Constant

Three sensitivities were performed on spring constants (i.e., stiffness) in the model, as shown in:

- The rack-to-floor stiffness was evaluated at $\pm 20\%$ of the nominal value.
- The rack-to-rack stiffness was evaluated at $\pm 20\%$ of the nominal value.
- The fuel-to-rack stiffness was evaluated at $\pm 20\%$ of the nominal value.

The effect of the sensitivities was a change in predicted loads within the variation found for different time histories and less than the variation for different COFs.

Impact on DCD

There is no impact on the DCD.

Impact on PRA

There is no impact on the PRA.

Impact on Technical Specifications

There is no impact on the Technical Specifications.

Impact on Technical/Topical/Environmental Reports

[APR1400-H-N-NR-14012-NP \(Rev. 3\)](#), Sections 3.7.1.3 and 3.7.4.3 will be revised as shown in Attachment 1 to this response.

The combined maximum impact loads on fuel support grid of the NFSRs and the SFSTRs are shown in Table 3-8.

(2) Impacts of Rack-to-Rack and Rack-to-Pool Wall

SFSTRs are installed as closely as possible with the protruding baseplate intended to be in contact with the adjacent baseplates. If the racks were initially installed with slight separation, conclusions would not change since it would be no different than a few time steps into a transient when the rack bases have moved slightly apart. As reported in Section 3.7.1.1, the upper part of the racks do not come into contact. Therefore, the only rack-to-rack contact is between the baseplate of racks. The maximum impact load at the SFSTR baseplates is shown in Table 3-8.

Also as reported in Section 3.7.1.1, the racks do not contact the SFP wall. Therefore, no rack to pool wall impact loads are calculated. This is consistent with SRP Section 3.8.4, Appendix D, Structural Acceptance Criteria, which states:

“In the consideration of the effects of seismic loads, factors of safety against gross sliding and overturning of racks and rack modulus [sic] under all probable service conditions should be in accordance with SRP Section 3.8.5, Subsection II.5. This position on factors of safety against sliding and tilting need not be met provided that the applicant meets any one of the following conditions:

“a. Detailed nonlinear dynamic analyses show that the amplitudes of sliding motion are minimal and impact between adjacent rack modules or between a rack module and the pool walls is prevented provided that the factors of safety against tilting are within the allowable values provided in SRP Section 3.8.5, Subsection II.5....”

3.7.2 Fuel Structural Evaluation

Lateral impact load on the spent fuel assembly is evaluated for two acceptance criteria: fuel spacer grid buckling and fuel cladding yield stress.

The maximum impact load per cell applied to fuel assembly is evaluated for the peak load shown in Table 3-8. Therefore, the maximum acceleration load that the rack imparts on the fuel assembly can be conservatively calculated as follows:

$$a = \frac{F}{w}$$

Where,

- a = Maximum lateral acceleration in g's (= 22.8 g) per section 7.2 of Reference 17,
- F = Maximum fuel-to-cell wall impact load per cell, and
- w = Weight of one fuel assembly (6.27 kN (1408.6 lbf)).

The structural integrity of fuel assembly cladding is evaluated for the maximum lateral acceleration load, obtained by combining (i.e., SRSS) the simultaneous impact load in the E-W and N-S directions to find the maximum value at any time step. The fuel assembly spacer grid is evaluated for the maximum grid impact load, obtained by combining (i.e., SRSS) the simultaneous impact load in the E-W and N-S directions at the same time.

3.7.2.1 Structural Integrity Evaluation of Fuel Spacer Grid

The lateral impact loads on a single fuel spacer grid is compared against its buckling load capacity, which is shown in the Table 3-3. The critical buckling load of the fuel spacer grid for the APR1400 design is 31.3 kN (7,045 lbf) and compared with the combined fuel grid impact load as shown in Table 3-8.

3.7.4.1 Rack EI

For both the NFSR and SFSR, sensitivities of $\pm 20\%$ of the product of rack elastic modulus and moment of inertia are evaluated in runs 21 through 24. For the NFSR, fuel assembly grid to cell impact loads were similar. For the SFSR, all loads were similar to those for the base case.

3.7.4.2 Coefficient of Friction

Each of the five time histories was applied to both Region I and Region II racks at COF values of 0.2, 0.5, and 0.8, as shown in Table 3-5 and

Figure 3-20. The following trends were noted:

- For loads on a single pedestal, horizontal loads increase with increasing COF
- Baseplate-to-baseplate impact loads increase with increasing COF
- COF does not affect the other loads.

3.7.4.3 Spring constant

Three sensitivities were performed on spring constants (i.e., stiffness) in the model, as shown in:

- The rack-to-floor stiffness was evaluated at $\pm 20\%$ of the nominal value.
- The rack-to-rack stiffness was evaluated at $\pm 20\%$ of the nominal value.
- The fuel-to-rack stiffness was evaluated at $\pm 20\%$ of the nominal value.

The effect of the sensitivities was a change in predicted loads within the variation found for different time histories and less than the variation for different COFs. Figure 3-24 show the effect on pedestal and baseplate impact loads, respectively.

3.7.4.4 Fuel Assembly EI

One case (Run 33) evaluates the effect of end of life fuel assembly properties. Fuel-to-cell wall and fuel assembly grid impact loads were consistent with those of the BOL case.

3.7.4.5 Rack Loading

The free standing SFSRs do slide and different fuel loading arrangements were considered. Run34 in Table 3-5 evaluates the all racks being empty. Run35 in Table 3-5 evaluates the one quarter full rack / two half full racks loaded (see Figure 3-4). The results showed that the displacements of empty fuel racks were less than those of fully loaded racks.

3.7.4.6 Computational Time Step

Comparison of a run at one half the fixed time step used for all other runs showed small changes in calculated results comparable to the run to run variation with different time histories. Small differences, vice identical results, are expected because the time step used affects where in each time history the acceleration is taken and how long it is applied. The 5% convergence value for dynamic simulation is applied to calculate the force and displacement quantities of interest. Displacement plots of one of the racks to compare results between time steps for the time step sensitivity are as shown in Figure 3-27.

3.7.5 Conservatism in Seismic Analysis

The APR1400 fuel rack seismic analytical approach includes significant conservatism:

- All of the fuel mass at each elevation in the rack is assumed to move as a unit, resulting in a conservative impact force and rack response.

REVISED RESPONSE TO REQUEST FOR ADDITIONAL INFORMATION**APR1400 Design Certification****Korea Electric Power Corporation / Korea Hydro & Nuclear Power Co., LTD****Docket No. 52-046**

RAI No.: 287-8272
SRP Section: 09.01.02 – New and Spent Fuel Storage
Application Section: 9.1.2
Date of RAI Issue: 11/02/2015

Question No. 09.01.02-32

The 10 CFR Part 50, Appendix A, General Design Criteria (GDC) 1, 2, 4, 5, 63, and 10CFR 52.80 (a) provide the regulatory requirements for the design of the new and spent fuel storage facilities. Standard Review Plan (SRP) Sections 9.1.2 and 3.8.4, Appendix D describes specific SRP acceptance criteria for the review of the fuel racks that are acceptable to meet the relevant requirements of the Commission's regulations identified above. In DCD Tier 2, Section 9.1.2.2.3, "New and Spent Fuel Storage Rack Design", the applicant stated that "The dynamic and stress analyses are performed as described in report APR1400-H-N-NR-14012-P & NP". In the technical report APR1400-H-N-NR-14012-P, Rev 0, Subsection 3.1.2.1 (2) "General Considerations" the applicant included the pedestal-to-bearing pad interface in the dynamic model of the rack for the impact loads. However, the staff did not find any acceptance criteria for the bearing pad. In order for the staff to perform its safety evaluation of the rack supports, the applicant in accordance with SRP 3.8.4 Appendix D I (3), is requested to provide a sketch showing the bearing pad dimensions and a layout of bearing pad with respect to the rack pedestal and the pool floor and acceptance criteria for the bearing pads including the maximum calculated and allowable bearing stress. The applicant is requested to identify any proposed changes to and provide a mark-up of Subsections in the DCD Tier 2 and the report APR1400-HN-NR-14012-P, Rev.0, as appropriate.

Response – (Rev. 0)

In the designing of spent fuel storage racks for the APR1400, bearing pads are not used. The spent fuel storage rack modules are free standing on embedments in the pool floor as specified on DCD Tier 2 Subsection 9.1.2.2.2.

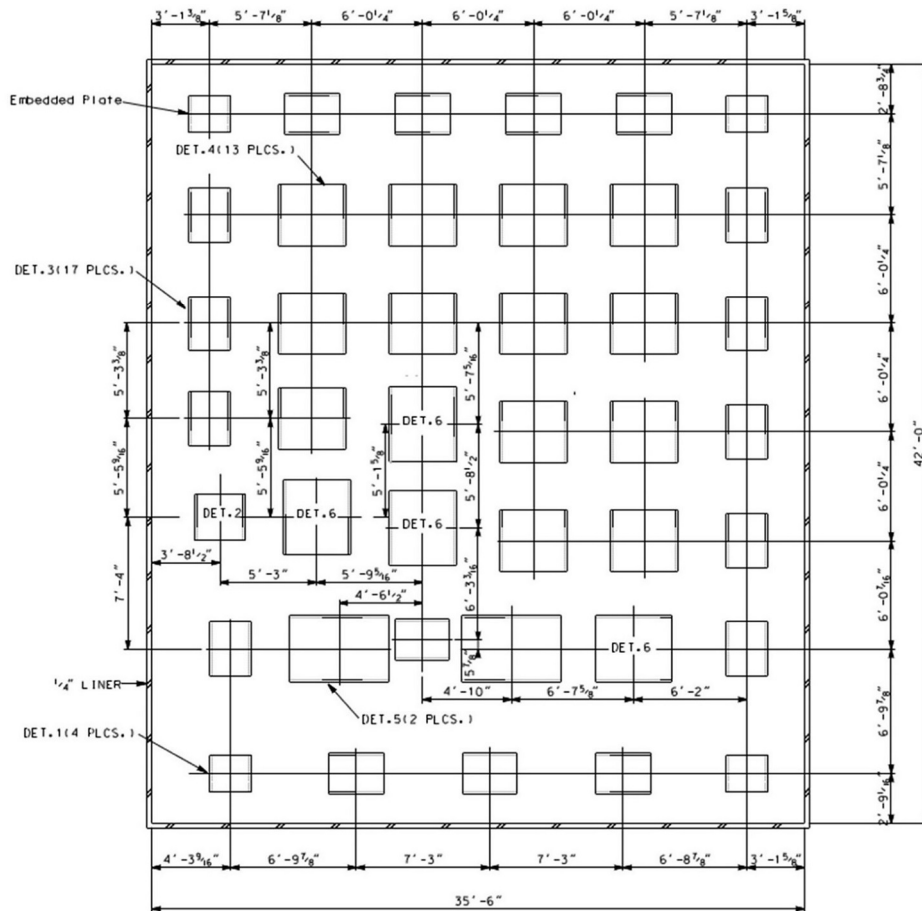
Therefore, the paragraph of Section 3.1.2.1(2) of technical report APR1400-H-N-NR-14012-NP will be corrected from "~ interfaces for the pedestal-to-bearing pad interface ~" to "~interfaces for the pedestal-to-embedments interface ~".

Response – (Rev. 1)

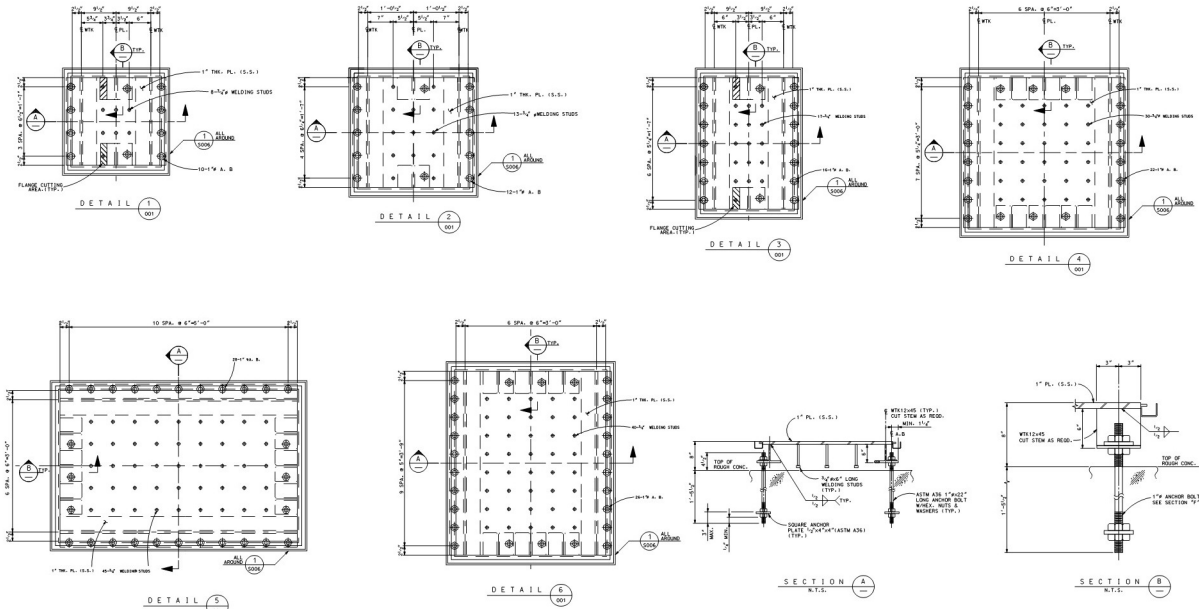
Technical report, APR1400-H-N-NR-14012-NP was submitted as Rev. 0 in December, 2014. KHNP responses to RAI 287-8272 were based in part on the Technical Report. Subsequent to issuance of the Technical Report and RAI responses, the NRC provided feedback on both the Technical Report and RAI 287-8272 responses. In response to this NRC feedback, Technical report, APR1400-H-N-NR-14012-NP will be revised (as Rev. 3) to incorporate additional information pertaining to the fuel racks. This RAI revision contains the specific Technical Report revisions relevant to this response and associated DCD changes, where necessary. A summary of the additional information is in the below paragraphs.

The SFSR modules are free-standing with pedestals resting on embedment plates (the SFSRs do not rest on the liner or use bearing pads), which distribute the dead weight of the loaded racks to the reinforced concrete structure of the floor.

As described in the DCD section 9.1.2.2, the spent fuel rack modules are laid as free standing on the embedments in the spent fuel pool floor. The layouts and dimensions for the embedments including spent fuel rack modules refers to the figures below.



Layout of embedments in the spent fuel pool floor



Dimensions of embedments

Impact on DCD

There is no impact on the DCD.

Impact on PRA

There is no impact on the PRA.

Impact on Technical Specifications

There is no impact on the Technical Specifications.

Impact on Technical/Topical/Environmental Reports

APR1400-H-N-NR-14012-NP (Rev. 3), Section 2.2 will be revised as shown in Attachment 1 to this response.

2 FUEL RACKS

2.1 Description of New Fuel Storage Racks

Figure 2-1 shows the layout and the plan view of the two NFSR modules in the dry, unlined new fuel storage pit (NFP). Each rack module consists of a 7 x 8 array of storage cells that are bolted to the pit floor and supported by top, middle, and base plates and stiffeners as shown in Figure 2-2 and Figure 2-3. The NFSR modules have 112 storage cells, which provide more than enough locations to store a refueling batch. The center-to-center spacing between adjacent fuel assemblies is 35.5 cm (14 in) to maintain subcriticality without the use of neutron absorbers. The NFSR cell wall thickness is 6 mm (0.236 in). SA-240 Type 304L material is used for the cell walls, plates, stiffeners, and pedestals, and SA-564 Grade 630 is used for the stud bolt. The basic dimensions of the NFSR modules are summarized in Table 2-1.

2.2 Description of Spent Fuel Storage Racks

Figure 2-4 shows the layout of the SFSR modules in the spent fuel pool (SFP), which consists of two regions, Region I and Region II. Fresh fuel assemblies, spent fuel assemblies, and damaged fuel in canisters can be stored in Region I, which has the capacity to store one full core, one refueling batch, and five damaged fuel canisters. Region I consists of four 8 x 8 cell modules (A1-1, A1-2, A1-3 and A1-4) and two 6 x 8 cell modules (A2-1 and A2-2). Module A2-1 has five cells that can each contain a damaged fuel canister. Region II consists of nineteen 8 x 8 cell modules (B1, B2-1, B2-2, B2-3, B3, B4, B5-1, B5-2, B5-3, B5-4, B5-5, B5-6, B6-1, B6-2, B6-3, B7, B8, B9 and B10) and four 8 x 7 cell modules (C1, C2, C3 and C4). Figure 2-5 gives the dimensions of the gaps between cell walls when the rack baseplates are installed touching, as indicated in Figure 2-6.

As shown in Figure 2-7 through 2-10, the SFSR modules are free-standing with pedestals resting on embedment plates (the SFSRs do not rest on the liner or use bearing pads), which distribute the dead weight of the loaded racks to the reinforced concrete structure of the floor. Each SFSR module is supported by four pedestals, and each pedestal has a 7-inch diameter leveling foot that can be adjusted with a long-handled tool. The SFSR modules are submerged in boric acid water with space between the racks and the cell walls. Therefore, the motions of racks and the fuel assemblies will be influenced by fluid-structure interactions.

To maintain subcriticality, the center-to-center spacing between adjacent fuel assemblies is 27.5 cm (10.83 in) for Region I racks and 22.5 cm (8.86 in) for Region II racks. The cell wall thickness of the SFSRs is 2.5 mm (0.098 in). SA-240 Type 304L material is used for the cell walls, baseplate, and pedestal; SA-564 Grade 630 is used for the leveling foot; and a hot-rolled composite plate material (METAMIC™) is used as a neutron absorber. The basic dimensions of the SFSRs are summarized in Table 2-2.

2.3 Fuel Storage Rack Fabrication

As described above, all of the fuel storage racks are similar in concept. However, the NFSRs and the SFSRs for Regions I and II have slightly different fabrication sequences. Note that welds are visually inspected in each step before access to perform a weld inspection is blocked due to addition of subsequent parts.

2.3.1 Fabrication Procedure of NFSR and SFSR

The NFSRs and SFSRs are fabricated in accordance with a design specification (Reference 22) and manufacturing drawings. The following describes the expected fabrication sequence but actual work may differ, provided design specification and drawing requirements (e.g., dimensions, inspection acceptance criteria, quality assurance) are met.

REVISED RESPONSE TO REQUEST FOR ADDITIONAL INFORMATION**APR1400 Design Certification****Korea Electric Power Corporation / Korea Hydro & Nuclear Power Co., LTD****Docket No. 52-046**

RAI No.: 287-8272
SRP Section: 09.01.02 – New and Spent Fuel Storage
Application Section: 9.1.2
Date of RAI Issue: 11/02/2015

Question No. 09.01.02-33

1. The 10 CFR Part 50, Appendix A, General Design Criteria (GDC) 1, 2, 4, 5, 63, and 10CFR 52.80 (a) provide the regulatory requirements for the design of the new and spent fuel storage facilities. Standard Review Plan (SRP) Sections 9.1.2 and 3.8.4, Appendix D describes specific SRP acceptance criteria for the review of the fuel racks that are acceptable to meet the relevant requirements of the Commission's regulations identified above. In DCD Tier 2, Section 9.1.2.2.3, "New and Spent Fuel Storage Rack Design", the applicant stated that "The dynamic and stress analyses are performed as described in report APR1400-H-N-NR-14012-P & NP". In the technical report APR1400-H-N-NR-14012-P, Rev 0, Section 4, "MECHANICAL ACCIDENTS ANALYSIS", Subsection 4.3, "Analysis Method", states that "This calculation covers the new fuel storage racks in NFP and the spent fuel storage racks of Region I and Region II in SFP. Region I racks are structurally stronger than Region II racks. To conservatively estimate the damage of the racks due to the postulated drop accidents, the calculation is performed for Region II racks. Since the new fuel storage rack is held down by firmly attached to the embedment plates of NFP using a stud bolt and is supported by additional intermediate plate, and has no "poison zone", the drop accident evaluation is performed only for the case of drop (away from pedestal) on baseplate of the fuel rack". The applicant is requested to provide the technical basis for concluding that the spent fuel storage racks of Region I are structurally stronger than the Region II racks and also provide a technical justification that the dynamic response and the design safety factors for the Region II racks will bound the Region I racks and the design stress limits for region I racks will not be exceeded under the required load combinations in the Table 3-1. The applicant is requested to identify any proposed changes to and provide a mark-up of Subsections in the DCD Tier 2 and the report APR1400-H-N-NR-14012-P, Rev.0, as appropriate.

Response – (Rev. 0)

In the report APR1400-H-N-NR-14012-P, Section 4.3, the sentence “Region I racks are structurally stronger than Region II racks” will be deleted. And the sentence “To conservatively estimate the damage of the racks due to the postulated drop accidents, the calculation is performed for Region II racks” will be revised as “To conservatively estimate the damage of the racks due to the postulated drop accidents, a calculation is performed for Region II racks using the damaged fuel canister inside dimension of Region I rack” regarding the mechanical accident evaluation.

Stress evaluation for Region I racks is shown in the table 3-12 in the report APR1400-H-N-NR-14012-P.

Response – (Rev. 1)

Technical report, APR1400-H-N-NR-14012-NP was submitted as Rev. 0 in December, 2014. KHNP responses to RAI 287-8272 were based in part on the Technical Report. Subsequent to issuance of the Technical Report and RAI responses, the NRC provided feedback on both the Technical Report and RAI 287-8272 responses. In response to this NRC feedback, Technical report, APR1400-H-N-NR-14012-NP will be revised (as Rev. 3) to incorporate additional information pertaining to the fuel racks. This RAI revision contains the specific Technical Report revisions relevant to this response and associated DCD changes, where necessary. A summary of the additional information is in the below paragraphs.

Impact Velocity

Some of the Region II periphery cells, which are formed by welding a panel plate to three adjacent box cells, are structurally weaker. Therefore, a shallow drop over a Region II rack periphery panel plate governs.

For deep drops over a pedestal, impact velocities are the same for both regions. For deep drops away from a pedestal, the impact velocities for Region I and Region II SFSTRs are calculated based on the inner dimension of damaged fuel canister cells and that of other cells, respectively. It cause different drag conditions of Region I and Region II SFSTRs. Therefore, the impact velocity for Region I SFSTRs is greater than that of Region II, as shown in Table below.

Rack	Cases		Drop Weight, kN (lbf)	Drop Height, m (in)	Impact Velocity, m/sec (in/sec)
SFSTR	Straight Deep Drop (Away from Pedestal)	Region I	10.8 (2,425)	5.2 (204.7)	8.22 (323.5)
		Region II			7.36 (289.6)

Impact on DCD

There is no impact on the DCD.

Impact on PRA

There is no impact on the PRA.

Impact on Technical Specifications

There is no impact on the Technical Specifications.

Impact on Technical/Topical/Environmental Reports

[APR1400-H-N-NR-14012-NP \(Rev. 3\), Section 4.3.2 will be revised as shown in Attachment 1 to this response.](#)

4.3.2 Calculation of Impact Velocity

The objective of the analysis is to calculate the final velocity of the dropping object. A dropping object is modeled as a single lumped mass under the influence of gravity in a drag inducing medium. The effects of buoyant mass, gravity, and fluid drag are accounted for in the model. The drag force is based on the exposed frontal area of the fuel assembly. The governing equation to calculate the impact velocity for a body of mass subject to gravity and drag effects is

TS

However, some of the Region II periphery cells, which are formed by welding a panel plate to three adjacent box cells, are structurally weaker. Therefore, a shallow drop over a Region II rack periphery panel plate governs.

For deep drops over a pedestal, impact velocities are the same for both regions. For deep drops away from a pedestal, the impact velocities for Region I and Region II SFSRs are calculated based on the inner dimension of damaged fuel canister cells and that of other cells, respectively. It cause different drag conditions of Region I and Region II SFSRs. Therefore, the impact velocity for Region I SFSRs is greater than that of Region II.

Since a drop into a NFSR is through air, rather than water, it has a higher impact velocity.

4.3.3 Finite Element Model

All drops were analyzed by developing a finite element model in ANSYS LS-DYNA. The impactor (e.g., the fuel assembly and its handling tool, dropped transport container handling tool) is conservatively modeled as a rigid solid with no energy absorption capacity except for drop scenario 3. The detailed configurations of the impact target (i.e., the rack) are modeled in all analyzed events. The deep drop analysis model considers the effects of all of the stored fuel assemblies in the rack by modifying the density of the baseplate to simulate the loading effects of the other fuel assemblies. In most cases, the model of the rack did not include any the structure underneath the rack, but for the deep drop over a pedestal, the effect of the impact on concrete underneath the pedestal baseplate was evaluated. Figure 4-4 through Figure 4-16 show the finite element models and results for individual scenarios, which are discussed in the following sections. ANSYS LS-DYNA Elements, SHELL163 (explicit thin structural shell) and SOLID164 (explicit 3-D structural solid), are used to mesh the cell walls, baseplate and rack feet. SHELL163 is a 4-node element with both bending and membrane capabilities. Both in-plane and normal loads are permitted. The element has 12 degrees of freedom at each node: translations, accelerations, and velocities in the nodal x, y, and z directions and rotations about the nodal x, y, and z-axes. SOLID164 is used for the 3-D modeling of solid structures. The element is defined by eight nodes having the degrees of freedom at each node: translations, velocities, and accelerations in the nodal x, y, and z directions. The bottom of the modeled rack feet is fixed in the finite element model because the NFSRs are bolted and horizontal motion is not relevant to a SFSR or NFSR straight vertical drop.

4.3.4 Methodology for Straight Shallow Drop Accident onto a SFSR

The straight shallow drop accident analysis determines the extent of the damage to the rack structure due to the impact of the dropping object. The impact velocity of the dropping mass is calculated first to determine the bounding kinetic energy that will be used to evaluate the postulated shallow drop accident. In analyzing the shallow drop, the rack model consists of 25 cells as shown in Figure 4-4. Modeling only 25 of 56 or 64 SFSR cells has negligible effect since damage is locally limited to the top of cell walls at the point of impact.

4.3.5 Methodology for Straight Deep Drop Accident (Away from Pedestal)

When a dropping object impacts the baseplate of a rack, the deformation of the baseplate and the potential for impact on the pool liner is evaluated. In analyzing the deep drop scenario 1 (away from the pedestal), the NFSR model consists of 56 cells as shown in Figure 4-5. Figure 4-7 shows the 16 cell model used for the SFSR. The deep drop analysis model considers the effects of all of the stored fuel assemblies in the rack by modifying the density of the baseplate to simulate the dynamic effects of the other fuel assemblies.

REVISED RESPONSE TO REQUEST FOR ADDITIONAL INFORMATION**APR1400 Design Certification****Korea Electric Power Corporation / Korea Hydro & Nuclear Power Co., LTD****Docket No. 52-046**

RAI No.: 287-8272
SRP Section: 09.01.02 – New and Spent Fuel Storage
Application Section: 9.1.2
Date of RAI Issue: 11/02/2015

Question No. 09.01.02-34

The 10 CFR Part 50, Appendix A, General Design Criteria (GDC) 1, 2, 4, 5, 63, and 10CFR 52.80 (a) provide the regulatory requirements for the design of the new and spent fuel storage facilities. Standard Review Plan (SRP) Sections 9.1.2 and 3.8.4, Appendix D describes specific SRP acceptance criteria for the review of the fuel racks that are acceptable to meet the relevant requirements of the Commission's regulations identified above. In DCD Tier 2, Section 9.1.2.2.3, "New and Spent Fuel Storage Rack Design", the applicant stated that "The dynamic and stress analyses are performed as described in report APR1400-H-N-NR-14012-P & NP". In the technical report APR1400-H-N-NR-14012-P, Rev 0, Subsections 3.2.2.1 and 3.2.2.2, the applicant provided the acceptance criteria for normal and upset conditions, Service Level A and Service Level B respectively, but did not discuss or provide the evaluation results for the normal and upset conditions. In accordance with SRP 3.8.4 Appendix D I (6), the applicant is requested to provide its evaluation results for the normal and upset conditions. The applicant is requested to identify any proposed changes to and provide a mark-up of Subsections in the DCD Tier 2 and the report APR1400-H-N-NR-14012-P, Rev.0, as appropriate.

Response – (Rev. 0)

As described in DCD 3.7.1, the APR1400 seismic Category I SSCs are designed for the safe shutdown earthquake (SSE). The SSE is defined as the maximum potential vibratory ground motion at the generic plant site. Since the operating basis earthquake (OBE) is defined as one third the SSE, the design of the APR1400 seismic Category I SSCs based on OBE are not required in accordance with Appendix S of 10 CFR Part 50. Moreover thermal loads applied to the racks are not included in the stress combinations involving seismic loadings; since the thermal stresses are a secondary stress, and have no stipulated stress limits for Class 3 structures or components when acting in concert with seismic loadings.

Therefore, the primary stress evaluation for the normal and upset conditions is performed for dead weight, which includes only of the racks and the fuel assembly weight, in accordance with Table 3-1 of technical report APR1400-H-N-NR-14012-P.

Technical report APR1400-H-N-NR-14012-P will be revised to include the evaluation results for the normal condition of the pedestal and cell wall of the racks.

Response – (Rev. 1)

Technical report, APR1400-H-N-NR-14012-NP was submitted as Rev. 0 in December, 2014. KHNP responses to RAI 287-8272 were based in part on the Technical Report. Subsequent to issuance of the Technical Report and RAI responses, the NRC provided feedback on both the Technical Report and RAI 287-8272 responses. In response to this NRC feedback, Technical report, APR1400-H-N-NR-14012-NP will be revised (as Rev. 3) to incorporate additional information pertaining to the fuel racks. This RAI revision contains the specific Technical Report revisions relevant to this response and associated DCD changes, where necessary. A summary of the additional information is in the below paragraphs.

Seismic Analysis

For the APR1400, the operating basis earthquake (OBE) ground motion is defined as one-third the SSE ground motion design response spectra. Therefore, in accordance with 10 CFR Part 50, Appendix S, an OBE design analysis is not required. The primary stress evaluation for the normal condition is performed for dead weight, which includes only of the racks and the fuel assembly weight. Therefore, maximum stress factors on rack for the Service Level A and D are provided as shown in Table 1.

Table 1 Maximum Stress Factors on Racks

Service Level	Rack	Pedestal Stress Factors			Cell Wall Stress Factors			COF
		FACT1	FACT2	FACT3	FACT1	FACT2	FACT3	
A	NFSRs	0.060	0.044	-	0.030	0.032	-	N/A
	SFSRs (Region I)	0.032	0.024	-	$\frac{0.034}{0.779^{(2)}} = 0.044$	0.037	-	N/A
	SFSRs (Region II)	0.034	0.026	-	$\frac{0.042}{0.779^{(2)}} = 0.054$	0.045	-	N/A
D	NFSRs	0.731	0.829	0.617	0.067	0.073	0.049	N/A
	SFSRs (Region I)	0.148	0.125	0.130	$\frac{0.181}{0.779^{(2)}} = 0.235$	0.194	0.045	0.8
	SFSRs (Region II)	0.168	0.140	0.155	$\frac{0.376}{0.779^{(2)}} = 0.483$	0.401	0.097	0.8

Notes:

- (1) Dimensionless stress factors, FACT1, FACT2, and FACT3
- (2) Stress correction factor considering slenderness ratio
- (3) Since the width-thickness ratio of NFSR is not greater than 51.4, no additional adjustment for the stress is necessary.

Mechanical Accident Analysis

The stuck fuel assembly is evaluated to Level B service limits to ensure the integrity of the rack is unaffected.

The fuel racks are adequate to withstand the uplift force of 22.2 kN (5,000 lbf) due to a stuck fuel assembly because the neutron absorbing poison plate is not damaged and structural integrity of the rack is maintained. Two cases are considered:

- (a) For vertical uplift when a fuel assembly was nearly free of the top of a SF SR, the effect is concentrated at the top of the rack structure along a single cell wall. If the vertical uplift force is resisted only by shear stress, the allowable shear stress level be limit is:

$$\tau_y = 1.33 * 0.4 * S_y = 1.33 * 0.4 * 21,400 \text{ psi} = 11,385 \text{ psi}$$

The depth of the cell structure h_{sf} that can support the load is obtained from

$$h_{sf} = \frac{F_e}{2 * \tau_y * t_{cell}} = \frac{5000 \text{ lbf}}{2 * 11,385 \text{ psi} * 0.098 \text{ in}} = 2.24 \text{ in}$$

Where,

$$t_{cell} = \text{cell wall thickness of } 0.098 \text{ in}$$

The top of the neutron absorbing plate is at about 24.0 inches below the top of the cell wall. Since the damaged area is above the location of the neutron absorber and is limited to a small section of one cell wall, margin to criticality and structural integrity are not affected.

- (b) For vertical uplift when a fuel assembly is fully seated, the force is assumed to be resisted by a single cell wall, which is 0.098 in thick and 8.66 in wide. If the stress is uniformly distributed across that cross section, it is equal to

$$\sigma = \frac{F_e}{D_{cell} * t_{cell}} = \frac{5000 \text{ lbf}}{8.66 \text{ in} * 0.098 \text{ in}} = 5892 \text{ psi}$$

The calculated stress is less than allowable tensile stress ($1.33 * 0.6 * S_y = 17,077 \text{ psi}$), which means that damage to the cell wall will not occur.

The forces caused by uplift of a stuck fuel assembly does not cause damage that affects the margin to criticality or structural integrity.

Impact on DCD

DCD Tier 2 Section 9.1.2.1 and Table 3.8-9C will be revised as indicated in Attachment 1 to this response.

Impact on PRA

There is no impact on the PRA.

Impact on Technical Specifications

There is no impact on the Technical Specifications.

Impact on Technical/Topical/Environmental Reports

APR1400-H-N-NR-14012-NP (Rev. 3), Sections 3.2.2.1, 3.2.2.2, 3.7.1, 4.5, and Table 3-9 will be revised as shown in Attachment 2 to this response.

Table 3.8-9C

Spent Fuel Storage Rack – Design Loading Combination Table

Load Combination	Acceptance Limit
D + L D + L + T _o D + L + T_o + E	ASME Code Section III, Subsection NF Level A Service Limits for Class 3
D + L + T_a + E D + L + T _o + P _f	ASME Code Section III, Subsection NF Level B Service Limits for Class 3
D + L + T _a + E'	ASME Code Section III, Subsection NF Level D Service Limits for Class 3
D + L + F _d	The functional capability of the fuel racks should be demonstrated.

Where,

D : Deadweight including fuel assembly weight

L : Live load

~~E : Operating basis earthquake (OBE)~~

E' : Safe shutdown earthquake (SSE)

T_o : Differential temperature-induced loads, based on the most critical transient or steady-state condition under normal operation or shutdown conditions

T_a : Highest temperature associated with the postulated abnormal design conditions

F_d : Force caused by the accidental drop of the heaviest load from maximum possible height

P_f : Upward force on the racks caused by a postulated stuck fuel assembly

← Note: For the APR1400, the operating basis earthquake (OBE) ground motion is defined as one-third the SSE ground motion design response spectra. Therefore, in accordance with 10 CFR Part 50, Appendix S, an OBE design analysis is not required and load combinations involving E have been removed.

- g. No CEAs or burnable poison rods in the fuel assembly, and no neutron absorption effect in the fuel assembly support materials are assumed to be present.
- h. The rack is filled with fuel assemblies up to the initial onsite storage capacity with the SFP filled with water.
- i. The bias and bias uncertainty obtained from benchmark calculation are reflected in the calculated K_{eff} . Uncertainties from mechanical tolerances and variations in the design parameters are added to the total uncertainty. For region II analyses, the effects of axial burnup profile and burnable poison rods, and uncertainty from the depletion calculation methodology are considered in the calculation K_{eff} .

Calculated K_{eff} including all biases and uncertainties is compared with design criterion in 10 CFR 50.68 in order to show the subcriticality of the new and spent fuel storage racks for normal conditions and postulated accidents. For the spent fuel pool region II, the curve for the minimum-burnup and initial loading enrichment is generated based on the K_{eff} s calculated for each enrichment and burnup.

9.1.1.3.4 Criticality Analysis for New and Spent Fuel Storage Racks

Criticality analyses for new and spent fuel storage racks are performed. The results show that the design criterion in 10 CFR 50.68 is met and that the subcriticality is maintained (Reference 10).

9.1.2 New and Spent Fuel Storage

9.1.2.1 Design Bases

The following design bases are imposed on the storage of new and spent fuel assemblies:

New Fuel Storage

- a. The new fuel storage pit is protected from the effects of natural phenomena, including earthquakes, tornadoes, hurricanes, floods, and external missiles. The new fuel storage racks meet the guidance in NRC RG 1.13 (Reference 11), NRC RG 1.29 (Reference 12), NRC RG 1.115 (Reference 13), NRC RG 1.117

(Reference 14), and ANSI/ANS 57.3 (Reference 15), as applicable to General Design Criterion (GDC) 2.

- b. All requirements of NRC RG 1.13 are met excluding those regarding the spent fuel pool water supply because new fuel storage is dry condition. The new fuel storage pit is designed to provide reasonable assurance that any light load, as described in Subsection 9.1.4.2.1, does not exceed the design impact energy capacity of the rack if the load is postulated to fall from its operational height over the new fuel storage racks. In addition, all heavy loads, as described in Subsection 9.1.4.2.1, are prevented from traveling over the new fuel storage racks by the use of mechanical and electrical interlocks on the cask handling hoist.
- c. The new fuel storage racks and facilities are designed to meet GDC 2, 5, 61, 62 and 63 of 10 CFR Part 50 Appendix A and qualified as seismic Category I per NRC RG 1.29, as described in Subsection 9.1.1.3.3.
- d. The fuel handling equipment located in the new fuel storage area meets the requirements of ANSI/ANS 57.1 (Reference 16). The new fuel storage racks meet the requirements of ANSI/ANS 57.3.
- e. The new fuel storage racks provide onsite storage capacity of 112 new fuel assemblies. This capacity, which represents 46 percent of the fuel assemblies in the core, envelops a reload batch based on a refueling cycle of 18 months.

applicable acceptance criteria

- f. The new fuel storage racks are designed to meet the ~~requirements~~ of Standard Review Plan (SRP) 3.8.4, Appendix D, which addresses appropriate combinations of ~~seismic and dropped loads with~~ allowable stress/deformation limits.

and

load

The applicable loads and load combinations used in the structural analysis of the new fuel storage racks are provided in Table 3.8-9C. The acceptance criteria are defined in ASME Code Section III, Subsection NF requirements for Class 3 component supports.

Spent Fuel Storage

- a. The spent fuel pool is protected from the effects of natural phenomena, including earthquakes, tornadoes, hurricanes, floods, and external missiles. The spent fuel storage racks meet the guidance in NRC RG 1.13, NRC RG 1.29, NRC RG 1.115, NRC RG 1.117, and ANSI/ANS 57.2 as applicable to GDC 2.
- b. All requirements of NRC RG 1.13 are met. The spent fuel pool is designed to prevent a loss of water in the spent fuel pool resulting in uncovering of the fuel, to prevent heavy loads from traversing over the spent fuel storage racks when the racks contain fuel assemblies, to withstand the impact of fuel assembly or a handling tool or a combination of both falling from the maximum handling elevation, to incorporate components that meet the seismic classification designated in Table 3.2-1, and to incorporate water level and radiation monitoring instrumentation. a
- c. The spent fuel storage racks and facilities are designed to meet the GDC 2, 4, 5, 61, and 62 of 10 CFR Part 50 Appendix A and qualified as seismic Category I per NRC RG 1.29, as described Subsection 9.1.1.3.3.
- d. The fuel handling equipment in the spent fuel storage area meets the requirements of ANSI/ANS 57.1. The spent fuel pool meets the requirements of ANSI/ANS 57.2 (Reference 17).
- e. The spent fuel storage racks provide onsite storage capability for one full core and one maximum refueling batch including the storage of five damaged fuel canisters plus a 20-year quantity of discharged fuel based on a refueling cycle of 18 months. All components within the area of the fuel racks meet the requirements of Table 3.2-1 to preclude rack damage.
- f. The spent fuel storage racks are designed to meet the applicable acceptance criteria ~~requirements~~ of SRP 3.8.4 Appendix D, which addresses appropriate combinations of seismic and ~~dropped loads with~~ allowable stress/deformation limits. load and

9. NUREG/CR-6979, "Evaluation of the French Haut Taux de Combustion (HTC) Critical Experiment Data," U.S. Nuclear Regulatory Commission, September 2008.
10. APR1400-Z-A-NR-14011-P, "Criticality Analysis of New and Spent Fuel Storage Racks," KHNP, November 2014.
11. Regulatory Guide 1.13, "Spent Fuel Storage Facility Design Basis," Rev. 2, U.S. Nuclear Regulatory Commission, March 2007.
12. Regulatory Guide 1.29, "Seismic Design Classification," Rev. 4, U.S. Nuclear Regulatory Commission, March 2007.
13. Regulatory Guide 1.115, "Protection Against Low-Trajectory Turbine Missiles," U.S. Nuclear Regulatory Commission, January 2012.
14. Regulatory Guide 1.117, "Tornado Design Classification," U.S. Nuclear Regulatory Commission, April 1978.
15. ANSI/ANS 57.3, "Design Requirements for New Fuel Storage Facilities at Light-Water Reactor Plants," American Nuclear Society, 1983.
16. ANSI/ANS 57.1, "Design Requirements for Light Water Reactor Fuel Handling System," American Nuclear Society, 1992.
17. ANSI/ANS 57.2, "Design Requirements for Light Water Reactor Spent Fuel Storage Facilities at Nuclear Power Plants," American Nuclear Society, 1983.
18. 10 CFR 20.1406, "Radiological Criteria for Unrestricted Use," U.S. Nuclear Regulatory Commission.
19. Regulatory Guide 4.21, "Minimization of Contamination and Radioactive Waste Generator: Life – Cycle Planning," U.S. Nuclear Regulatory Commission, June 2008.
20. APR1400-H-N-NR-14012-P & NP, "Mechanical Analysis for New and Spent Fuel Storage Racks," KHNP, ~~December 2014~~.

21. ASME NOG-1, "Rules for Construction of Overhead and Gantry Cranes," The American Society of Mechanical Engineers, 2010.

The APR1400 SFSTRs are free-standing; thus, there is no or minimal restraint against free thermal expansion at the base of the rack. Moreover, stresses induced due to thermal expansion will be secondary stresses since they are self-limiting, and have no stipulated stress limits in Class 3 structures or components when acting in concert with seismic loadings. Therefore, thermal loads applied to the racks are not included in the stress combinations involving seismic loadings. ASME Code Section III, Division 1, Subsection NF and Appendix F are applied as stress limits criteria of fuel storage rack for service conditions.

Material properties for analysis and stress evaluation are provided in subsection 3.4.4.

3.2.2.1 Normal Conditions (Level A)

(1) Stress in Tension

The allowable stress in tension on a net section (F_t) is given in NF-3321.1(a)(1).

$$F_t = 0.6 S_y \text{ [but not more than } 0.5 S_u \text{]}$$

Where,

S_y = yield strength of material at a given temperature, and
 S_u = ultimate strength of material at a given temperature.

(2) Stress in Shear

The allowable stress in shear on a net section (F_v) is given in NF-3322.1(b)(1).

$$F_v = 0.4 S_y$$

(3) Stress in Compression

The allowable stress in compression on a net section (F_a) of austenitic stainless steel is given in NF-3322.1(c)(2).

$$F_a = S_y (0.47 - k \cdot l/444r)$$

Where,

kl/r is less than or equal to 120 for all sections,

l = unsupported length of component,

k = length coefficient which gives influence of boundary conditions, e.g.,

$k = 1$; simple support both ends,

$k = 2$; cantilever beam, conservatively used for evaluations,

$k = 0.5$; clamped at both ends, and

r = radius of gyration of component.

(4) Stress in Bending

The allowable bending stress (F_b) resulting from tension and compression on extreme fibers of box-type flexural members is given in NF-3322.1(d)(4).

$$F_b = 0.60 S_y$$

(5) Combined Stress (Combined Bending and Compression Loads)

Combined bending and compression load on a net section per NF-3322.1(e)(1) satisfies the following equation.

$$f_a/F_a + C_{mx}f_{bx}/D_xF_{bx} + C_{my}f_{by}/D_yF_{by} \leq 1.0$$

Where,

- f_a = Direct compressive stress in the section,
 f_{bx} = Maximum bending stress along x-axis,
 f_{by} = Maximum bending stress along y-axis,
 C_{mx} = 0.85,
 C_{my} = 0.85,
 D_x = $1 - (f_a/F'_{ex})$,
 D_y = $1 - (f_a/F'_{ey})$,
 F'_{ex}, F'_{ey} = $(\pi^2 E)/(2.15 (kl/r)_{x,y}^2)$,
 and subscripts x and y reflect the particular bending plane.

(6) Combined Stress (Combined Flexure and Tension Loads)

Combined flexure and tension/compression load on a net section satisfies the following equation given in NF-3322.1(e).

$$(f_a/0.6 S_y) + (f_{bx}/F_{bx}) + (f_{by}/F_{by}) \leq 1.0$$

(7) Welds

The allowable maximum shear stress on the net section of a weld (F_w) is given in Table NF-3324.5(a)-1.

$$F_w = 0.3 S_u$$

Where, S_u is the weld material ultimate strength at temperature. For the area in contact with the base metal, the shear stress on the gross section is limited to $0.4 S_y$. Where, S_y is the yield strength of material at a given temperature.

3.2.2.2 Upset Conditions (Level B)

The stress limits for Level B are those for Level A multiplied by the stress limit factor specified in Table NF-3523(b)-1 (Reference 4).

3.2.2.3 Faulted/Abnormal (Level D)

Article F-1334 (ASME Section III, Appendix F (Reference 4), states that limits for the Level D condition are the smaller of 2 or $1.167 S_u/S_y$ times the corresponding limits for the Level A condition if $S_u > 1.2 S_y$, or 1.4 if $S_u \leq 1.2 S_y$ except for requirements specifically listed below. S_u and S_y are the ultimate strength and yield strength at the specified rack design temperature. Examination of material properties for 304L stainless demonstrates that 1.2 times the yield strength is less than the ultimate strength. Since $1.167 \times (66,100/21,400) = 3.60$, the multiplier of 2.0 controls.

Exceptions to the above general multiplier are the following:

- (1) The tensile stress on the net section shall not exceed the lesser of $1.2 S_y$ and $0.7 S_u$.
- (2) The shear stress on the gross section shall not exceed the lesser of $0.72 S_y$ or $0.42 S_u$. In the case of the austenitic stainless steel material used here, $0.72 S_y$ governs.
- (3) Combined axial compression and bending - The equations for Level A conditions shall apply except that $F_a = 2/3 \times$ Buckling Load, and F'_{ex} and F'_{ey} may be increased by the factor 1.65.

- Rack weld stresses and safety factors – used to confirm racks maintain their structural integrity [Table 3-12]
- Stress on fuel assembly – used to confirm fuel assemblies are not damaged to the extent that cladding is breached [Table 3-11]
- Stresses on the threads of the SFSR pedestal leveling feet – used to assess damage to threads [Table 3-13]
- Stresses on the NFSR stud bolt - used to confirm NFSR stud bolts maintain their structural integrity [Table 3-14]

The seismic responses in the horizontal directions are combined using the square root of the sum of the squares (SRSS) method in the analysis of the fuel assembly, rack structure, welded connections, and the rack supports of NFSR and SFSR. For all horizontal loads except fuel assembly grid impact, the SRSS combination uses the maximum E-W and the maximum N-S load at any time during the transient, even if they do not occur during the same time step. The grid impact loads use the values during the same time step to find the maximum.

3.7.1 Time History Simulation Results

The loads and the displacements by dynamic simulations are summarized in Table 3-6 through Table 3-8 and in Figure 3-20 through Figure 3-26. Note that the values shown are maximum values found for any of the racks for each run. Where horizontal loads are reported, they are for the same rack, but the vertical load reported for that run may be from a different rack. For the SFSRs, results are reported for both Region I and Region II racks since they are slightly different structurally and have different rack-to-rack spacing.

3.7.1.1 Displacements of Rack

The NFSRs are fixed and not subject to displacement at their bases provided their stud bolts remain intact, as shown in Figure 2-3. The displacement of the NFSRs at their top is determined to confirm there is no contact between adjacent cells or with the new fuel storage pit walls.

The SFSRs are specified to be installed with pedestals and baseplates as close as possible, as shown in Figure 2-6. Therefore, during a seismic event they will initially move apart, although they could again slide together during the transient. Due to the random nature of the seismic acceleration, the racks will move in different directions by different amounts, and this can be affected by the time step and COF used in the analysis. This randomness would be true even if experiments were run repeatedly using different time histories. The initial movement can determine the ultimate relative position of racks to each other. As discussed in Section 3.1.1, a baseline correction process has been used to eliminate unrealistic cumulative displacement leading to large final displacements. The use of five independent time histories with sensitivities for COF and rack loading provides a reasonable range of possible displacements. Since none of the runs predicted displacements of more than a small fraction of the gap between the outermost racks to SFP wall, contact of cells between SFSRs and the SFP walls is not expected. The baseplates of adjacent racks can come into contact at some velocity if they initially move apart and then back together, as discussed in Section 3.7.1.3.

Presuming that the racks are in contact at their bases, flexure of the racks along their height could cause the top ends of adjacent racks to come into contact. The maximum reduction in gap between adjacent racks (i.e., larger values indicate the rack upper structures to be closer to each other) are shown in Table 3-6. The minimum gap for the cell-to-cell contact in Region I is 60.0 mm (2.36 in), and that of Region II is 30.0 mm (1.18 in), as shown in Figure 2-5. Therefore, there is no impact on the rack cells by each other, because the maximum relative displacements of racks are smaller than the cell wall separation with baseplates touching.

Table 3-9 Maximum Stress Factors on Racks

Service Level	Rack	Pedestal Stress Factors			Cell Wall Stress Factors			COF
		FACT1	FACT2	FACT3	FACT1	FACT2	FACT3	
A	NFSRs	0.060	0.044	-	0.030	0.032	-	N/A
	SFSRs (Region I)	0.032	0.024	-	$\frac{0.034}{0.779^{(2)}} = 0.044$	0.037	-	N/A
	SFSRs (Region II)	0.034	0.026	-	$\frac{0.042}{0.779^{(2)}} = 0.054$	0.045	-	N/A
D	NFSRs	0.731	0.829	0.617	0.067	0.073	0.049	N/A
	SFSRs (Region I)	0.148	0.125	0.130	$\frac{0.181}{0.779^{(2)}} = 0.235$	0.194	0.045	0.8
	SFSRs (Region II)	0.168	0.140	0.155	$\frac{0.376}{0.779^{(2)}} = 0.483$	0.401	0.097	0.8

Notes:

- (1) Dimensionless stress factors, FACT1, FACT2, and FACT3, are described in Section 3.2.3.
- (2) Stress correction factor considering slenderness ratio (from Appendix F.3 through F.5 of Reference 17)
- (3) Since the width-thickness ratio of NFSR is not greater than 51.4, no additional adjustment for the stress is necessary.

Table 3-10 Overturning Evaluation of Racks

Run No.	Rack No.	Relative Displacement	Angle of Rotation	Allowable Rotation	Safety Factor (1.5 required)
24	B5-4	10 mm (0.392 in)	0.12°	18.5°	154

(4) Stuck Fuel Assembly (Scenario 4)

The fuel racks are adequate to withstand the uplift force of 22.2 kN (5,000 lbf) due to a stuck fuel assembly because the neutron absorbing poison plate is not damaged and structural integrity of the rack is maintained. Two cases are considered:

- (a) For vertical uplift when a fuel assembly was nearly free of the top of a SFSR, the effect is concentrated at the top of the rack structure along a single cell wall. If the vertical uplift force is resisted only by shear stress, the allowable shear stress level be limit is:

$$\tau_y = 1.33 * 0.4 * S_y = 1.33 * 0.4 * 21,400 \text{ psi} = 11,385 \text{ psi}$$

The depth of the cell structure h_{sf} that can support the load is obtained from

$$h_{sf} = \frac{F_e}{2 * \tau_y * t_{cell}} = \frac{5000 \text{ lbf}}{2 * 11,385 \text{ psi} * 0.098 \text{ in}} = 2.24 \text{ in}$$

Where,

t_{cell} = cell wall thickness of 0.098 in

The top of the neutron absorbing plate is at about 24.0 inches below the top of the cell wall. Since the damaged area is above the location of the neutron absorber and is limited to a small section of one cell wall, margin to criticality and structural integrity are not affected.

- (b) For vertical uplift when a fuel assembly is fully seated, the force is assumed to be resisted by a single cell wall, which is 0.098 in thick and 8.66 in wide. If the stress is uniformly distributed across that cross section, it is equal to

$$\sigma = \frac{F_e}{D_{cell} * t_{cell}} = \frac{5000 \text{ lbf}}{8.66 \text{ in} * 0.098 \text{ in}} = 5892 \text{ psi}$$

The calculated stress is less than allowable tensile stress ($1.33 * 0.6 * S_y = 17,077 \text{ psi}$), which means that damage to the cell wall will not occur.

The results of the evaluation for the cell wall tensile stress, cell to cell weld shear stress, and the base metal shear stress for stuck fuel assembly accident scenario are summarized in Table 4-2.

The forces caused by uplift of a stuck fuel assembly does not cause damage that affects the margin to criticality or structural integrity.

REVISED RESPONSE TO REQUEST FOR ADDITIONAL INFORMATION**APR1400 Design Certification****Korea Electric Power Corporation / Korea Hydro & Nuclear Power Co., LTD****Docket No. 52-046**

RAI No.: 287-8272
SRP Section: 09.01.02 – New and Spent Fuel Storage
Application Section: 9.1.2
Date of RAI Issue: 11/02/2015

Question No. 09.01.02-35

The 10 CFR Part 50, Appendix A, General Design Criteria (GDC) 1, 2, 4, 5, 63, and 10CFR 52.80 (a) provide the regulatory requirements for the design of the new and spent fuel storage facilities. Standard Review Plan (SRP) Sections 9.1.2 and 3.8.4, Appendix D describes specific SRP acceptance criteria for the review of the fuel racks that are acceptable to meet the relevant requirements of the Commission's regulations identified above. In DCD Tier 2, Section 9.1.2.2.3, "New and Spent Fuel Storage Rack Design", the applicant stated that "The dynamic and stress analyses are performed as described in report APR1400-H-N-NR-14012-P & NP". In the technical report APR1400-H-N-NR-14012-P, Rev 0, Subsection 3.2.2.2, "Upset Conditions (Level B)", the Service Level B acceptance criteria states that "allowable stress of Level A is used for Level B for conservatism". The staff notes that in Section 4.3.5, "Methodology for Stuck Fuel Accident", the applicant did not use the allowable stress of Level A but instead increased the Service Level A allowable in shear to Service Level B allowable. In accordance with SRP 3.8.4 Appendix D I (6), the applicant is requested to clarify the apparent inconsistency in the implementation of its Service Level B acceptance criteria for the stuck fuel assembly scenario. The applicant is also requested to provide the results of its evaluation and safety factors for the cell wall tensile stress, cell to cell weld shear stress, and the base metal shear stress for this accident scenario. The applicant is requested to identify any proposed changes to and provide a mark-up of Subsections in the DCD Tier 2 and the report APR1400-H-N-NR-14012-P, Rev.0, as appropriate.

Response – (Rev. 0)

In technical report APR1400-H-N-NR-14012-P, Section 3.2.2.2, the sentence "The stress limit factors for Level B are larger than those for Level A. However, allowable stress of Level A is used for Level B for conservatism" will be deleted to be consistent with the Section 4.3.5, "Methodology for Stuck Fuel Accident".

For the stuck fuel accident analysis, the critical location for load application is to have the uplift load applied near the top of the rack along a single cell wall. This set of assumptions induces the maximum tensile stress in the cellular region of the rack due to the vertical force. The stress calculations are performed manually using the strength of materials formula and the results of the stuck fuel assembly are summarized in the table below:

Region	Stress Category	Calculated Stress MPa (psi)	Allowable Stress ⁽¹⁾ MPa (psi)	Safety Factor
Cell Wall	Tensile	36.9 (5,354)	117.7 (17,077)	2.9
Cell-to-Cell Weld	Shear	8.9 (1,294)	136.7 (19,830)	15.3
Base Metal	Shear	8.9 (1,294)	78.5 (11,385)	8.8

Note)

(1) Per Appendix D of SRP 3.8.4, the allowable stresses for Level B service condition were applied to the stuck fuel assembly load.

Response – (Rev. 1)

Technical report, APR1400-H-N-NR-14012-NP was submitted as Rev. 0 in December, 2014. KHNP responses to RAI 287-8272 were based in part on the Technical Report. Subsequent to issuance of the Technical Report and RAI responses, the NRC provided feedback on both the Technical Report and RAI 287-8272 responses. In response to this NRC feedback, Technical report, APR1400-H-N-NR-14012-NP will be revised (as Rev. 3) to incorporate additional information pertaining to the fuel racks. This RAI revision contains the specific Technical Report revisions relevant to this response and associated DCD changes, where necessary. A summary of the additional information is in the below paragraphs.

Acceptance Criteria for Stuck Fuel Assembly

The stuck fuel assembly is evaluated to Level B service limits to ensure the integrity of the rack is unaffected.

Results of Stuck Fuel Assembly

The fuel racks are adequate to withstand the uplift force of 22.2 kN (5,000 lbf) due to a stuck fuel assembly because the neutron absorbing poison plate is not damaged and structural integrity of the rack is maintained. Two cases are considered:

- (a) For vertical uplift when a fuel assembly was nearly free of the top of a SF/SR, the effect is concentrated at the top of the rack structure along a single cell wall. If the vertical uplift force is resisted only by shear stress, the allowable shear stress level be limit is:

$$\tau_y = 1.33 * 0.4 * S_y = 1.33 * 0.4 * 21,400 \text{ psi} = 11,385 \text{ psi}$$

The depth of the cell structure h_{sf} that can support the load is obtained from

$$h_{sf} = \frac{F_e}{2 * \tau_y * t_{cell}} = \frac{5000 \text{ lbf}}{2 * 11,385 \text{ psi} * 0.098 \text{ in}} = 2.24 \text{ in}$$

Where,

t_{cell} = cell wall thickness of 0.098 in

The top of the neutron absorbing plate is at about 24.0 inches below the top of the cell wall. Since the damaged area is above the location of the neutron absorber and is limited to a small section of one cell wall, margin to criticality and structural integrity are not affected.

- (b) For vertical uplift when a fuel assembly is fully seated, the force is assumed to be resisted by a single cell wall, which is 0.098 in thick and 8.66 in wide. If the stress is uniformly distributed across that cross section, it is equal to

$$\sigma = \frac{F_e}{D_{cell} * t_{cell}} = \frac{5000 \text{ lbf}}{8.66 \text{ in} * 0.098 \text{ in}} = 5892 \text{ psi}$$

The calculated stress is less than allowable tensile stress ($1.33 * 0.6 * S_y = 17,077 \text{ psi}$), which means that damage to the cell wall will not occur.

The results of the evaluation for the cell wall tensile stress, cell to cell weld shear stress, and the base metal shear stress for stuck fuel assembly accident scenario are summarized in Table 1.

The forces caused by uplift of a stuck fuel assembly does not cause damage that affects the margin to criticality or structural integrity.

Table 1 Stress Evaluation for Stuck Fuel Assembly

Region	Stress Category	Calculated Stress MPa (psi)	Allowable Stress ⁽¹⁾ MPa (psi)
Cell Wall	Tensile	40.6 (5,892)	117.7 (17,077)
Cell-to-Cell Weld	Shear	8.9 (1,294)	136.7 (19,830)
Base Metal	Shear	8.9 (1,294)	78.5 (11,385)

Note:

- (1) Per Appendix D of SRP 3.8.4, the allowable stresses for Level B service condition were applied to the stuck fuel assembly load.

Impact on DCD

There is no impact on the DCD.

Impact on PRA

There is no impact on the PRA.

Impact on Technical Specifications

There is no impact on the Technical Specifications.

Impact on Technical/Topical/Environmental Reports

[APR1400-H-N-NR-14012-NP \(Rev. 3\)](#), Sections 4.2(4), 4.5(4) and Table 4-2 will be revised as shown in Attachment 1 to this response.

SFSR (limited by the motor stall torque or load-limiting device of the crane used to load fuel into the racks) represents the maximum uplift force of a stuck fuel assembly.

4.2 Acceptance Criteria

For mechanical accidents above, the acceptance criteria to ensure damage of the racks is limited as described below:

(1) Straight Shallow Drop (Scenario 1)

For the postulated shallow drop event, the crushed rack walls must not extend down into the "poison zone" that shadows the entire length of the active fuel. This will ensure that the configuration analyzed in the criticality evaluation remains valid. The distance measured from the top of the rack to the upper boundary of the "poison zone" is 610 mm (24.0 in). The depth of damage to the impacted cell walls must be demonstrated to remain limited to the portion of the cell above the top of the "poison zone", which is the elevation of the top of the neutron absorber. This will ensure that the configuration analyzed in the criticality evaluation remains valid. The distance measured from the top of the rack to the upper boundary of the "poison zone" is 0.61 m (2 ft).

(2) Straight Deep Drop (Scenario 2; Away from the pedestal)

The dropping mass impacts the rack baseplate. The acceptance criteria are that the baseplate is not pierced and that the deformed baseplate of the rack must not impact the concrete floor (NFSRs) or pool liner (SFSRs). The normal separation between the underside of the NFSR baseplate and the pit floor is 185 mm (7.28 in) and between the underside of the SFSR baseplate and pool liner is 160 mm (6.30 in).

(3) Straight Deep Drop (Scenario 3; Over a pedestal)

For the postulated deep drop event (over a pedestal), the compressive stress on the concrete floor underneath the embedment plates shall not exceed the maximum allowable stress of 16.4 MPa (2,375 psi) as specified on the paragraph 5.3.4.4 of design specification (Reference 22).

(4) Stuck Fuel Assembly (Scenario 4)

The stuck fuel assembly is evaluated to Level B service limits to ensure the integrity of the rack is unaffected.

4.3 Analysis Method

The finite element method is used for the impact analysis of the postulated drop accidents. ANSYS LS-DYNA, a commercial computer code that has been independently validated by Doosan (Reference 30), is used to numerically simulate the impact events. For uplift force, a classical strength of materials calculation is used to determine the amount of area needed to support the forces.

4.3.1 Assumptions

- Scenario masses and heights are constrained as follows:
 - Fuel assembly plus handling tool (1,100 kg (2,425 lbm)) drops from a maximum initial height of 0.61 m (2 ft) above the top of the rack in accordance with paragraph 5.3.4.4.2 of the rack design specification (Reference 22) for all drop scenarios.
 - Transport container handling tool (214.55 kg (473 lbm)) drops from a maximum initial height of 5.0 m (196.8 in) above the top of the rack for shallow drop scenario rack in accordance with paragraph 5.3.4.4.2 of the rack design specification (Reference 22).

(4) Stuck Fuel Assembly (Scenario 4)

The fuel racks are adequate to withstand the uplift force of 22.2 kN (5,000 lbf) due to a stuck fuel assembly because the neutron absorbing poison plate is not damaged and structural integrity of the rack is maintained. Two cases are considered:

- (a) For vertical uplift when a fuel assembly was nearly free of the top of a SFSR, the effect is concentrated at the top of the rack structure along a single cell wall. If the vertical uplift force is resisted only by shear stress, the allowable shear stress level be limit is:

$$\tau_y = 1.33 * 0.4 * S_y = 1.33 * 0.4 * 21,400 \text{ psi} = 11,385 \text{ psi}$$

The depth of the cell structure h_{sf} that can support the load is obtained from

$$h_{sf} = \frac{F_e}{2 * \tau_y * t_{cell}} = \frac{5000 \text{ lbf}}{2 * 11,385 \text{ psi} * 0.098 \text{ in}} = 2.24 \text{ in}$$

Where,

t_{cell} = cell wall thickness of 0.098 in

The top of the neutron absorbing plate is at about 24.0 inches below the top of the cell wall. Since the damaged area is above the location of the neutron absorber and is limited to a small section of one cell wall, margin to criticality and structural integrity are not affected.

- (b) For vertical uplift when a fuel assembly is fully seated, the force is assumed to be resisted by a single cell wall, which is 0.098 in thick and 8.66 in wide. If the stress is uniformly distributed across that cross section, it is equal to

$$\sigma = \frac{F_e}{D_{cell} * t_{cell}} = \frac{5000 \text{ lbf}}{8.66 \text{ in} * 0.098 \text{ in}} = 5892 \text{ psi}$$

The calculated stress is less than allowable tensile stress ($1.33 * 0.6 * S_y = 17,077 \text{ psi}$), which means that damage to the cell wall will not occur.

The results of the evaluation for the cell wall tensile stress, cell to cell weld shear stress, and the base metal shear stress for stuck fuel assembly accident scenario are summarized in Table 4-2.

The forces caused by uplift of a stuck fuel assembly does not cause damage that affects the margin to criticality or structural integrity.

Table 4-1 Impact Evaluation Data

Rack	Cases		Drop Weight ^(*) , kN (lbf)	Drop Height, m (in)	Impact Velocity, m/sec (in/sec)
NFSR	Straight Deep Drop (Away from Pedestal)		10.8 (2,425)	5.18 (203.9)	10.1 (396.8)
SFSR	Straight Shallow Drop		10.8 (2,425)	0.61 (24.0)	3.14 (123.6)
			2.1 (473)	4.98 (196.0)	7.15 (281.3)
	Straight Deep Drop (Away from Pedestal)	Region I	10.8 (2,425)	5.2 (204.7)	8.22 (323.5)
		Region II			7.36 (289.6)
Straight Deep Drop (Over a Pedestal)		10.8 (2,425)	5.2 (204.7)	3.93 (154.9)	

(*) Drop Weight = Fuel assembly along with the handling tool (2,425 lbf) or transport container handling tool (473 lbf)

Table 4-2 Stress Evaluation for Stuck Fuel Assembly

Region	Stress Category	Calculated Stress MPa (psi)	Allowable Stress ⁽¹⁾ MPa (psi)
Cell Wall	Tensile	40.6 (5,892)	117.7 (17,077)
Cell-to-Cell Weld	Shear	8.9 (1,294)	136.7 (19,830)
Base Metal	Shear	8.9 (1,294)	78.5 (11,385)

Note:

(1) Per Appendix D of SRP 3.8.4, the allowable stresses for Level B service condition were applied to the stuck fuel assembly load.

REVISED RESPONSE TO REQUEST FOR ADDITIONAL INFORMATION**APR1400 Design Certification****Korea Electric Power Corporation / Korea Hydro & Nuclear Power Co., LTD****Docket No. 52-046**

RAI No.: 287-8272

SRP Section: 09.01.02 – New and Spent Fuel Storage

Application Section: 9.1.2

Date of RAI Issue: 11/02/2015

Question No. 09.01.02-36

1. The 10 CFR Part 50, Appendix A, General Design Criteria (GDC) 1, 2, 4, 5, 63, and 10CFR 52.80 (a) provide the regulatory requirements for the design of the new and spent fuel storage facilities. Standard Review Plan (SRP) Sections 9.1.2 and 3.8.4, Appendix D describes specific SRP acceptance criteria for the review of the fuel racks that are acceptable to meet the relevant requirements of the Commission's regulations identified above. In DCD Tier 2, Section 9.1.2.2.3, "New and Spent Fuel Storage Rack Design", the applicant stated that "The dynamic and stress analyses are performed as described in report APR1400-H-N-NR-14012-P & NP". In the technical report APR1400-H-N-NR-14012-P, Rev 0, Subsection 3.7.1.1, "Displacements of Rack", it is stated that "Actually, impact on rack-to-rack occurs at baseplate of the SFSRs because the installed racks are in contact with each other. The maximum impact loads generated at the NFSRs and the SFSRs are summarized in Table 3-10." In Subsection 3.7.1.3 (2), "Impact Loads", it is stated that "The prominent baseplate of the fuel storage rack for the APR1400 design is installed almost in contact with the adjacent baseplate."

In accordance with SRP 3.8.4 Appendix D I (3, 5), the applicant is requested to provide the following information so that the staff can perform its safety evaluation of the seismic analysis of new and spent fuel storage racks (NFSR and SFSR).

- a. For NFSR and SFSR, provide the baseplate dimensions and layout and plan view clearly showing gap or no gap between the adjacent baseplates; the gaps between the baseplates and the spent fuel pool walls; and the rack-to-rack gaps at midheight and at the top of the racks. Identify the elevation of the gaps shown in Figure 2-4.
- b. Discuss how the effect of adjacent baseplates that are in contact is modeled in the nonlinear dynamic models.

- c. The pool multi-rack dynamic analysis model in Figure 3-2 shows gaps between the adjacent base plates of all 29 racks. Describe how the contact between the baseplates is modeled in the whole pool multi-rack model. If the racks are installed such that their baseplates are in contact, provide the technical basis why the whole pool multi-rack model, with gaps, shown in Figure 3-2, predicts conservative dynamic responses for the racks and SFP walls.
- d. Discuss how the thermal load effects are considered for the installed racks that are in contact (no gap) with each other at the baseplate. Also discuss the effect on the design forces at the pedestal due to the thermal expansion of the installed racks.
- e. The applicant is requested to provide COL information items that include the development of post seismic event inspection procedures to measure gaps between the new and spent fuel storage racks.

The applicant is requested to identify any proposed changes to and provide a mark-up of Subsections in the DCD Tier 2 and the report APR1400-H-N-NR-14012-P, Rev.0, as appropriate.

Response – (Rev. 0)

- a. The baseplate dimensions and layout and plan view for NFSR and SF SR as below figures.



TS

New Fuel Storage Rack Layout



Spent Fuel Storage Rack Layout

Spent Fuel Storage Rack Layout

- b. The adjacent baseplates are connected by a spring element and the stiffness value of the baseplate is assigned to the impact spring for impact phenomena. Figure 3-4 of the report APR1400-H-N-NR-14012-P shows schematic of spring element used for SFSR.
- c. The baseplate of the fuel storage rack is installed barely in contact with the adjacent baseplate.
Therefore, the contact between the baseplates in the whole pool multi-rack model is modeled by ANSYS CONTAC52 element. Figure 3-2 shows the simplified rack beam model except ANSYS CONTAC52 element.
- d. The effect of the thermal load and the thermal expansion for the installed racks is addressed in the report APR1400-H-N-NR-14012-P, Section 3.2.2 and the response for question number 09.01.02-11. The APR1400 SFSRs are free-standing; thus, there is no or minimal restraint against free thermal expansion at the base of the pedestal.
Therefore, the effect of thermal load on the rack baseplate was not considered.

- e. A COL item for including the development of post seismic event inspection procedures will be added in DCD Tier 2 Subsection 9.1.2.3.1 and 9.1.2.3.2.

Response – (Rev. 1)

Technical report, APR1400-H-N-NR-14012-NP was submitted as Rev. 0 in December, 2014. KHNP responses to RAI 287-8272 were based in part on the Technical Report. Subsequent to issuance of the Technical Report and RAI responses, the NRC provided feedback on both the Technical Report and RAI 287-8272 responses. In response to this NRC feedback, Technical report, APR1400-H-N-NR-14012-NP will be revised (as Rev. 3) to incorporate additional information pertaining to the fuel racks. This RAI revision contains the specific Technical Report revisions relevant to this response and associated DCD changes, where necessary. A summary of the additional information is in the below paragraphs.

- a. Figures 1, 2, and 3 show the layout and plan view for NFSR and SFSR



Figure 1 Layout and Plan View of NFSR



Figure 2 Plan View of SFSR Showing Rack Gaps above Baseplate Level

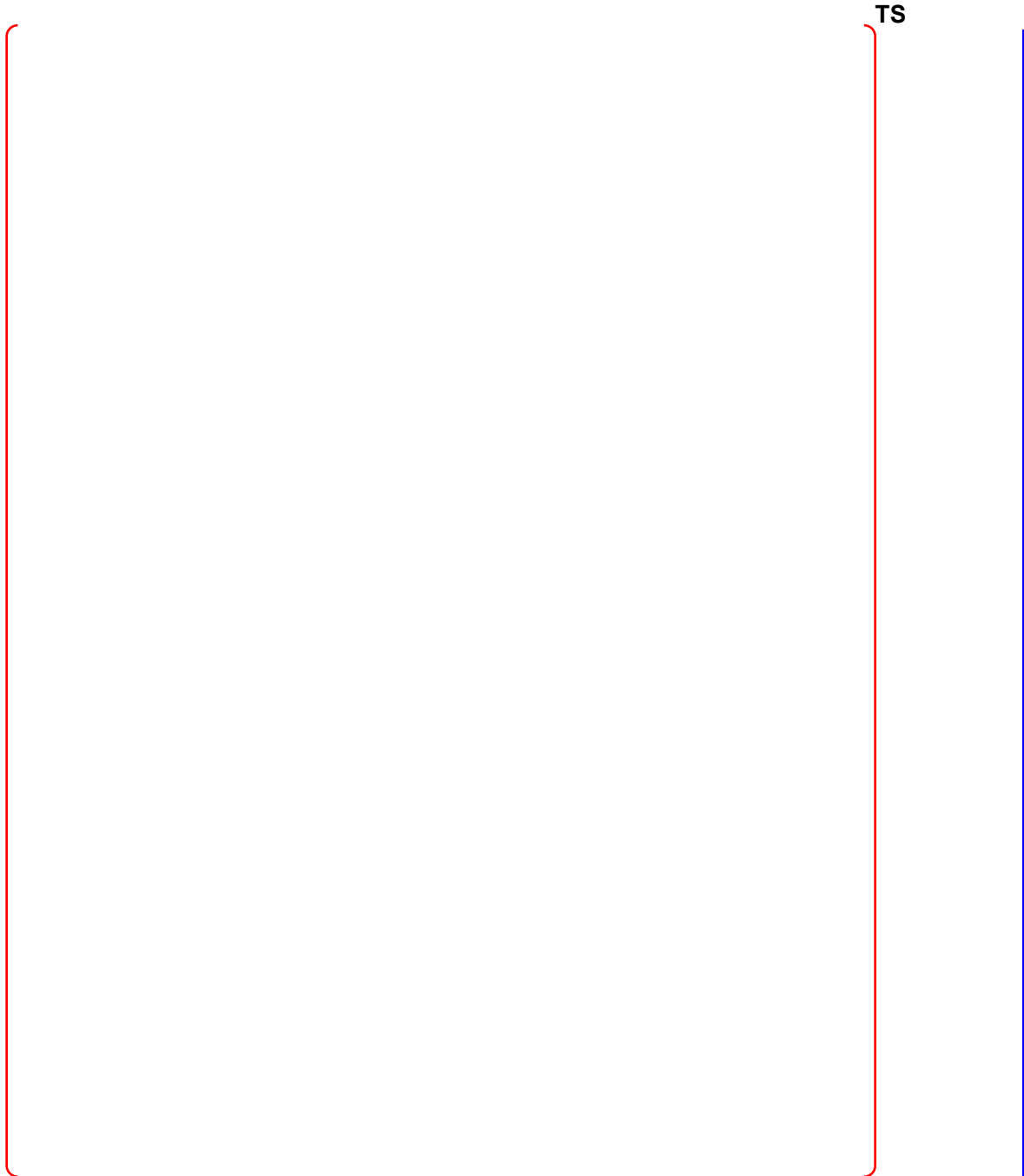


Figure 3 Plan View of SFSR Showing Rack Gaps at Baseplates

b. Gaps between fuel assemblies and rack cell walls/baseplate, adjacent rack baseplates, and pedestals and embedment plates are modeled with contact elements in the WPMR analysis.

Contact (i.e., gap) elements are used in the representation of rack sliding and impact. A directional stiffness is assigned to the contact element. The pool floor is assumed to be a rigid body initially in contact with the rack pedestals. The contact elements are used to represent

potential impact of a rack pedestal on the pool floor. The coefficient of friction between the rack pedestals and pool floor is incorporated into a contact (gap) element.

Two types of stiffness are used in the SFSR model: 3-D elastic beam elements, as discussed above, and contact elements. The contact elements are used to calculate horizontal loads due to friction (between the rack pedestal and embedment plate) and impacts (fuel-to-cell wall, rack-to-rack, and pedestal-to-embedment plate). The contact element used is ANSYS CONTAC52.

CONTAC52 represents two surfaces that may maintain or break physical contact and may slide relative to each other. This element is capable of supporting only compression in the direction normal to the surfaces and shear (coulomb friction) in the tangential direction. The element has three degrees of freedom at each node (x, y, and z). A specified stiffness acts in the normal and tangential directions when the gap is closed.

c. The SFSRs are specified to be installed with pedestals and baseplates as close as possible, as shown in Figure 3. Therefore, during a seismic event they will initially move apart, although they could again slide together during the transient. Due to the random nature of the seismic acceleration, the racks will move in different directions by different amounts, and this can be affected by the time step and COF used in the analysis. This randomness would be true even if experiments were run repeatedly using different time histories. The initial movement can determine the ultimate relative position of racks to each other. A baseline correction process has been used to eliminate unrealistic cumulative displacement leading to large final displacements. The use of five independent time histories with sensitivities for COF and rack loading provides a reasonable range of possible displacements. Since none of the runs predicted displacements of more than a small fraction of the gap between the outermost racks to SFP wall, contact of cells between SFSRs and the SFP walls is not expected. The baseplates of adjacent racks can come into contact at some velocity if they initially move apart and then back together.

d. A temperature induced stress is expansion of adjacent SFSRs with increased temperature resulting in a contact load between pedestals and baseplates of adjacent racks. As for the load due to expansion of each SFSR causing a contact stress, assuming the racks are installed touching at 21°C (70°F) and heat up to 48.9°C (120°F), the expansion of each rack is about 0.43 mm (0.017 in). In order to develop a load due to constraint of free end displacement, more than two adjacent racks must be in hard contact this is extremely unlikely. Therefore, the development of any significant thermal load due to restraint of free end displacement is not considered credible. Any incidental forces that might develop if some baseplates are in contact are self-limiting as a very small displacement, or shifting of the racks, relieves the stress. Self-limiting stresses developed by constraint of the structure and relieved by minor deformation are, by definition (NF-3121.3), secondary stresses.

According SRP Section 3.8.4, Appendix D, Section I.2, "Design, fabrication, and installation of fuel racks of stainless steel material may be performed based on ASME Code, Section III, Division 1, Subsection NF requirements for Class 3 component supports." For the design of Class 3 component supports, Table NF-3251.2-1, does not require the evaluation of secondary stresses. Based on this, it is concluded that the development of significant thermal loads due to constraint of the baseplates is not credible and any postulated incidental loads

need not be considered since they result in secondary stresses. Therefore, loads from the restraint of adjacent racks do not need to be explicitly considered in the design analysis.

Impact on DCD

DCD Tier 2 Section 9.1.2.3.1, 9.1.2.3.2, 9.1.6 and Table 1.8-2 will be revised as indicated in Attachment 1 to this response.

Impact on PRA

There is no impact on the PRA.

Impact on Technical Specifications

There is no impact on the Technical Specifications.

Impact on Technical/Topical/Environmental Reports

The following sections of APR1400-H-N-NR-14012-NP (Rev. 3) will be revised as shown in Attachment 2 to this response.

- a) Figure 2-1, 2-5, and 2-6
- b) Section 3.1.2.1 and 3.1.2.2
- c) Section 3.1.2.1, 3.1.2.2, and 3.7.1.1
- d) Section 3.2.2 and 3.7.3.5(3)

The new fuel assemblies are stored dry. The rack structure is designed to maintain a safe geometric array for normal and postulated accident conditions. The rack structure maintains the required degree of subcriticality for normal and postulated accident conditions such as flooding with pure water and worst-case moderator density.

9.1.2.3.2 Spent Fuel Storage Racks

The COL applicant is to provide post seismic event inspection procedures to measure gaps between the new fuel storage racks (COL 9.1(7)).

The spent fuel storage racks are designed to seismic Category I requirements (described in Section 3.2) and are capable of withstanding normal and postulated dead loads, live loads, loads resulting from thermal effects, and loads caused by an SSE.

The spent fuel racks are designed with adequate energy absorption capabilities to withstand the impact of a dropped fuel assembly from the maximum lift height of the fuel handling machine, as described in Subsection 9.1.2.3.3. Handling equipment capable of carrying loads heavier than fuel components (e.g., spent fuel cask handling crane) is prevented by design from carrying heavy loads over the spent fuel storage area. The spent fuel storage racks can withstand an uplift force greater than or equal to the uplift capability of the fuel handling machine (2,268 kg [5,000 lb]).

Materials used in rack fabrication are compatible with the storage pool environment, and surfaces that come into contact with the fuel assemblies are made of annealed austenitic stainless steel. Structural materials are corrosion resistant and do not contaminate the fuel assemblies or pool environment. The neutron absorbing material used in the rack design is suitable for the storage environment.

Design of the spent fuel storage facility is in accordance with NRC RG 1.13 (Reference 11).

The thermal-hydraulic analysis demonstrating that the flow through the spent fuel rack is adequate for decay heat removal from the spent fuel assemblies during anticipated operating conditions is provided in the thermal-hydraulic analysis report.

The spent fuel storage racks and storage facility are designed to seismic Category I requirements. The spent fuel storage rack is designed to meet the following criteria under plant conditions such as seismic or fuel handling accidents:

- a. Prevent physical damage to the stored fuel

- b. Maintain the stored fuel in a subcritical configuration
- c. Maintain the capability to remove and insert fuel assemblies
- d. Maintain the stored fuel in a coolable geometry

The spent fuel storage racks and storage facility are designed to maintain the minimum allowable fuel spacing during the fuel storage. The structural material of the spent fuel storage rack is designed to withstand corrosion from contact with the cooling water.

9.1.2.3.3 Fuel Assembly Drop Analysis

The COL applicant is to provide post seismic event inspection procedures to measure gaps between the spent fuel storage racks (COL 9.1(7)).

New and spent fuel storage racks are evaluated for withstanding a postulated drop of a fuel assembly and its associated handling tool to maintain a subcritical array assuming the maximum weight handled on each rack and the maximum drop height, as described in Table 9.1.2-1.

9.1.2.4 Inspection and Testing Requirements

Refer to Subsection 14.2.12.1.33 for the initial plant startup test program related to the proper operation of the fuel handling equipment, including the spent fuel storage rack positions.

A coupon surveillance program monitors the neutron absorbing material (METAMIC™) over the lifetime of the racks to verify their integrity. The coupons are taken from the same production lot as used for fabrication of the rack and characterized for comparison with subsequent measurements. At least one archive specimen is retained for later comparison with the irradiated coupons.

A minimum of 14 coupons are immersed into the storage racks in the SFP. Additional coupons may be used to address potential license extensions and post-shutdown fuel storage. Each coupon is large enough to obtain a tensile test specimen (approximately 10.16 × 20.32 cm [4 × 8 in]). The coupons are adjacent to freshly discharged irradiated fuel in an empty fuel compartment in regions I and II.

COL 9.1(4) The COL applicant is to provide plant procedures for preventing and mitigating inadvertent reactor cavity drain down events, maintenance procedures for the maintenance and inspection of refueling pool seal, and emergency response procedures for the proper measures during pool drain down events.

COL 9.1(5) The COL applicant is to provide plant operating procedure guidelines for preoperational load testing and checks of interlocks, blocks, hoisting cables, control circuitry, and lubrication of fuel handling equipment.

9.1.7 References

1. 10 CFR Part 50, Appendix A, General Design Criterion 62, "Prevention of Criticality in Fuel Storage and Handling," U.S. Nuclear Regulatory Commission.
2. 10 CFR 50.68, "Criticality Accident Requirements," U.S. Nuclear Regulatory Commission, November 1998.
3. DSS-ISG-2010-01, "Staff Guidance Regarding the Nuclear Criticality Safety Analysis for Spent Fuel Pools," U.S. Nuclear Regulatory Commission, October 2011.
4. NUREG/CR-6698, "Guide for Validation of Nuclear Criticality Safety Computational Methodology," U.S. Nuclear Regulatory Commission, January 2001.
5. ORNL/TM-2005/39, "Scale: A Comprehensive Modeling and Simulation Suite for Nuclear Safety Analysis and Design," Version 6.1, ORNL, June 2011.
6. M. B. Chadwick et al., "ENDF/B-VII.0 Next Generation Evaluated Nuclear Data Library for Nuclear Science and Technology," Special Issue on Evaluated Nuclear Data File ENDF/B-VII.0 Nuclear Data Sheets, 107(12), 2931-3059, December 2006.
7. NEA/NSC/DOC(95), "International Handbook of Evaluated Criticality Safety Benchmark Experiments," OECD NEA Nuclear Science Committee, September 2008.
8. NUREG/CR-6361, "Criticality Benchmark Guide for LWR Fuel in Transportation and Storage Packages," U.S. Nuclear Regulatory Commission, September 2008.

COL 9.1(7) The COL applicant is to provide post seismic event inspection procedures to measure gaps between the new and spent fuel storage racks.

Table 1.8-2 (12 of 29)

Item No.	Description
COL 9.1(4)	The COL applicant is to provide plant procedures for preventing and mitigating inadvertent reactor cavity drain down events, maintenance procedures for the maintenance and inspection of refueling pool seal, and emergency response procedures for the proper measures during pool drain down events.
COL 9.1(5)	The COL applicant is to provide plant operating procedure guidelines for preoperational load testing and checkouts of interlocks, blocks, hoisting cables, control circuitry and lubrication of fuel handling equipment.
COL 9.2(1)	The COL applicant is to develop procedures for system filling, venting, and operational procedures to minimize the potential for water hammer; to analyze the system for water hammer impacts; to design the piping system to withstand potential water hammer forces; and to analyze inadvertent water hammer events in accordance with NUREG-0927 in the ESWS.
COL 9.2(2)	The COL applicant is to develop layout of the site-specific portion of the system to minimize the potential for water hammer in the ESWS.
COL 9.2(3)	The COL applicant is to (1) to determine required pump design head, using pressure drop from the certified design portion of the plant and adding site-specific head requirements, (2) determine pump shutoff head to establish system design pressure, which is not to exceed APR1400 system design pressure, and (3) evaluate potential for vortex formation at the pump suction based on the most limiting applicable conditions in the ESWS.
COL 9.2(4)	The COL applicant is to determine the design details of the backwashing line, vent line, and their discharge locations in the ESWS.
COL 9.2(5)	The COL applicant is to provide the evaluation of the ESW pump at the high and low water levels of the UHS. In the event of approaching low UHS water level, the COL applicant is to develop a recovery procedure.
COL 9.2(6)	The COL applicant is to provide measures to prevent long-term corrosion and organic fouling that may degrade system performance in the ESWS.
COL 9.2(7)	The COL applicant is to evaluate the need and design and install freeze protection in the ESWS if required.
COL 9.2(8)	The COL applicant is to conduct periodic inspection, monitoring, maintenance, performance, and functional testing of the ESWS and UHS piping and components, including the heat transfer capability of the CCW heat exchangers based on GL 89-13 and GL 89-13 Supplement 1.

COL 9.1(7) The COL applicant is to provide post seismic event inspection procedures to measure gaps between the new and spent fuel storage racks.

TS



Figure 2-1 Layout and Plan View of NFSR

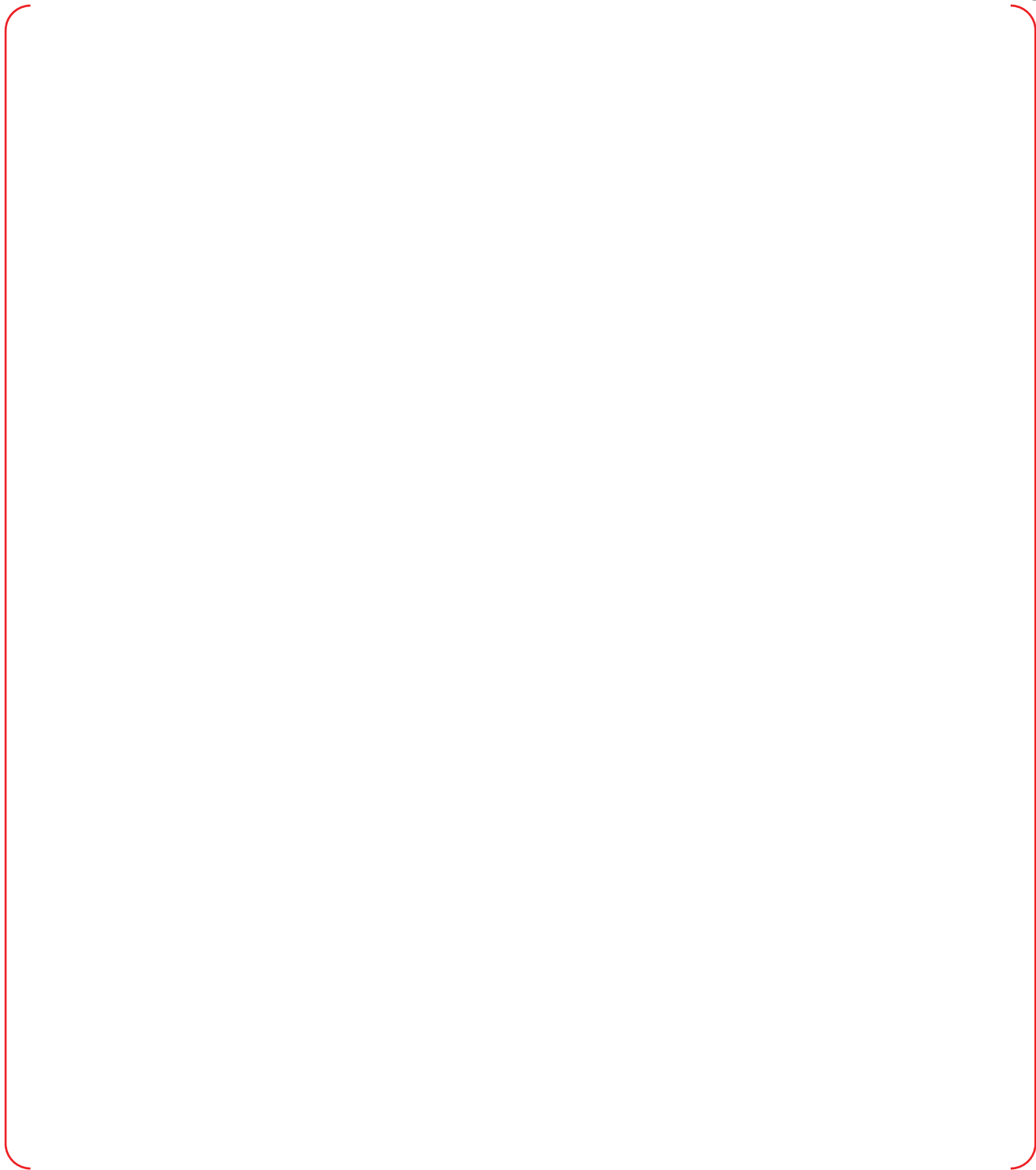


Figure 2-5 Plan View of SF SR Showing Rack Gaps above Baseplate Level

RAI 287-8272 - Question 09.01.02-36_Rev.1

TS

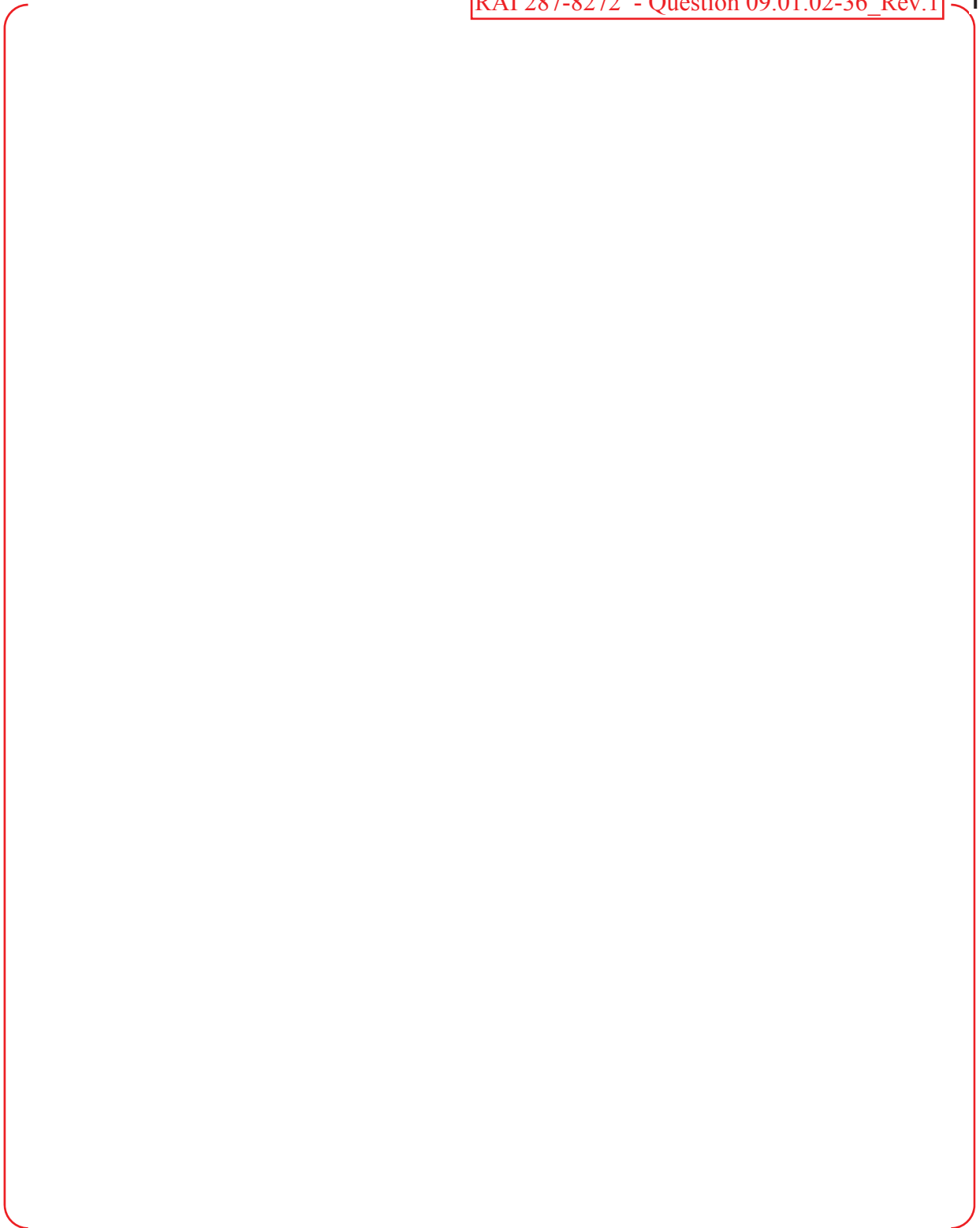


Figure 2-6 Plan View of SFSR Showing Rack Gaps at Baseplates

(3) Contact Elements

Gaps between fuel assemblies and rack cell walls/baseplate, adjacent rack baseplates, and pedestals and embedment plates are modeled with contact elements in the WPMR analysis, as described in Section 3.1.2.4.

(4) Coefficient of Friction

Because the SFSTRs are free-standing, they may slide during an earthquake. The pedestal-to-embedment plate interface is assigned a coefficient of friction (COF) that represents contact between stainless steel surfaces in a wet environment. Based on experimental data (Reference 14), the COF is bounded within the range from 0.2 to 0.8 with a mean value of 0.5.

Since the NFSTRs are attached to the floor, COF is not applicable as long as the stud bolts remain intact.

For both the NFSTRs and SFSTRs, a COF of 0.5 between the fuel assembly and the rack was used.

(5) Fluid Coupling

For seismic conditions, the submerged SFSTR is influenced by fluid coupling as well as by mechanical contact. When the racks displace toward each other and the gaps between them are reduced, the fluid coupling effect increases. Because the racks are densely arranged in the spent fuel pool, the fluid coupling effect can be significant. Fluid coupling is included in the SFSTR models by use of hydrodynamic mass based on the potential flow theory of Fritz (References 15 and 16).

Hydrodynamic masses are defined at fuel assembly-to-cell wall gaps, rack-to-rack gaps, rack-to-pool wall gaps, and rack baseplate-to-pool floor gaps based on the size of the gaps at those locations. Figure 2-5 and Figure 2-6 show the installation gaps for the SFSTRs.

As gap size is increased, the hydrodynamic mass decreases. The hydrodynamic mass is calculated based upon the initial gap sizes. The initial SFSTR rack-to-rack baseplate gaps are the minimum physically possible. Although the hydrodynamic mass increases as the rack moves to close the gap, the increase is not meaningful until the gap becomes very small. Therefore, hydrodynamic mass is not updated during a seismic response run because the maximum displacement of the outermost rack is small in comparison with the gap size of the outermost rack and the pool wall. If applied, the increase in hydrodynamic mass would reduce the sliding response of the racks. Therefore, it is conservative for maximizing the amount of rack sliding and the potential for rack-to-pool wall and rack-to-rack impacts to not increase the hydrodynamic mass. This is also consistent with the discussion of fluid effects in NUREG/CR-5912, Section 6.4.3, Fluid Effects, which states "...the change was not significant and that the practice of using a constant hydrodynamic mass based on initial gaps is reasonable."

Therefore, a sensitivity analysis of variation in gaps (i.e., installation tolerances for the gap) was not performed.

Hydrodynamic mass is calculated based on Fritz's classical two-body fluid coupling model (Reference 16) extended to multiple bodies. In its simplest form, the fluid coupling effect can be explained by considering the proximate motion of two bodies (such as a rack and a wall) under water.

The effect of hydrodynamic mass is implemented through the use of the ANSYS MATRIX27 element as discussed in Section 3.1.2.3.

The NFSTRs have no hydrodynamic effect because they are installed in air.

3.1.2.2 Details for Rack and Fuel Assembly Model

The sections below provide details on the rack and fuel assembly modeling.

(1) New Fuel Storage Rack Model

The dynamic analysis model for the NFSR and fuel assemblies are shown in Figure 3-1. The NFSR and fuel assembly model are of a single rack and includes 3-D elastic beam elements (ANSYS BEAM4) and lumped mass elements (ANSYS MASS21) with properties derived from the dynamic characteristics of the detailed 3-D shell model of the NFSR. Effective structural properties for the dynamic model are determined from the natural frequencies and mode shapes of the detailed model (see Section 3.1.2.7). Details of effective structural properties for fuel racks are shown in Appendix H of Reference 17. Structural properties (i.e. Young's modulus and flexural rigidity) for fuel assemblies are shown in Table 3-3.

Vertical portions of the NFSR cells and fuel assemblies are each represented by five nodes. Nodes are located at the rack baseplate, $\frac{1}{4} H$, $\frac{1}{2} H$, $\frac{3}{4} H$, and H (where H is the rack height measured above the baseplate). Each rack node has six degrees of freedom (three translations and three rotations) and a lumped mass associated with it. The nodes for the rack and the fuel assembly are connected by contact elements (ANSYS CONTAC52) in the horizontal direction. There is a single contact element in the vertical direction between the fuel assembly bottom node and the baseplate node.

Lumped masses of the NFSR and fuel assemblies are distributed among the five nodes for rack cells and fuel assemblies as shown in the table below:

Node No. (Figure 3-1)		Location	Total Mass Distribution
Rack	Fuel Assembly		
13	18	Top of Rack	12.5 %
12	17	3/4 Height	25 %
11	16	1/2 Height	25 %
10	15	1/4 Height	25 %
9	14	Bottom (Baseplate) of Rack	12.5 %

(2) Spent Fuel Storage Rack Model

To model the interaction among the multiple SFSTRs, the WPMR shown in Figure 3-3 is comprised of a dynamic analysis model for individual SFSTRs, as shown in Figure 3-2. This model is similar to the NFSR model and is composed of elastic beam elements and lumped mass elements with properties derived from the dynamic characteristics of the detailed 3-D shell model of the SFSTR. An underlying assumption in the modeling of the rack as a single beam using the overall bending stiffness of the entire rack is that the cell-to-cell welds remain intact and can carry the internal forces. This assumption is confirmed by structural evaluation of the welds (see Section 3.7.3.3).

Effective structural properties for the dynamic model are determined from the natural frequencies and mode shapes of the detailed model (see Section 3.1.2.7).

Figure 3-2 shows a schematic depicting five nodes representing masses of fuel and rack cells and their associated elements, which are used to represent the interactions and vertical and horizontal motions of support pedestals, respectively. Contact (i.e., gap) elements are used in the representation of rack sliding and impact. A directional stiffness is assigned to the contact element. The pool floor is assumed to be a rigid body initially in contact with the rack pedestals. The contact elements are used to represent potential impact of a rack pedestal on the pool floor. The coefficient of friction between the rack pedestals and pool floor is incorporated into a contact (gap) element.

RAI 287-8272 - Question 09.01.02-36_Rev.1

The hydrodynamic masses for the fuel assembly-to-cell wall, rack-to-rack and rack-to-pool wall are modeled as ANSYS mass MATRIX27 elements. The hydrodynamic masses for rack baseplate-to-pool floor are considered as added masses to each rack baseplate.

Lumped masses of the rack and fuel assemblies are distributed among the five nodes for spent fuel storage rack cells and fuel assemblies as shown in the table below.

Node No. (Figure 3-2)		Location	Total Mass Distribution
Rack	Fuel Assembly		
13	18	Top of Rack	12.5 %
12	17	3/4 Height	25 %
11	16	1/2 Height	25 %
10	15	1/4 Height	25 %
9	14	Bottom (Baseplate) of Rack	12.5 %

All the fuel assemblies in each storage rack module are modeled as one beam of which the mass equals the sum of the masses of all the fuel assemblies in a rack module. Structural properties (i.e. Young's modulus and flexural rigidity) for fuel assemblies are shown in Table 3-3. Because the fuel assemblies in a rack module are modeled together, all fuel assemblies move simultaneously in one direction. This assumption results in larger impact forces on the rack module than the actual case and results in conservative loads on the storage rack. Because the fuel assembly is modeled with five nodes, the calculated impact loads on the nodes will be larger than the actual value because the fuel assembly actually has eleven spacer grids. The maximum fuel assembly grid horizontal impact load is determined by dividing the maximum impact load at each node by the number of grids associated with that node (2.75 for Nodes 10, 11, and 12, and 1.375 for Nodes 9 and 13).

Fluid damping and form drag are conservatively omitted.

Figure 3-3 shows the WPMR analysis model, which combines the single rack models described above to represent the entire spent fuel pool.

3.1.2.3 Hydrodynamic Mass

In addition to the structural mass of racks and fuel assemblies, hydrodynamic masses are included in the SFSR model to account for fluid coupling. Hydrodynamic mass is included in the SFSR model with the ANSYS MATRIX27 element and added mass, which represents an arbitrary element whose geometry is undefined but whose kinematic response can be specified by mass coefficients. Details of hydrodynamic masses are shown in Appendix H of Reference 17.

(1) Fuel Assembly-to-Cell Wall

A fuel assembly consists of fuel rods, guide tubes, top and bottom nozzles, and spacer grids. The hydrodynamic mass coefficients between the rack cell wall and the fuel assembly are calculated assuming the rack cell and fuel assembly are long coaxial cylinders. Hydrodynamic masses acting at the centers of two rigid cylinders with a fluid-filled annulus are represented using the following formula in Reference 15:

$$\begin{pmatrix} F_1 \\ F_2 \end{pmatrix} = \begin{bmatrix} -M_H & M_1 + M_H \\ M_1 + M_H & -(M_1 + M_2 + M_H) \end{bmatrix} \begin{pmatrix} X_1'' \\ X_2'' \end{pmatrix}$$

$$M_H = \left[\frac{R_2^2 + R_1^2}{R_2^2 - R_1^2} \right] \pi \rho R_1^2 h$$

RAI 287-8272 - Question 09.01.02-36_Rev.1

At any given time, t , these equations can be thought of as a set of “static” equilibrium equations that also take into account inertia forces and damping forces. Displacement and loads of each storage rack are obtained by post-processing the results of the WPMR analysis.

- (3) Apply a constant time step size and a single computer processor to ensure repeatability. Repeatability of the solution results was confirmed by rerunning one of the base transient cases with unaltered input and confirming the same results would be obtained if the case were rerun.
- (4) Perform stress analyses of the racks using the loads from the transient dynamic analyses. Evaluate calculated stresses based on the criteria in ASME Code Section III, Subsection NF (Reference 4) and perform local evaluation for the bounding case to show that the structural integrity of the fuel is maintained under all impact loads.

The analysis for the NFSR is performed in a similar manner except that only a single rack module is modeled. This simplification is appropriate because of the large separation between the two rack modules (approximately 24 inches) and the absence of water.

3.2 Acceptance Criteria

The composite dynamic simulation wherein all racks in the pool are modeled is used 1) to determine the loads and displacements for each fuel storage rack in the pool and the relative motion between racks, and 2) to evaluate the potential damage and consequences of inter-rack and rack-wall impact phenomena in the racks.

The NFSRs and the SFSRs are designed as seismic Category I. The structural analysis of fuel storage rack is performed for all load conditions of the fuel storage rack in accordance with NRC SRP 3.8.4 (Reference 1) and NRC SRP 3.8.5 (Reference 20). This includes loads on the racks when fuel assemblies are normally stored in the racks; when a SSE occurs; and when the fuel assembly or other permitted items handled over the racks falls down onto or into them. The principal design criteria of the racks are shown in Sections 3.2.1 and 3.2.2.

Per Section I.3 of SRP 3.8.4 (Reference 1), the impact loads on the fuel assembly should not lead to damage of the fuel. Damage of the fuel is evaluated for structural elements of a fuel assembly including the fuel rod cladding to verify they are not stressed beyond the material allowable limits such that the fuel rods are no longer able to provide confinement for contained radioactive fission materials. In addition, an evaluation considering pertinent failure modes such as buckling should be performed to demonstrate that when subject to the consequent loads resulting from the load combinations described in Table 3-1, the structural elements of the fuel assembly will not exceed the material allowable limits.

3.2.1 Kinematic Criteria

Because the SFSRs are not fixed, overturning or sliding could happen due to external load. According to the NRC SRP 3.8.5 (Reference 20), the minimum acceptable factor of safety against overturning under the seismic event is 1.5. This ensures that the rack does not exhibit a rotation sufficient to bring the center of mass over the corner pedestal. Because NFSRs are attached to the floor, they were confirmed not susceptible to overturning by showing that their stud bolt stresses are acceptable (Section 3.2.2.4).

3.2.2 Stress Limit Criteria

Stress limits must not be exceeded under the required load combinations. The applicable loads and load combinations of structural analysis for the rack are defined in the Table 3-1, based on NRC SRP 3.8.4, Appendix D (Reference 1). For the APR1400, the operating basis earthquake (OBE) ground motion is defined as one-third the SSE ground motion design response spectra. Therefore, in accordance with 10 CFR Part 50, Appendix S, an OBE design analysis is not required and load

combinations involving "E" have been removed. The acceptance limits are defined in ASME Code Section III, Subsection NF (Reference 4), as applicable for Class 3 component supports.

The APR1400 SFSTRs are free-standing; thus, there is no or minimal restraint against free thermal expansion at the base of the rack. Moreover, stresses induced due to thermal expansion will be secondary stresses since they are self-limiting, and have no stipulated stress limits in Class 3 structures or components when acting in concert with seismic loadings. Therefore, thermal loads applied to the racks are not included in the stress combinations involving seismic loadings. ASME Code Section III, Division 1, Subsection NF and Appendix F are applied as stress limits criteria of fuel storage rack for service conditions.

Material properties for analysis and stress evaluation are provided in subsection 3.4.4.

3.2.2.1 Normal Conditions (Level A)

(1) Stress in Tension

The allowable stress in tension on a net section (F_t) is given in NF-3321.1(a)(1).

$$F_t = 0.6 S_y \text{ [but not more than } 0.5 S_u\text{]}$$

Where,

S_y = yield strength of material at a given temperature, and
 S_u = ultimate strength of material at a given temperature.

(2) Stress in Shear

The allowable stress in shear on a net section (F_v) is given in NF-3322.1(b)(1).

$$F_v = 0.4 S_y$$

(3) Stress in Compression

The allowable stress in compression on a net section (F_a) of austenitic stainless steel is given in NF-3322.1(c)(2).

$$F_a = S_y (0.47 - k \cdot l / 444r)$$

Where,

kl/r is less than or equal to 120 for all sections,

l = unsupported length of component,

k = length coefficient which gives influence of boundary conditions, e.g.,

$k = 1$; simple support both ends,

$k = 2$; cantilever beam, conservatively used for evaluations,

$k = 0.5$; clamped at both ends, and

r = radius of gyration of component.

(4) Stress in Bending

The allowable bending stress (F_b) resulting from tension and compression on extreme fibers of box-type flexural members is given in NF-3322.1(d)(4).

$$F_b = 0.60 S_y$$

- Margin to overturning – used to verify rack does not tip [Table 3-10]
- Stress factors – used to compare calculated loads to allowable stresses (i.e., values <1.0 have margin to allowable [Table 3-9]
- Rack weld stresses and safety factors – used to confirm racks maintain their structural integrity [Table 3-12]
- Stress on fuel assembly – used to confirm fuel assemblies are not damaged to the extent that cladding is breached [Table 3-11]
- Stresses on the threads of the SFSR pedestal leveling feet – used to assess damage to threads [Table 3-13]
- Stresses on the NFSR stud bolt - used to confirm NFSR stud bolts maintain their structural integrity [Table 3-14]

The seismic responses in the horizontal directions are combined using the square root of the sum of the squares (SRSS) method in the analysis of the fuel assembly, rack structure, welded connections, and the rack supports of NFSR and SFSR. For all horizontal loads except fuel assembly grid impact, the SRSS combination uses the maximum E-W and the maximum N-S load at any time during the transient, even if they do not occur during the same time step. The grid impact loads use the values during the same time step to find the maximum.

3.7.1 Time History Simulation Results

The loads and the displacements by dynamic simulations are summarized in Table 3-6 through Table 3-8 and in Figure 3-20 through Figure 3-26. Note that the values shown are maximum values found for any of the racks for each run. Where horizontal loads are reported, they are for the same rack, but the vertical load reported for that run may be from a different rack. For the SFSRs, results are reported for both Region I and Region II racks since they are slightly different structurally and have different rack-to-rack spacing.

3.7.1.1 Displacements of Rack

The NFSRs are fixed and not subject to displacement at their bases provided their stud bolts remain intact, as shown in Figure 2-3. The displacement of the NFSRs at their top is determined to confirm there is no contact between adjacent cells or with the new fuel storage pit walls.

The SFSRs are specified to be installed with pedestals and baseplates as close as possible, as shown in Figure 2-6. Therefore, during a seismic event they will initially move apart, although they could again slide together during the transient. Due to the random nature of the seismic acceleration, the racks will move in different directions by different amounts, and this can be affected by the time step and COF used in the analysis. This randomness would be true even if experiments were run repeatedly using different time histories. The initial movement can determine the ultimate relative position of racks to each other. As discussed in Section 3.1.1, a baseline correction process has been used to eliminate unrealistic cumulative displacement leading to large final displacements. The use of five independent time histories with sensitivities for COF and rack loading provides a reasonable range of possible displacements. Since none of the runs predicted displacements of more than a small fraction of the gap between the outermost racks to SFP wall, contact of cells between SFSRs and the SFP walls is not expected. The baseplates of adjacent racks can come into contact at some velocity if they initially move apart and then back together, as discussed in Section 3.7.1.3.

Presuming that the racks are in contact at their bases, flexure of the racks along their height could cause the top ends of adjacent racks to come into contact. The maximum reduction in gap between adjacent racks (i.e., larger values indicate the rack upper structures to be closer to each other) are shown in Table 3-6. The minimum gap for the cell-to-cell contact in Region I is 60.0 mm (2.36 in), and that of Region II is 30.0 mm (1.18 in), as shown in Figure 2-5. Therefore, there is no impact on the rack cells by each

other, because the maximum relative displacements of racks are smaller than the cell wall separation with baseplates touching.

The maximum relative displacement of the rack pedestal from its starting point is 104.3 mm (4.1 in) as shown in Table 3-6. The minimum size of the embedment plate is about 610 mm (24 in) x 610 mm (24 in) (Reference 27). Therefore, rack pedestals do not slide off the embedment plates onto the spent fuel pool liner because the maximum displacement of rack pedestal is not large enough to move off of the embedment plate.

The maximum rotations of the rack are obtained from a post-processing of the rack time history response output. The SFSR should not exhibit rotations sufficient to cause the rack to overturn (i.e., the rack does not exhibit a rotation sufficient to bring the center of mass over the corner pedestal). Based on the width and height of a 8x7 rack, the rotation required to produce incipient tipping for this rack is approximately equal to:

$$\tan^{-1}[(1/2 * \text{Distance to bring center of gravity over pedestal}) / (1/2 * \text{Height of rack})]$$

$$\tan^{-1}[(1,610/2) / (4,775/2)] = 18.5^\circ$$

As shown in Table 3-10, the safety factor for allowable angle is greater than the acceptance criteria of 1.5 from SRP 3.8.5. Therefore, overturning of a rack module does not occur.

3.7.1.2 Support Pedestal Loads of Rack

The maximum horizontal and vertical loads generated on support pedestal with the application of SSE loads are shown in Table 3-7 and Figure 3-22 and are used to perform structural integrity evaluation of support pedestal and rack. The dynamic simulations of the racks give results for the vertical and two horizontal forces (i.e., E-W and N-S directions) throughout the transient. From those values, the maximum axial force in the vertical direction and the maximum shear forces of the two horizontal directions per pedestal are determined. The resultant shear force for each run is conservatively calculated by combining the maximum horizontal loads on any single pedestal as shown in Table 3-7 using the square root of the sum of the squares (SRSS) method. The maximum bending moment at the bottom baseplate-to-pedestal interface is computed by multiplying the maximum shear force and the distance from the bottom baseplate to the contact point surface underneath of the NFSRs and SFSRs, which is 185 mm (7.28 inches) and 160 mm (6.3 inches) as shown in Tables 2-1 and 2-2, respectively. Additional detail is provided in Appendix F of Reference 17.

3.7.1.3 Impact Loads

The impact loads for fuel-to-cell wall, rack-to-rack and rack-to-pool wall of the NFP and SFP are calculated as follows:

(1) Fuel-to-Cell Wall

For purposes of assessing the effect on rack structural integrity, the maximum impact loads of fuel assembly-to-cell wall for the NFSRs and the SFSRs are as shown in Table 3-8. These loads are determined by dividing the maximum total fuel assembly beam to cell wall load by the number of fuel assemblies in the rack under evaluation (e.g., divide by 64 for a full rack, 32 for a half full rack).

For purposes of determining the effect on the fuel assembly grids, the impact load on each of the fuel support grids at each time step is determined by dividing the maximum calculated impact load per cell at each of the five nodes by number of spacer grids at each of the nodes. For each run, the impact loads in the East-West and North-South directions are combined using the SRSS method at the same time.

3.7.3.5 Local Stress Evaluation

(1) Cell Wall Impact

The maximum fuel-to-cell wall impact loads for the NFSRs and the SFSRs are as shown in Table 3-8. The evaluation for cell wall for impact is performed to guarantee that local impact does not affect criticality of stored fuel. Integrity of local cell wall is evaluated conservatively using the peak impact load. The limiting impact load to induce overall permanent deformation is calculated by plastic analysis. The cell walls of the new and the spent fuel storage racks can withstand a side load of a maximum of 273.2 kN (61,410 lbf) and 47.4 kN (10,660 lbf), respectively (Reference 17). Therefore, the cell wall of racks satisfies the requirement with the maximum impact loads less than the allowable loads.

(2) Cell Wall Buckling

The cell wall buckling analysis is performed to evaluate the buckling capacity of the spent fuel storage rack cells at the base of the racks using ANSYS program. The cell wall acts alone in compression for a length of about 130 mm (5.12 in) up to the point where the neutron absorbing material sheathing is attached. The sheathing provides additional strength against cell wall buckling. Therefore, the buckling analysis is considered on the lower 130 mm (5.12 in) of the cell wall.

The analysis is evaluated for Region II cells because the maximum stress factor on Region I racks is less than the maximum stress factor (i.e. FACT 2) for the region II racks as shown in Table 3-9.

A compressive force for cell wall buckling evaluation is calculated as follows:

$$\sigma_{\text{comp}} = 1.2 \times 21400 \times \text{FACT2} = 71.0 \text{ MPa (10,298 psi)}$$

Where,

FACT2 = 0.401, the stress factor is taken from Table 3-9.

Above calculation is based on the maximum stress factor for the net vertical force on the gross cell cross-section. The vertical forces on the rack support pedestal reflects the weight of the rack plus the stored fuel assemblies during the seismic event. Since the stored fuel assemblies are supported by the rack baseplate, the actual compressive load on the rack cell structure is significantly less than the value determined by the results of dynamic simulations. It is appropriate to use a FACT2 value for cell wall buckling evaluation.

The critical elastic buckling load of cell wall is calculated by ANSYS eigenvalue analysis. Two by two cells of spent fuel storage rack are considered in the buckling analysis. The FE model reflects a reinforcement plate that is welded to outer side of cells. The boundary condition and applied unit load (1 MPa) of FE mode is shown in Figure 3-28. Fixed boundary condition is applied on bottom surface of FE model. Figure 3-29 shows the results of buckling analysis. The minimum value of load multiplier represents the critical elastic buckling pressure of fuel rack cell wall, which is 136.68 MPa (19,823 psi). Therefore, two-thirds of the critical buckling stress as the limit under Service Level D condition is calculated as 91.12 MPa (13,215 psi).

The ANSYS analysis demonstrates that the spent fuel storage rack cells remain in a stable configuration under the maximum seismic load without any gross yielding of the storage cell wall, which satisfies the ASME Code requirements for Level D conditions. Therefore, a buckling of the rack cell wall does not occur.

(3) Secondary Stress by Temperature Effects

The temperature gradients across the rack structure caused by differential heating effects between one or more filled cells and one or more adjacent empty cells are considered. The worst thermal stress in a fuel rack is obtained when a storage cell has a fuel assembly generating heat at the maximum postulated rate and the surrounding storage cells contain no fuel. The thermal stress stresses that occur in this scenario

are secondary stresses as defined by the ASME Code Section III, Division 1. Therefore, it is independently evaluated without combining with primary stress of other load conditions.

A conservative estimate of the weld stresses along the length of an isolated hot cell is obtained by considering a beam strip uniformly heated by $\Delta T = 36\text{ }^{\circ}\text{C}$ ($65\text{ }^{\circ}\text{F}$), and restrained from growth along one long edge. The temperature rise envelops the difference between the maximum local spent fuel pool water temperature ($76.2\text{ }^{\circ}\text{C}$ ($169\text{ }^{\circ}\text{F}$) bounding) inside a storage cell and the bulk pool temperature ($48.9\text{ }^{\circ}\text{C}$ ($120\text{ }^{\circ}\text{F}$)) based on the thermal-hydraulic analysis of the spent fuel pool (Reference 29). This analysis assumes an almost full SFP to which freshly discharged fuel with worst case decay heat is added in adjacent cells and SFP thermal capacity of only the water above the top of the SFRs. The maximum shear stress due to temperature change for isolated hot cell weld is calculated as follows:

$$\tau_{max} = E \times \alpha \times \Delta T$$

Where,

$$E = 1.896\text{E}+05\text{ N/mm}^2\text{ (}27.5\text{E}+06\text{ psi),}$$

$$\alpha = 9.5\text{E}-06\text{ in/in-}^{\circ}\text{F, and}$$

$$\Delta T = 36\text{ }^{\circ}\text{C (}65\text{ }^{\circ}\text{F).}$$

The maximum shear stress due to the temperature gradient for an isolated hot cell is calculated given that this thermal stress is classified as secondary stress, the allowable shear stress criteria for Level D condition ($0.42 S_u = 191.4\text{ MPa}$ ($27,762\text{ psi}$)) is used as the limit of allowable. Therefore, the maximum shear stress due to the temperature gradient is acceptable.

Another possible source of temperature induced stress is expansion of adjacent SFSRs with increased temperature resulting in a contact load between pedestals and baseplates of adjacent racks or relatively different expansion for a fuel assembly and the cell surrounding it. For the former, it is likely that a fuel assembly would cool over time so that it would not generate an increase stress. However, in the event of a loss of SFP cooling, the fuel and the surrounding cell could heat up at different rates. The fuel assembly grid typical dimension is 206.45 mm (8.128 in) square, and a SFSR cell inner dimension is $220.0 \pm 3\text{ mm}$ square, for a gap of 10.55 mm (0.415 in). Assuming that thermal expansion of the fuel assembly and the rack material is identical, the elongation of SA-240 Type 304L material due to thermal expansion is:

$$\epsilon = \alpha (T_2 - T_1) = 0.001\text{ in/in}$$

Where,

ϵ : Differential thermal expansion elongation (in/in),

α : Thermal expansion coefficient of SA-240 Type 304L = $8.9\text{E}-6\text{ (in/in-}^{\circ}\text{F)}$,

T_2 : Temperature = $223.7\text{ }^{\circ}\text{F}$ [Maximum fuel clad cladding temperature of spent fuel assembly at abnormal condition per thermal-hydraulic analysis], and

T_1 : Temperature = $115.5\text{ }^{\circ}\text{F}$ [Bulk temperature on normal condition of spent fuel pool].

Given the fuel assembly dimensions, the total differential expansion is 0.21 mm (0.008 in), which is a small fraction of the available gap.

As for the load due to expansion of each SFSR causing a contact stress, assuming the racks are installed touching at $21\text{ }^{\circ}\text{C}$ ($70\text{ }^{\circ}\text{F}$) and heat up to $48.9\text{ }^{\circ}\text{C}$ ($120\text{ }^{\circ}\text{F}$), the expansion of each rack is about 0.43 mm (0.017 in). In order to develop a load due to constraint of free end displacement, more than two adjacent racks must be in hard contact this is extremely unlikely. Therefore, the development of any significant thermal load due to restraint of free end displacement is not considered credible. Any incidental forces that might develop if some baseplates are in contact are self-limiting as a very small displacement, or shifting of the racks, relieves the stress. Self-limiting stresses developed by constraint of the structure and relieved by minor deformation are, by definition (NF-3121.3), secondary stresses.

RAI 287-8272 - Question 09.01.02-36_Rev.1

According to SRP Section 3.8.4, Appendix D, Section I.2, "Design, fabrication, and installation of fuel racks of stainless steel material may be performed based on ASME Code, Section III, Division 1, Subsection NF requirements for Class 3 component supports." For the design of Class 3 component supports, Table NF-3251.2-1, does not require the evaluation of secondary stresses. Based on this, it is concluded that the development of significant thermal loads due to constraint of the baseplates is not credible and any postulated incidental loads need not be considered since they result in secondary stresses. Therefore, loads from the restraint of adjacent racks do not need to be explicitly considered in the design analysis.

(4) Punching Shear Analysis of Rack Baseplate

a. Punching due to Vertical Pedestal Load

A punching shear analysis has been performed for the rack baseplate under seismic loading conditions. The analysis demonstrates that the maximum vertical load on a single support pedestal is less than the force necessary for the 285 mm (11.2 in) square pedestal block to punch through the 25 mm (0.984 in) thickness of the baseplate. The punching shear capacity of the baseplate (F_v) can be calculated by following equation.

$$F_v = \frac{S_y}{\sqrt{3}} \times 4 \times L \times t$$

Where,

$\frac{S_y}{\sqrt{3}}$ (shear stress limit according to the distortion energy theory of yielding),

S_y (yield strength of baseplate) = 147.5 MPa (21,400 psi),

L (side length of the pedestal block) = 285 mm (11.2 in), and

t (thickness of the baseplate) = 25 mm (0.984 in).

The punching shear capacity of the baseplate calculated using the above equation exceeds the maximum pedestal load per Table 3-7 as shown in Table 3-15. Therefore, a punching shear failure of the rack baseplate will not occur.

b. Punching due to Fuel Impact Load

A punching shear analysis due to the maximum impact load of fuel assembly-to-baseplate is performed for the rack baseplate under seismic loading conditions and compared with the allowable stress limit ($0.72 \times S_y = 106.2$ MPa (15,408 psi)) for the Level D condition as follows:

$$\sigma_{\text{shear}} = F_{\text{impact}} / (4 \times L \times t/2)$$

Where,

F_{impact} (Maximum fuel assembly-to-baseplate impact load in vertical direction)
= 55.7 kN (12,516 lbf) per Table 3-8,

L (Side length of the square cross-section of fuel assembly) = 206.5 mm (8.128 in), and

t (Thickness of the baseplate) = 25 mm (0.984 in).

The resultant stress (σ_{shear}) does not exceed the allowable stress limit as shown in Table 3-15. Therefore, a punching shear failure of the rack baseplate will not occur.

3.7.4 Sensitivity Studies

Since the NFSRs are secured in place and do not slide, the following sensitivities (except for the first, rack EI) are not considered applicable. Therefore, discussion of these sensitivities is for the SFSTRs only.

REVISED RESPONSE TO REQUEST FOR ADDITIONAL INFORMATION**APR1400 Design Certification****Korea Electric Power Corporation / Korea Hydro & Nuclear Power Co., LTD****Docket No. 52-046**

RAI No.: 287-8272
SRP Section: 09.01.02 – New and Spent Fuel Storage
Application Section: 9.1.2
Date of RAI Issue: 11/02/2015

Question No. 09.01.02-37

1. The 10 CFR Part 50, Appendix A, General Design Criteria (GDC) 1, 2, 4, 5, 63, and 10CFR 52.80 (a) provide the regulatory requirements for the design of the new and spent fuel storage facilities. Standard Review Plan (SRP) Sections 9.1.2 and 3.8.4, Appendix D describes specific SRP acceptance criteria for the review of the fuel racks that are acceptable to meet the relevant requirements of the Commission's regulations identified above. In DCD Tier 2, Section 9.1.2.2.3, "New and Spent Fuel Storage Rack Design", the applicant stated that "The dynamic and stress analyses are performed as described in report APR1400-H-N-NR-14012-P & NP". In the technical report APR1400-H-N-NR-14012-P, Rev 0, Table 3-9, "Maximum Loads on single Pedestal", the applicant provided the pedestal forces for the new and spent fuel racks. In accordance with SRP 3.8.4 Appendix D I (5), the applicant is requested to provide the details how the pedestal forces were converted to the bending moment and shear force at the bottom baseplate-to-pedestal interface. The applicant is requested to identify any proposed changes to and provide a mark-up of Subsections in the DCD Tier 2 and the report APR1400-H-N-NR-14012-P, Rev.0, as appropriate.

Response – (Rev. 0)

The dynamic simulations of the racks give results for the vertical and two horizontal forces (i.e. east-west and north-south directions) at that instant. From those values, the maximum axial force of the vertical direction and the maximum shear forces of the two horizontal directions per pedestal are determined. The resultant shear force is conservatively calculated by combining the maximum horizontal loads (i.e. east-west and north-south directions) on a single pedestal in Table 3-9 of technical report APR1400-H-N-NR-14012-P using the square root of the sum of the squares (SRSS) method. The maximum bending moment at the bottom baseplate-to-pedestal interface is computed by multiplying the maximum shear force and the distance from the bottom baseplate to the liner plate of the new fuel storage rack and the spent fuel storage racks, which is 185 mm (7.28 inches) and 160 mm (6.3 inches) as shown in Tables 2-1 and 2-2 of technical report APR1400-H-N-NR-14012-P, respectively.

Response – (Rev. 1)

Technical report, APR1400-H-N-NR-14012-NP was submitted as Rev. 0 in December, 2014. KHNP responses to RAI 287-8272 were based in part on the Technical Report. Subsequent to issuance of the Technical Report and RAI responses, the NRC provided feedback on both the Technical Report and RAI 287-8272 responses. In response to this NRC feedback, Technical report, APR1400-H-N-NR-14012-NP will be revised (as Rev. 3) to incorporate additional information pertaining to the fuel racks. This RAI revision contains the specific Technical Report revisions relevant to this response and associated DCD changes, where necessary. A summary of the additional information is in the below paragraphs.

Support Pedestal Loads of Rack

The maximum horizontal and vertical loads generated on support pedestal with the application of SSE loads are used to perform structural integrity evaluation of support pedestal and rack. The dynamic simulations of the racks give results for the vertical and two horizontal forces (i.e., E-W and N-S directions) throughout the transient. From those values, the maximum axial force in the vertical direction and the maximum shear forces of the two horizontal directions per pedestal are determined. The resultant shear force for each run is conservatively calculated by combining the maximum horizontal loads on any single pedestal using the square root of the sum of the squares (SRSS) method. The maximum bending moment at the bottom baseplate-to-pedestal interface is computed by multiplying the maximum shear force and the distance from the bottom baseplate to the contact point surface underneath of the NFSRs and SFSRs, which is 185 mm (7.28 inches) and 160 mm (6.3 inches), as shown in Tables 2-1 and 2-2 of technical report APR1400-H-N-NR-14012-P, respectively.

Impact on DCD

There is no impact on the DCD.

Impact on PRA

There is no impact on the PRA.

Impact on Technical Specifications

There is no impact on the Technical Specifications.

Impact on Technical/Topical/Environmental Reports

APR1400-H-N-NR-14012-NP (Rev. 3), Sections 3.2.2.1, 3.2.2.3(3), 3.2.3, 3.7.1.2, and 3.7.3.1 will be revised as shown in Attachment 1 to this response.

combinations involving “E” have been removed. The acceptance limits are defined in ASME Code Section III, Subsection NF (Reference 4), as applicable for Class 3 component supports.

The APR1400 SFSTRs are free-standing; thus, there is no or minimal restraint against free thermal expansion at the base of the rack. Moreover, stresses induced due to thermal expansion will be secondary stresses since they are self-limiting, and have no stipulated stress limits in Class 3 structures or components when acting in concert with seismic loadings. Therefore, thermal loads applied to the racks are not included in the stress combinations involving seismic loadings. ASME Code Section III, Division 1, Subsection NF and Appendix F are applied as stress limits criteria of fuel storage rack for service conditions.

Material properties for analysis and stress evaluation are provided in subsection 3.4.4.

3.2.2.1 Normal Conditions (Level A)

(1) Stress in Tension

The allowable stress in tension on a net section (F_t) is given in NF-3321.1(a)(1).

$$F_t = 0.6 S_y \text{ [but not more than } 0.5 S_u \text{]}$$

Where,

S_y = yield strength of material at a given temperature,

and S_u = ultimate strength of material at a given temperature.

(2) Stress in Shear

The allowable stress in shear on a net section (F_v) is given in NF-3322.1(b)(1).

$$F_v = 0.4 S_y$$

(3) Stress in Compression

The allowable stress in compression on a net section (F_a) of austenitic stainless steel is given in NF-3322.1(c)(2).

$$F_a = S_y (0.47 - k \cdot l / 444r)$$

Where,

kl/r is less than or equal to 120 for all sections,

l = unsupported length of component,

k = length coefficient which gives influence of boundary conditions,

e.g., $k = 1$; simple support both ends,

$k = 2$; cantilever beam, conservatively used for evaluations, $k = 0.5$; clamped at both ends, and

r = radius of gyration of component.

(4) Stress in Bending

The allowable bending stress (F_b) resulting from tension and compression on extreme fibers of box-type flexural members is given in NF-3322.1(d)(4).

$$F_b = 0.60 S_y$$

(5) Combined Stress (Combined Bending and Compression Loads)

Combined bending and compression load on a net section per NF-3322.1(e)(1) satisfies the following equation.

$$f_a/F_a + C_{mx}f_{bx}/D_xF_{bx} + C_{my}f_{by}/D_yF_{by} \leq 1.0$$

Where,

$$\begin{aligned} f_a &= \text{Direct compressive stress in the section,} \\ f_{bx} &= \text{Maximum bending stress along x-axis,} \\ f_{by} &= \text{Maximum bending stress along y-axis,} \\ C_{mx} &= 0.85, \\ C_{my} &= 0.85, \\ D_x &= 1 - (f_a/F'_{ex}), \\ D_y &= 1 - (f_a/F'_{ey}), \\ F'_{ex}, F'_{ey} &= (\pi^2 E)/(2.15 (kl/r)_{x,y}^2), \end{aligned}$$

and subscripts x and y reflect the particular bending plane.

(6) Combined Stress (Combined Flexure and Tension Loads)

Combined flexure and tension/compression load on a net section satisfies the following equation given in NF-3322.1(e).

$$(f_a/0.6 S_y) + (f_{bx}/F_{bx}) + (f_{by}/F_{by}) \leq 1.0$$

(7) Welds

The allowable maximum shear stress on the net section of a weld (F_w) is given in Table NF-3324.5(a)-1.

$$F_w = 0.3 S_u$$

Where, S_u is the weld material ultimate strength at temperature. For the area in contact with the base metal, the shear stress on the gross section is limited to $0.4 S_y$. Where, S_y is the yield strength of material at a given temperature.

3.2.2.2 Upset Conditions (Level B)

The stress limits for Level B are those for Level A multiplied by the stress limit factor specified in Table NF-3523(b)-1 (Reference 4).

3.2.2.3 Faulted/Abnormal (Level D)

Article F-1334 (ASME Section III, Appendix F (Reference 4), states that limits for the Level D condition are the smaller of 2 or $1.167 S_u/S_y$ times the corresponding limits for the Level A condition if $S_u > 1.2 S_y$, or 1.4 if $S_u \leq 1.2 S_y$ except for requirements specifically listed below. S_u and S_y are the ultimate strength and yield strength at the specified rack design temperature. Examination of material properties for 304L stainless demonstrates that 1.2 times the yield strength is less than the ultimate strength. Since $1.167 \times (66,100/21,400) = 3.60$, the multiplier of 2.0 controls.

Exceptions to the above general multiplier are the following:

- (1) The tensile stress on the net section shall not exceed the lesser of $1.2 S_y$ and $0.7 S_u$.
- (2) The shear stress on the gross section shall not exceed the lesser of $0.72 S_y$ or $0.42 S_u$. In the case of the austenitic stainless steel material used here, $0.72 S_y$ governs.

RAI 287-8272 - Question 09.01.02-37_Rev.1

- (3) Combined axial compression and bending - The equations for Level A conditions shall apply except that $F_a = 2/3 \times$ Buckling Load, and F'_{ex} and F'_{ey} may be increased by the factor 1.65.
- (4) For welds, the Level D allowable weld stress is not specified in Appendix F of the ASME Code. Therefore, a limit for weld throat stress is used conservatively as follows:

$$F_w = (0.3 S_u) \times \text{Factor}$$

Where,

$$\text{Factor} = (\text{Level D shear stress limit})/(\text{Level A shear stress limit}) = 0.72 \times S_y / 0.4 \times S_y = 1.8$$

3.2.2.4 Stress Limit for NFSR Stud Bolt

The allowable tensile and shear stresses in the stud bolt are in accordance with ASME Code Section III, Subsection NF and Appendix F for Service Level A and D, respectively. The appropriate stress limit factors K_{bo} are given in Table NF-3225.2-1 in accordance with the load condition. The NFSR stud bolt subjected to combined shear and tension shall be proportioned so that the combined effects of shear and tensile stress satisfy the ellipse equation as shown below.

Load Condition	Tensile (F_{tb})	Shear (F_{vb})	Combined ⁽¹⁾
Level A	$S_u/3.33$	$0.62S_u/5$	$\frac{f_t^2}{F_{tb}^2} + \frac{f_v^2}{F_{vb}^2} \leq 1$
Level D ⁽²⁾	$\text{Min}(0.7S_u, S_y)$	$\text{Min}(0.42S_u, 0.6S_y)$	

(1) f_t and f_v are calculated tensile and shear stresses, respectively.

(2) Specified in Appendix F-1335 of ASME Code, Section III, Division 1.

3.2.3 Dimensionless Stress Factors

Dimensionless stress factors are calculated by the ratio of the calculated stress to the allowable stress for the combined and the individual loads according to ASME Code Section III, Division 1, Subsection NF. When the calculated stress factor does not exceed 1.0, it is considered to meet stress limit requirements for each service condition. In this report, a stress factor as described below is calculated using the load combination for each service condition.

FACT1 = Stress factor of member subject to combined bending and compression (as defined in subsection 3.2.2.1(5)).

FACT2 = Stress factor of member subject to combined flexure and tension (or compression) (as defined in subsection 3.2.2.1(6)).

FACT3 = Stress factor of gross shear on a net section.

3.3 Assumptions

The following assumptions are used in the WPMR dynamic analysis:

- (1) Fluid damping is conservatively neglected.
- (2) Sloshing of the SFP water during a seismic event does not influence the dynamic response of the racks in either horizontal direction because the height of the racks is approximately equal to 3/8 times the depth of water in the spent fuel pool (see Reference 21).
- (3) The fuel assembly is considered as 3-D elastic beam with concentrated masses at the upper and lower ends and at three equally spaced intermediate points of the rack (total of 5 nodes).

other, because the maximum relative displacements of racks are smaller than the cell wall separation with baseplates touching.

The maximum relative displacement of the rack pedestal from its starting point is 104.3 mm (4.1 in) as shown in Table 3-6. The minimum size of the embedment plate is about 610 mm (24 in) x 610 mm (24 in) (Reference 27). Therefore, rack pedestals do not slide off the embedment plates onto the spent fuel pool liner because the maximum displacement of rack pedestal is not large enough to move off of the embedment plate.

The maximum rotations of the rack are obtained from a post-processing of the rack time history response output. The SF SR should not exhibit rotations sufficient to cause the rack to overturn (i.e., the rack does not exhibit a rotation sufficient to bring the center of mass over the corner pedestal). Based on the width and height of a 8x7 rack, the rotation required to produce incipient tipping for this rack is approximately equal to:

$$\tan^{-1}[(1/2 * \text{Distance to bring center of gravity over pedestal}) / (1/2 * \text{Height of rack})]$$

$$\tan^{-1}[(1,610/2) / (4,775/2)] = 18.5^\circ$$

As shown in Table 3-10, the safety factor for allowable angle is greater than the acceptance criteria of 1.5 from SRP 3.8.5. Therefore, overturning of a rack module does not occur.

3.7.1.2 Support Pedestal Loads of Rack

The maximum horizontal and vertical loads generated on support pedestal with the application of SSE loads are shown in Table 3-7 and Figure 3-22 and are used to perform structural integrity evaluation of support pedestal and rack. The dynamic simulations of the racks give results for the vertical and two horizontal forces (i.e., E-W and N-S directions) throughout the transient. From those values, the maximum axial force in the vertical direction and the maximum shear forces of the two horizontal directions per pedestal are determined. The resultant shear force for each run is conservatively calculated by combining the maximum horizontal loads on any single pedestal as shown in Table 3-7 using the square root of the sum of the squares (SRSS) method. The maximum bending moment at the bottom baseplate-to-pedestal interface is computed by multiplying the maximum shear force and the distance from the bottom baseplate to the contact point surface underneath of the NFSRs and SF SRs, which is 185 mm (7.28 inches) and 160 mm (6.3 inches) as shown in Tables 2-1 and 2-2, respectively. Additional detail is provided in Appendix F of Reference 17.

3.7.1.3 Impact Loads

The impact loads for fuel-to-cell wall, rack-to-rack and rack-to-pool wall of the NFP and SFP are calculated as follows:

(1) Fuel-to-Cell Wall

For purposes of assessing the effect on rack structural integrity, the maximum impact loads of fuel assembly-to-cell wall for the NFSRs and the SF SRs are as shown in Table 3-8. These loads are determined by dividing the maximum total fuel assembly beam to cell wall load by the number of fuel assemblies in the rack under evaluation (e.g., divide by 64 for a full rack, 32 for a half full rack).

For purposes of determining the effect on the fuel assembly grids, the impact load on each of the fuel support grids at each time step is determined by dividing the maximum calculated impact load per cell at each of the five nodes by number of spacer grids at each of the nodes. For each run, the impact loads in the East-West and North-South directions are combined using the SRSS method at the same time.

The resulting safety factor on fuel assembly spacer grid is as summarized in Table 3-11.

3.7.2.2 Stress Evaluation of Fuel Cladding

The maximum lateral acceleration acting on the fuel mass is used to calculate a load uniformly distributed over a single fuel rod modeled as a beam simply supported by the spacer grids, and the maximum fuel rod length between the spacer grids is 359.4 mm (14.148 in) as shown in Table 3-3.

The uniformly distributed load on the fuel rod is calculated as follows:

$$q = a \times W_{\text{fuel}}$$

Where,

a = Maximum lateral acceleration in g's (= 22.8 g) per section 7.2 of Reference 17, and
 W_{fuel} = Fuel assembly rod mass per unit length (0.61 kg/m).

The maximum bending moment for uniform load is calculated as

$$M = (q \times L_{\text{spacer}}^2) / 8$$

Where,

L_{spacer} = Maximum fuel rod length between spacer grids (359.4 mm (14.148 in)).

The resulting maximum bending stress in the fuel cladding is calculated from equation below.

$$\sigma_b = \frac{M \cdot R_o}{I}$$

Where,

R_o = Outer radius of fuel rod (4.75 mm (0.187 in)), and
 I = Moment of inertia of fuel rod cladding (160.4 mm⁴ (3.853 x 10⁻⁴ in⁴)).

This bending stress is compared to the yield stress of 540.3 MPa (78,365 psi) per Table 3-3 for fuel rod cladding, the resulting safety factor is given in Table 3-11. The strain associated with this maximum stress is

$$\varepsilon = \sigma_b / E$$

The maximum impact load on an individual fuel grid spacer cell, the bending stress and the strain induced in the fuel rod cladding due to the maximum lateral acceleration are summarized in Table 3-11. The structural integrity of the stored fuel assemblies under the SSE event is maintained, because the safety factors are greater than 1.0.

3.7.3 Rack Structural Evaluation

To ensure that the fuel racks have adequate safety margins, all stress evaluations for the fuel racks are performed based on the worst-case results in any rack at any time during multiple simulations. In this section, the structural integrity of welds and racks is evaluated by using the maximum loads in vertical and horizontal direction calculated by time-history analysis of the racks.

3.7.3.1 Stress Factors for Racks

Using the time-history analysis results for pedestal normal and lateral interface forces, the limiting bending moment and shear force at the baseplate-to-pedestal interface may be computed as a function of

RAI 287-8272 - Question 09.01.02-37_Rev.1

time. In particular, maximum values for the stress factors which are defined in Section 3.2.2 can be determined for each pedestal in each rack. Using this information, the structural integrity of the pedestals can be assessed.

The net section maximum bending moments and shear forces can also be determined at the bottom of the rack structure. From these loads, the stress factors for the NFSRs and the SFSR cell walls just above the baseplate can be also determined in the rack. Because they are at the end of fuel rack beam, these locations are the most heavily loaded net sections in the structure so that satisfaction of the stress factor criteria at these locations ensures that the overall structural criteria set forth in Section 3.2 are met.

As shown in Table 3-9:

- Maximum pedestal stress factors for the NFSRs and SFSRs are less than the allowable of 1.0.
- Maximum cell wall stress factors for the NFSRs and SFSRs are less than the allowable of 1.0.

Therefore, the rack cells and the support pedestals are able to maintain their structural integrity under the worst loading conditions.

3.7.3.2 Pedestal Thread Stress Evaluation

The integrity for the support pedestal thread is evaluated using the maximum load on the support pedestal in vertical direction as shown in Table 3-7. Using this load, the maximum shear stress of thread in the engagement region is calculated. The allowable shear stress of SA-240 Type 304L material for Level D condition is the lesser of $0.72 S_y = 106.2 \text{ MPa}$ (15,408 psi) or $0.42 S_u = 191.4 \text{ MPa}$ (27,762 psi) as stated on Section 3.2.2. Therefore, the former criteria controls, and the calculated shear stress of pedestal thread is acceptable, as shown on Table 3-13.

3.7.3.3 Stresses on Welds

Weld locations of the NFSRs subjected to SSE loading are at the bottom of the rack at the cell-to-baseplate connection, and at the top of the pedestal support at the baseplate connection.

SFSR welds are at the bottom of the rack at the cell-to-baseplate connection, at the top of the pedestal support at the baseplate connection, and at cell-to-cell connections. The maximum values of resultant loads are used to evaluate the structural integrity of these welds. The calculated stresses on fuel rack welds are summarized in Table 3-12.

(1) Cell-to-Baseplate Weld

As given in ASME Code Section III, Subsection NF, for Level A or B conditions, an allowable shear stress of a weld is $0.3 S_u = 136.7 \text{ MPa}$ (19,830 psi) conservatively based on the base metal material. As stated in Section 3.2.2.3, the allowable weld stress may be increased for Level D by a factor of 1.8, giving an allowable of $0.54 S_u = 246.1 \text{ MPa}$ (35,694 psi).

Stresses in the cell-to-baseplate welds are determined through the use of a simple conversion factor (ratio) applied to the corresponding stress factor in the adjacent rack material. This stress factor is discussed in Section 3.2.3, and given in Table 3-9. The conversion factor (ratio) values are developed from consideration of the differences in material thickness and length versus weld throat dimension and length, as follows:

$$\text{Ratio} = [(220 + 2.5) \times 2.5] / (180 \times 2.5 \times 0.707) = 1.75 \text{ (for the SFSRs)}$$

Where,

Inner cell dimension (220 mm (8.66 in)),

REVISED RESPONSE TO REQUEST FOR ADDITIONAL INFORMATION**APR1400 Design Certification****Korea Electric Power Corporation / Korea Hydro & Nuclear Power Co., LTD****Docket No. 52-046**

RAI No.: 287-8272
SRP Section: 09.01.02 – New and Spent Fuel Storage
Application Section: 9.1.2
Date of RAI Issue: 11/02/2015

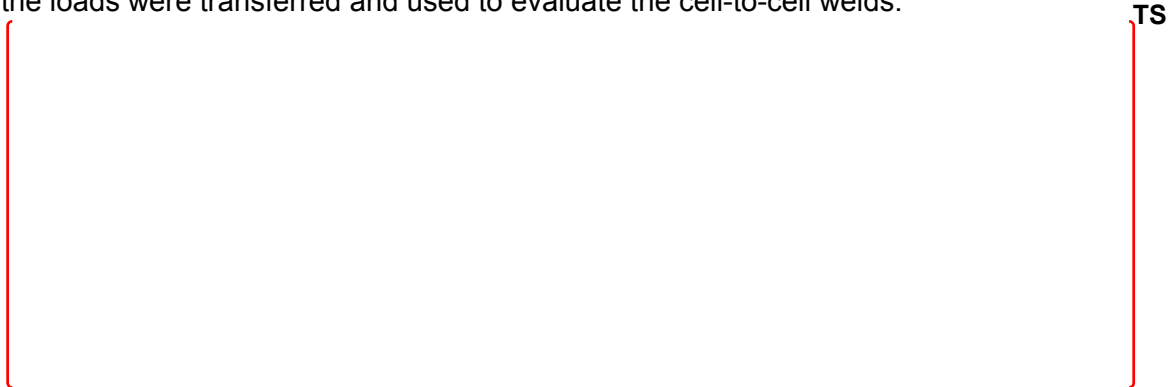
Question No. 09.01.02-38

The 10 CFR Part 50, Appendix A, General Design Criteria (GDC) 1, 2, 4, 5, 63, and 10CFR 52.80 (a) provide the regulatory requirements for the design of the new and spent fuel storage facilities. Standard Review Plan (SRP) Sections 9.1.2 and 3.8.4, Appendix D describes specific SRP acceptance criteria for the review of the fuel racks that are acceptable to meet the relevant requirements of the Commission's regulations identified above. In DCD Tier 2, Section 9.1.2.2.3, "New and Spent Fuel Storage Rack Design", the applicant stated that "The dynamic and stress analyses are performed as described in report APR1400-H-N-NR-14012-P & NP". In the technical report APR1400-H-N-NR-14012-P, Rev 0, Subsection 3.7.3.3 (3) "Cell-to-Cell Weld" provides a general description of the forces considered in the evaluation of cell-to-cell welds but did not provide any descriptions of how the stresses in the weld were calculated. In accordance with SRP 3.8.4 Appendix D I (3, 4, 5, 6), the applicant is requested to provide details of how the stresses in the cell-to-cell welds were determined, including a free-body diagram explaining how the loads were transferred and used to evaluate the cell-to-cell welds. The applicant is requested to identify any proposed changes to and provide a mark-up of Subsections in the DCD Tier 2 and the report APR1400-H-N-NR-14012-P, Rev.0, as appropriate.

Response – Rev. 0

Cell-to-cell connections are a series of connecting welds along the cell height. Stresses in the storage rack cell to cell welds develop due to fuel assembly impacts with the cell wall. Weld stress is calculated based on the maximum fuel-to-cell impact load and shear stress, which is obtained by using the cell wall shear stress coefficient under Level D conditions from the dynamic analysis results. The maximum fuel-to-cell impact load (= 25,000 lbf) is taken from Table 3-10 of technical report APR1400-H-N-NR-14012-P. The shear stress on the cell wall is calculated by multiplying shear allowable stress under Level D conditions and the cell wall stress coefficient, $FACT3 = 0.07$, per Table 3-12 of technical report APR1400-H-N-NR-14012-P.

The total shear stress acting on the weld is calculated by combining the shear stress acting on cell wall with the fuel-to-cell impact stress using the square root of the sum of the squares (SRSS) method. Then the safety factors of the storage rack cell-to-cell weld and base material adjacent to the weld are calculated as summarized in Table 3-13 of technical report APR1400-H-N-NR-14012-P. Below are figures that show a free-body diagram explaining how the loads were transferred and used to evaluate the cell-to-cell welds.



In summary, the stress on the cell-to-cell weld is calculated using the following formula.

- 1) Stress calculation of base metal adjacent to weld due to impact load:

$$S_{impact} = \frac{Impact_{sse}}{A_{weld}}$$

Where, $Impact_{sse}$ is the maximum cell to fuel assembly impact load in Table 3-10 of technical report APR1400-H-N-NR-14012-P and A_{weld} is the total area of weld.

- 2) Shear stress calculation on the cell wall:

$$S_{shear} = StressFactor \cdot V_{sse}$$

Where, $StressFactor$ is the shear stress factor of cell wall in Table 3-12 of technical report APR1400-H-N-NR-14012-P and V_{sse} is the allowable stress of cell wall under Level D condition.

- 3) Total shear stress calculation acting at cell-to-cell weld:

$$S_{combined} = \sqrt{(S_{impact}^2 + S_{shear}^2)}$$

Response – Rev. 1

Technical report, APR1400-H-N-NR-14012-NP was submitted as Rev. 0 in December, 2014. KHNP responses to RAI 287-8272 were based in part on the Technical Report. Subsequent to issuance of the Technical Report and RAI responses, the NRC provided feedback on both the Technical Report and RAI 287-8272 responses. In response to

this NRC feedback, Technical report, APR1400-H-N-NR-14012-NP will be revised (as Rev. 3) to incorporate additional information pertaining to the fuel racks. This RAI revision contains the specific Technical Report revisions relevant to this response and associated DCD changes, where necessary. A summary of the additional information is in the below paragraphs.

Cell-to-Cell Weld

Cell-to-cell connections are a series of connecting welds along the cell height. Stresses in the SFSR cell-to-cell welds develop due to fuel assembly impacts with the cell wall. Weld stress is calculated based on the maximum fuel-to-cell wall impact load and shear stress, which is obtained by using the cell wall shear stress coefficient under Level D conditions from the dynamic analysis results. These weld stresses are conservatively considered by assuming that fuel assemblies in adjacent cells are moving out of phase with one another so that impact loads in two adjacent cells are in opposite directions and are applied simultaneously. This load application tends to separate the two cells from each other at the weld.

Stress in the cell-to-cell weld is combined by the square root of the sum of the squares (SRSS) method for the shear stress due to horizontal load acting on rack and the shear stress due to impact load of rack fuel-to-cell wall, and the stress due to cell wall axial shear load.

Figure 1 shows a free-body diagram explaining how the loads were transferred and used to evaluate the cell-to-cell welds.

In summary, the stress on the cell-to-cell weld is calculated using the following formulas as described in Reference 1.

1) Stress calculation of base metal adjacent to weld due to impact load:

$$S_{impact} = \frac{F_{impact}}{A_{weld}}$$

Where,

F_{impact} : Maximum fuel assembly to cell impact load, and

A_{weld} : Total area of weld.

2) Shear stress calculation of the cell wall:

$$S_{shear} = FACT3 * V_{sse}$$

Where,

FACT3 : Shear stress factor of cell wall, and

V_{sse} : Allowable stress of cell wall under Level D condition.

3) Axial shear stress calculation of the cell wall:

$$S_{a_shear} = \frac{F_{a_shear}}{A_{weld}}$$

Where,

F_{a_shear} : Axial shear force of cell wall,

$$= FACT2 * V_{sse_axial} * A_{cell}$$

FACT2 : Tensile or bending stress factor of cell wall,

V_{sse_axial} : Allowable stress of cell wall under Level D condition, and

A_{cell} : Area of cell.

4) Total shear stress calculation acting at cell-to-cell weld:

$$S_{combined} = \sqrt{S_{impact}^2 + S_{shear}^2 + S_{a_shear}^2}$$



Figure 1 SFSR Weld Stress Diagram

Reference:

1. Doosan, "Structural and Seismic Analysis Report for New and Spent Fuel Storage Racks," N14014-224CN-0001, Rev.3, Aug. 2017 (Doosan Proprietary).

Impact on DCD

There is no impact on the DCD.

Impact on PRA

There is no impact on the PRA.

Impact on Technical Specifications

There is no impact on the Technical Specifications.

Impact on Technical/Topical/Environmental Reports

APR1400-H-N-NR-14012-NP (Rev. 3), Section 3.7.3.3(3) and Figure 3-19 will be revised as shown in Attachment 1 to this response.

Cell wall thickness (2.5 mm (0.098 in)),
Weld length (180 mm (7.09 in)), and
Weld throat thickness (= 2.5 x 0.707 = 1.767 mm (0.069 in)) are used.

For the NFSRs, the cell wall thickness and weld thickness are 6.0 mm (0.236 in) and 4.24 mm (0.167 in), respectively. The conversion factor (ratio) for the NFSRs is calculated as 1.54.

The highest predicted cell-to-baseplate weld stress is conservatively calculated based on the highest FACT2 for the rack cell region tension stress factor and FACT3 for the rack cell region shear stress factor. The maximum stress factors used do not all occur at the same time instant and the shear stress factors are the maximum for all load conditions. The total cell-to-baseplate weld stress is calculated by combining the shear stress on the weld with the axial shear stress on the weld by tension stress using the SRSS method. The stress on the weld of cell-to- baseplate is calculated as follows:

1) Shear stress calculation of cell-to-baseplate weld:

$$S_{\text{shear}} = (\text{FACT3}) \times \text{Min.}(0.72 \times S_y \text{ or } 0.42 \times S_u) \times \text{Ratio}$$

Where, FACT3 : Shear stress factor of cell wall in Table 3-9, and

0.72 x S_y or 0.42 x S_u : Allowable stress of cell wall under Level D condition.

2) Axial shear stress calculation of cell-to-baseplate weld:

$$S_{\text{axialshear}} = (\text{FACT2}) \times \text{Min.}(1.2 \times S_y \text{ or } 0.7 \times S_u) \times \text{Ratio}$$

Where, FACT2 : Tension stress factor of cell wall in Table 3-9, and

1.2 x S_y or 0.7 x S_u : Allowable stress of cell wall under Level D condition.

3) The total cell-to-baseplate weld stress:

$$S_{\text{combined}} = \sqrt{S_{\text{shear}}^2 + S_{\text{axialshear}}^2}$$

The calculated stress value is less than the allowable weld stress value of 246.1 MPa (35,694 psi). Therefore, all weld stresses between the cell wall and the baseplate are acceptable.

(2) Baseplate-to-Pedestal Weld

The stress in the baseplate-to-pedestal weld is evaluated using the maximum horizontal pedestal load and the maximum compressive vertical load. The weld stress is derived from simultaneous application of the maximum tensile force obtained from ANSYS and the maximum pedestal friction forces in the horizontal directions in Table 3-7. The calculated maximum stress identified in Table 3-12 is well below the Level D allowable of 246.1 MPa (35,694 psi). Therefore, all weld stresses between baseplate and support pedestal are acceptable.

(3) Cell-to-Cell Weld

Cell-to-cell connections are a series of connecting welds along the cell height. Stresses in the SF SR cell-to-cell welds develop due to fuel assembly impacts with the cell wall. Weld stress is calculated based on the maximum fuel-to-cell wall impact load and shear stress, which is obtained by using the cell wall shear stress coefficient under Level D conditions from the dynamic analysis results. These weld stresses are conservatively considered by assuming that fuel assemblies in adjacent cells are moving out of phase with one another so that impact loads in two adjacent cells are in opposite directions and are applied simultaneously. This load application tends to separate the two cells from each other at the weld.

RAI 287-8272 - Question 09.01.02-38_Rev.1

Stress in the cell-to-cell weld is combined by the square root of the sum of the squares (SRSS) method for the shear stress due to horizontal load acting on rack and the shear stress due to impact load of rack fuel-to-cell wall, and the stress due to cell wall axial shear load.

The maximum fuel-to-cell wall impact load is taken from Table 3-8. The shear stress on the cell wall is calculated by multiplying shear allowable stress under Level D conditions and the cell wall stress coefficient, FACT3 from Table 3-9. The total shear stress acting on the weld is calculated by combining the shear stress acting on cell wall with the fuel-to-cell impact stress using the SRSS method. The calculated stresses of the cell-to-cell weld and the base metal shear are well below the allowable, and the results are summarized in Table 3-12.

Figure 3-19 shows a free-body diagram explaining how the loads were transferred and used to evaluate the cell-to-cell welds.

In summary, the stress on the cell-to-cell weld is calculated using the following formulas as described in Reference 17.

1) Stress calculation of base metal adjacent to weld due to impact load:

$$S_{impact} = \frac{F_{impact}}{A_{weld}}$$

Where,

F_{impact} : Maximum fuel assembly to cell impact load in Table 3-8,
and A_{weld} : Total area of weld.

2) Shear stress calculation of the cell wall:

$$S_{shear} = FACT3 * V_{sse}$$

Where, FACT3 : Shear stress factor of cell wall in Table 3-9, and

V_{sse} : Allowable stress of cell wall under Level D condition.

3) Axial shear stress calculation of the cell wall:

$$S_{a_shear} = \frac{F_{a_shear}}{A_{weld}}$$

Where,

F_{a_shear} : Axial shear force of cell wall,
= $FACT2 * V_{sse_axial} * A_{cell}$

FACT2 : Tensile or bending stress factor of cell wall in Table 3-9,

V_{sse_axial} : Allowable stress of cell wall under Level D condition, and

A_{cell} : Area of cell.

4) Total shear stress calculation acting at cell-to-cell weld:

$$S_{combined} = \sqrt{S_{impact}^2 + S_{shear}^2 + S_{a_shear}^2}$$

3.7.3.4 Stress Evaluation of Stud Bolt for NFSR

The integrity for the stud bolt is evaluated for the maximum loads on NFSR module. Detailed calculation is provided in Appendix F (Reference 17). Stud bolt stress is evaluated against the criteria for Level D. The calculated stresses of stud bolt are well below the allowable, and the results are summarized in Table 3-14.

RAI 287-8272 - Question 09.01.02-38_Rev.1

TS

Figure 3-19 SFSR Weld Stress Diagram

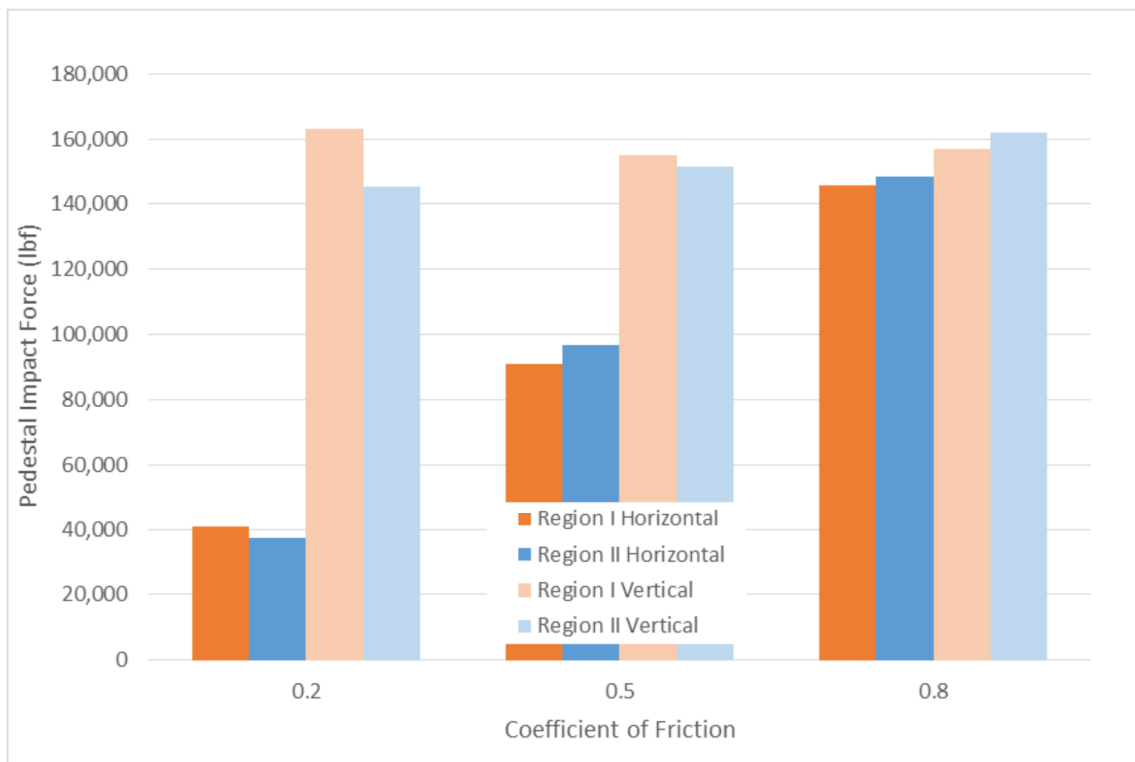


Figure 3-20 SFSR Loads for Varying Coefficients of Friction

REVISED RESPONSE TO REQUEST FOR ADDITIONAL INFORMATION**APR1400 Design Certification****Korea Electric Power Corporation / Korea Hydro & Nuclear Power Co., LTD****Docket No. 52-046**

RAI No.: 287-8272
SRP Section: 09.01.02 – New and Spent Fuel Storage
Application Section: 9.1.2
Date of RAI Issue: 11/02/2015

Question No. 09.01.02-39

1. The 10 CFR Part 50, Appendix A, General Design Criteria (GDC) 1, 2, 4, 5, 63, and 10CFR 52.80 (a) provide the regulatory requirements for the design of the new and spent fuel storage facilities. Standard Review Plan (SRP) Sections 9.1.2 and 3.8.4, Appendix D describes specific SRP acceptance criteria for the review of the fuel racks that are acceptable to meet the relevant requirements of the Commission's regulations identified above. In DCD Tier 2, Section 9.1.2.2.3, "New and Spent Fuel Storage Rack Design", the applicant stated that "The dynamic and stress analyses are performed as described in report APR1400-H-N-NR-14012-P & NP". In the technical report APR1400-H-N-NR-14012-P, Rev 0, Subsection 3.7.3.3(2) "Baseplate-to-Pedestal Weld", it is stated that "The weld between baseplate and support pedestal is checked using finite element analysis to determine that the maximum stress is 124.1 MPa (17,992 psi) under a Level D condition". In accordance with SRP 3.8.4 Appendix D I (3, 4, 5, 6), the applicant is requested to provide details of the finite element analysis performed, including the finite element computer program, the computer model, and the loads considered in the weld stress analysis. The applicant is requested to identify any proposed changes to and provide a mark-up of Subsections in the DCD Tier 2 and the report APR1400-H-N-NR-14012-P, Rev.0, as appropriate.

Response – (Rev. 0)

The stress evaluation of the welds between the pedestal and the rack baseplate were performed using the finite element analysis program, ANSYS and manual calculations.

An ANSYS model as shown below was used to develop the load along the welds surrounding the pedestal. The maximum horizontal loads on a single pedestal are applied to the top of the beam element.

TS

The weld stress is derived from the simultaneous application of the maximum tensile force, as obtained from ANSYS, and the maximum pedestal friction forces in the horizontal directions ($F_{xs}=756.2$ kN (170,000 lbf) and $F_{ys}= 660.1$ kN (148,400 lbf)), as determined by dynamic analysis. This is conservative, since these maximum loads may not occur at the same pedestal or at the same time instant. The maximum pedestal friction forces in any single direction are reported in Table 3-9 of technical report, APR1400-H-N-NR-14012-P. Therefore, stress on the weld is calculated by combining the horizontal load due to dynamic analysis and maximum tensile load, which is obtained from the ANSYS program.

Response – (Rev. 1)

Technical report, APR1400-H-N-NR-14012-NP was submitted as Rev. 0 in December, 2014. KHNP responses to RAI 287-8272 were based in part on the Technical Report. Subsequent to issuance of the Technical Report and RAI responses, the NRC provided feedback on both the Technical Report and RAI 287-8272 responses. In response to this NRC feedback, Technical report, APR1400-H-N-NR-14012-NP will be revised (as Rev. 3) to incorporate additional information pertaining to the fuel racks. This RAI revision contains the specific Technical Report revisions relevant to this response and associated DCD changes, where necessary. A summary of the additional information is in the below paragraphs.

The stress in the baseplate-to-pedestal weld is evaluated using the maximum horizontal pedestal load and the maximum compressive vertical load. The weld stress is derived from simultaneous application of the maximum tensile force obtained from ANSYS and the maximum pedestal friction forces in the horizontal directions in Table 3-7 of the Technical report, APR1400-H-N-NR-14012-NP. The calculated maximum stress (= 123.3 MPa (17,885 psi) for NFSR and 99.6 MPa (14,443 psi) for SFSR) is well below the Level D allowable of 246.1 MPa (35,694 psi). Therefore, all weld stresses between baseplate and support pedestal are acceptable.

Impact on DCD

There is no impact on the DCD.

Impact on PRA

There is no impact on the PRA.

Impact on Technical Specifications

There is no impact on the Technical Specifications.

Impact on Technical/Topical/Environmental Reports

APR1400-H-N-NR-14012-NP (Rev. 3), Section 3.7.3.3(2) will be revised as shown in Attachment 1 to this response.

Cell wall thickness (2.5 mm (0.098 in)),
Weld length (180 mm (7.09 in)), and
Weld throat thickness (= 2.5 x 0.707 = 1.767 mm (0.069 in)) are used.

For the NFSRs, the cell wall thickness and weld thickness are 6.0 mm (0.236 in) and 4.24 mm (0.167 in), respectively. The conversion factor (ratio) for the NFSRs is calculated as 1.54.

The highest predicted cell-to-baseplate weld stress is conservatively calculated based on the highest FACT2 for the rack cell region tension stress factor and FACT3 for the rack cell region shear stress factor. The maximum stress factors used do not all occur at the same time instant and the shear stress factors are the maximum for all load conditions. The total cell-to-baseplate weld stress is calculated by combining the shear stress on the weld with the axial shear stress on the weld by tension stress using the SRSS method. The stress on the weld of cell-to- baseplate is calculated as follows:

1) Shear stress calculation of cell-to-baseplate weld:

$$S_{\text{shear}} = (\text{FACT3}) \times \text{Min.}(0.72 \times S_y \text{ or } 0.42 \times S_u) \times \text{Ratio}$$

Where, FACT3 : Shear stress factor of cell wall in Table 3-9, and

0.72 x S_y or 0.42 x S_u : Allowable stress of cell wall under Level D condition.

2) Axial shear stress calculation of cell-to-baseplate weld:

$$S_{\text{axialshear}} = (\text{FACT2}) \times \text{Min.}(1.2 \times S_y \text{ or } 0.7 \times S_u) \times \text{Ratio}$$

Where, FACT2 : Tension stress factor of cell wall in Table 3-9, and

1.2 x S_y or 0.7 x S_u : Allowable stress of cell wall under Level D condition.

3) The total cell-to-baseplate weld stress:

$$S_{\text{combined}} = \sqrt{S_{\text{shear}}^2 + S_{\text{axialshear}}^2}$$

The calculated stress value is less than the allowable weld stress value of 246.1 MPa (35,694 psi). Therefore, all weld stresses between the cell wall and the baseplate are acceptable.

(2) Baseplate-to-Pedestal Weld

The stress in the baseplate-to-pedestal weld is evaluated using the maximum horizontal pedestal load and the maximum compressive vertical load. The weld stress is derived from simultaneous application of the maximum tensile force obtained from ANSYS and the maximum pedestal friction forces in the horizontal directions in Table 3-7. The calculated maximum stress identified in Table 3-12 is well below the Level D allowable of 246.1 MPa (35,694 psi). Therefore, all weld stresses between baseplate and support pedestal are acceptable.

(3) Cell-to-Cell Weld

Cell-to-cell connections are a series of connecting welds along the cell height. Stresses in the SFSR cell-to-cell welds develop due to fuel assembly impacts with the cell wall. Weld stress is calculated based on the maximum fuel-to-cell wall impact load and shear stress, which is obtained by using the cell wall shear stress coefficient under Level D conditions from the dynamic analysis results. These weld stresses are conservatively considered by assuming that fuel assemblies in adjacent cells are moving out of phase with one another so that impact loads in two adjacent cells are in opposite directions and are applied simultaneously. This load application tends to separate the two cells from each other at the weld.

REVISED RESPONSE TO REQUEST FOR ADDITIONAL INFORMATION**APR1400 Design Certification****Korea Electric Power Corporation / Korea Hydro & Nuclear Power Co., LTD****Docket No. 52-046**

RAI No.: 287-8272
SRP Section: 09.01.02 – New and Spent Fuel Storage
Application Section: 9.1.2
Date of RAI Issue: 11/02/2015

Question No. 09.01.02-40

1. The 10 CFR Part 50, Appendix A, General Design Criteria (GDC) 1, 2, 4, 5, 63, and 10CFR 52.80 (a) provide the regulatory requirements for the design of the new and spent fuel storage facilities. Standard Review Plan (SRP) Sections 9.1.2 and 3.8.4, Appendix D describes specific SRP acceptance criteria for the review of the fuel racks that are acceptable to meet the relevant requirements of the Commission's regulations identified above. In DCD Tier 2, Section 9.1.2.2.3, "New and Spent Fuel Storage Rack Design", the applicant stated that "The dynamic and stress analyses are performed as described in report APR1400-H-N-NR-14012-P & NP". In the technical report APR1400-H-N-NR-14012-P, Rev 0, the applicant in Subsection 3.2.2.3 "Faulted (Abnormal) Conditions (Level D)", specified the allowable compressive stress as two-thirds of the critical buckling stress for the stress limit criteria for combined axial compression + bending loads,. However, in subsection 3.7.3.4(2), "Local Stress Evaluation", the applicant calculated the critical buckling stress of 12,731 psi but did not reduce it to two-thirds to obtain allowable compressive stress for the rack cell wall. In accordance with SRP 3.8.4 Appendix D I (3), the applicant is requested to provide the technical justification for using the calculated critical buckling stress as the limit under Service Level D condition, instead of the two-thirds of the critical buckling stress as stated in the Level D stress limit criteria. Also, in the calculation of critical buckling stress, BETA (value of coefficient) = 4.0 is used. The applicant is requested to explain what boundary conditions are assumed on the long edges of the simplified cell wall buckling model, and provide the technical basis for this designation. The applicant is requested to identify any proposed changes to and provide a mark-up of Subsections in the DCD Tier 2 and the report APR1400-H-N-NR-14012-P, Rev.0, as appropriate.

Response – (Rev. 0)

The evaluation for cell wall buckling will be revised to reflect the two-thirds of the critical buckling stress as stated in the Level D stress limit criteria.
Section 3.7.3.4(2) of the report APR1400-H-N-NR-14012-P, will be revised as shown below.

“(2) Cell Wall Buckling

The allowable local buckling stresses of the cell walls for the fuel storage rack are obtained by using classical plate buckling analysis on the lower portion of the cell walls. A critical buckling stress of cell walls can be calculated by following equation (Reference 19).

$$\sigma_{cr} = K \frac{E}{(1-\nu^2)} \left(\frac{t}{b} \right)^2$$

Where, E (Young’s modulus) = 1.896E+05 N/mm²(27.5E+06 psi), ν (Poisson’s ratio) = 0.3, t (Cell Thickness) = 2.5 mm(0.098 in), b (Cell width) = 220 mm (8.66 in). The K factor varies depending on the plate length/width ratio and the boundary support conditions at the side of the plate. At the base of the rack, the cell wall acts alone in compression for a length of about 5.1 inch up to the point where the cover plate for the neutron absorber sheathing is attached. Above this level, the cover plate for the neutron absorber sheathing provides additional strength against buckling, which is not considered here. Therefore, the length/width ratio for the 220 mm (8.66 in) wide cell wall will be taken as 0.59. From Table 35 of Roark’s Formulas for stress & strain, 6th edition (Reference 19), the value of K is taken as 5.80, which is the corresponding value for a/b (length/width ratio) = 0.6, for two edges simply supported and two opposite edges clamped.

For the given data above, two-thirds of the critical buckling stress (σ_{cr}) as the limit under Service Level D condition is calculated as 103.2 MPa (14,964 psi) for all racks. It should be noted that this calculation is based on the applied stress being uniform along the entire length of the cell wall. In the actual fuel rack, the compressive stress comes from consideration of the overall bending of the rack structures during a seismic event and as such is negligible at the rack top. In the simulation, the maximum compressive stress due to overall bending is generated near the baseplate. This local buckling stress limit is not violated anywhere in the body of the rack modules, since the maximum compressive stress in the outermost cell is $\sigma = 2 \times 0.6 \times 147.5 \times \text{FACT2}$ (from Table 3-12 with FACT2 = 0.314) = 55.6 MPa (8,061 psi) and is within the allowable value of 103.2 MPa (14,964 psi). Therefore, a buckling of the rack cell wall does not occur.”

Response – (Rev. 1)

Technical report, APR1400-H-N-NR-14012-NP was submitted as Rev. 0 in December, 2014. KHNP responses to RAI 287-8272 were based in part on the Technical Report. Subsequent to issuance of the Technical Report and RAI responses, the NRC provided feedback on both the Technical Report and RAI 287-8272 responses. In response to this NRC feedback, Technical Report APR1400-H-N-NR-14012-NP will be revised (as Rev. 3) to incorporate additional information pertaining to the fuel racks. This RAI revision contains the specific Technical Report revisions relevant to this response and associated DCD changes, where necessary. A summary of the additional information is in the below paragraphs.

Cell Wall Buckling

The cell wall buckling analysis is performed to evaluate the buckling capacity of the spent fuel storage rack cells at the base of the racks using ANSYS program. The cell wall acts alone in compression for a length of about 130 mm (5.12 in) up to the point where the neutron absorbing material sheathing is attached. The sheathing provides additional strength against cell wall buckling. Therefore, the buckling analysis is considered on the lower 130 mm (5.12 in) of the cell wall.

The analysis is evaluated for Region II cells because the maximum stress factor on Region I racks is less than the maximum stress factor (i.e. FACT 2) for the region II racks. A compressive force for cell wall buckling evaluation is calculated as follows:

$$\begin{aligned}\sigma_{\text{comp}} &= 1.2 \times 21400 \times \text{FACT2} \\ &= 71.0 \text{ MPa (10,298 psi)}\end{aligned}$$

Where,

FACT2 = 0.401, the maximum stress factor of the Region II racks.

The above calculation is based on the maximum stress factor for the net vertical force on the gross cell cross-section. The vertical forces on the rack support pedestal reflects the weight of the rack plus the stored fuel assemblies during the seismic event. Since the stored fuel assemblies are supported by the rack baseplate, the actual compressive load on the rack cell structure is significantly less than the value determined by the results of dynamic simulations. It is appropriate to use a FACT2 value for cell wall buckling evaluation.

The critical elastic buckling load of cell wall is calculated by ANSYS eigenvalue analysis. Two by two cells of spent fuel storage rack are considered in the buckling analysis. The FE model reflects a reinforcement plate that is welded to outer side of cells. The boundary condition and applied unit load (1 MPa) of FE mode is as shown in Figure 1. Fixed boundary condition is applied on bottom surface of FE model. Figure 2 shows the results of buckling analysis. The minimum value of load multiplier represents the critical elastic buckling pressure of fuel rack cell wall, which is 136.68 MPa (19,823 psi). Therefore, two-thirds of the critical buckling stress as the limit under Service Level D condition is calculated as 91.12 MPa (13,215 psi).

The ANSYS analysis demonstrates that the spent fuel storage rack cells remain in a stable configuration under the maximum seismic load without any gross yielding of the storage cell wall, which satisfies the ASME Code requirements for Level D conditions. Therefore, a buckling of the rack cell wall does not occur.



Figure 1 Boundary Condition and Applied Load of FE Model



Figure 2 Results of Buckling Analysis

Impact on DCD

There is no impact on the DCD.

Impact on PRA

There is no impact on the PRA.

Impact on Technical Specifications

There is no impact on the Technical Specifications.

Impact on Technical/Topical/Environmental Reports

[APR1400-H-N-NR-14012-NP \(Rev. 3\)](#), Sections 3.2.2.3 and 3.7.3.5(2) will be revised as shown in Attachment 1 to this response.

(5) Combined Stress (Combined Bending and Compression Loads)

Combined bending and compression load on a net section per NF-3322.1(e)(1) satisfies the following equation.

$$f_a/F_a + C_{mx}f_{bx}/D_xF_{bx} + C_{my}f_{by}/D_yF_{by} \leq 1.0$$

Where,

$$\begin{aligned} f_a &= \text{Direct compressive stress in the section,} \\ f_{bx} &= \text{Maximum bending stress along x-axis,} \\ f_{by} &= \text{Maximum bending stress along y-axis,} \\ C_{mx} &= 0.85, \\ C_{my} &= 0.85, \\ D_x &= 1 - (f_a/F'_{ex}), \\ D_y &= 1 - (f_a/F'_{ey}), \\ F'_{ex}, F'_{ey} &= (\pi^2 E)/(2.15 (kl/r)_{x,y}^2), \end{aligned}$$

and subscripts x and y reflect the particular bending plane.

(6) Combined Stress (Combined Flexure and Tension Loads)

Combined flexure and tension/compression load on a net section satisfies the following equation given in NF-3322.1(e).

$$(f_a/0.6 S_y) + (f_{bx}/F_{bx}) + (f_{by}/F_{by}) \leq 1.0$$

(7) Welds

The allowable maximum shear stress on the net section of a weld (F_w) is given in Table NF-3324.5(a)-1.

$$F_w = 0.3 S_u$$

Where, S_u is the weld material ultimate strength at temperature. For the area in contact with the base metal, the shear stress on the gross section is limited to $0.4 S_y$. Where, S_y is the yield strength of material at a given temperature.

3.2.2.2 Upset Conditions (Level B)

The stress limits for Level B are those for Level A multiplied by the stress limit factor specified in Table NF-3523(b)-1 (Reference 4).

3.2.2.3 Faulted/Abnormal (Level D)

Article F-1334 (ASME Section III, Appendix F (Reference 4), states that limits for the Level D condition are the smaller of 2 or $1.167 S_u/S_y$ times the corresponding limits for the Level A condition if $S_u > 1.2 S_y$, or 1.4 if $S_u \leq 1.2 S_y$ except for requirements specifically listed below. S_u and S_y are the ultimate strength and yield strength at the specified rack design temperature. Examination of material properties for 304L stainless demonstrates that 1.2 times the yield strength is less than the ultimate strength. Since $1.167 \times (66,100/21,400) = 3.60$, the multiplier of 2.0 controls.

Exceptions to the above general multiplier are the following:

- (1) The tensile stress on the net section shall not exceed the lesser of $1.2 S_y$ and $0.7 S_u$.
- (2) The shear stress on the gross section shall not exceed the lesser of $0.72 S_y$ or $0.42 S_u$. In the case of the austenitic stainless steel material used here, $0.72 S_y$ governs.

RAI 287-8272 - Question 09.01.02-40_Rev.1

- (3) Combined axial compression and bending - The equations for Level A conditions shall apply except that $F_a = 2/3 \times$ Buckling Load, and F'_{ex} and F'_{ey} may be increased by the factor 1.65.
- (4) For welds, the Level D allowable weld stress is not specified in Appendix F of the ASME Code. Therefore, a limit for weld throat stress is used conservatively as follows:

$$F_w = (0.3 S_u) \times \text{Factor}$$

Where,

$$\text{Factor} = (\text{Level D shear stress limit})/(\text{Level A shear stress limit}) = 0.72 \times S_y / 0.4 \times S_y = 1.8$$

3.2.2.4 Stress Limit for NFSR Stud Bolt

The allowable tensile and shear stresses in the stud bolt are in accordance with ASME Code Section III, Subsection NF and Appendix F for Service Level A and D, respectively. The appropriate stress limit factors K_{bo} are given in Table NF-3225.2-1 in accordance with the load condition. The NFSR stud bolt subjected to combined shear and tension shall be proportioned so that the combined effects of shear and tensile stress satisfy the ellipse equation as shown below.

Load Condition	Tensile (F_{tb})	Shear (F_{vb})	Combined ⁽¹⁾
Level A	$S_u/3.33$	$0.62S_u/5$	$\frac{f_t^2}{F_{tb}^2} + \frac{f_v^2}{F_{vb}^2} \leq 1$
Level D ⁽²⁾	$\text{Min}(0.7S_u, S_y)$	$\text{Min}(0.42S_u, 0.6S_y)$	

(1) f_t and f_v are calculated tensile and shear stresses, respectively.

(2) Specified in Appendix F-1335 of ASME Code, Section III, Division 1.

3.2.3 Dimensionless Stress Factors

Dimensionless stress factors are calculated by the ratio of the calculated stress to the allowable stress for the combined and the individual loads according to ASME Code Section III, Division 1, Subsection NF. When the calculated stress factor does not exceed 1.0, it is considered to meet stress limit requirements for each service condition. In this report, a stress factor as described below is calculated using the load combination for each service condition.

FACT1 = Stress factor of member subject to combined bending and compression (as defined in subsection 3.2.2.1(5)).

FACT2 = Stress factor of member subject to combined flexure and tension (or compression) (as defined in subsection 3.2.2.1(6)).

FACT3 = Stress factor of gross shear on a net section.

3.3 Assumptions

The following assumptions are used in the WPMR dynamic analysis:

- (1) Fluid damping is conservatively neglected.
- (2) Sloshing of the SFP water during a seismic event does not influence the dynamic response of the racks in either horizontal direction because the height of the racks is approximately equal to 3/8 times the depth of water in the spent fuel pool (see Reference 21).
- (3) The fuel assembly is considered as 3-D elastic beam with concentrated masses at the upper and lower ends and at three equally spaced intermediate points of the rack (total of 5 nodes).

3.7.3.5 Local Stress Evaluation

(1) Cell Wall Impact

The maximum fuel-to-cell wall impact loads for the NFSRs and the SFSRs are as shown in Table 3-8. The evaluation for cell wall for impact is performed to guarantee that local impact does not affect criticality of stored fuel. Integrity of local cell wall is evaluated conservatively using the peak impact load. The limiting impact load to induce overall permanent deformation is calculated by plastic analysis. The cell walls of the new and the spent fuel storage racks can withstand a side load of a maximum of 273.2 kN (61,410 lbf) and 47.4 kN (10,660 lbf), respectively (Reference 17). Therefore, the cell wall of racks satisfies the requirement with the maximum impact loads less than the allowable loads.

(2) Cell Wall Buckling

The cell wall buckling analysis is performed to evaluate the buckling capacity of the spent fuel storage rack cells at the base of the racks using ANSYS program. The cell wall acts alone in compression for a length of about 130 mm (5.12 in) up to the point where the neutron absorbing material sheathing is attached. The sheathing provides additional strength against cell wall buckling. Therefore, the buckling analysis is considered on the lower 130 mm (5.12 in) of the cell wall.

The analysis is evaluated for Region II cells because the maximum stress factor on Region I racks is less than the maximum stress factor (i.e. FACT 2) for the region II racks as shown in Table 3-9.

A compressive force for cell wall buckling evaluation is calculated as follows:

$$\sigma_{\text{comp}} = 1.2 \times 21400 \times \text{FACT2} = 71.0 \text{ MPa (10,298 psi)}$$

Where,

FACT2 = 0.401, the stress factor is taken from Table 3-9.

Above calculation is based on the maximum stress factor for the net vertical force on the gross cell cross-section. The vertical forces on the rack support pedestal reflects the weight of the rack plus the stored fuel assemblies during the seismic event. Since the stored fuel assemblies are supported by the rack baseplate, the actual compressive load on the rack cell structure is significantly less than the value determined by the results of dynamic simulations. It is appropriate to use a FACT2 value for cell wall buckling evaluation.

The critical elastic buckling load of cell wall is calculated by ANSYS eigenvalue analysis. Two by two cells of spent fuel storage rack are considered in the buckling analysis. The FE model reflects a reinforcement plate that is welded to outer side of cells. The boundary condition and applied unit load (1 MPa) of FE mode is shown in Figure 3-28. Fixed boundary condition is applied on bottom surface of FE model. Figure 3-29 shows the results of buckling analysis. The minimum value of load multiplier represents the critical elastic buckling pressure of fuel rack cell wall, which is 136.68 MPa (19,823 psi). Therefore, two-thirds of the critical buckling stress as the limit under Service Level D condition is calculated as 91.12 MPa (13,215 psi).

The ANSYS analysis demonstrates that the spent fuel storage rack cells remain in a stable configuration under the maximum seismic load without any gross yielding of the storage cell wall, which satisfies the ASME Code requirements for Level D conditions. Therefore, a buckling of the rack cell wall does not occur.

(3) Secondary Stress by Temperature Effects

The temperature gradients across the rack structure caused by differential heating effects between one or more filled cells and one or more adjacent empty cells are considered. The worst thermal stress in a fuel rack is obtained when a storage cell has a fuel assembly generating heat at the maximum postulated rate and the surrounding storage cells contain no fuel. The thermal stress stresses that occur in this scenario

REVISED RESPONSE TO REQUEST FOR ADDITIONAL INFORMATION**APR1400 Design Certification****Korea Electric Power Corporation / Korea Hydro & Nuclear Power Co., LTD****Docket No. 52-046**

RAI No.: 287-8272

SRP Section: 09.01.02 – New and Spent Fuel Storage

Application Section: 9.1.2

Date of RAI Issue: 11/02/2015

Question No. 09.01.02-41

1. The 10 CFR Part 50, Appendix A, General Design Criteria (GDC) 1, 2, 4, 5, 63, and 10CFR 52.80 (a) provide the regulatory requirements for the design of the new and spent fuel storage facilities. Standard Review Plan (SRP) Sections 9.1.2 and 3.8.4, Appendix D describes specific SRP acceptance criteria for the review of the fuel racks that are acceptable to meet the relevant requirements of the Commission's regulations identified above. In DCD Tier 2, Section 9.1.2.2.3, "New and Spent Fuel Storage Rack Design", the applicant stated that "The dynamic and stress analyses are performed as described in report APR1400-H-N-NR-14012-P & NP". In accordance with SRP 3.8.4 Appendix D I (3, 4, 5, 6), the applicant is requested to provide the following additional information in the technical report.

(a) In the technical report APR1400-H-N-NR-14012-P, Rev 0, Subsection 3.7.2, "Fuel structural Evaluation", the applicant did not discuss the location of the impact on the fuel where the maximum impact force occurs. The applicant is requested to provide the impact load for both the top and at the mid height of the fuel assembly. The staff notes in Subsection 3.1.2.2, "Details for Rack and Fuel Assembly", that "The mass of the upper, the central and the lower nodes is 1/4, 1/2 and 1/4 of the total mass, respectively". Since only 25 percent of the mass is assumed at the ends of the fuel assembly, there is a potential for a higher g-load on the fuel assembly at the top compared to that at the mid height if the impact load at the top of the fuel assembly is more than half the impact load calculated at the mid height. The applicant is requested to provide a technical justification for not determining the g-load on the fuel assembly at the top and at the mid-height and then using the maximum of the g-load in subsequent fuel assembly structural integrity evaluations.

(b) The staff in reviewing Table 3-10, "Impact Loads on Rack", notes that the impact load on the fuel assembly in the East-West and North-South directions is 25000 lbf and 18,594 lbf respectively. In subsection 3.7.2, "Fuel structural Evaluation", the applicant considered only the 25000 lbf load in evaluation the fuel assembly. The applicant is requested to provide the technical basis for not combining the impact load on the fuel assembly in the north-south and

east-west directions simultaneously to obtain the total lateral impact load for use in evaluating the structural integrity of the fuel assembly.

(c) The applicant is also requested to provide the general criteria used for combining the seismic responses in the design and analysis of the fuel assembly, rack structure, welded connections, and the rack supports of NFSR and SFSR due to the SSE excitation along the three orthogonal directions (2 horizontal and vertical) imposed simultaneously.

The applicant is requested to identify any proposed changes to and provide a mark-up of Subsections in the DCD Tier 2 and the report APR1400-H-N-NR-14012-P, Rev.0, as appropriate.

Response – (Rev. 0)

(a) The impact loads for both the top and at the mid height of the fuel assembly are as shown in the table below:

	TS
--	----

(b) The structural integrity of the fuel assembly will be evaluated by combining the impact load on the fuel assembly in the north-south and east-west directions simultaneously to obtain the total lateral impact load. The report APR1400-H-N-NR-14012-P including the structural integrity evaluation of the fuel assembly will be provided by April 30, 2016.

(c) Seismic loadings for the three orthogonal directions (2 horizontal and vertical) are applied simultaneously to the rack models. The seismic responses are combined using the square root of the sum of the squares (SRSS) method in the design and analysis of the fuel assembly, rack structure, welded connections, and the rack supports of NFSR and SFSR due to the SSE excitation.

Response – (Rev. 1)

Technical report, APR1400-H-N-NR-14012-NP was submitted as Rev. 0 in December, 2014. KHNP responses to RAI 287-8272 were based in part on the Technical Report. Subsequent to issuance of the Technical Report and RAI responses, the NRC provided feedback on both the Technical Report and RAI 287-8272 responses. In response to this NRC feedback, Technical Report APR1400-H-N-NR-14012-NP will be revised (as Rev. 3) to incorporate additional information pertaining to the fuel racks. This RAI revision contains the specific

Technical Report revisions relevant to this response and associated DCD changes, where necessary. A summary of the additional information is in the below paragraph).

Details for Rack and Fuel Assembly Model

The NFSR and fuel assembly model are of a single rack and includes 3-D elastic beam elements (ANSYS BEAM4) and lumped mass elements (ANSYS MASS21) with properties derived from the dynamic characteristics of the detailed 3-D shell model of the NFSR. Effective structural properties for the dynamic model are determined from the natural frequencies and mode shapes of the detailed model. Vertical portions of the NFSR cells and fuel assemblies are each represented by five nodes. Nodes are located at the rack baseplate, $\frac{1}{4} H$, $\frac{1}{2} H$, $\frac{3}{4} H$, and H (where H is the rack height measured above the baseplate). Each rack node has six degrees of freedom (three translations and three rotations) and a lumped mass associated with it. The nodes for the rack and the fuel assembly are connected by contact elements (ANSYS CONTAC52) in the horizontal direction. There is a single contact element in the vertical direction between the fuel assembly bottom node and the baseplate node.

The SFSR model is similar to the NFSR model and is composed of elastic beam elements and lumped mass elements with properties derived from the dynamic characteristics of the detailed 3-D shell model of the SFSR. All the fuel assemblies in each storage rack module are modeled as one beam of which the mass equals the sum of the masses of all the fuel assemblies in a rack module. Because the fuel assemblies in a rack module are modeled together, all fuel assemblies move simultaneously in one direction. This assumption results in larger impact forces on the rack module than the actual case and results in conservative loads on the storage rack. Because the fuel assembly is modeled with five nodes, the calculated impact loads on the nodes will be larger than the actual value because the fuel assembly actually has eleven spacer grids. The maximum fuel assembly grid horizontal impact load is determined by dividing the maximum impact load at each node by the number of grids associated with that node (2.75 for Nodes 10, 11, and 12, and 1.375 for Nodes 9 and 13). Lumped masses of the rack and fuel assemblies are distributed among the five nodes for spent fuel storage rack cells and fuel assemblies as shown in the table below.

Node No.		Location	Total Mass Distribution
Rack	Fuel Assembly		
13	18	Top of Rack	12.5 %
12	17	3/4 Height	25 %
11	16	1/2 Height	25 %
10	15	1/4 Height	25 %
9	14	Bottom (Baseplate) of Rack	12.5 %

Impact Load for Fuel Assembly-to-Cell Wall

Maximum impact loads of fuel assembly-to-cell wall are determined by dividing the maximum total fuel assembly beam to cell wall load by the number of fuel assemblies in the rack under evaluation (e.g., divide by 64 for a full rack, 32 for a half full rack). For purposes of determining the effect on the fuel assembly grids, the impact load on each of the fuel support

grids at each time step is determined by dividing the maximum calculated impact load per cell at each of the five nodes by number of spacer grids at each of the nodes. For each run, the impact loads in the East-West and North-South directions are combined using the SRSS method at the same time.

Fuel Structural Evaluation

Lateral impact load on the spent fuel assembly is evaluated for two acceptance criteria: fuel spacer grid buckling and fuel cladding yield stress. The maximum acceleration load that the rack imparts on the fuel assembly can be conservatively calculated as follows:

$$a = \frac{F}{w}$$

Where,

- a = Maximum lateral acceleration in g's (= 22.8 g) per section 7.2 of Reference 1,
- F = Maximum fuel-to-cell wall impact load per cell, and
- w = Weight of one fuel assembly (6.27 kN (1408.6 lbf)).

The structural integrity of fuel assembly cladding is evaluated for the maximum lateral acceleration load, obtained by combining (i.e., SRSS) the simultaneous impact load in the E-W and N-S directions to find the maximum value at any time step. The fuel assembly spacer grid is evaluated for the maximum grid impact load, obtained by combining (i.e., SRSS) the simultaneous impact load in the E-W and N-S directions at the same time.

Structural Integrity Evaluation of Fuel Spacer Grid

The lateral impact loads on a single fuel spacer grid is compared against its buckling load capacity. The critical buckling load of the fuel spacer grid for the APR1400 design is 31.3 kN (7,045 lbf) and compared with the combined fuel grid impact load.

Stress Evaluation of Fuel Cladding

The maximum lateral acceleration acting on the fuel mass is used to calculate a load uniformly distributed over a single fuel rod modeled as a beam simply supported by the spacer grids, and the maximum fuel rod length between the spacer grids is 359.4 mm (14.148 in).

The uniformly distributed load on the fuel rod is calculated as follows:

$$q = a \times W_{\text{fuel}}$$

Where,

- a = Maximum lateral acceleration in g's (= 22.8 g), and
- W_{fuel} = Fuel assembly rod mass per unit length (0.61 kg/m).

The maximum bending moment for uniform load is calculated as

$$M = (q \times L_{\text{spacer}}^2) / 8$$

Where,

- L_{spacer} = Maximum fuel rod length between spacer grids (359.4 mm (14.148 in)).

The resulting maximum bending stress in the fuel cladding is calculated from equation below.

$$\sigma_b = \frac{M \cdot R_o}{I}$$

Where,

R_o = Outer radius of fuel rod (4.75 mm (0.187 in)), and

I = Moment of inertia of fuel rod cladding (160.4 mm⁴ (3.853 x 10⁻⁴ in⁴)).

This bending stress is compared to the yield stress of 540.3 MPa (78,365 psi) for fuel rod cladding. The strain associated with this maximum stress is

$$\varepsilon = \sigma_b / E$$

The maximum impact load on an individual fuel grid spacer cell, the bending stress and the strain induced in the fuel rod cladding due to the maximum lateral acceleration.

Seismic Input and Response Combination

Seismic inputs for the three orthogonal directions (east-west, north-south, and vertical) are applied simultaneously to the rack modules. The horizontal loads are combined using the square root sum of the squares (SRSS) method in the analysis of the fuel assembly, rack structure, welded connections, and rack supports.

Reference:

1. Doosan, "Structural and Seismic Analysis Report for New and Spent Fuel Storage Racks," N14014-224CN-0001, Rev.3, Aug. 2017 (Doosan Proprietary)

Impact on DCD

There is no impact on the DCD.

Impact on PRA

There is no impact on the PRA.

Impact on Technical Specifications

There is no impact on the Technical Specifications.

Impact on Technical/Topical/Environmental Reports

APR1400-H-N-NR-14012-NP (Rev. 3) will be revised as shown in Attachment 1 to this response.

- a) Sections 3.1.2.2(1), 3.7.1.3(1), and 3.7.2.1
- b) Sections 3.7.1.3, 3.7.2, Table 3-8, and Table 3-11
- c) Sections 3.1.2.1 and 3.7

because the PSDs shown in Figure 3-17 and Figure 3-18 have no abrupt dip or low points in power that could indicate insufficient energy input at a frequency in the range of interest.

- ✓ The time history for each of the three orthogonal directions is statistically independent from the others, as demonstrated by the absolute value of their correlation coefficient not exceeding 0.16 – met, largest value is 0.08 for both NFSR and SFSR.

Figure 3-11 through Figure 3-14 show the comparison between the target response spectrum (red) and the computed average response spectrum (black) for the five time histories for the E-W, N-S, and vertical directions for NFSR and SFSR, respectively. The two areas where the adequacy checks are not consistent with the guidance are the 30% exceedance and number of consecutive points below the target. Since the PSD check was performed for the each average of all time histories and showed no gaps (Figure 3-17 and Figure 3-18), the points of exceedance just result in additional energy input, which is conservative and judged acceptable.

In addition, a comparison of predicted results was performed to confirm that none of the time histories provided unexpected or inconsistent behavior, as described in Section 3.7.5.

The average of the generated response spectra is shown to envelope the corresponding target spectra (Figure 3-11 through Figure 3-14), meeting the intent of SRP 3.7.1 (Reference 9).

Based on the above, the use of the five time artificial histories shown in Figure 3-5 to Figure 3-10 is considered satisfactory for the nonlinear structural analysis of the fuel storage rack response to seismic conditions.

3.1.2 Modeling

3.1.2.1 General Considerations

Reliable assessment of the kinematic behavior of the rack modules requires suitable dynamic models that incorporate the key attributes of the structures. The SFSR model must have the ability to execute concurrent sliding, rocking, bending, twisting, and other motions associated with free-standing racks. Additionally, the SFSR model must possess the capability to simulate fuel assembly rattling, rack lift-off, and subsequent impact of support pedestals, while also considering the effect of the water mass in and around the rack modules. Similarly, the NFSR model must be able to simulate fuel assembly rattling and other motions associated with fixed-base racks.

The sections below describe individual features of the 3-D dynamic analysis model for the fuel racks.

(1) Seismic Input and Response Combination

Seismic inputs for the three orthogonal directions (east-west, north-south, and vertical) are applied simultaneously to the rack modules. The horizontal loads are combined using the square root sum of the squares (SRSS) method in the analysis of the fuel assembly, rack structure, welded connections, and rack supports.

(2) Fuel Loading

The dynamic analysis of the NFSR assumes the racks are fully loaded; the SFSR analysis considers various loading configurations (in most cases fully loaded, but also mixed/partially loaded and empty). When fuel assemblies are present in a rack, they are assumed to be fully seated (lowered all the way into a cell).

3.1.2.2 Details for Rack and Fuel Assembly Model

The sections below provide details on the rack and fuel assembly modeling.

(1) New Fuel Storage Rack Model

The dynamic analysis model for the NFSR and fuel assemblies are shown in Figure 3-1. The NFSR and fuel assembly model are of a single rack and includes 3-D elastic beam elements (ANSYS BEAM4) and lumped mass elements (ANSYS MASS21) with properties derived from the dynamic characteristics of the detailed 3-D shell model of the NFSR. Effective structural properties for the dynamic model are determined from the natural frequencies and mode shapes of the detailed model (see Section 3.1.2.7). Details of effective structural properties for fuel racks are shown in Appendix H of Reference 17. Structural properties (i.e. Young's modulus and flexural rigidity) for fuel assemblies are shown in Table 3-3.

Vertical portions of the NFSR cells and fuel assemblies are each represented by five nodes. Nodes are located at the rack baseplate, $\frac{1}{4} H$, $\frac{1}{2} H$, $\frac{3}{4} H$, and H (where H is the rack height measured above the baseplate). Each rack node has six degrees of freedom (three translations and three rotations) and a lumped mass associated with it. The nodes for the rack and the fuel assembly are connected by contact elements (ANSYS CONTAC52) in the horizontal direction. There is a single contact element in the vertical direction between the fuel assembly bottom node and the baseplate node.

Lumped masses of the NFSR and fuel assemblies are distributed among the five nodes for rack cells and fuel assemblies as shown in the table below:

Node No. (Figure 3-1)		Location	Total Mass Distribution
Rack	Fuel Assembly		
13	18	Top of Rack	12.5 %
12	17	3/4 Height	25 %
11	16	1/2 Height	25 %
10	15	1/4 Height	25 %
9	14	Bottom (Baseplate) of Rack	12.5 %

(2) Spent Fuel Storage Rack Model

To model the interaction among the multiple SFSRs, the WPMR shown in Figure 3-3 is comprised of a dynamic analysis model for individual SFSRs, as shown in Figure 3-2. This model is similar to the NFSR model and is composed of elastic beam elements and lumped mass elements with properties derived from the dynamic characteristics of the detailed 3-D shell model of the SFSR. An underlying assumption in the modeling of the rack as a single beam using the overall bending stiffness of the entire rack is that the cell-to-cell welds remain intact and can carry the internal forces. This assumption is confirmed by structural evaluation of the welds (see Section 3.7.3.3).

Effective structural properties for the dynamic model are determined from the natural frequencies and mode shapes of the detailed model (see Section 3.1.2.7).

Figure 3-2 shows a schematic depicting five nodes representing masses of fuel and rack cells and their associated elements, which are used to represent the interactions and vertical and horizontal motions of support pedestals, respectively. Contact (i.e., gap) elements are used in the representation of rack sliding and impact. A directional stiffness is assigned to the contact element. The pool floor is assumed to be a rigid body initially in contact with the rack pedestals. The contact elements are used to represent potential impact of a rack pedestal on the pool floor. The coefficient of friction between the rack pedestals and pool floor is incorporated into a contact (gap) element.

performed to verify that fuel rack response is reasonably bounded. These sensitivities were:

- Run numbers 21 and 22 are identical to the NFSR bounding run but vary the value of the rack elastic modulus times the moment of inertia (i.e., EI) $\pm 20\%$.
- Run numbers 23 and 24 are identical to the bounding run but vary the value of the rack elastic modulus times the moment of inertia (i.e., EI) $\pm 20\%$.
- Run numbers 25 through 32 vary impact spring constants of rack-to-floor, rack-to-rack baseplate, and fuel-to-cell wall by $\pm 20\%$.
- Run number 33 evaluates EOL fuel elastic modulus times the moment of inertia (i.e., EI)
- Run numbers 34 and 35 assume empty racks and a mix of full, 50%, 25%, and empty racks (see Figure 3-4).
- Run number 36 was performed with a fixed time step of one half that used for all other runs in order to demonstrate convergence.

Conclusions from these sensitivity cases are discussed in Section 3.7.4.

3.7 Results of Analyses

This section discusses the results, which are presented in tables and figures at the end of the section. Detailed results are provided in Reference 17. Structural evaluation results according to load combination of Table 3-1 are meet the ASME Code Section III, Subsection NF.

Although runs are performed with five different time histories, note that individual runs shown are not independent. For example, runs 6, 11, and 16 are identical inputs except for the rack pedestal coefficient of friction. Also, sensitivities runs were performed using the base runs (i.e., runs 6 through 20 for the SFSR and 1 through 5 for the NFSR) giving the most limiting results. For example, the sensitivity on rack-to-rack stiffness (i.e., runs 31 and 32) used base run 12 since it had the highest baseplate-to-baseplate impact load, leading to results of runs 31 and 32 being biased high. Since all sensitivities were performed this way, the sensitivity run loads will average higher than the loads from the base runs.

For the SFSRs, each run was performed for all racks, and results are reported separately for region I and region II. The heaviest region I rack weighs almost twice as much as the lightest in region II (see Table 3-2), leading to different magnitudes of some responses between regions.

The following results are presented in the identified tables:

- Displacements of racks:
 - (1) SFSR baseplates relative to pool floor (i.e., where they were at start of transient)[Table 3-6]
 - (2) NFSR and SFSR tops in relation to their bases (i.e., flexing of rack upper structure that could lead to contact even if bases are not touching)[Table 3-6]
- Loads on supports:
 - (1) NFSR and SFSR pedestal loads in vertical direction and horizontal directions [Table 3-7]
- Loads on structure:
 - (1) Impact loads on SFSR baseplates (i.e., adjacent racks bump into each other) – used to assess integrity of baseplate to cell welds [Table 3-8]
 - (2) Impact loads on cell walls (i.e., fuel assemblies rattle against walls of cell containing them) – used to assess integrity of cell-to-cell welds [Table 3-8]
 - (3) Impact loads on fuel assembly grids (i.e., not all grids along the height impact cell walls uniformly) [Table 3-8]
- Margin to overturning – used to verify rack does not tip [Table 3-10]
- Stress factors – used to compare calculated loads to allowable stresses (i.e., values < 1.0 have margin to allowable [Table 3-9])

RAI 287-8272 - Question 09.01.02-41_Rev.1

- Rack weld stresses and safety factors – used to confirm racks maintain their structural integrity [Table 3-12]
- Stress on fuel assembly – used to confirm fuel assemblies are not damaged to the extent that cladding is breached [Table 3-11]
- Stresses on the threads of the SFSR pedestal leveling feet – used to assess damage to threads [Table 3-13]
- Stresses on the NFSR stud bolt - used to confirm NFSR stud bolts maintain their structural integrity [Table 3-14]

The seismic responses in the horizontal directions are combined using the square root of the sum of the squares (SRSS) method in the analysis of the fuel assembly, rack structure, welded connections, and the rack supports of NFSR and SFSR. For all horizontal loads except fuel assembly grid impact, the SRSS combination uses the maximum E-W and the maximum N-S load at any time during the transient, even if they do not occur during the same time step. The grid impact loads use the values during the same time step to find the maximum.

3.7.1 Time History Simulation Results

The loads and the displacements by dynamic simulations are summarized in Table 3-6 through Table 3-8 and in Figure 3-20 through Figure 3-26. Note that the values shown are maximum values found for any of the racks for each run. Where horizontal loads are reported, they are for the same rack, but the vertical load reported for that run may be from a different rack. For the SFSRs, results are reported for both Region I and Region II racks since they are slightly different structurally and have different rack-to-rack spacing.

3.7.1.1 Displacements of Rack

The NFSRs are fixed and not subject to displacement at their bases provided their stud bolts remain intact, as shown in Figure 2-3. The displacement of the NFSRs at their top is determined to confirm there is no contact between adjacent cells or with the new fuel storage pit walls.

The SFSRs are specified to be installed with pedestals and baseplates as close as possible, as shown in Figure 2-6. Therefore, during a seismic event they will initially move apart, although they could again slide together during the transient. Due to the random nature of the seismic acceleration, the racks will move in different directions by different amounts, and this can be affected by the time step and COF used in the analysis. This randomness would be true even if experiments were run repeatedly using different time histories. The initial movement can determine the ultimate relative position of racks to each other. As discussed in Section 3.1.1, a baseline correction process has been used to eliminate unrealistic cumulative displacement leading to large final displacements. The use of five independent time histories with sensitivities for COF and rack loading provides a reasonable range of possible displacements. Since none of the runs predicted displacements of more than a small fraction of the gap between the outermost racks to SFP wall, contact of cells between SFSRs and the SFP walls is not expected. The baseplates of adjacent racks can come into contact at some velocity if they initially move apart and then back together, as discussed in Section 3.7.1.3.

Presuming that the racks are in contact at their bases, flexure of the racks along their height could cause the top ends of adjacent racks to come into contact. The maximum reduction in gap between adjacent racks (i.e., larger values indicate the rack upper structures to be closer to each other) are shown in Table 3-6. The minimum gap for the cell-to-cell contact in Region I is 60.0 mm (2.36 in), and that of Region II is 30.0 mm (1.18 in), as shown in Figure 2-5. Therefore, there is no impact on the rack cells by each other, because the maximum relative displacements of racks are smaller than the cell wall separation with baseplates touching.

The maximum relative displacement of the rack pedestal from its starting point is 104.3 mm (4.1 in) as shown in Table 3-6. The minimum size of the embedment plate is about 610 mm (24 in) x 610 mm (24 in) (Reference 27). Therefore, rack pedestals do not slide off the embedment plates onto the spent fuel pool liner because the maximum displacement of rack pedestal is not large enough to move off of the embedment plate.

The maximum rotations of the rack are obtained from a post-processing of the rack time history response output. The SF SR should not exhibit rotations sufficient to cause the rack to overturn (i.e., the rack does not exhibit a rotation sufficient to bring the center of mass over the corner pedestal). Based on the width and height of a 8x7 rack, the rotation required to produce incipient tipping for this rack is approximately equal to:

$$\tan^{-1}[(1/2 * \text{Distance to bring center of gravity over pedestal}) / (1/2 * \text{Height of rack})]$$

$$\tan^{-1}[(1,610/2) / (4,775/2)] = 18.5^\circ$$

As shown in Table 3-10, the safety factor for allowable angle is greater than the acceptance criteria of 1.5 from SRP 3.8.5. Therefore, overturning of a rack module does not occur.

3.7.1.2 Support Pedestal Loads of Rack

The maximum horizontal and vertical loads generated on support pedestal with the application of SSE loads are shown in Table 3-7 and Figure 3-22 and are used to perform structural integrity evaluation of support pedestal and rack. The dynamic simulations of the racks give results for the vertical and two horizontal forces (i.e., E-W and N-S directions) throughout the transient. From those values, the maximum axial force in the vertical direction and the maximum shear forces of the two horizontal directions per pedestal are determined. The resultant shear force for each run is conservatively calculated by combining the maximum horizontal loads on any single pedestal as shown in Table 3-7 using the square root of the sum of the squares (SRSS) method. The maximum bending moment at the bottom baseplate-to-pedestal interface is computed by multiplying the maximum shear force and the distance from the bottom baseplate to the contact point surface underneath of the NFSRs and SF SRs, which is 185 mm (7.28 inches) and 160 mm (6.3 inches) as shown in Tables 2-1 and 2-2, respectively. Additional detail is provided in Appendix F of Reference 17.

3.7.1.3 Impact Loads

The impact loads for fuel-to-cell wall, rack-to-rack and rack-to-pool wall of the NFP and SFP are calculated as follows:

(1) Fuel-to-Cell Wall

For purposes of assessing the effect on rack structural integrity, the maximum impact loads of fuel assembly-to-cell wall for the NFSRs and the SF SRs are as shown in Table 3-8. These loads are determined by dividing the maximum total fuel assembly beam to cell wall load by the number of fuel assemblies in the rack under evaluation (e.g., divide by 64 for a full rack, 32 for a half full rack).

For purposes of determining the effect on the fuel assembly grids, the impact load on each of the fuel support grids at each time step is determined by dividing the maximum calculated impact load per cell at each of the five nodes by number of spacer grids at each of the nodes. For each run, the impact loads in the East-West and North-South directions are combined using the SRSS method at the same time. The combined maximum impact loads on fuel support grid of the NFSRs and the SF SRs are shown in Table 3-8.

(2) Impacts of Rack-to-Rack and Rack-to-Pool Wall

RAI 287-8272 - Question 09.01.02-41_Rev.1

SFSRs are installed as closely as possible with the protruding baseplate intended to be in contact with the adjacent baseplates. If the racks were initially installed with slight separation, conclusions would not change since it would be no different than a few time steps into a transient when the rack bases have moved slightly apart. As reported in Section 3.7.1.1, the upper part of the racks do not come into contact. Therefore, the only rack-to-rack contact is between the baseplate of racks. The maximum impact load at the SFSR baseplates is shown in Table 3-8.

Also as reported in Section 3.7.1.1, the racks do not contact the SFP wall. Therefore, no rack to pool wall impact loads are calculated. This is consistent with SRP Section 3.8.4, Appendix D, Structural Acceptance Criteria, which states:

“In the consideration of the effects of seismic loads, factors of safety against gross sliding and overturning of racks and rack modulus [sic] under all probable service conditions should be in accordance with SRP Section 3.8.5, Subsection II.5. This position on factors of safety against sliding and tilting need not be met provided that the applicant meets any one of the following conditions:

“a. Detailed nonlinear dynamic analyses show that the amplitudes of sliding motion are minimal and impact between adjacent rack modules or between a rack module and the pool walls is prevented provided that the factors of safety against tilting are within the allowable values provided in SRP Section 3.8.5, Subsection II.5....”

3.7.2 Fuel Structural Evaluation

Lateral impact load on the spent fuel assembly is evaluated for two acceptance criteria: fuel spacer grid buckling and fuel cladding yield stress.

The maximum impact load per cell applied to fuel assembly is evaluated for the peak load shown in Table 3-8. Therefore, the maximum acceleration load that the rack imparts on the fuel assembly can be conservatively calculated as follows:

$$a = \frac{F}{w}$$

Where,

a = Maximum lateral acceleration in g's (= 22.8 g) per section 7.2 of Reference 17, F = Maximum fuel-to-cell wall impact load per cell, and
w = Weight of one fuel assembly (6.27 kN (1408.6 lbf)).

The structural integrity of fuel assembly cladding is evaluated for the maximum lateral acceleration load, obtained by combining (i.e., SRSS) the simultaneous impact load in the E-W and N-S directions to find the maximum value at any time step. The fuel assembly spacer grid is evaluated for the maximum grid impact load, obtained by combining (i.e., SRSS) the simultaneous impact load in the E-W and N-S directions at the same time.

3.7.2.1 Structural Integrity Evaluation of Fuel Spacer Grid

The lateral impact loads on a single fuel spacer grid is compared against its buckling load capacity, which is shown in the Table 3-3. The critical buckling load of the fuel spacer grid for the APR1400 design is 31.3 kN (7,045 lbf) and compared with the combined fuel grid impact load as shown in Table 3-8. The resulting safety factor on fuel assembly spacer grid is as summarized in Table 3-11.

3.7.2.2 Stress Evaluation of Fuel Cladding

The maximum lateral acceleration acting on the fuel mass is used to calculate a load uniformly distributed

Table 3-8 Maximum Impact Loads of Each Simulation⁽¹⁾

Rack	Run No.	Rack-to-Rack Baseplate Impact Load (lbf)	Fuel-to-Cell Wall Impact Load per Cell (lbf)			Combined Fuel Grid ⁽²⁾ Impact Load (lbf)	Coefficient of Friction
			Horizontal		Vertical		
			E-W	N-S			
NFSR	1	-	10,304	14,380	6,477	4,018	N/A
	2	-	11,127	14,913	6,491	3,748	
	3	-	11,432	14,950	7,534	4,481	
	4	-	11,298	14,573	5,089	3,869	
	5	-	10,395	13,646	4,288	4,481	
SFSR (Region I)	6	215,000	17,969	13,656	9,063	3,405	0.2
	7	210,000	17,031	18,906	11,406	3,300	
	8	231,000	18,563	16,167	10,516	3,311	
	9	158,000	19,219	15,563	8,292	3,268	
	10	161,000	19,375	14,781	6,229	3,216	
	11	241,000	17,344	15,938	8,922	3,215	
	12	320,000	17,969	15,781	9,578	3,112	0.5
	13	215,000	21,563	15,125	12,516	3,168	
	14	193,000	19,063	15,229	8,292	3,416	
	15	205,000	17,969	16,875	6,203	3,737	
	16	226,000	18,125	17,031	9,188	3,279	0.8
	17	197,000	17,396	17,344	9,234	3,258	
	18	271,000	18,125	15,938	7,625	3,244	
	19	227,000	18,281	15,625	7,344	3,052	
20	157,000	18,281	15,484	6,047	3,220		
SFSR (Region II)	6	157,000	19,844	16,719	7,375	3,397	0.2
	7	144,000	20,313	15,781	7,891	3,495	
	8	176,000	20,469	17,188	6,911	3,421	
	9	123,000	20,313	16,875	10,286	3,204	
	10	189,000	18,281	16,875	5,625	3,090	
	11	180,000	18,906	15,781	9,781	3,247	0.5
	12	184,000	19,844	17,500	7,203	3,452	
	13	192,000	20,313	18,281	7,446	3,222	
	14	162,000	18,750	17,500	9,946	3,351	
15	174,000	19,063	17,054	5,161	3,538		

Mechanical Analysis for New and Spent Fuel Storage Racks

APR1400-H-N-NR-14012-NP, Rev.3

RAI 287-8272 - Question 09.01.02-41_Rev.1

SFSR (Region II)	16	193,000	22,031	16,094	11,688	3,543	0.8
	17	245,000	19,286	17,500	7,734	3,353	
	18	213,000	24,063	17,656	6,109	3,196	
	19	182,000	19,375	17,344	10,304	3,807	
	20	191,000	18,906	19,844	6,188	3,250	
Sensitivity Runs							
NFSR	21	-	12,750	11,688	4,286	3,595	N/A
	22	-	13,596	14,557	4,288	3,970	
SFSR (Region I)	23	239000	19,375	16,250	8,125	3,154	0.8
	24	188000	15,667	16,563	9,719	3,154	
	25	167000	19,500	15,417	7,516	3,252	0.8
	26	245000	18,125	15,438	7,979	3,846	
	27	328000	20,938	15,547	9,141	3,459	0.5
	28	290000	15,729	16,094	9,563	3,364	
	29	188000	20,156	18,750	6,938	3,734	0.8
	30	217000	16,875	13,984	9,344	3,472	
	31	206000	18,438	21,250	8,167	3,322	0.8
	32	203000	16,719	15,688	10,604	3,011	
	33	259000	20,625	16,563	7,813	3,366	0.8
	34	123000	-	-	-	-	0.5
	35	244000	16,958	14,458	7,844	3,140	0.5
	36	198000	17,188	14,313	9,203	3,349	0.8
SFSR (Region II)	23	147,000	19,688	17,500	6,359	3,445	0.8
	24	240,000	19,063	17,031	10,109	3,445	
	25	239,000	22,344	16,089	6,828	3,764	0.8
	26	223,000	17,344	17,214	9,391	3,278	
	27	205,000	17,813	17,031	6,813	3,664	0.5
	28	142,000	18,438	15,781	7,984	3,243	
	29	163,000	21,406	16,563	7,411	3,712	0.8
	30	184,000	19,844	16,563	6,484	3,352	
	31	170,000	22,969	18,438	11,875	3,522	0.8
	32	222,000	22,031	15,375	10,304	2,975	
	33	175,000	20,313	15,281	9,607	3,248	0.8
	34	68,800	-	-	-	-	0.5
	35	147,000	19,156	18,281	7,172	3,197	0.5
	36	224000	19,844	17,500	6,859	3,257	0.8

Notes:

- (1) Reported values are maximum for a run for any rack of that type (e.g., Region II SFSR). Although the horizontal loads are for the same rack, the maximum loads listed in other columns for a run may be from different racks.
- (2) Combined fuel grid impact loads are calculated by SRSS of horizontal (E-W and N-S) fuel impact loads for the most highly loaded grid. Since horizontal loads calculated at five vertical nodes are not uniform, and a different number of grids shares the load, the SRSS of the fuel-to-fuel impact loads does not yield the combined fuel grid impact load for a run.

Table 3-11 Stress Evaluation for Fuel Assembly

Location	Category	Calculated Value	Allowable Limit	Safety Factor (-)
Fuel spacer grid	Buckling Load	19.9 kN (4,481 lbf)	31.3 kN (7,045 lbf)	1.57
Fuel rod cladding	Bending Stress	65.2 MPa (9,449 psi)	540.3 MPa (78,365 psi)	8.3
	Yield Strain	0.0007 in/in	0.0058 in/in	8.3

Table 3-12 Stress Evaluation for Fuel Racks

Region	Rack	Type	Calculated Stress, MPa (psi)	Allowable Stress, MPa (psi)	Safety Factor (-)
Rack Cell-to-Baseplate	SFSR	Weld	154.3 (22,379)	246.1 (35,694)	1.59
		Base Metal Shear	109.1 (15,824)	118.0 ⁽²⁾ (17,120)	1.08
Baseplate-to-Pedestal ⁽¹⁾	NFSR	Weld	92.2 (20,725)	246.1 (35,694)	2.67
		Base Metal Shear	65.2 (14,653)	118.0 ⁽²⁾ (17,120)	1.81
	SFSR	Weld	55.5 (12,476)	246.1 (35,694)	4.43
		Base Metal Shear	39.2 (8,820)	118.0 ⁽²⁾ (17,120)	3.01
Cell-to-Cell	SFSR	Weld	66.4 (9,630)	246.1 (35,694)	3.71
		Base Metal Shear	46.9 (6,808)	118.0 ⁽²⁾ (17,120)	2.51

Notes:

- (1) Stresses on weld of the baseplate-to-support pedestal of the rack are conservatively evaluated by applying the maximum support loads acting on the NFSRs to the weld of the support pedestal of the SFSRs, as described in Appendix G.2 of Reference 17.
- (2) The allowable stress is calculated using 304 material yield strength.

REVISED RESPONSE TO REQUEST FOR ADDITIONAL INFORMATION**APR1400 Design Certification****Korea Electric Power Corporation / Korea Hydro & Nuclear Power Co., LTD****Docket No. 52-046**

RAI No.: 287-8272
SRP Section: 09.01.02 – New and Spent Fuel Storage
Application Section: 9.1.2
Date of RAI Issue: 11/02/2015

Question No. 09.01.02-42

The 10 CFR Part 50, Appendix A, General Design Criteria (GDC) 1, 2, 4, 5, 63, and 10CFR 52.80 (a) provide the regulatory requirements for the design of the new and spent fuel storage facilities. Standard Review Plan (SRP) Sections 9.1.2 and 3.8.4, Appendix D describes specific SRP acceptance criteria for the review of the fuel racks that are acceptable to meet the relevant requirements of the Commission's regulations identified above. In DCD Tier 2, Section 9.1.2.2.3, "New and Spent Fuel Storage Rack Design", the applicant stated that "The dynamic and stress analyses are performed as described in report APR1400-H-N-NR-14012-P & NP". In the technical report APR1400-H-N-NR-14012-P, Rev 0, Table 3-11, "Stress Evaluation for Fuel Assembly", the applicant provides allowable limit for fuel grid spacer and fuel rod cladding. The staff did not find the basis for the bending stress calculation in the fuel rod cladding reported in the Table 3-11. In order for the staff to perform its safety evaluation of the fuel assembly, the applicant in accordance with SRP 3.8.4 Appendix D I (6) is requested to provide the technical basis for calculating the bending stress and the acceptance criteria used for the evaluation the fuel cladding. The applicant is also requested to provide the stress/strain evaluation of fuel cladding and an evaluation of the fuel channel. The applicant is requested to identify any proposed changes to and provide a mark-up of Subsections in the DCD Tier 2 and the report APR1400-H-N-NR-14012-P, Rev.0, as appropriate.

Response – (Rev. 0)

The details for the bending stress calculation in the fuel rod cladding are described in Section 3.7.2.2 of the report APR1400-H-N-NR-14012-NP. Section 3.7.2.2 of the report APR1400-H-N-NR-14012-NP will be revised to include the strain evaluation of fuel cladding.

But the fuel channel evaluation is not included because a fuel channel is not part of the Plus7 fuel assembly design.

Response – (Rev. 1)

Technical report, APR1400-H-N-NR-14012-NP was submitted as Rev. 0 in December, 2014. KHNP responses to RAI 287-8272 were based in part on the Technical Report. Subsequent to issuance of the Technical Report and RAI responses, the NRC provided feedback on both the Technical Report and RAI 287-8272 responses. In response to this NRC feedback, Technical Report APR1400-H-N-NR-14012-NP will be revised (as Rev. 3) to incorporate additional information pertaining to the fuel racks. This RAI revision contains the specific Technical Report revisions relevant to this response and associated DCD changes, where necessary. A summary of the additional information is in the below paragraph).

Stress Evaluation of Fuel Cladding

The maximum lateral acceleration acting on the fuel mass is used to calculate a load uniformly distributed over a single fuel rod modeled as a beam simply supported by the spacer grids, and the maximum fuel rod length between the spacer grids is 359.4 mm (14.148 in). The uniformly distributed load on the fuel rod is calculated as follows:

$$q = a \times W_{\text{fuel}}$$

Where,

$$\begin{aligned} a &= \text{Maximum lateral acceleration in g's (= 22.8 g), and} \\ W_{\text{fuel}} &= \text{Fuel assembly rod mass per unit length (0.61 kg/m).} \end{aligned}$$

The maximum bending moment for uniform load is calculated as

$$M = (q \times L_{\text{spacer}}^2) / 8$$

Where,

$$L_{\text{spacer}} = \text{Maximum fuel rod length between spacer grids (359.4 mm (14.148 in)).}$$

The resulting maximum bending stress in the fuel cladding is calculated from equation below.

$$\sigma_b = \frac{M \cdot R_o}{I}$$

Where,

$$\begin{aligned} R_o &= \text{Outer radius of fuel rod (4.75 mm (0.187 in)), and} \\ I &= \text{Moment of inertia of fuel rod cladding (160.4 mm}^4 \text{ (3.853} \times 10^{-4} \text{ in}^4 \text{)).} \end{aligned}$$

This bending stress (= 65.2 MPa (9,449 psi)) is compared to the yield stress of 540.3 MPa (78,365 psi) for fuel rod cladding. The strain associated with this maximum stress is

$$\epsilon = \sigma_b / E$$

The maximum impact load on an individual fuel grid spacer cell, the bending stress and the strain induced in the fuel rod cladding due to the maximum lateral acceleration.

Impact on DCD

DCD Tier 2 Sections 9.1.2.2.1 and 9.1.2.2.2 will be revised as indicated in Attachment 1 to this response.

Impact on PRA

There is no impact on the PRA.

Impact on Technical Specifications

There is no impact on the Technical Specifications.

Impact on Technical/Topical/Environmental Reports

APR1400-H-N-NR-14012-NP (Rev. 3), Section 3.7.2.2 and Table 3-11 will be revised as shown in Attachment 2 to this response.

All cells of the new fuel storage racks are each designed with openings on the bottom that can drain an unanticipated release of water.

New Fuel Storage Rack

The rack is an assembly ^{of} cells. The minimum edge-to-edge spacing between fuel assemblies in adjacent rows is maintained to keep the fuel assemblies in a subcritical configuration. The minimum spacing is satisfied even after allowances are made for the rack fabrication tolerances and the predicted deflections resulting from postulated accident conditions. The stainless steel used for fabrication of the new fuel storage racks is physically and chemically compatible with ~~clad fuel made of Zircaloy~~. All cells have openings on the bottom to facilitate drainage in a flooding accident. Each storage cell in the racks has a lead-in guide to facilitate fuel assembly insertion without damaging the assembly. ^{cladding}

The racks are bolted to embedments at the bottom of the rack storage cavity to preclude tipping.

A new fuel inspection area is provided for the inspection of new fuel assemblies after they are withdrawn from their shipping container and before being placed in the new or spent fuel racks. It contains a seismic Category II inspection device to ascertain whether the fuel assemblies meet the dimensional requirements for installation into the reactor vessel. Visual inspection is also performed to check for shipping damage and to provide reasonable assurance that all protective wrapping material has been removed.

The center-to-center spacing between adjacent fuel assemblies is designed to be 35.5 cm (14 in) to the north and south and 35.5 cm (14 in) to the east and west to maintain subcriticality.

9.1.2.2.2 Spent Fuel Storage

Spent Fuel Pool

The spent fuel handling area consists of three separate water-filled fuel storage ^{which} and handling areas—the spent fuel cask loading pit, SFP, and fuel transfer canal—and are designed as seismic Category I within the seismic Category I auxiliary building in accordance with Chapter 3, Table 3.2-1. The design of the spent fuel cooling system

including related connections to the SFP is described in Subsection 9.1.3. Each area can be sealed from its adjacent area by a hinged gate equipped with elastomer seals. The gates are designed as seismic Category I and allow the spent fuel cask loading pit and the fuel transfer canal to be drained without affecting the water level in the SFP. The gates are designed to withstand the water pressure in the SFP when the adjacent areas are dewatered.

The fuel transfer canal contains the fuel transfer system that is used for transporting fuel assemblies to and from the containment building. The spent fuel cask loading pit contains the spent fuel cask that is used for the transport of spent fuel assemblies from the fuel storage area in the auxiliary building.

All the preceding areas are stainless-steel-lined and concrete-walled pools that are integral parts of the fuel handling area building structure.

The SFP is approximately 7.31 m (42 ft) deep and made of reinforced concrete lined with stainless steel plate. The SFP is sufficiently deep that when a spent fuel assembly is being carried over the spent fuel storage racks by the spent fuel handling machine (SFHM) at its maximum lift height, there is sufficient water coverage to provide reasonable assurance that personnel on the SFHM or on the operating floor around the pool are not exposed to radiation levels exceeding 0.025 mSv per hour.

Piping penetrations to the SFP are at least 3.05 m (10 ft) above the top of the fuel assemblies seated in the spent fuel storage racks. The bottom of the gates that lead from the SFP to the fuel transfer canal and the spent fuel cask loading pit are above the top of the stored fuel assemblies. The spent fuel storage racks and the pool floor are designed to withstand the maximum impact energy of a fuel handling tool or a fuel assembly with its handling tool dropped from the maximum lift height. Redundant low- and high-level water alarms and temperature measurement instruments, as described in Subsection 9.1.3.5, minimize the potential for overfilling the pool. The ventilation system for the SFP area is described in Subsection 9.1.3.1.

Pipes that discharge into the spent fuel pool include siphon breaker holes as an anti-siphon device between the normal water level and the level of the SFP pumps' suction connection.

The makeup water to the SFP is provided by a safety Class 3, seismic Category I water supply, as described in Subsection 9.1.3.2.

A liner leakage collection system is provided to collect possible leakage from liner plate welds on the pool walls and floor. The stainless steel liners are welded to the C-shaped embedment in the pool walls, and the floors and embedment are interconnected and drain through the leakage collection pipe to a monitored collection point.

The SFP leakage collection pipes connected to the C-shaped embedment are closed by valves or caps in the collection points. Any leakage from liner plate welds is detected by opening the valves or caps during weekly patrols. To meet the requirements of 10 CFR 20.1406 (Reference 18), the inside of the leakage collection pipes is inspected using a device (e.g., fiberscope) approximately every refueling outage. If any materials (e.g., accumulated boric acid residue, minerals) are detected, the pipes are cleaned. The leakage collection pipes are sized to allow cleaning as specified in NRC RG 4.21 (Reference 19).

Spent Fuel Storage Racks

in plates attached to all four sides of each cell (with the exception a the outer side of some cells on the periphery).

Spent fuel storage racks used for high-density storage are typically stainless steel structures with rectangular fuel storage cells coated with neutron absorbing material (see Figure 9.1.2-2).

Although free

Spent fuel storage rack modules are free standing on embedments in the pool floor. ~~Sufficient space is provided between adjacent modules and between modules and other obstructions in the SFP to allow the modules to slide without contacting each other or other obstructions~~ during a seismic event. The modules are equipped with stable, adjustable feet that rest on the embedments. The adjustable feet and lifting lugs permit the modules to be installed in the pool. The stainless steel used for the fabrication of the racks is compatible with fuel assembly materials and the spent fuel borated water environment.

Neutron absorbing material is used for reactivity control in spent fuel storage rack. Neutron absorbing material is inserted between the fuel storage cell and the cover plate. Stainless steel plate for cover plate is welded to each side of the fuel storage cell with the neutron absorbing material installed in the cover plate cavity. The objective of cover plate design is to secure the neutron absorbing material to be installed safety. The cover plate serves to locate and position the neutron absorbing material accurately and to preclude its movement under seismic conditions. The cover plate also isolates the neutron absorbing material from the fuel. The neutron absorbing material covers the full length of the active fuel. Provisions are made for installing surveillance specimens of the neutron absorbing material

analysis of loads imparted by baseplate-to-baseplate contact demonstrates not damage occurs

SFSRs are installed as closely as possible with the protruding baseplate intended to be in contact with the adjacent baseplates. If the racks were initially installed with slight separation, conclusions would not change since it would be no different than a few time steps into a transient when the rack bases have moved slightly apart. As reported in Section 3.7.1.1, the upper part of the racks do not come into contact. Therefore, the only rack-to-rack contact is between the baseplate of racks. The maximum impact load at the SFSR baseplates is shown in Table 3-8.

Also as reported in Section 3.7.1.1, the racks do not contact the SFP wall. Therefore, no rack to pool wall impact loads are calculated. This is consistent with SRP Section 3.8.4, Appendix D, Structural Acceptance Criteria, which states:

“In the consideration of the effects of seismic loads, factors of safety against gross sliding and overturning of racks and rack modulus [sic] under all probable service conditions should be in accordance with SRP Section 3.8.5, Subsection II.5. This position on factors of safety against sliding and tilting need not be met provided that the applicant meets any one of the following conditions:

“a. Detailed nonlinear dynamic analyses show that the amplitudes of sliding motion are minimal and impact between adjacent rack modules or between a rack module and the pool walls is prevented provided that the factors of safety against tilting are within the allowable values provided in SRP Section 3.8.5, Subsection II.5....”

3.7.2 Fuel Structural Evaluation

Lateral impact load on the spent fuel assembly is evaluated for two acceptance criteria: fuel spacer grid buckling and fuel cladding yield stress.

The maximum impact load per cell applied to fuel assembly is evaluated for the peak load shown in Table 3-8. Therefore, the maximum acceleration load that the rack imparts on the fuel assembly can be conservatively calculated as follows:

$$a = \frac{F}{w}$$

Where,

- a = Maximum lateral acceleration in g's (= 22.8 g) per section 7.2 of Reference 17,
- F = Maximum fuel-to-cell wall impact load per cell, and
- w = Weight of one fuel assembly (6.27 kN (1408.6 lbf)).

The structural integrity of fuel assembly cladding is evaluated for the maximum lateral acceleration load, obtained by combining (i.e., SRSS) the simultaneous impact load in the E-W and N-S directions to find the maximum value at any time step. The fuel assembly spacer grid is evaluated for the maximum grid impact load, obtained by combining (i.e., SRSS) the simultaneous impact load in the E-W and N-S directions at the same time.

3.7.2.1 Structural Integrity Evaluation of Fuel Spacer Grid

The lateral impact loads on a single fuel spacer grid is compared against its buckling load capacity, which is shown in the Table 3-3. The critical buckling load of the fuel spacer grid for the APR1400 design is 31.3 kN (7,045 lbf) and compared with the combined fuel grid impact load as shown in Table 3-8. The resulting safety factor on fuel assembly spacer grid is as summarized in Table 3-11.

3.7.2.2 Stress Evaluation of Fuel Cladding

The maximum lateral acceleration acting on the fuel mass is used to calculate a load uniformly distributed

over a single fuel rod modeled as a beam simply supported by the spacer grids, and the maximum fuel rod length between the spacer grids is 359.4 mm (14.148 in) as shown in Table 3-3.

The uniformly distributed load on the fuel rod is calculated as follows:

$$q = a \times W_{\text{fuel}}$$

Where,

a = Maximum lateral acceleration in g's (= 22.8 g) per section 7.2 of Reference 17, and
 W_{fuel} = Fuel assembly rod mass per unit length (0.61 kg/m).

The maximum bending moment for uniform load is calculated as

$$M = (q \times L_{\text{spacer}}^2) / 8$$

Where,

L_{spacer} = Maximum fuel rod length between spacer grids (359.4 mm (14.148 in)).

The resulting maximum bending stress in the fuel cladding is calculated from equation below.

$$\sigma_b = \frac{M \cdot R_o}{I}$$

Where,

R_o = Outer radius of fuel rod (4.75 mm (0.187 in)), and
 I = Moment of inertia of fuel rod cladding (160.4 mm⁴ (3.853 x 10⁻⁴ in⁴)).

This bending stress is compared to the yield stress of 540.3 MPa (78,365 psi) per Table 3-3 for fuel rod cladding, the resulting safety factor is given in Table 3-11. The strain associated with this maximum stress is

$$\varepsilon = \sigma_b / E$$

The maximum impact load on an individual fuel grid spacer cell, the bending stress and the strain induced in the fuel rod cladding due to the maximum lateral acceleration are summarized in Table 3-11. The structural integrity of the stored fuel assemblies under the SSE event is maintained, because the safety factors are greater than 1.0.

3.7.3 Rack Structural Evaluation

To ensure that the fuel racks have adequate safety margins, all stress evaluations for the fuel racks are performed based on the worst-case results in any rack at any time during multiple simulations. In this section, the structural integrity of welds and racks is evaluated by using the maximum loads in vertical and horizontal direction calculated by time-history analysis of the racks.

3.7.3.1 Stress Factors for Racks

Using the time-history analysis results for pedestal normal and lateral interface forces, the limiting bending moment and shear force at the baseplate-to-pedestal interface may be computed as a function of time. In particular, maximum values for the stress factors which are defined in Section 3.2.2 can be determined for each pedestal in each rack. Using this information, the structural integrity of the pedestals can be assessed.

Table 3-11 Stress Evaluation for Fuel Assembly

Location	Category	Calculated Value	Allowable Limit	Safety Factor (-)
Fuel spacer grid	Buckling Load	19.9 kN (4,481 lbf)	31.3 kN (7,045 lbf)	1.57
Fuel rod cladding	Bending Stress	65.2 MPa (9,449 psi)	540.3 MPa (78,365 psi)	8.3
	Yield Strain	0.0007 in/in	0.0058 in/in	8.3

Table 3-12 Stress Evaluation for Fuel Racks

Region	Rack	Type	Calculated Stress, MPa (psi)	Allowable Stress, MPa (psi)	Safety Factor (-)
Rack Cell-to-Baseplate	SFSR	Weld	154.3 (22,379)	246.1 (35,694)	1.59
		Base Metal Shear	109.1 (15,824)	118.0 ⁽²⁾ (17,120)	1.08
Baseplate-to-Pedestal ⁽¹⁾	NFSR	Weld	92.2 (20,725)	246.1 (35,694)	2.67
		Base Metal Shear	65.2 (14,653)	118.0 ⁽²⁾ (17,120)	1.81
	SFSR	Weld	55.5 (12,476)	246.1 (35,694)	4.43
		Base Metal Shear	39.2 (8,820)	118.0 ⁽²⁾ (17,120)	3.01
Cell-to-Cell	SFSR	Weld	66.4 (9,630)	246.1 (35,694)	3.71
		Base Metal Shear	46.9 (6,808)	118.0 ⁽²⁾ (17,120)	2.51

Notes:

(1) Stresses on weld of the baseplate-to-support pedestal of the rack are conservatively evaluated by applying the maximum support loads acting on the NFSRs to the weld of the support pedestal of the SFSRs, as described in Appendix G.2 of Reference 17.

(2) The allowable stress is calculated using 304 material yield strength.